CONFERENCE SERIES

David Stock, Roland Wester, Paul Scheier (Eds.)

XIXth Symposium on Atomic, Cluster and Surface Physics 2014 (SASP 2014)

February 8 – 14, 2014

Obergurgl, Austria

Contributions

XIXth Symposium on Atomic, Cluster and Surface Physics 2014 (SASP 2014)

February 8 – 14, 2014 Obergurgl, Austria

International Scientific Committee:

Davide Bassi (Universitá degli Studi di Trento)
Tilmann D. Märk (Universität Innsbruck)
Nigel Mason (Open University, UK)
Martin Quack (Eidgenössische Technische Hochschule Zürich)
Tom Rizzo (EPFL Lausanne)
Paul Scheier (Universität Innsbruck)

Organizing Committee:

Institut für Ionenphysik und Angewandte Physik, Universität Innsbruck

Stephan Denifl, Paul Scheier and Roland Wester (chairpersons)
Arntraud Bacher

Preface

The international Symposium on Atomic, cluster and Surface Physics, SASP, is a continuing biennial series of conferences, founded in 1978 by members of the Institute of Atomphysik, now Institute of Ionphysics and Applied Physics of the University of Innsbruck, Austria. SASP symposia aim to promote the growth of scientific knowledge and effective exchange of information among scientists in the field of atomic, molecular, cluster and surface physics, stressing both fundamental concepts and applications across these areas of interdisciplinary science. A major focus of SASP 2014 is on ion-molecule reactions.

Since the beginning, the SASP format has been similar to that of a Gordon Conference, with invited lectures, hot topic oral presentations, posters and ample time for discussions. The attendance to the symposium has been kept to about 100 participants to favor interdisciplinary and multidisciplinary discussions.

SASP usually takes place in Austria, but every second time, it may be held in another alpine country. So far, the SASP conferences were held in the following locations:

1978 Zirog, Italy	1998 Going, Austria
1980 Maria Alm, Austria	2000 Folgaria, Italy
1982 Maria Alm, Austria	2002 Going, Austria
1984 Maria Alm, Austria	2004 La Thuile, Italy
1986 Obertraun, Austria	2006 Obergurgl, Austria
1988 La Plagne, France	2008 Les Diablerets, Switzerland
1990 Obertraun, Austria	2010 Obergurgl, Austria
1992 Pampeago, Italy	2012 Alpe d´Huez, France
1994 Maria Alm, Austria	2014 Obergurgl, Austria
1996 Engelberg, Switzerland	

SASP Erwin Schrödinger Gold Medal 2014

The „SASP Award for Outstanding Scientific Achievements" was initiated in 1992 by the SASP International Scientific Committee. This award is granted during the bienniel SASP meeting to one or two scientists, chosen among those who have strong connections to the activities of SASP.

The recipient of the SASP award 2014 – in the form of the "Erwin Schrödinger Gold Medal" designed by Zdenek Herman – will be

Stephen D. Price, University College London,
United Kingdom

Stephen D. Price, from the University College London, United Kingdom, will receive this award for his outstanding contributions to ion chemistry, in particular to ion-molecule reactions of singly and multiply charged ions in the gas phase.

At previous SASP meetings the Schrödinger Gold Medal was awarded to:

1992   David Smith, Birmingham, UK
1994   Zdenek Herman, Praha, Czech Republic
1996   Werner Lindinger and Tilmann Märk, Innsbruck, Austria
1998   Eldon Ferguson, Boulder, USA and Chava Lifshitz, Jerusalem, Israel
2000   Jean H. Futrell, Richland, USA
2002   Eugen Illenberger, Berlin, Germany
2004   Anna Giardini-Guidoni, Roma, Italy
2006   Davide Bassi, Trento, Italy and Martin Quack, Zürich, Switzerland
2008   Helmut Schwarz, Berlin, Germany
2010   Kurt Becker, New York, USA
2012   Dieter Gerlich, Chemnitz, Germany and John Maier, Basel, Switzerland

Program

	Sun, Feb 9	Mon, Feb 10	Tue, Feb 11	Wed, Feb 12	Thu, Feb 13	Fri, Feb 14
8:30				Chair: A. Mauracher		
				Alkwin Slenczka		
9:00		Chair: Martin Quack	Chair: H. Haberland		Chair: Rainer Beck	Chair: John Maier
		Marc Brouard	Alexander Dorn	Wolfgang E. Ernst	Olivier Dulieu	Veronique Vuitton
9:30		Piergiorgio Casavecchia	Markus Oster	Marius Lewerenz	Bill Hase	Gary E. Douberly
10:00		Regina de Vivie-Riedle	Beate Paulus	Oleg Boyarkine	Stefan Matejcik	Philippe Dugourd
10:30						
11:00		Coffee				
		Jochen Küpper	Karl-Michael Weitzel	*Thomas Rizzo*	Roberto Marquardt	*G. Niedner-Schatteburg*
11:30		Bas van de Meerakker	*Katharina Dobes*	*Ewen Campbell*	*Oliver Buenermann*	Martin Beyer
				Marc van Hemert		
12:00		*Albrecht Lindinger*	*Tim Schäfer*	*Oskar Asvany*	*Jana Roithova*	Jürgen Stohner
12:30		*Markus Kowalewski*	*Morten Hundt*		*Henning Zettergren*	End
			Break			
16:00						
			Snack			
16:30		Chair: Paul Scheier	Chair: E. Illenberger	Chair: Stephan Denifl	Chair: R. Wester	
		Nigel Mason	Oddur Ingolfson	Frank Hagelberg	*Christian Alcaraz*	
17:00					*Sieghard Albert*	
		Helmut Schwarz	Marcio Varella	Andrew M. Ellis	*Karl-Heinz Ernst*	
17:30			*Petra Swiderek*	*Daniela Ascenzi*	Violaine Vizcaino	
18:00		Tilmann Märk special	*Fabio Zappa*	*Štěpán Roučka*		
			Juraj Fedor	*Ralf Zimmermann*	Stephen Price	
18:30						
20:15		Dinner			SASP Award	
20:30	Welcome					
	Mark Johnson		Armin Wisthaler		Conf Dinner	
21:00	Frederic Merkt	Poster	Chris A. Mayhew	Poster		

Contents

Invited Papers

Hot Topic Papers

Contributed Papers

Invited Papers

Cryogenic ion vibrational and electronic predissociation spectroscopy

Mark A. Johnson
Yale University

I will discuss how the cooling, mass selection, and processing of cryogenic ions provides powerful opportunities for the detailed characterization of their structures as well as the rational synthesis of labile reaction intermediates. This is accomplished by first cooling the ions close to 10K and condensing onto them dozens of weakly bound, chemically inert small molecules or rare gas atoms. This assembly can then be used as a medium in which to quench reactive encounters by rapid evaporation of the adducts, as well as provide a universal means for acquiring highly resolved vibrational action spectra of the embedded species by photoinduced mass-loss. Moreover, the spectroscopic measurements can be obtained with readily available, broadly tunable pulsed infrared lasers because absorption of a single photon is sufficient to induce evaporation. The method is implemented with a hybrid photofragmentation mass spectrometer involving two stages of mass selection with two laser excitation regions interfaced to the cryogenic ion source. Specific recent examples include the structure of small building blocks of ionic liquids and the temperature dependence of the electronic spectrum of Rhodamine 6G.
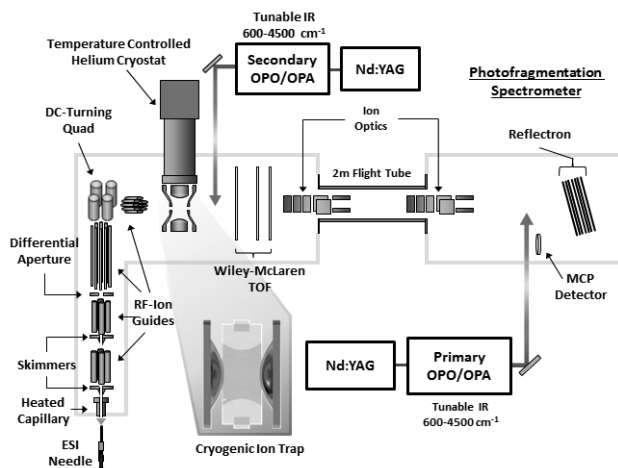
Molecular Rydberg states and ions: high-resolution spectroscopy and electrostatic trapping

Daniel Sprecher, Christian Seiler and <u>Frédéric Merkt</u>
Laboratorium für Physikalische Chemie, ETH Zürich

Molecular Rydberg states are electronically excited states in which the electron can be described as moving in a distant orbit around the molecular ion core. High-resolution spectroscopy of such states provides information on the interaction between the electron and the ion core and, by extrapolation of the Rydberg series, on the energy level structure of the ion core. Multichannel quantum defect theory (MQDT) is very powerful tool to analyze the Rydberg spectrum of a molecule and to derive sets of physically meaningful parameters describing the interaction between the Rydberg electron and the molecular ion core [1]. In the past ten years, we have combined high-resolution spectroscopy in the vacuum-ultraviolet and the sub-millimeter-wave ranges of the electromagnetic spectrum and MQDT to study the rovibrational structure (including the fine and hyperfine structures) of molecular Rydberg states. In these studies, we have obtained new information on the role of nuclear spins in photoionization and have developed reliable methods to measure the rovibrational and hyperfine energy level structures of molecular ions [2,3]. Results of recent investigations of the Rydberg spectrum of H_2 and He_2 will be presented which have served, among others, (i) to determine the dissociation energies of H_2, HD and D_2 and the hyperfine structure of H_2^+, HD^+ and D_2^+ with high accuracy, and (ii) to study the interaction between Rydberg levels of *gerade* and *ungerade* electronic symmetry in HD [4]. Given the focus of SASP 2014 on molecular ions, I shall also briefly present results on the electrostatic trapping of Rydberg molecules [5] and argue that a Rydberg-molecule trap is a trap in which ions are doubly trapped, by the Rydberg electron *and* by the weak electrostatic potential. Such traps may offer advantages over more conventional ion traps.

References

[1] Ch. Jungen, Elements of quantum defect theory, in Handbook of high-resolution spectroscopy, Eds. M. Quack and F. Merkt (Wiley, Chichester, 2011)

[2] J. Liu, E. J. Salumbides, U. Hollenstein, J. C. J. Koelemeij, K. S. E. Eikema, W. Ubachs and F. Merkt, J. Chem. Phys. 130, 174306 (2009)

[3] D. Sprecher, Ch. Jungen, W. Ubachs and F. Merkt, Faraday Discussions 150, 51 − 70 (2011)

[4] D. Sprecher, Rovibronic and hyperfine interactions in Rydberg states of molecular hydrogen, Dissertation, ETH Zürich, 2013

[5] Ch. Seiler, Rydberg-*Stark deceleration and trapping of atoms and molecules*, Dissertation, ETH Zürich, 2013

The stereodynamics of inelastic scattering of NO(X) by Ar

Mark Brouard*, Helen Chadwick, Chris Eyles, Sean D.S. Gordon, Balazs Hornung,
Bethan Nichols,
Department of Chemistry, University of Oxford,
The Physical and Theoretical Chemistry, Laboratory, South Parks Road,
Oxford OX1 3QZ, United Kingdom

F. Javier Aoiz
Departamento de Química Física, Facultad de Química,
Universidad Complutense, 28040 Madrid, Spain.

Arjan Gijsbertsen
Laser Center and Department of Physical Chemistry, Vrije Universiteit,
Amsterdam, De Boelelaan 1083, 1081 HV Amsterdam, The Netherlands

Steven Stolte
Laser Center and Department of Physical Chemistry, Vrije Universiteit,
Amsterdam, De Boelelaan 1083, 1081 HV Amsterdam, The Netherlands, and
Atomic and Molecular Physics Institute, Jilin University, Changchun 130012, China.
and
Laboratoire Francis Perrin, Bâtment 522, DRECEM/SPAM/CEA Saclay, 91191 Gif
sur Yvette, France

New velocity map ion-imaging results will be presented for the inelastic scattering of
NO(X) by Ar, and other rare gases, in which the NO(X) molecule is fully quantum
state-selected both before and after collision. State-to-state differential cross-sections
(DCSs) and collision-induced angular momentum orientation and alignment of the
fully Λ-doublet resolved inelastic scattering of NO($X^2\Pi_{1/2}$,v=0,j=1/2,f) with Ar have
been measured at a collision energy of 530 cm^{-1}.

The dependence of the DCSs and angular momentum polarization on rotational and
Λ-doublet state will be discussed in detail, with reference to simple classical and
semi-classical models, as well as to exact quantum scattering calculations. A
particular focus of the talk will be a discussion of the quantum mechanical origin of
collision induced angular momentum orientation.

New experimental results will also be presented in which we have measured the DCSs and polarization on the inelastically scattered NO(X) products arising from collisions with oriented NO molecules. These results may be considered the first 'complete' experiment on the inelastic scattering of NO(X) by the rare gases.

*email address: mark.brouard@chem.ox.ac.uk

Molecular beam studies of polyatomic multichannel nonadiabatic reaction dynamics of oxygen atoms

Piergiorgio Casavecchia, Francesca Leonori, Nadia Balucani
Dipartimento di Chimica, Università degli Studi di Perugia
Via Elce di Sotto, 8 - 06123 Perugia, Italy

Small unsaturated hydrocarbons, such as C_2H_2 (acetylene), C_2H_4 (ethylene), C_3H_4 (allene and methylacetylene) and C_3H_6 (propene), are crucial intermediates in hydrocarbon combustion, where their dominant consumption pathways are reactions with ground-state oxygen atoms, $O(^3P)$ [1,2]. These reactions are characterized by a variety of energetically open, competing radical and molecular product channels, some of which can take place only via intersystem crossing (ISC) from triplet to singlet potential energy surfaces (PES). In combustion modelling, among the most important information needed for each of these elementary multichannel reactions of $O(^3P)$ are: (*a*) the overall rate constant, (*b*) the identity of the primary products, and (*c*) the branching ratios (BRs) possibly as a function of collision energy E_c (temperature). While kinetics experiments are able to satisfy point (*a*), point (*b*) and (*c*) still represent a challenge for kinetics, although considerable progress has recently been made [3]. The method most suitable to tackle this challenge is the crossed molecular beams (CMB) scattering technique with "universal" mass spectrometric detection [4] based on "soft" ionization by tunable energy electrons [5] or VUV synchrotron radiation [6].

In this talk we will report on our recent investigations of the reaction dynamics of $O(^3P)$ with acetylene [7], ethylene [8], allene [9], methylacetylene [10] and propene [11] using the CMB method. By exploiting "soft" electron-ionization we have probed all energetically allowed product channels (up to ten in $O+C_3H_4$) and characterized the dynamics, branching ratios and extent of ISC. The BRs for the five competing channels leading to $H+CH_2CHO$, $H+CH_3CO$, H_2+CH_2CO, CH_3+HCO, and CH_2+HCHO from $O+C_2H_4$ are analyzed together with those obtained from kinetics studies at room temperature [12] ($E_c \approx 0.9$ kcal/mol). The combined kinetics and dynamics results have allowed us to examine the BRs and the extent of ISC in a wide range of E_cs (temperature), from ~1 kcal/mol (300 K) up to ~13 kcal/mol (4300 K). Experimental results are compared with those of available statistical calculations on *ab initio* PESs for all systems and with those of quasiclassical trajectory surface-hopping computations carried out in a synergic fashion by the group of Bowman on coupled *ab initio* triplet and singlet PESs for the benchmark multichannel nonadiabatic reaction $O+C_2H_4$. ISC is found to increase strongly with molecular complexity (from about 0% in $O+C_2H_2$ up to about 50% in $O+C_2H_4$ and more than

90% in O+CH$_2$CCH$_2$) and to depend on molecular structure (about 80% in O+CH$_3$CCH).

References

[1] N. Balucani, F. Leonori and P. Casavecchia, in *Cleaner Combustion,* Green Energy and Technology, eds. F. Battin-Leclerc, J. M. Simmie and E. Blurok, Ch. 22, pp 577-606, Springer-Verlag London, 2013.

[2] J. A. Miller, M. J. Pilling, J. Troe, *Proc. Comb. Inst.* **30**, 43 (2005); D. J. Hucknall, *Chemistry of Hydrocarbon Combustion*, Chapman Hall, New York, 1985.

[3] J.D.Savee, O.Welz, C.A.Taatjes, D.L.Osborn, *PCCP* **14**, 10410 (2012).

[4] P. Casavecchia, *Rep. Prog. Phys.* **63**, 355-414 (2000).

[5] P. Casavecchia, F. Leonori, N. Balucani, R. Petrucci, G. Capozza and E. Segoloni, *PCCP* **11,** 46 (2009) (*Perspective*); N. Balucani, G. Capozza, F. Leonori, E. Segoloni and P. Casavecchia, *Int. Rev. Phys. Chem.* **25**, 109 (2006).

[6] S.-H.Lee, W.-K.Chen, W.-J.Huang, *J.Chem.Phys.***130**,054301 (2009).

[7] G.Capozza *et al. JCP* **120**, 4557 (2004); F. Leonori, N. Balucani, G. Capozza, E. Segoloni, G. G. Volpi and P. Casavecchia, *PCCP*, submitted.

[8] P. Casavecchia, G. Capozza, E. Segoloni, F. Leonori, N. Balucani, G. G. Volpi, *J. Phys. Chem. A* **109**, 3527 (2005); B. Fu, Y.-C. Han, J. M. Bowman, L. Angelucci, N. Balucani, F. Leonori and P. Casavecchia, *Proceedings of the National Academy of Sciences USA (PNAS)* **109**, 9733 (2012); B. Fu, Y.-C. Han, J. M. Bowman, F. Leonori, N. Balucani, L. Angelucci, A. Occhiogrosso, R. Petrucci and P. Casavecchia, *J. Chem. Phys.* **137**, 22A532 (2012); P. Casavecchia, J. Bowman, *et al.*, *in prep.*

[9] F. Leonori, A. Occhiogrosso, N. Balucani, A. Bucci, R. Petrucci and P. Casavecchia*.*, *J. Phys. Chem. Lett.* **3**, 75 (2012).

[10] N. Balucani, F. Leonori, V. Nevrly, S. Falcinelli, D. Stranges, A. Bergeat and P. Casavecchia, *in preparation.*

[11] V. Nevrly, A. Bergeat, F. Leonori, N. Balucani, S. Falcinelli, S. Chefdeville, and P. Casavecchia, *work in progress*.

[12] T. L. Nguyen, L. Vereecken, X. J. Hou, M. T. Nguyen, and J. Peeters **109**, 7489 (2005); A. Miyoshi *et al.*, *PCCP* **11**, 7318 (2009).

Molecular features in complex environment: cooperative team players during excited state bond cleavage

Sebastian Thallmair, Matthias Roos, Benjamin Fingerhut, <u>Regina de Vivie-Riedle</u>
rdvpc@cup.uni-muenchen.de

Department Chemie, Ludwig-Maximilians-Universität, München

Photoinduced bond cleavage is often employed for the generation of carbocations, which are central to S_N1 reactions. Benzhydryl derivates are prominent precursors in organic chemistry. Depending on the leaving group, the photoinduced bond cleavage occurs on a femtosecond to picosecond time scale and typically leads to two distinguishable products, the desired benzhydryl cations and as competing by-product the benzhydryl radicals. Conical intersections are the chief suspects for such ultrafast branching processes. We show for two typical examples, the neutral benzhydrylchloride and the charged diphenylmethyltriphenyl-phosphonium ions that the role of the conical intersections depends on the interplay of molecular features with the environment. It turns out to differ significantly for both precursors.

Our analysis is based on quantum chemical, quantum dynamical and on-the-fly calculations. The experimental optical signal we use for comparison is recorded by the Riedle group (LMU, Physik) with high temporal resolution. In case of benzhydrylchloride we can directly connect the observed signals to two early conical intersections close to the Franck Condon region, in case of the diphenylmethyltriphenylphosphonium ion dynamic solvent effects are needed to activate a conical intersection at larger distances along the reaction coordinate. Including the dynamic effect of the solvent, we could clarify the individual bond cleavage mechanism and outline how chemical modifications can be used to control the dissociation and the stability of the carbocations independently.

Controlled complex molecules for cool chemistry and hot imaging

Jochen Küpper

Center for Free-Electron Laser Science, DESY, Notkestrasse 85, 22607 Hamburg, Germany
Department of Physics, University of Hamburg, Luruper Chausse 149, 22761 Hamburg, Germany
The Hamburg Center for Ultrafast Imaging, Luruper Chaussee 149, 22761 Hamburg, Germany

The structure function relationship is still a largely open area of molecular sciences. On the one hand there is vast evidence for structural influence in chemistry and biology, with highly successful abstractions even at the textbook level. On the other hand, there is very little direct experimental evidence for the details of this structure-function relationship. We have demonstrated a new approach toward the investigation of the influence of conformational details in the molecular structure on the reactivity of gas-phase reactions. In a benchmark experiment, we measured the chemical reactivities of the *cis* and *trans* conformers of 3-aminophenol with Ca^+ ions [1].

In the second part I will discuss approaches toward the disentangling of the chemical dynamics of individual molecular species with temporal and spatial atomic resolution. The recording of these so-called molecular movies, the atomically resolved structural dynamics of complex molecules, is within reach. Corresponding modern experiments in the molecular sciences range from ultrafast attosecond electron dynamics investigations of diatomic molecules to the coherent diffractive imaging of nanocrystals or viruses of biological samples [2]. The successful filming will often rely on strongly controlled molecular samples. This includes the separation of individual structural isomers [3,4] or even single quantum states of complex molecules [5,6], but also the ability to strongly fix complex molecules in space [7,8], and to deliver them to the interaction point of the probe experiment, such as modern table-top laser systems, free-electron lasers, or electron beams.

In this presentation I will discuss our endeavors to get complex molecules under control, including the spatial separation of different species and the one- and three-dimensional alignment and orientation. I will discuss the chemical reactivities of conformers and discuss future possibilities to study the structure-function

relationship in bimolecular reactions. Moreover, the controlled samples of such many-body quantum systems have been successfully employed in various benchmark experiments toward the recording of molecular movies and I will discuss the state-of-the art and future possibilities.

References

[1] Y. P. Chang, K. Długołęcki, J. Küpper, D. Rösch, D. Wild, and S. Willitsch, *Science* **342**, 98 (2013).

[2] A. Barty, J. Küpper, and H. N. Chapman, *Annu. Rev. Phys. Chem*. **64**, 415 (2013).

[3] F. Filsinger, U. Erlekam, G. von Helden, J. Küpper, and G. Meijer, *Phys. Rev. Lett*. **100**, 133003 (2008).

[4] F. Filsinger, J. Küpper, G. Meijer, J. L. Hansen, J. Maurer, J. H. Nielsen, L. Holmegaard, and H. Stapelfeldt, *Angew. Chem. Int. Ed*. **48**, 6900 (2009).

[5] J. H. Nielsen, P. Simesen, C. Z. Bisgaard, H. Stapelfeldt, F. Filsinger, B. Friedrich, G. Meijer, and J. Küpper, *Phys. Chem. Chem. Phys*. **13**, 18971 (2011).

[6] S. Putzke, F. Filsinger, H. Haak, J. Küpper, and G. Meijer, *Phys. Chem. Chem. Phys*. **13**, 18962 (2011).

[7] L. Holmegaard, J. H. Nielsen, I. Nevo, H. Stapelfeldt, F. Filsinger, J. Küpper, and G. Meijer, *Phys. Rev. Lett*. **102**, (2009).

[8] I. Nevo, L. Holmegaard, J. H. Nielsen, J. L. Hansen, H. Stapelfeldt, F. Filsinger, G. Meijer, and J. Küpper, *Phys. Chem. Chem. Phys*. **11**, 9912 (2009).

Cold and Controlled Collisions using Stark-decelerated molecular beams

Sebastiaan Y.T. van de Meerakker

Radboud University Nijmegen, Institute for Molecules and Materials, Nijmegen, the Netherlands

Over the last years methods have been developed to get improved control over molecules in a molecular beam [1]. With the Stark decelerator, a part of a molecular beam can be selected to produce bunches of molecules with a computer-controlled velocity and with longitudinal temperatures as low as a few mK. The molecular packets that emerge from the decelerator have small spatial and angular spreads, and have almost perfect quantum state purity.

These tamed molecular beams are ideally suited for molecular scattering experiments, and allow for precise state-to-state scattering experiments as a function of the collision energy. I will report on low-energy scattering of OH with rare gas atoms, revealing the quantum threshold behavior of state-to-state inelastic cross sections [2,3]. Recently, we have exploited the state purity of Stark decelerated beams to study inelastic scattering between *two* state-selected molecules, using the two open shell radicals OH + NO as a model system [4]. Finally, I will present our first results on the combination of Stark deceleration and velocity map imaging. The narrow velocity spread of Stark-decelerated beams results in scattering images with an unprecedented sharpness and angular resolution. This has facilitated the observation of diffraction oscillations in the state-to-state differential cross sections for NO + Ar.

The study of molecular collisions at low collision energies (1- 20 cm^{-1}) is another exciting avenue. I will report on recent measurements (performed at the University of Bordeaux) of scattering resonances for inelastic collisions between O_2 and H_2 [5], and our future plans to scatter Stark-decelerated with Zeeman-decelerated molecules.

References

[1] S.Y.T. van de Meerakker, H.L. Bethlem, N. Vanhaecke, and G. Meijer *Chemical Reviews* **112**, 4828 (2012).
[2] J.J. Gilijamse, S. Hoekstra, S.Y.T. van de Meerakker, G.C. Groenenboom, and

    G. Meijer *Science* **313**, 1617 (2006).

[3] L. Scharfenberg, J. Kłos, P.J. Dagdigian, M.H. Alexander, G. Meijer, and S.Y.T. van de Meerakker *Phys. Chem. Chem. Phys.* **12**, 10660 (2010).

[4] M. Kirste, X. Wang, H.C. Schewe, G. Meijer, K. Liu, A. van der Avoird, L.M.C. Janssen, K.B. Gubbels, G.C. Groenenboom, and S.Y.T. van de Meerakker *Science* **338**, 1060 (2012).

[5] S. Chefdeville, Y. Kalugina, S.Y.T. van de Meerakker, Ch. Naulin, F. Lique, and M. Costes, *Science* **341**, 1094 (2013).

The advantages and potential of drift-tube chemical ionisation mass spectrometric techniques for the detection of threat agents

Chris A. Mayhew

School of Physics and Astronomy, University of Birmingham, UK

It is a considerable pleasure to have the opportunity to formally thank Professor Tilmann Märk for not only our many fruitful collaborative projects during the last ten years, but also for the kindness and generosity he has shown to me. It has been a privilege to have had the opportunity to work with Tilmann and his colleagues in Innsbruck. I therefore wish to dedicate this presentation to Tilmann on the occasion of his 70th birthday.

1. Background

Two major drift-tube analytical instruments are widely used for trace gas detection in many areas of application, ranging from tree emissions through to breath analysis. These are the ion mobility spectrometer (IMS) and the proton transfer reaction mass spectrometer (PTR-MS). Of the two, PTR-MS is perhaps the more versatile of the two [1,2]. A review of the literature shows that approximately 50% of reported PTR-MS activities involve VOCs (anthropogenic and biogenic) in the environment. Another 30% of publications are associated with food science, while health science accounts for approximately 15% of publications. The remaining 5% of papers deal with a multitude of topics, including homeland security (the focus of this presentation). In contrast to PTR-MS, IMS has been predominantly used for chemical warfare agent and explosive detection [3].

The majority of analytical research has on the whole been the result of individual groups working in their own particular fields, with little communication between them. However, there is considerable synergy and complementarity associated with these applications, as schematically represented in the diagram on the next page. The intention of this diagram is to illustrate that developments made in one area of application could be easily used to great effect in another. For example, the more established atmospheric areas of PTR-MS research could aid the development of the new and emerging area of Homeland Security. Sampling techniques developed for the environmental sciences could potentially find use in homeland security (e.g. thermal desorption).

The historical development of PTR-MS can be traced back to the measurements of the rates of fast ion-molecule reactions in the 1960s and

Fundamental Research & Development
Reliable & reproducible sampling techniques
Improved inlet systems (*e.g.* rapid cycle times)
Analytical techniques and procedures
Calibration, transmission, sensitivity, resolution
Signal processing, analysis techniques, statistical analyses
Mass spectral profiles/fingerprinting
Changing operational parameters (e.g. humidity, *E/N*)
Switching reagent ion
Evaluation and validation of PTR-MS in complex multicomponent environments
Electronic structure calculations
Software development (user friendly interfaces)

Environmental Sciences

Real-World Applications

Homeland Security

Food Science and Technology

Diet & Health
Diet & Disease
Intra- & inter individual differences

Health Science

1970s using flow tube methods. The technology used for measuring the kinetics of these reactions morphed in the middle 1990s into the PTR-MS analytical technique. The seminal work in this area was carried out by Professor Werner Lindinger and his team at the University of Innsbruck. By the time of his untimely death in 2001, Werner and his colleagues had demonstrated the applicability of PTR-MS as an analytical tool for monitoring trace gases in several environments and had established a spin-off company (Ionicon Analytik GmbH) for the commercial exploitation of this novel technology [4]. His legacy was successfully carried forward, developed and expanded by his colleagues in the company, and most notably by Tilmann Märk (the first Chief Executive Officer after Werner Lindinger). Tilmann's creativity, enthusiasm, drive and warmth have significantly contributed to the successful development of PTR-MS and to the success of Ionicon Analytik GmbH. Importantly, Tilmann and colleagues have uniquely combined instrumental development with an active and internationally leading research programme. An important area of recent development is that associated with threat agent detection. This is an area of research that I have had the opportunity of working on with Tilmann and his colleagues.

The aim of this presentation is to review our work on threat agent detection, which ultimately involves an understanding of fundamental ion-molecule processes, the subject of SASP 2014, and highlight how it compares with current research involving IMS-MS.

2. The Detection of Threat Agents

Both PTR-MS and IMS are drift-tube based technologies that can be used for the detection of threat agents. In positive ion mode protonated molecular species are

generally used as reagent ions. There are, of course, differences. IMS relies on pulsing ions into a drift region and then the different arrival times of the ions at the end of the drift region are used to provide selectivity. Furthermore, IMS operates with the drift tube at high pressures (typically one atmosphere) so that protonated water clusters are the dominant reagent ions. Given that the proton affinities of $(H_2O)_n$ clusters ($n > 1$) are greater than that of the H_2O monomer, this limits the range of chemicals that can be detected, which can be beneficial, e.g. for example by eliminating certain VOCs. However, it can equally well lead to limitations. For example, in positive ion mode IMS cannot easily detect solid explosives (TNT, PETN, HMX, etc.) and so for the detection of such compounds an IMS operates in negative ion mode.

IMS is currently the most commonly deployed chemical analysis technology for the detection of threat agents in trace amounts in security areas. Despite its sensitivity and robustness, IMS has certain disadvantages; the most critical is its limited chemical specificity. This can cause false positive signals resulting from the erroneous identification of harmless interferents as a threat agent. The rapid detection of traces of threat agents adhered to people or objects with a high level of confidence (low rate of false positives) in ambient air with a sensitivity that equals or surpasses that of IMS, but has a superior selectivity, requires a new analytical approach. PTR-MS does not only have a comparable if not higher sensitivity, but it also provides a higher selectivity than is possible with IMS and hence a higher confidence in compound assignments. PTR-MS has therefore an as yet untapped potential to support security personnel in detecting threat agents and to identify people who have handled such agents (e.g. through traces on hands, clothing, etc.). The rapid identification of trace quantities of threat agents with a high level of confidence is of great importance to the military and emergency responders, and as well as applications in checkpoint security areas such as airports, harbours and train stations.

In this presentation we will illustrate the capabilities of both IMS and PTR-MS for the rapid detection of a broad range of threat agents (explosives, chemical warfare agents and illicit drugs). One of our most interesting findings to date was the observed dependence of the intensity of protonated TNT as a function of the reduced electric field (the ratio of the electric field, E, and the buffer gas number density, N). (E/N is a key PTR-MS operational parameter defining the collisional energy.) This dependence is illustrated in figure 1 (a) and is compared to that for PETNH[+] shown in figure 1 (b), which shows the more usual behaviour of decreasing protonated ion intensity with increasing E/N. The explanation for the behaviour of TNTH[+] lies in unusual secondary ion-molecule chemistry taking place in the drift tube [5].
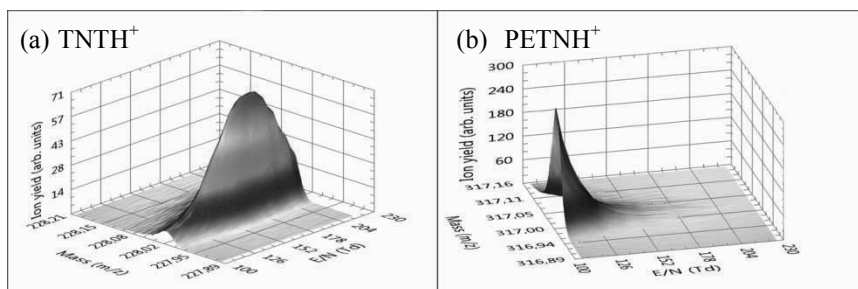
Figure 1: *Ion signal intensities for protonated (a) TNT and (b) PETN as a function of E/N recorded using a PTR TOF-MS instrument.*

In another study we have demonstrated the use of a switchable reagent ion source to improve the PTR-MS instrument's selectivity for the detection of TNT, TNB, PETN and RDX [6]. Selectivity is improved owing to the production of different product ions resulting from changes in the reagent ion-molecule chemistry. Furthermore, we have shown that under the right conditions the switching of the ion chemistry can be rapid (seconds), making PTR-MS an ideal complementary instrument to IMS for use in the world of homeland security.

3. Acknowledgements

References

[1] Blake, R. S., Monks, P. S., Ellis, A. M. (2009) Chem. Rev. 109, 861.
[2] Ellis, A. M. And Mayhew, C. A. (2014) Proton Tanfer reaction Mass Spectrometry, 1st ed.,Wiley.
[3] Eiceman, G.A., Karpas, Z. (2005) Ion Mobility Spectrometry, 2nd ed., Taylor and Francis,Boca Raton FA.
[4] http://www.ionicon.com/
[5] Sulzer, P., Petersson, F., Agarwal, B. et al. (2012) Anal. Chem. 84, 4161.
[6] Sulzer, P., Agarwal, B., Jürschik, S. et al. (2013) Int. J. Mass Spectrom. doi:10.1016/j.ijms.2013.05.004.

Mass Spectrometry and Catalysis Research: A Happy Marriage

Helmut Schwarz, Nicolas Dietl, Maria Schlangen

Institut für Chemie, Technische Universität Berlin, 10623 Berlin (Germany)

We shall present selected examples of gas-phase reactions which are of timely interest for the catalytic activation of small molecules. Due to the very nature of the experiments, detailed insight in the *active site* of catalysts is provided and – in combination with computational chemistry – mechanistic aspects of as well as the elementary steps involved in the making and breaking of chemical bonds are revealed.

Examples to be discussed include *inter alia*: (i) Metal-mediated carbon-carbon bond formation; (ii) low-temperature, catalytic oxidation of CO; (iii) oxygen-centered radicals as active sites in catalytic hydrocarbon activation, e.g. the oxidative coupling of methane $2CH_4 \rightarrow C_2H_6$.

It will be shown that mass-spectrometry based studies on 'isolated' reactive species provide an ideal arena for probing experimentally the energetics and kinetics of a chemical reaction in an unperturbed environment at a strictly molecular level, and thus enable the characterization of crucial intermediates that have previously not been within the reach of conventional condensed-phase techniques [1].

References

[1] For recent review articles, see: (a) M. Schlangen, H. Schwarz, *Catal. Lett.* **2012**, *142*, 1265; (b) N. Dietl, M. Schlangen, H. Schwarz, *Angew. Chem. Int. Ed.* **2012**, *51*, 5544; (c) H. Schwarz, *Angew. Chem. Int. Ed.* **2011**, *50*, 10096; (d) D. K. Bohme, H. Schwarz, *Angew. Chem. Int. Ed.* **2005**, *44*, 2336.

The Method of Increments applied to Adsorption on Surfaces

Beate Paulus

Institut für Chemie und Biochemie, FU Berlin, Takustr. 3, 14195 Berlin

The method of increments [1] for the correlation energy in solids is based on the expansion of the correlation energy in terms of localized orbital groups. Any size-extensive correlation method like coupled cluster can be used for the correlations, the Hartree-Fock treatment is performed for the extended systems. The methods will be used for the determination of highly accurate adsorption energies especially in the case of physisirption, where dispersion effects play an significant role. We have applied the method of increments to the adsorption of small molecules on ionic surfaces [2]. Here I want to present the results for water on graphene [3] and carbon nanotubes as example for a purely van der Waals bound system an compare with dispersion corrected DFT functionals.

References

[1] (a) H. Stoll, Phys. Rev. B 1992, 46, 6700;
    (b) B. Paulus, Phys. Rep. 2006, 428, 1 (review);
    (c) C. Müller, B. Paulus, Phys. Chem. Chem. Phys. 2012, 14, 7605;
[2] (a) C. Müller, B. Herschend, K. Hermansson, B. Paulus, J. Chem. Phys. 2008, 128, 214701.
    (b) C. Müller, K. Hermansson, B. Paulus, Chem. Phys. 2009, 362, 91;
    (c) C. Müller, B. Paulus, K. Hermansson, Surf. Sci. 2009, 603, 2619;
    (d) L. Hammerschmidt, C. Müller, B. Paulus, J. Chem. Phys. 2012, 136, 124117;
[3] (a) K. Rosciszewski, B. Paulus, Int. J. Quantum Chem. 2009, 109, 3055;
    (b) E. Voloshina, D. Usvyat, M. Schütz, Yu. S. Dedkov, and B. Paulus, Phys. Chem. Chem. Phys. 2011, 13, 12041

Bombardment induced ion transport through glasses and polymers: conductivity measurements and diffusion profiles

David Budina, Pramod V. Menezes, Martin Schäfer, Susanne Schulze, Julia Zakel, Karl-Michael Weitzel

Chemistry Department, Philipps-Universität Marburg, Marburg, Germany

Recently, we have reported a new experimental approach for determining the ionic conductivity of a broad range of materials ranging from ion conducting glasses to polymer films [1,2,3]. The approach is based on bombarding the surface of the sample with an alkali ion beam. The adsorption of ions on the sample surface causes a well defined surface potential. The backside of the sample is connected to a grounded metal electrode. The potential gradient and the concentration gradient arising from this adsorption induce ion transport through the sample which is detected as a current on the backside electrode. The conductivity of the sample can be determined by measuring the ion current at the backside electrode as a function of the kinetic energy of the bombarding ions. The technique is termed bombardment induced ion transport (BIIT).

In general the BIIT experiment induces an electro-diffusion profile in the sample, which we are able to analyze by means of ToF-SIMS (time of flight secondary ion mass spectrometry). The entire diffusion profile can be quantitatively described based on a Nernst-Planck-Poisson model both in the case of a glass [4] and of a polymer film [5]. This analysis provides additional information on the space and concentration dependence of diffusion coefficients.

In this contribution we wish to demonstrate the current capabilities and limitations of the technique. As a matter of fact the technique is particularly powerful for extremely small conductivities. In the case of glasses the experiment is capable of addressing the mixed alkali effect by bombarding e.g. a sodium ion conductor with a potassium ion beam. In the case of polymer films employing the correspondingly high ion beam energies we can address the regime of dielectric breakthrough.

References

[1]   M. Schäfer and K.-M. Weitzel, *Physical Chemistry Chemical Physics* **2011**, 13, 20112-20122

[2] P.V. Menezes, J. Martin, M. Schäfer, H. Staesche, B. Roling, and K.-M. Weitzel, *Physical Chemistry Chemical Physics* **2011**, 13, 20123-20128

[3] S. Schulze, J. Zakel, M. Schäfer, A. Greiner, K.-M. Weitzel, *Physical Chemistry Chemical Physics 2013, 15, 1481-1487*

[4] L. Rossrucker, P.V. Menezes, J. Zakel, M. Schäfer, B. Roling, K.-M. Weitzel *Z. Phys. Chem.* **2012**, 226, 341-353

[5] S. Schulze, J. Zakel, M. Schäfer and K.-M. Weitzel, *IEEE-TDEI* **2012**, 19, 1167-1174

Single particle aerosol mass spectrometry

Markus Oster, Matthias Bente-von Frowein, Jürgen Schnelle-Kreis, Ralf Zimmermann

Joint Mass Spectrometry Centre, Cooperation Group Comprehensive Molecular Analytics, Helmholtz Zentrum München, Ingolstädter Landstr. 1, 85764 Neuherberg, Germany

1. Introduction

Laser based mass spectrometry is a convenient method for the on-line analysis of aerosols on single particle level. Thereby, the identification of organic molecules that are of great interest because of their effects on human health is often complicated due to a high degree of fragmentation during the ionization process. To achieve a good identification of these organic compounds, the commonly used one-step laser desorption/ionization can be replaced by a two-step approach. Hereby, particle bound molecules are desorbed either by thermal desorption or by laser desorption in a first step. These volatilized molecules are ionized in a second step with a subsequent laser pulse. The selection of the wavelength and the energy density of the ionization laser can hereby have a large influence on the selectivity of the ionization process.

2. Methods

A differentially pumped inlet system is used to remove the gas phase of an aerosol sample and to generate a particle beam. The particle beam crosses two cw-laser beams and the light they scatter is detected and the time shift between the two scattering events is measured. That provides information about the aerodynamic diameter and velocity of single particles (SP). A CO_2-laser that is triggered according to the individual particle velocimetry is used for laser desorption (LD), and a KrF-excimer laser for resonance-enhanced multiphoton ionisation (REMPI), that is selective for polycyclic aromatic hydrocarbons (PAH). Alternatively, the KrF-laser can also be used for a one-step laser desorption/ionisation, which allows the detection of inorganic compounds but causes fragmentation of organic molecules. Furthermore, laser desorption can be replaced by thermal desorption (TD) by impingement of the particles on a heated metal surface. All three modes (LD-REMPI, TD-REMPI and LDI) can be performed with the same setup by choosing accordant trigger settings for the lasers. The produced ions are detected by means of a bipolar reflectron time-of-flight mass spectrometer (TOF-MS).

3. Results

Several aerosol samples were investigated with the three different modes mentioned above (LDI, LD-REMPI, and TD-REMPI) of a SP-TOFMS. While the LDI-mode mainly provides information on inorganic compounds, the LD-REMPI-mode delivers information on organic compounds, especially on PAH and alkylated PAH. It was also possible to differentiate particles according to their origin by means of the LD-REMPI-technique by their detected PAH patterns. It could be shown, that particles deriving from combustion of hard and soft wood and particles deriving from diesel and gasoline car exhaust, show different PAH patterns. For example retene, a C4-alkylated phenanthrene, (m/z = 234) is a marker for the combustion of coniferous wood. This also allows the source identification of ambient aerosols on a single particle level in some respects. Furthermore, the field capability of the TD-REMPI-SP-TOFMS setup was proven in the scope of a measurement campaign in Augsburg, Germany in winter 2010 with the aim to investigate the impact of wood combustion on ambient aerosol, since thermal desorption is more robust and field suited than laser desorption. The detection of wood combustion related aerosol particles in a size range from ~400 nm to 5 µm was successful with this method. The detection of retene was also successful on several particles, so particles containing retene are dedicated to domestic heating. By analysing the sizing data, it could be shown, that particles containing PAH exhibit a different size distribution than PAH-free particles. The temporal variations of the occurrence of the observed particles indicate, that an important fraction of these particles derive from re-suspension and agglomeration processes in the atmosphere. In future work, the two-step LD-REMPI-mode will be combined with a one-step LDI-process. By means of this method, information of organic (specially PAH and alkylated PAH) and inorganic compounds will be gained on a single particle level.

4. References

[1] Bente, M., Adam, T., Ferge, T., Gallavardin, S., Sklorz, M., Streibel, T., and Zimmermann, R. International Journal of Mass Spectrometry **258**(1-3), 86-94 (2006).
[2] Bente, M., Sklorz, M., Streibel, T., and Zimmermann, R. Analytical Chemistry **80**(23), 8991-9004 (2008).
[3] Bente, M., Sklorz, M., Streibel, T., and Zimmermann, R. Anal. Chem. **81**(7), 2525-2536 (2009).
[4] Oster, M., Elsasser, M., Schnelle-Kreis, J., and Zimmermann, R. Analytical and Bioanalytical Chemistry **401**(10), 3173-3182 (2011).

Novel Studies of Electron-Impact Induced Ionization of Atoms, Molecules and Clusters

Alexander Dorn, Khokon Hossen

Max-Planck-Institut für Kernphysik, Saupfercheckweg 1, 69117 Heidelberg, Germany

Xueguang Ren, Thomas Pflüger, Marvin Weyland

Physikalisch-Technische Bundesanstalt, Bundesallee 100, 38116 Braunschweig, Germany

In kinematically complete experiments on electron impact ionization the momentum vectors of all particles in the initial and final collision state fixed. Therefore, such studies give detailed insight into the scattering process and can be used to critically test ab-initio calculations, e.g. for the ionization of atoms [1]. For more complex targets like molecules and clusters the momentum vectors of ionic fragments yields information on reaction channels and for linear molecules on their spatial alignment. Using the experimental technique of the reaction microscope such multi-particle coincidence experiments become feasible due to its high detection efficiency covering essentially the complete solid angle for electrons and ions.

In Figure 1 a schematic view of the reaction microscope is shown. Charged particles produced in the overlap region of a pulsed electron beam and a supersonic gas jet are extracted by means of homogenous electric and magnetic fields and projected onto time and position sensitive detectors. The data for each collision event are stored and evaluated in an offline analysis in order to determine the particle momentum vectors and the cross sections of interest.

Here results of a few exemplary studies for targets of increasing size will be presented: For ionization of H_2 a strong dependence of the collision dynamics on the spatial alignment of the target molecules is observed. Low energetic ionized electrons are predominantly emitted along the molecular axis [2].
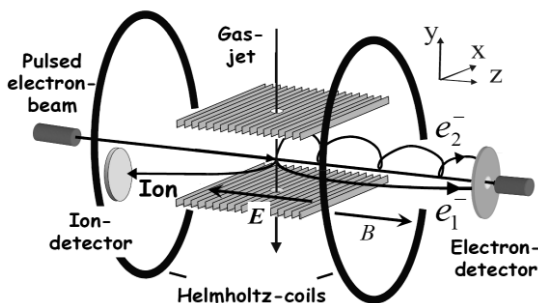
Figure 1*: The reaction microscope*

Collisions involving small noble gas clusters reveal multiple scattering processes and various cluster dissociation mechanisms [3].

For more complex molecules like CH_4 we demonstrate how the detailed knowledge on the kinematics of the final state particles allows disentangling the molecular states involved in the dissociation process [4].

Finally, future experiments on the ionization of biologically relevant molecules by low energy electrons ($E_0 < 20$ eV) will be discussed.

References

[1] Th. Pflüger, O. Zatsarinny, K. Bartschat, A. Senftleben, X. Ren, J. Ullrich, and Alexander Dorn, Phys. Rev. Lett. **110**, 153202

[2] X. Ren, T. Pflüger, S. Xu, J. Colgan, M. S. Pindzola, A. Senftleben, J. Ullrich, and A. Dorn, Phys. Rev. Lett. **109**, 123202

[3] Thomas Pflüger, Arne Senftleben, Xueguang Ren, Alexander Dorn, and Joachim Ullrich, Phys. Rev. Lett. **107**, 223201

[4] Sh. Xu , X. Ma , X. Ren , A. Senftleben , Th. Pflüger , Sh. Yan, P. Zhang , J. Yang , J. Ullrich and A. Dorn, J. Chem. Phys. **138,** 134307 (2013)

Velocity Slice Imaging in Dissociative Electron Attachment studies

Oddur Ingólfsson and Frímann H. Ómarsson
Department of Chemistry and Science Institute, University of Iceland, Dunhaga 3, 107 Reykjavík, Iceland

Ewelina Szymanska, Nigel J. Mason
Department of Physical Sciences, The Open University, Walton Hall, MK7 6AA, Milton Keynes, UK

E. Krishnakumar
Tata Institute of Fundamental Research, Homi Bhabha Road, Colaba, Mumbai 400005, India

Velocity slice imaging is discussed in context to dissociative electron attachment of CF_4, CF_3Cl and CF_3I, the underlying resonances and the energetics and dynamics of the formation of selected fragments.

Introduction

In the last decades the importance of Dissociative Electron Attachment (DEA) processes in a variety of industrial processing techniques as well as in naturally occurring phenomenon has become increasingly clear. These include plasma-processing and plasma based devices, nano-technological writing methods, such as Focused Electron Beam Induced Processing (FEBIP), [1,2] and biologically relevant processes such as radiation damage to biologically important molecules. [3] In this context the importance of a deeper understanding of the physics, energetics and dynamics behind these processes has become increasingly clear.

Conventionally, gas phase DEA experiments are mainly conducted in crossed-beam experiments where target molecules are exposed to a quasi-monochromatic low energy electron beam and the negative ion yield is recorded in dependency of the electron energy. Such experiments reveal branching ratios, and in some cases absolute cross sections for fragment ion formation and also give a fair picture of the energy associated with the underlying negative ion resonances. Quantum chemical calculations and comparison with other scattering and photo-excitation experiments, often allow for the deduction of the nature of the underlying resonances, the composition of the neutral fragments and the dissociation dynamics.

Velocity Slice Imaging is a powerful technique that has recent found application in Dissociative Electron Attachment (DEA) studies, and has proven valuable in accessing information on DEA processes that is not accessible with conventional experimental methods.[4-6] In this contribution we present VSI-DEA data for selected fragments from CF_4, [5] CF_3Cl [6] and CF_3I as examples of such processes.

Experimental

The current VSI-DEA instrument, was constructed by E Krisnakumar (TIFR, India) in collaboration with N. J Mason at the Open University, UK. It consists of crossed electron and molecular beams and a detection system composed of a time of flight (ToF) mass spectrometer with a position sensitive detector. The electron beam is pulsed with an on-time of 200 ns, in which the initial negative ions are formed. The electron pulse is then followed by a time delay of about 200 ns, in which the kinetic energy release in the respective DEA processes leads to spatial expansion of the fragments formed, i.e., the formation of a Newton sphere that reflects the angular distribution of the fragments, and their kinetic energy. The Newton sphere of the anions formed is then extracted in to the ToF and detected on a position sensitive detector consisting of a Z stack of three 75 mm micro channel plates, and a phosphorous screen. By timing of the detector pulse, the central slice of the Newton sphere of the anionic fragments can be obtained and thus their kinetic energy and angular distribution. Figure 1 shows an example of such distributions recorded for the F^- and CF_3^- ion yield from CF_4 at two different incident electron energies for each fragment [5].
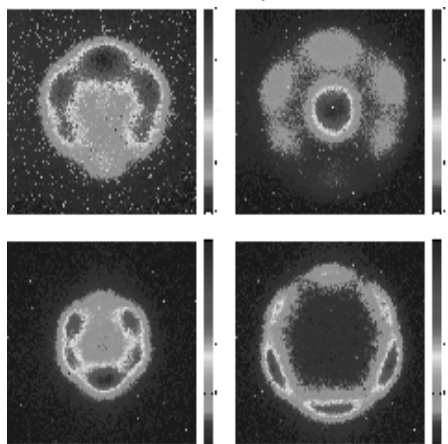
Note, that by using this method the angular distribution of the negative fragment ions can be obtained simultaneously over the whole (0-360°) angular range, without any reconstructing algorithms like inverse Abel transformation and at the same time the kinetic energy can be measured.

To obtain information on the symmetry of the resonances the angular distribution can be fitted with a polyatomic extension [7] of the diatomic model proposed by O'Malley and Taylor [8].

Figure 1: *Velocity Slice Images of F^- (upper) at 5.5 eV (left) and 7.5 eV (right) and of CF_3^- (lower) at 5.5 eV (left) and 8.5 eV (right). The electron beam traverses downwards and through the center of each figure. Adapted from ref. [5].*

VSI of selected DEA fragments from CF$_4$, CF$_3$Cl and CF$_3$I

Here we describe VSI experiments on the halogenated methane derivatives CF$_4$ [5] CF$_3$Cl [6] and CF$_3$I and we show that in each of these cases the VSI technique allows for insight in to the DEA processes that would not be accessible with conventional methods.

Tetrafluoromethane, CF$_4$ is a tetrahedral molecule that falls within the T$_d$ symmetry group while the expected elongation of one of the C−F bonds in the DEA process should lead to a temporary negative ion (TNI) of C$_{3v}$ symmetry. This is reflected in the angular distribution observed [5], which we find only adequately described through linear combination of both the target and product state, and we argue that the DEA process needs to be described as a quantum superposition of both these sates. Hence, both the T$_d$ symmetry of the target and the C$_{3v}$ symmetry of the product temporary negative ion must be accounted for to describe this reactive scattering process. Furthermore, the strong coupling of the electronic and nuclear kinetic energy in this highly symmetric molecule is reflected in the total kinetic energy release (KER), upon DEA. This is especially clear in the KER in the CF$_3^-$ formation where two distinct processes are observed. We attribute these to a geometrical relaxation of this fragment in the DEA process, at incident electron energies below the threshold of the ion formation, and the formation of a geometrically restrained fragment when the electron energy is sufficiently high and the energy release through the adiabatic electron affinity of the relaxed ion is not necessary to enable the process.

Trifluorochloromethane, CF$_3$Cl is another example where VSI reviles features in the electron attachment process that are not accessible in conventional experimental setups [6]. This is most noticeably for the F$^-$ formation, which appears in the DEA ion yield through one broad contribution centered around 4 eV. In this case the velocity slice images revile two distinct components, one with high KER and the second with close to thermal kinetic energy distribution. Hence this contribution is composed of two distinct resonances not distinguishable in conventional DEA experiments [9, 10]. While the angular distribution of the high KER F$^-$ ions agrees well with a shape resonance of A$_1$ symmetry where the incoming electron is trapped into the low-lying a$_1$(C-F σ*) orbital. The low KER through the second resonance, however, does not allow us to acquire the angular distribution associated with this resonance.

Trifluoroiodomethane; CF$_3$I, is another example where the VSI reveals features that are not accessible in conventional DEA experiments. For this molecule it is well established that the CF$_3^-$ formation is associated with exceptionally high KER [11]. This is also clear from the expansion of the Newtons sphere in the velocity slice

images of this fragment. However, in the velocity slice images a low KER component is also clearly visible, indicating that two different processes are responsible for the CF_3^- production in this range. Our current analyses of these data lead us to propose that the high KER channel in this case is associated the ground state if the neutral iodine $^2I_{2/3}$ as the complementary fragment to CF_3^-, while the low KER component is associated with the excited state $^2I_{1/2}$. Hence, the data on the kinetic energy of the CF_3^- ions, and thus the KER in this dissociation process, reviles information on the electronic state of the neutral counterpart.

Acknowledgements

References

[1] I. Utke, P. Hoffmann and J. Melngailis, J. Vac. Sci. Technol. B, 2008, 26, 1197–1276.
[2] W. F. Van Dorp and C. W. Hagen, Journal of Applied Physics, 2008, 104, 081301–081301–42.
[3] I. Baccarelli, I. Bald, F.A. Gianturco, E. Illenberger, J. Kopyra, Phys. Rep. 508 (2011) 1.
[4] D. Nandi, V. S. Prabhudesai, E. Krishnakumar, and A. Chatterjee, Rev. Sci. Instrum., 76 053107, (2005)
[5] F. H. Ómarsson, E. Szymanska, N. J. Mason, E. Krishnakumar, O. Ingólfsson, Submitted (2013)
[6] F. H. Ómarsson, O. Ingólfsson, N. J. Mason, E. Krishnakumar, Eur. Phys. J. D., 66, 12, (2012).
[7] R. Azria, Y. Le Coat, G. Lefevre, and D. Simon, J. Phys B: At. Mol. Phys., 12, 1–10, (1979).
[8] T. F. O'Malley and H. S. Taylor, Phys. Rev, 176, 1–15, (1968)
[9] E. Illenberger, H.U. Scheunemann, H. Baumgärtel, Chem. Phys. 37(1), 21 (1979)
[10] E. Illenberger, Chem. Phys. Lett. 80(1), 153 (1981)
[11] T. Oster, O. Ingólfsson, M. Meinke and E. Illenberger J. Chem. Phys, 99(7) 5141 (1993).

Transient Anion States of 5-Halouracils

Fábris Kossoski and Márcio T. do N. Varella
*Instituto de Física, Universidade de São Paulo, CP 66318, 05314-970,
São Paulo, SP, Brazil*

Márcio H. F. Bettega
*Departamento de Física, Universidade Federal do Paraná, CP 19044, 81531-990,
Curitiba, PR, Brazil*

The radiosensitizing activity of 5-halouracils have long been known [1]. These halogenated molecules replace thymine units in DNA and increase the sensitivity to ionizing and UV radiation [2]. Theses properties would arise, at least in part, from efficient mechanisms for dissociative electron attachment (DEA). It is well-known that free electrons are the most abundant secondary species generated by ionizing radiation in the biological matter, and the formation of transient negative ion (TNI) states often give rise to dissociative processes that may damage the DNA and other biomolecules. In halo-uracils, the substituents are heavy atoms with high electron affinities and polarisabilities that tend to stabilize the TNI's, thus allowing for significant vibrational relaxation.
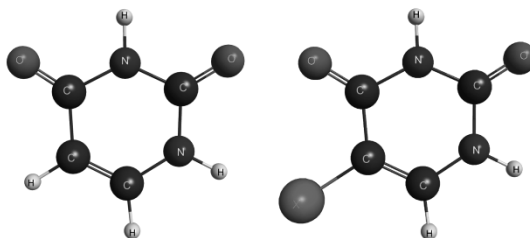
Figure 1: *Geometrical structures of uracil (left) and 5-X-uracils (right), where the halogen atom (X=F, Cl, Br, I) is indicated in green.*

In spite of their importance, the literature on electron interactions with halouracils is relatively scarce, especially on the theory side. In this work, we report on the shape resonance spectra of 5-X-uracils (X=F, Cl, Br, I), as obtained from elastic scattering calculations. Shape resonances are TNI's formed by electron attachment to vacant virtual orbitals of the molecular ground state (core-excited anion states are not accounted for). The scattering calculations were performed with the parallel version of the Schwinger Multichannel Method implemented with Pseudopotentials (SMCPP) [3] and indicate a rich spectrum of π^* resonances and π^* bound anion

states, as well as σ* states arising from the C_5–X bonds (see Fig. 1). We also survey the potential energy surfaces of the bound states of these molecular anions employing standard electronic structure techniques, namely density functional theory (DFT) with the hybrid B3LYP correlation-exchange functional.

The calculated resonance spectra are in good agreement in the available electron transmission (ET) data for the 5-halouracils [4] (although, to our present knowledge, no calculated scattering cross sections have been reported for the 5-halouracils, our results for uracil are in agreement with the available calculations). While our DFT results are also consistent with those reported by Li *et al*. [5], we further explore the potential surfaces of the valence bound states. While we have not performed dynamics simulations, both the present scattering and bound-state calculations are compatible with the very rich DEA data [6] that points out a complex branching of the dissociation cross section.

Acknowledgments

References
[1] S. Zamenhof, R. Degiovanni, and S. Greer, Nature **81**, 827 (1958).

[2] H. Abdoul-Carime, M. A. Huels, E. Illernberger, and L. Sanche, J. Am. Chem. Soc. **123**, 5354 (2001).

[3] M. H. F. Bettega, L. G. Ferreira, and M. A. P. Lima, Phys. Rev. A **47**, 1111 (1993); J. S. dos Santos, R. F. da Costa, and M. T. do N. Varella, J. Chem. Phys. **136**, 084307 (2012).

[4] A. Scheer, K. Aflatooni, G. Gallup, and P. Burrow, Phys. Rev. Lett. **92**, 068102 (2004).

[5] X. Li, L. Sanche, and M. D. Sevilla, J. Phys. Chem. A **106**, 11248 (2002).

[6] S. Denifl, S. Matejcik, B. Gstir, G. Hanel, M. Probst, P. Scheier, and T. D. Märk, J. Chem. Phys. **118**, 4107 (2003).

Application of Ion-Molecule-Reactions for Atmospheric Composition Research

Armin Wisthaler
Department of Chemistry, University of Oslo, Norway

The Earth's atmosphere is mainly composed of nitrogen, oxygen, argon and water vapor. In addition, it contains inorganic trace gases and a myriad of organic trace gases that are either directly emitted from biogenic and anthropogenic sources or formed in atmospheric chemical reactions. Organic trace gases have been detected in the Earth's atmosphere at ppq-to-ppm (10^{-15} to 10^{-6} v/v) levels and many of them have been linked to climate change, air quality deterioration and human health effects. Organic trace gases affect the Earth's radiative budget; they alter photochemical oxidant levels in the atmosphere and influence the formation, growth and properties of aerosol particles.

The huge number and complexity of organic trace gases in the atmosphere, their reactivity and low abundances pose a great challenge to the environmental analytical chemist. Chromatography is still the method of choice for many applications but the analysis is slow and often prone to artifacts. Based on the initial work by F. Arnold in the 1980ies, on-line chemical ionization mass spectrometry (CIMS) has become an important analytical tool for real-time detection of organic trace gases in the atmosphere. On-line CIMS relies on direct and continuous sample injection into an ion source, trace gas ionization via ion-molecule reactions and mass spectrometric detection of diagnostic ions that preserve the compositional information of the neutral analyte molecules (e.g. protonated analyte ions or ion-analyte adducts).

The currently most widely used on-line CIMS instrument in atmospheric composition research is the proton-transfer-reaction mass spectrometer (PTR-MS) which was originally conceived in W. Lindinger's group in Innsbruck in the mid-1990ies. Recent years have, however, seen the emergence of a series of innovative on-line CIMS methods and instruments that have led to the discovery of previously undetected trace gas species in the atmosphere. In my talk, I will review the state-of-the-art of atmospheric organic trace gas detection by on-line CIMS and demonstrate how ion-molecule reactions are currently used for analytical purposes in atmospheric composition research.

Reactivity in electronically excited and ionized biomolecules and clusters

M. Ryszka, B. Barc, R. Pandey, M. Dampc, <u>S. Eden</u>
Department of Physical Sciences, The Open University, Milton Keynes, MK7 6AA,
United Kingdom

Radiation induced processes in nucleobases have been investigated intensively in recent years in order to better understand the fundamental processes that can initiate DNA and RNA lesions [1]. Further interest relates to the mechanisms underpinning the remarkable photo-stability of DNA bases and their possible evolutionary implications. While studies of isolated molecules generally provide the clearest data interpretations, equivalent measurements on hydrogen-bonded complexes enable closer analogies to be drawn with biological environments where different isomeric forms, excited state dynamics, energy dissipation processes, and (unimolecular or intermolecular) reactive pathways can be significant.
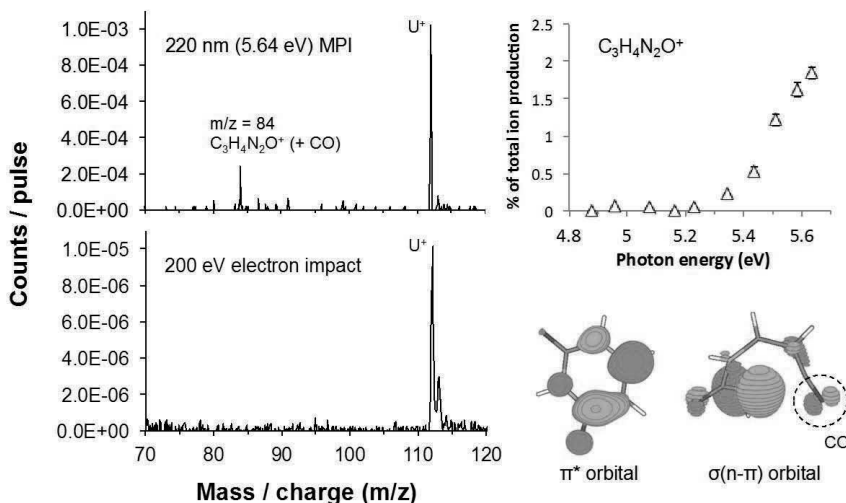
Figure 1: *(Left) Comparison of MPI (220 nm, 6×10^7 Wcm^{-2}) and EI (200 eV) mass spectra or uracil [2]. (Top right) Photon energy dependence of $C_3H_4N_2O^+$ production as a percentage of the total signal for uracil MPI [2]. (Bottom right) Two orbitals [3] involved in the ring-opening excitation that we associate with $C_3H_4N_2O^+$ production (the CO group that we expect to be abstracted is circled).*

By comparing dissociative ionization by electron impact (EI) and UV multi-photon ionization (MPI) of isolated and clustered nucleobases, we have obtained evidence indicating isomeric transitions in neutral electronic excited states. In particular, a new fragment ion ($C_3H_4N_2O^+$) has been observed from gas-phase uracil by single-color 2-photon absorption at photon energies below 5.29 ± 0.06 eV (see Fig. 1 for MPI and EI mass spectra as well as the MPI photon energy dependence for $C_3H_4N_2O^+$ production) [2]. This channel is not activated by EI and the threshold agrees closely with the minimum calculated activation energy (5.25 eV, CASSCF) for a ring opening conical intersection from the lowest-lying $^1\pi\pi^*$ state to a $^1\sigma(n-\pi)\pi^*$ closed shell state [3]. Moreover, the predicted ring opening transition leaves a CO group at one end of the isomer (see Fig. 1 for the optimized geometry of the $\sigma(n-\pi)$ orbital), apparently vulnerable to abstraction. Further results include identifying $C_3H_3NO^+$ production via metastable dissociation of the uracil radical cation (1.3-13 μs after ionization) and detecting neutral CO fragments.
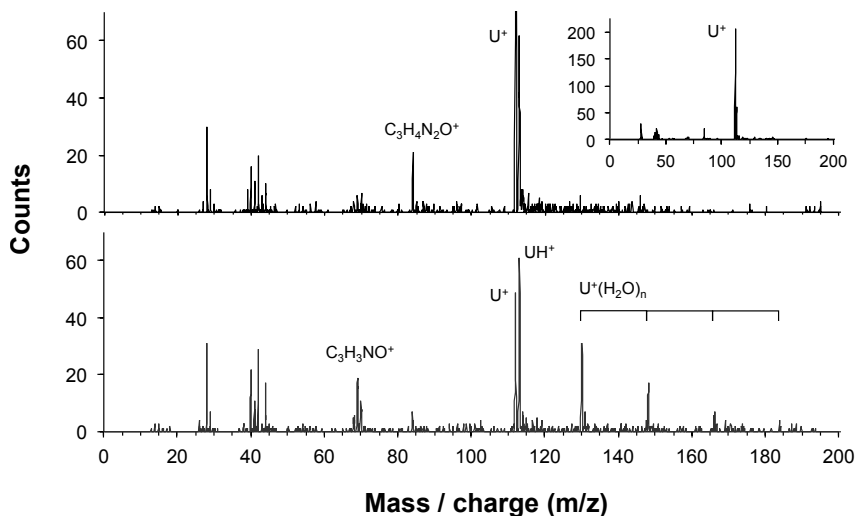
Figure 2: *MPI (220 nm, 4×10^6 Wcm^{-2}) of uracil in dry (upper plot and inset) and hydrated conditions (lower plot).*

EI and MPI mass spectra of nucleobase-water clusters have been compared with equivalent dry measurements to assess hydrogen-bonding effects on dissociative ionization. In general, increased production of relatively large fragment ions (e.g. $C_3H_3NO^+$ from uracil – see Fig. 2) due to hydration can attributed to energy dissipation via cluster dissociation limiting sequential dissociation processes.

However, hydration suppresses the $C_3H_4N_2O^+$ channel highlighted above, indicating a different process by which the hydrogen-bonded environment stabilizes uracil with respect to excited state ring opening [3]. The result may be due to the presence of hydrogen-bonded water moieties decoupling the excited states involved in the ring-opening conical intersection associated with this dissociative MPI channel.
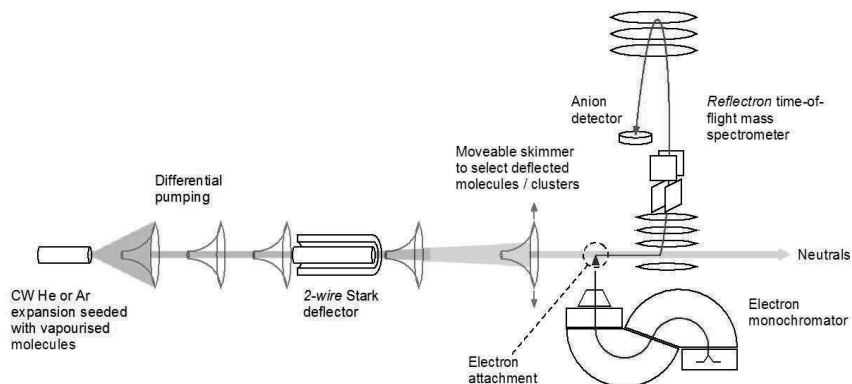
Figure 3: *Experiment to probe electron attachment to selected clusters.*

A major challenge in analyzing radiation-induced processes in clusters is the broad distribution of sizes and configurations produced by supersonic expansion sources (or alternative cluster sources, for example utilizing laser ablation). The last part of the talk will report progress in the development of a new experiment to analyze low energy electron interactions with selected neutral isomers and clusters (Fig. 3) [4]. This exploits a Stark deflection system developed by Küpper and co-workers at DESY. They have recently applied the method to separate singly hydrated indole from momomers and larger clusters in a mixed beam [5].

References

[1] C. T. Middleton, K. de La Harpe, C. Su, Y. K. Law, C. E. Crespo- Hernandez, B. Kohler, Annu. Rev. Phys. Chem., 2009, 60, 217.

[2] B. Barc, M. Ryszka, J. Spurrell, M. Dampc, P. Limão-Vieira, R. Parajuli, N.J. Mason, S. Eden, J. Chem. Phys., 2013, 139, 244311.

[3] D. Nachtigallova, A. J. A. Aquino, J. J. Szymczak, M. Barbatti, P. Hobza, H. Lischka, J. Phys. Chem. A, 2011, 115, 5247.

[4] S. Eden, EPSRC CAF project EP/J002577/1

[5] S. Trippel, Y-P. Chang, S. Stern, T. Mullins, L. Holmegaard, J. Küpper, Phys. Rev. A, 2012, 86, 033202.

Prospects and limitations of electronic spectroscopy in superfluid helium nano droplets

Alkwin Slenczka

Institut für Physikalische und Theoretische Chemie, Universität Regensburg, 93040 Regensburg, Germany

Molecular spectroscopy in superfluid helium nanodroplets has become a widely recognized technique to prepare and study molecules and molecular aggregates at low temperatures [1]. Compared to "classical" host systems such as solid matrices, helium droplets have been shown to exhibit greatly reduced inhomogeneity and to allow for free rotation [2]. This is a consequence of the quantum nature of superfluid helium. From the very beginning the experimental data favoured a dopant species to be surrounded by a non-superfluid helium solvation layer in order to explain helium induced spectroscopic features [3]. While experimental results provide much evidence for this model one might think of alternative explanations. We present a critical review of our own work on electronic spectroscopy which includes spectroscopy of molecules, molecular aggregates and photochemical reactions. As a result the electronic degree of freedom appears to be a key quantity which is responsible for many of the helium induced features observed in electronic spectra. This may be of consequence for further experimental and theoretical activities.

References

[1] J. P. Toennies, A. F. Vilesov, Angew. Chem. Int. Ed. (2004).
[2] M. Hartmann, R. E. Miller, J. P. Toennies, A. F. Vilesov, Science **272**, 1631 (1996).
[3]   M. Hartmann, A. Lindinger, J.P. Toennies, A.F. Vilesov, Chem. Phys. **239**, 139 (1998).

Dynamics of molecules and clusters in helium droplets

Wolfgang E. Ernst

Institute of Experimental Physics, Graz University of Technology, Petersgasse 16, A-8010 Graz, Austria

1. Introduction

Droplets of about 10^4 helium atoms (He_N) represent a nanometer-sized superfluid medium of 0.4 K temperature and the least interacting matrix material for molecular spectroscopy. They can be doped with one or several atoms or molecules that move freely in or on the droplets and may form complexes in this cold environment. Very weakly bound species and even unusual conformers are observed and can be investigated with any method that is commonly applied to molecular beams: laser spectroscopy and ionization, mass spectrometry, spin resonance, measurements in external electric or magnetic fields [1].

Although the dopant-helium interaction is very weak, the influence of the quantum solvent helium may alter relaxation pathways after electronic excitation or barrier heights towards dopant aggregation. In the following, three examples from our recent work on metal doped helium droplets will be discussed.

2. Formation of cold alkali-alkaline earth molecules

While most atomic or molecular dopants are localized in the center of a helium droplet, alkali and some alkaline earth species remain at the droplet surface due to their very weak He-dopant binding potential [1]. A large difference in the respective solvation energies for different dopants can even give rise to a potential barrier against the reaction between two dopants as we have recently shown for the van der Waals interaction between heliophilic rare gas and heliophobic alkali dopants [2]. In contrast, two heliophobic dopants like one alkali (Ak) and one alkaline earth (Ake) atom can very well form a diatomic molecule on the droplet surface. Ak-Ake molecules have attracted considerable attention as candidates for the formation of ultracold molecules with a magnetic and an electronic dipole moment. In order to explore this interesting group of molecules, we recently recorded laser excitation spectra of LiCa [3] and RbSr on helium droplets. Our own quantum chemistry calculations allowed the assignment of 6 electronic band systems [3].
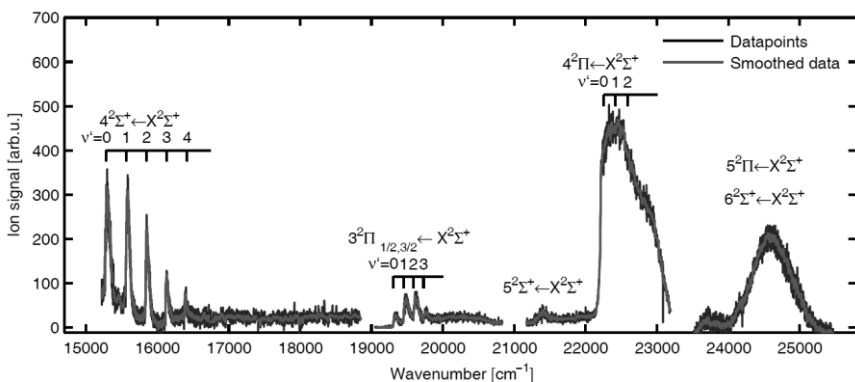
Figure 1: *Excitation spectrum of LiCa on He$_N$ as recorded by REMPI-TOF spectroscopy*

3. Chromium in helium droplets:
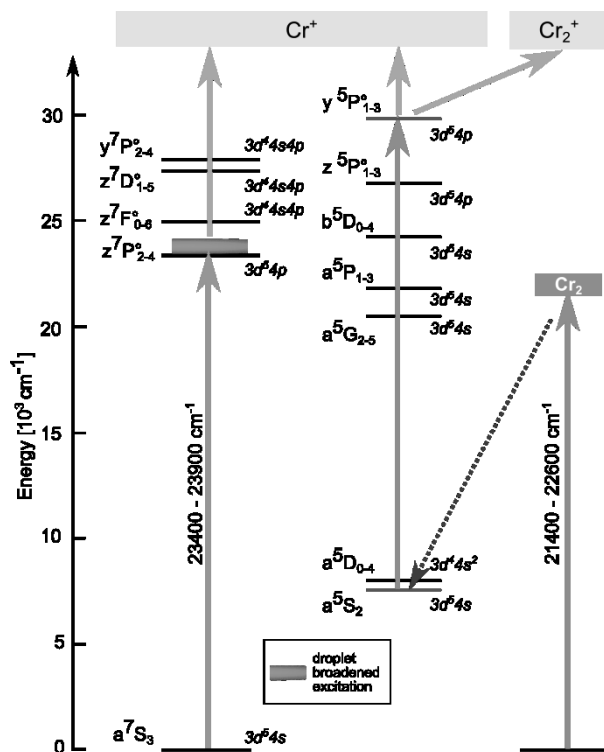
Figure 2:
Energy level scheme for septet and quintet states of Cr that are accessed by resonant two photon ionization spectroscopy of Cr-He$_N$ and the excitation of a predissociating Cr$_2$ system in He$_N$ with subsequent atomic Cr quintet state excitation and ionization.

In contrast to the surface located Ak and Ake species, transition metals like chromium show a much more complex behaviour when placed on a helium droplet and excited by lasers. In its ground state, the Cr atom is localized in the center of the droplet while different electronically excited states exhibit different solvation energies in helium which gives rise to complex relaxation patterns after laser excitation: Among these, septet-quintet transitions and expulsion of Cr from the droplet after electronic excitation were observed [4, 5]. Laser excitation of Cr_2 in He_N around 22000 cm^{-1} results in predissociation whereupon the Cr quintet state dissociation products could be further excited in the droplet and recombined as observed in the resulting mass spectra [6].

4. Silver clusters formed in helium droplets followed by surface deposition
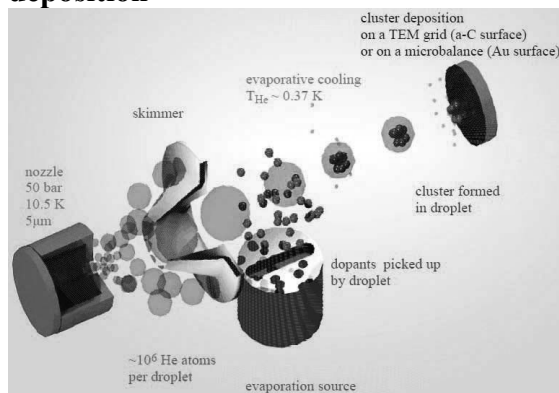
Figure 3:
Experimental scheme for the doping of large He_N ($N \approx 10^6$) with metal atoms that form cold clusters in He_N and are deposited on a solid surface.
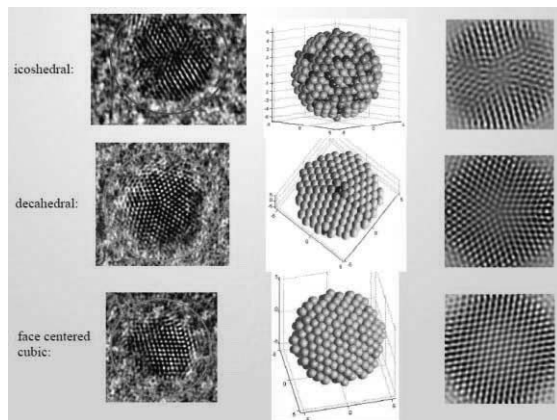
Figure 4:
Silver clusters of 2 to 5 nm diameter formed in He droplets and deposited on an amorphous carbon substrate: left column – TEM images, center column – calculated 3D-morphology, right column – TEM simulations for calc. morphologies.

Clusters and nanoparticles of transition or coinage metals can be formed inside large helium droplets by employing an electron bombardment oven for evaporating high temperature metals [7]. Silver clusters of 500 to 3000 atoms were produced this way, deposited on amorphous carbon substrates and analyzed by transmission electron microscopy. The results were compared to morphologies obtained by molecular dynamics simulations and indicate that the metal clusters experience a rather soft landing on the substrate "cushioned" by the evaporating helium surroundings [8].

References

[1] "Helium Droplets as Nanocryostats for Molecular Spectroscopy—from the Vacuum Ultraviolet to the Microwave Regime" by C. Callegari and W. E. Ernst in: *Handbook of High Resolution Spectroscopy*, Eds. F. Merkt and M. Quack, 1st Edition, Vol. 3, p. 1551-1594, ISBN-10: 0-470-06653-9, ISBN-13: 978-0-470-06653-9 - John Wiley & Sons, Chichester, 2011.

[2] J. Poms, A. W. Hauser, and W. E. Ernst, PCCP **14**, 15158-15165 (2012), *DOI: 10.1039/c2cp42333b*.

[3] G. Krois, J. V. Pototschnig, F. Lackner, and W. E. Ernst, J. Phys. Chem. A 2013 online, *DOI: 10.1021/jp407818k* (Festschrift in honor of Terry Miller).

[4] A. Kautsch, M. Hasewend, M. Koch, and W. E. Ernst, Phys. Rev. A **86**, 033428-1-4 (2012).

[5] A. Kautsch, M. Koch, and W. E. Ernst, J. Phys. Chem. A**117**, 9621-9625 (2013), *DOI: 10.1021/jp312336m* (Festschrift in honor of Takeshi Oka).

[6] A. Kautsch, F. Lindebner, M. Koch, and W. E. Ernst, manuscript in prep.

[7] M. Ratschek, M. Koch, and W. E. Ernst, J. Chem. Phys. **136**, 104201-1-6 (2012).

[8] A. Volk, P. Thaler, M. Koch, E. Fisslthaler, W. Grogger, and W. E. Ernst, J. Chem. Phys. **138**, 214312-1-7 (2013).

Cluster size dependence of vibrational frequency shifts of small molecular ions inside helium clusters

Marius Lewerenz and Mirjana Mladenović

Laboratoire MSME, UMR 8208 CNRS, Université Paris Est,
5, Blvd. Descartes, 77454 Marne la Vallée Cedex 2, France

1. Introduction

Since its introduction about twenty years ago, helium nano droplet isolation spectroscopy (HENDI) has evolved into an almost routinely applied and very versatile variant of matrix isolation spectroscopy. As opposed to other matrix techniques, spectra of molecules embedded into the cold (< 0.5 K) quantum liquid helium clusters usually exhibit resolved rotational structure. The weakness of the helium-molecule interaction ensures that vibrational band origins are only slightly shifted relative to the free molecule situation. Most spectroscopic data were obtained for large helium clusters (10^3 – 10^5 atoms) with broad size distributions. Helium cluster size resolved infrared or microwave spectra have been observed only for a very limited number of systems like OCS@He$_n$ [1] and CO@He$_n$ [2]. The low temperature conditions lead to compact rotation-vibration bands which typically cover only about 1 cm^{-1} such that bands arising from different simultaneously present cluster sizes can be sufficiently well separated to allow their assignment. Size assignment is vastly simplified for charged species by standard ion mass selection techniques such that size specific spectra can be measured. In spite of the low number densities achievable for ions, high resolution spectra have been observed by sensitive depletion techniques [3,4] which exploit the predissociation of the weakly bound complexes following vibrational or electronic excitation. Even though the existence of stable complexes between helium atoms and diverse molecular ions is well known from the mass spectra routinely recorded in experiments on neutral precursors only N_2^+He$_n$ and OH$^+$He have been spectroscopically characterised. The observed ion yield distributions often exhibit distinct stability patterns.

We identified the systems CO$^+$He$_n$ and OH$^+$He$_n$ as excellent candidates for a theoretical exploration of their intermolecular potential [5] and the prediction of their structure, stability, and vibrational properties. He-CO$^+$ is also an interesting astrophysical collision system.

2. Computational methods

We performed (R)CCSD(T) calculations with large diffuse basis Dunning type basis sets to construct accurate potential surfaces for the interaction between helium atoms and the diatomic molecular ions CO^+, NO^+, and OH^+. The ab initio interaction energies were converted into analytical two- or three-dimensional representations. The two-dimensional representations for the CO^+He and NO^+He potentials V(R, ϑ ;v) depend explicitly on intermolecular Jacobi coordinates R and ϑ and parametrically on the diatomic vibrational quantum number v and were obtained by computing the interaction energies for a large grid of R and ϑ values with the diatomic distance frozen at its expectation value in a given vibrational state. The strong proton affinity of rare gases requires a more advanced treatment for OH^+He: The adiabatic two-dimensional surface V(R, ϑ ;v) is constructed from the original full three-dimensional surface by solving the intramolecular OH vibrational problem for each (R, ϑ) cut and adding the (R, ϑ)-dependent vibrational term in state v to the electronic minimum [6]. These surfaces are used to construct many body models including the He-He dispersion interaction and additional induction terms. We solve the vibrational many body problem with a special version of diffusion quantum Monte Carlo (DMC) technique which allows rigid body constraints [7] to predict the cohesive energies, quantum averaged structures and size dependent vibrational frequency shifts of these species. For the triatomic clusters we also employ a discrete variable approach using an exact expression for the kinetic energy operator to compute rovibrational states.

3. Results

For CO^+He we find an electronically bent minimum energy arrangement with a Jacobi angle near 45°, a electronic binding energy of 275 cm^{-1} and a barrier to linearity of about 60 cm^{-1}. The ground state vibrational wave function shows significant floppiness and a noticeable amplitude for the linear particle arrangement. Our rovibrational calculations for CO^+He show this triatomic complex to belong to the class of quasi linear molecules [5]. Our DMC calculations for CO^+He_n clusters with n up to 50 yield a stability pattern with magic numbers at n=6, 8, and 11 and closure of a first shell of helium atoms around the CO^+ ion at n=14 (see Fig. 1). We predict a blue shift reaching a peak value of about 2.7 cm^{-1} at the magic number n=11, then dropping to about 2 cm^{-1}, and passing through another weak maximum near n=20 before reaching about 1.8 cm^{-1} for the largest clusters.
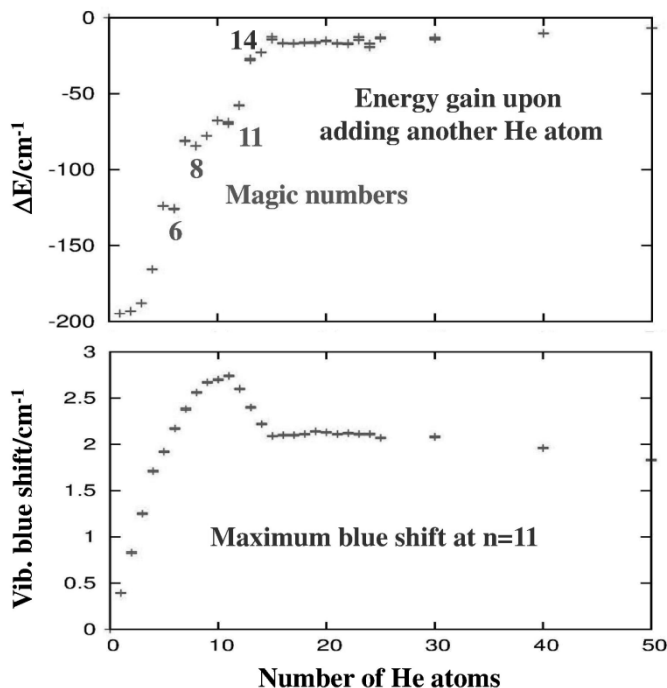
Figure 1: *Incremental binding energy and vibrational frequency shift for* CO^+He_n *clusters*

The OH^+He triatomic complex has a relatively rigid linear structure with an electronic interaction energy of 690 cm⁻¹. This value increases to 750 and 894 cm⁻¹ for the adiabatic v=0 and v=1 surfaces, indicating a very pronounced red shift of the OH vibration. The tightening of the complex upon OH vibrational excitation also affects the intermolecular zero point energy which partially compensates the deepening of the surface such that the final prediction of the n=1 frequency shift is 64 cm⁻¹, very close to the experimental value of 66 cm⁻¹ [3], see Fig. 2. We find a magic number at n=12 indicating shell closure which coincides with a minimum of the size dependent red shift of 34 cm⁻¹. This reduction of the red shift is related to a blue shifting effect of helium atoms located on the O side of OH^+. The onset of a second helium shell leads to an initial slight rebound of the frequency shift before receding again.
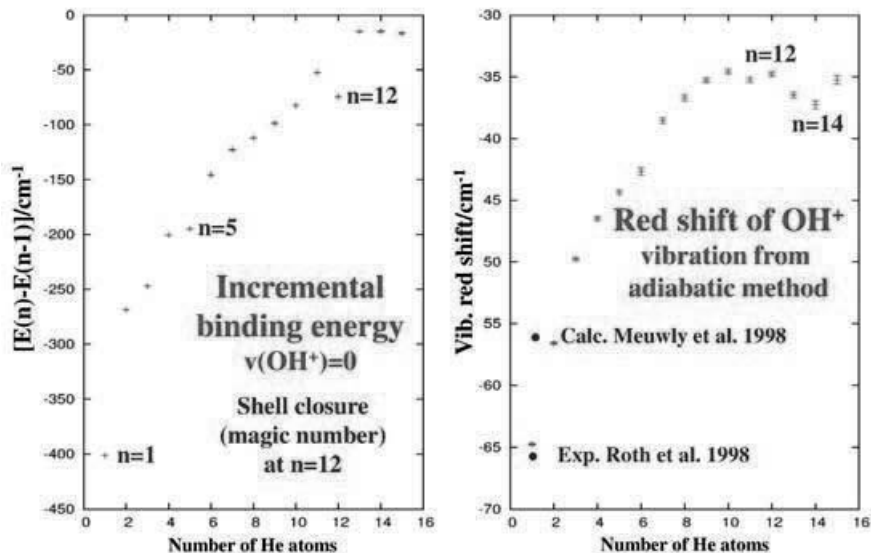
Figure 2: *Incremental binding energy and vibrational frequency shift for OH^+He_n clusters*

4. Concluding remarks

The strong permanent dipole moments and computed large dipole transition moments of CO^+He_n and OH^+He_n should allow the observation of their infrared predissociation spectra. Comparison with the known spectra of neutral CO inside helium clusters can shed new light on the role of superfluidity in molecular rotation inside liquid helium.

References

[1] A. R. W. McKellar, Y. Xu and W. Jäger, *Phys. Rev. Lett.* **97**, 183401 (2006)
[2] A. R. W. McKellar, *J. Chem. Phys.* **125**, 164328 (2006)
[3] D. Roth, S. A. Nizkorodov, J. P. Maier, and O. Dopfer, *J. Chem. Phys.* **109**, 3841 (1998)
[4] E. J. Bieske and J. P. Maier, *Chem. Rev.* **93**, 2603 (1993)
[5] M. Mladenović and M. Lewerenz, *Mol. Phys.* **111**, 2068 (2013)
[6] M. Meuwly, J. P. Maier and P. Rosmus, *J. Chem. Phys.* **109**, 3850 (1998)
[7] D. Blume, M. Lewerenz, F. Huisken, and M. Kaloudis, *J. Chem. Phys.* **105**, 8666 (1996)

Cold Ion Spectroscopy for Structural Determination of Peptides and Proteins

Natalia S. Nagornova, Vladimir Kopysov, <u>Oleg V. Boyarkin</u>

Laboratoire de Chimie Physique Moléculaire, École Polytechnique Fédérale de Lausanne, Station-6, CH-1015 Lausanne, Switzerland

Spectroscopy of protonated biomolecules provides benchmarks for calculations of intrinsic three-dimensional structures of these large species. We employ double-resonance photo-fragmentation approach to measure UV and conformer-selective IR spectra of cryogenically cooled, protonated biomolecules as large as decapeptides, their water complexes and small proteins. Cooling of the molecules is essential to suppress thermal congestion and achieve vibrational resolution in the spectra, thus providing a significant number of details – a molecular fingerprint. These fingerprints reveal frequencies and, since recently, absolute intensities of vibrations, which must be reproduced by theory for validation of the correct ion structure. To view more details of such fingerprints we are adding one more dimension to UV photofragmentation spectroscopy by combining it with high mass-resolution analysis of UV-induced fragments. We report on progress in coupling our cold ion instrument to a commercial Orbitrap mass-spectrometer.

For large molecules structural calculations with spectroscopic accuracy become too lengthy and challenging to rely on. We present a few examples, where certain important structural determinations can be obtained directly from spectroscopy of biomolecules, yet without calculations.

Computational Studies on Magnetism in Carbon Nanostructures

Frank Hagelberg

Department of Physics and Astronomy, East Tennessee State University, Johnson City, TN 37614, USA

Jianhua Wu

Department of Physics, Atmospheric Sciences, and Geoscience, Jackson State University, Jackson, MS 39217, USA

Within in the current effort of designing novel nanomaterials, carbon nanostructures occupy a special place. This is due to the broad range of their properties which can be tuned to match an equally broad variety of actual or potential applications. While carbon nanostructures have been established as promising candidates for new electric devices, their magnetic properties have received attention only quite recently. Magnetic carbon nanostructures, however, hold great promise for potential applications in nanodevices based on spintronics [1-3], operating with spin currents rather than currents of electric charge, as employed in conventional electronics [4]. While basic carbon nanostructures, such as graphene, periodic carbon nanotubes, or fullerenes are spin zero systems in their ground states, magnetism may be induced in these structures by encapsulating magnetic components into the interior of the nanosystem [5].

Also, radiation damage [6,7] and defect formation [8, 9], as achieved by irradiating the nanosystem with high-energy particles, have been shown to give rise to magnetic ordering. However, extended carbon structures can also acquire magnetic ground states as a consequence of dimensional reduction. As is well known, graphene strips of finite width with zigzag-structured edges, zigzag graphene nanoribbons (ZGNRs), have been shown to be magnetic [10, 11], associated with lowering the dimension of graphene from two to one, and an analogous observation has been made for zigzag nanotubes if their dimension drops from one to zero [12, 13, 14].

The focus of this contribution is on single-walled carbon nanotubes (SWCNTs) of the zigzag type. The impact of various structural and environmental tube parameters on the magnetism of these systems, among them curvature, topological defects as well as metal atom impurities, will be discussed.

Among the axially confined hydrogenated $(n,0)$ SWCNTs examined in our work by plane-wave density functional theory (DFT), with tube indices n ranging from 5 to 24, and with lengths up to eleven transpolyene rings, antiferromagnetic (AFM)

coordination has been found to prevail for n = 7–24. Thus, beyond a threshold index of n = 6, the systems investigated here display the magnetic behaviour expected on the basis of Lieb's theorem [15]. For SWCNTs of higher curvature, as represented in this work by the systems with n = 5 and 6, distinct variations of the magnetic phase with the tube length were observed, in analogy to layered transition metal composites consisting of a spacer unit surrounded by two ferromagnetic segments.

With respect to the size of the magnetic moment generated by unpaired electrons in the ferromagnetic (FM) phase at the SWCNT edges, and its variation with n, an elementary pattern is identified, involving a universal relation between the magnetic moments of these finite ZGNRs in the asymptotic range and those of the longest SWCNTs analyzed in this work. Specifically, deforming the ZGNRs into SWCNTs of the zigzag type reduced their magnetic moment by $2\mu_B$.

Recent simulations [16] have extended these basic systems to cross-linked carbon nanotubes (CLCNTs), composed of three SWCNTs. These composites are of interest for both nanomechanics and nanoelectronics. Various CLCNT models, differing from each other by the structure of the contact regions of the three SWCNT constituents, were explored in terms of their geometric, electronic, and magnetic properties. Various magnetic phases, as obtained by combining finite SWCNTs in ferromagnetic (FM) or antiferromagnetic (AFM) coordination, were distinguished.

(a)   (b)   (c)
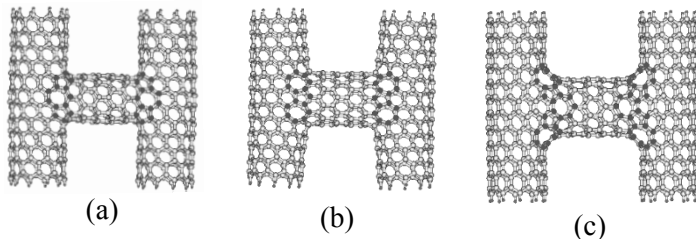
Figure 1. *The three prototypes of cross-linking architectures investigated in this work.*

Three types of CLCNTs were analyzed by use of plane-wave DFT, differing from each other by the structure of the contact region between the sidewalls and the bridge (see Figure 1). In particular, a previously established structure (connection (c)) with a complex arrangement of topological defects in the contact region, involving pentagons, heptagons, and octagons, is contrasted with two alternative structures with pentagons and heptagons only (connections (a) and (b)). In terms of magnetism, three configurations were distinguished: both sidewalls in AFM (FM) coordination, and a mixed case where one sidewall realizes AFM, the other FM coordination. Connections (a) and (c) were shown to display the expected hierarchy of magnetic phases, with the AFM-AFM (FM-FM) ordering at highest (lowest) stability.

Different stability sequences were found for connection (b), demonstrating that the structure of the contact region exerts a strong influence on the relative energies of the three magnetic phases. Inspection of the corresponding linear spin density distribution profiles in conjunction with the associated total magnetic moments suggest that these differences are correlated with the presence of finite magnetic moments in the contact regions of connections (a) and (b) which may exhibit AFM or FM order across the bridge.

The magnetic properties of the CLCNTs considered here provide the key to a closer understanding of their adsorption features. As established for connection (c), places of enhanced spin density along both the sidewalls and the bridge of the CLCNT emerge, by the criterion of the hydrogen atom adsorption energy, as preferred sites of hydrogen atom attachment. This pattern is related to an increased tendency of covalent bond formation at places where the density of unpaired electrons is high.

In continuation of this research, it will be interesting to determine the transport properties of the CLCNTs considered here. As shown in this work, the stabilities of selected magnetic configurations, involving AFM-AFM, FM-FM, and mixed junctions, can be sensitively manipulated by adjusting the structure of the contact region joining the bridge and the sidewalls. This effect might be exploited to generate a wide variety of magnetic networks of interest for spintronics applications.

References

[1] F. Kuemmeth, H.O.H. Churchill, P.K. Herring, C.M. Marcus, Materials Today 2009,13, 18.

[2] C.M. Schneider, Kohzuharova S. Groudeva-Zutova, B. Zao, T. Muehl, I. Moenchj, H. Vinschelberg, Rietschel A. Leonhardt, J. Fink, Nanotube Spintronics: Magnetic Systems Based on Carbon Nanotubes, in: Frontiers of Multifunctional Integrated Nanosystems, eds. E. Buzaneva, P. Scharff, Nato Science Series 2005, Vol.152, 359.

[3] S.H. Jhang, M. Marganska, Y. Skoursi, D. Preusche, B. Witkamp, M. Grifoni, H. van der Zant, C. Strunk, J. Wosnitza, Phys. Rev. B 2010, 82, 041404.

[4] O.V. Yazyev, ChemInform Abstract: Emergence of Magnetism in Graphene Materials and Nanostructures. ChemInform 2011, 42: no. doi: 10.1002/chin.201101219.

[5] J. Wu, F. Hagelberg, J. Phys. Chem. C 2011, 115, 4571.

[6] F. Banhart, Rep. Prog. Phys. 1999, 62, 1181.

[7]   A.V. Krasheninnikov, F. Banhart, Nature Mater. 2007, 6,723.

[8]   P. Lehtinen, A.S. Foster, Y. Ma, A.V. Krasheninnikov, R.M. Nieminen, Phys. Rev. Lett. 2004, 93, 187202.

[9]   R.H. Telling, C.P. Ewels, A.A. El-Barbary, M.I. Heggie, Nature Mater. 2003, 2, 333.

[10] M. Fujita, K. Wakabayashi, K. Nakada, K. Kusakabe, J. Phys. Soc. Jp. 1996 65, 1920.

[11] K. Nakada, M. Fujita, G. Dresselhaus, M. Dresselhaus, Phys. Rev.B 1996 54, 17954.

[12] A. J. Du, Y. Chen, G. Q. Lu, S.C. Smith, Appl. Phys. Lett. 2008 93, 073101.

[13] Y.H. Kim, J. Choi, K.J. Chang, Phys. Rev. B 2003, 68, 125420.

[14] O. Hod, G.E. Scuseria, ACS Nano 2008, 2, 2243.

[15] E.H. Lieb, Phys. Rev. Lett. 1989, 62, 1201.

[16] J. Wu, A. Ayasoufi, J. Leszczynski, F.Hagelberg, J. Phys. Chem. C 2013, 117, 3646.

Cluster and particle formation in helium droplets

Adrian Boatwright, Cheng Feng, Daniel Spence, Elspeth Latimer, Shengfu Yang and
Andrew M. Ellis

[1] *Department of Chemistry, University of Leicester, Leicester LE1 7RH*

Chris Binns

[2] *Department of Physics and Astronomy, University of Leicester, LE1 7RH*

Helium nanodroplets provide a convenient low temperature environment in which to study small clusters and complexes, particularly using spectroscopic techniques such as laser-induced depletion spectroscopy. A natural progression is to exploit helium droplets to grow larger objects, and in particular nanoparticles. Helium droplets offer some unique features as a medium for growing nanoparticles. These include: (1) chemical inertness; (2) a very low temperature (0.4 K); (3) the high thermal conductivity of superfluid helium, which leads to rapid cooling of dopants; (4) good dopant mobility; (5) the ability to add materials sequentially, enabling the easy formation of core-shell nanoparticles. In addition, there is an expectation, which seems to be borne out by the scarce experimental evidence available so far, that a nanoparticle encased in helium can be soft-landed onto a surface. These factors offer a route to a large array of new and interesting types of nanoparticles [1].

This presentation will provide an overview of recent work in our laboratory on the formation and deposition of nanoscale objects grown inside helium droplets. This will include preliminary studies of core-shell nanoparticles, including information on their magnetic properties. In addition the formation of narrow chain structures in large helium droplets will also be described (an example of a metallic chain is shown opposite). Here the evidence suggests that these long chains, typically hundreds of nm in length but very narrow (<10 nm), are formed by the 'pinning' of dopant atoms to quantized vortices in the
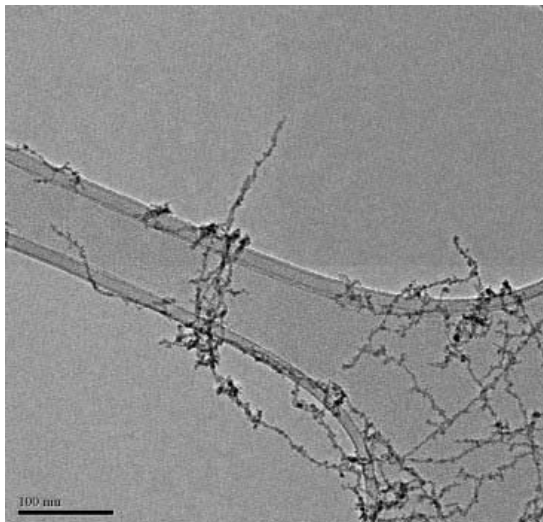
helium droplets, as first proposed by Gomez *et al.* [2]. The formation of these chains for a variety of dopants will be shown and a mechanism will be proposed which accounts for their dependence on droplet size.

References

[1] A. Boatwright, C. Feng, D. Spence, E. Latimer, C. Binns, A M. Ellis, S. Yang, *Faraday Discuss*. **162**, 113 (2013).
[2] L. F. Gomez, E. Loginov, A. F. Vilesov, *Phys. Rev. Lett*. **108**, 155302 (2012)

Direct dynamics simulations of gas-phase S_N2 nucleophilic substitution reactions. Atomistic mechanisms and comparisons with experiment

William L. Hase

Texas Tech University, Lubbock, Texas USA

Direct dynamics simulations have been performed for gas-phase S_N2 nucleophilic substitution reactions. An important component of these calculations are comparisons with molecular beam ion imaging experiments of the Roland Wester research group and gas kinetic experiments of the Albert Viggiano research group. Excellent agreement is found between the simulations and experiments. The simulations provide an atomistic understanding of the experimental results, which include product energy distributions, velocity scattering angle distributions, and gas kinetic rate constants. Important publications describing this research are references 1-6, and the review in reference 7.

References

[1] W. L. Hase, "Computer Simulation of Gas-Phase Chemical Reactions: Applications to S_N2 Nucleophilic Substitution", *Science* **266**, 1998 (1994)

[2] J. Mikosch, S. Trippel, C. Eichhorn, R. Otto, U. Lourderaj, J. X. Zhang, W. L. Hase, M. Weidemueller, and R. Wester, "Imaging Nucleophilic Substitution Dynamics", *Science* **319**, 183 (2008).

[3] J. Zhang, J. Mikosch, S. Trippel, R. Otto, M. Weidemueller, R. Wester, and W. L. Hase, "F^- + $CH_3I \rightarrow FCH_3$ + I^- Reaction Dynamics. Non-Traditional Atomistic Mechanisms and Formation of a Hydrogen-Bonded Complex", *J. Phys. Chem. Lett.* **1**, 2747 (2011).

[4] R. Otto, J. Xie, J. Brox, S. Trippel, M. Stei, T. Best, M. R. Siebert, W. L. Hase, and R. Wester, "Reaction Dynamics of Temperature-Variable Anion Water Clusters Studied with Crossed Beams and by Direct Dynamics", *Faraday Discuss. Chem. Soc.* **157**, 41 (2012).

[5] J. Mikosch, J. Zhang, S. Trippel, C. Eichhorn, R. Otto, R. Sun, W. A. de Jong, M. Weidemueller, W. L. Hase, and R. Wester, "Indirect Dynamics of a Highly Exoergic Substitution Reaction", *J. Am. Chem. Soc.* **135**, 4250 (2013).

[6] J. Zhang, U. Lourderaj, R. Sun, J. Mikosch, R. Wester, and W. L. Hase, "Simulation Studies of the Cl^- + CH_3I S_N2 Nucleophilic Substitution Reaction:

Comparison with Ion Imaging Experiments*", J. Chem. Phys.* **138**, 114309 (2013).

[7] P. Manikandan, J. Zhang, and W. L. Hase, "Chemical Dynamics Simulations of $X^- + CH_3Y \rightarrow XCH_3 + Y^-$ Gas-Phase S_N2 Nucleophilic Substitution Reactions. Non-Statistical Dynamics and Non-Traditional Reaction Mechanisms", *J. Phys. Chem. A* **116**, 3061 (2012).

Ion-neutral chemistry at ultralow energies: Dynamics of reactive collisions between laser-cooled ions and atoms in an ion-atom hybrid trap

O. Dulieu[b], F. H.J. Hall[a], P. Eberle[a], G. Hegi[a], M. Raoult[b], M. Aymar[b], and S. Willitsch[a]

[a] Department of Chemistry, University of Basel, Switzerland
[b] Laboratoire Aimé Cotton, CNRS/ Univ. Paris Sud/ ENS Cachan, Orsay, France

Cold chemical reactions between laser-cooled Ca^+ or Ba^+ ions and Rb atoms were studied in an ion-atom hybrid trap [1]. Reaction rate constants were determined in the collision energy range E_{coll}/k_B = 20 mK-20 K. Product branching ratios were studied using resonant-excitation mass spectrometry. The dynamics of the reactive processes including the radiative formation of $CaRb^+$ and $BaRb^+$ molecular ions has been analyzed using high-level quantum-chemical calculations of potential energy curves and quantum-scattering calculations for the radiative channels [2, 3]. It is shown that the energy dependence of the reaction rates is governed by long-range interactions, while its magnitude is determined by short-range non-adiabatic and radiative couplings which induce a chemical change. The quantum character of the collisions is predicted to manifest itself in the occurrence of narrow shape resonances at well-defined collision energies. The present results highlight both universal and system-specific phenomena in cold ion-neutral reactive collisions.

References

[1] F.H.J. Hall, M. Aymar, N. Bouloufa-Maafa, O. Dulieu and S. Willitsch, Phys. Rev. Lett. 107, 243202 (2011).
[2] F. H. J. Hall, P. Eberle, G. Hegi, M. Raoult, M. Aymar, O. Dulieu, S. Willitsch, Mol. Phys. 111, 2020 (2013)
[3] F. H. J. Hall, M. Aymar, M. Raoult, O. Dulieu, S. Willitsch, Mol. Phys. 111, 1683 (2013)

Scattering Quantum Dynamics of NO with Cu

B. Murali Krishna, J. Lefevre and Roberto Marquardt
Lab. de Chimie Quantique – UMR 7177 CNRS/Université de Strasbourg

Graham A. Worth
Department of Chemistry – University of Birmingham

1. Introduction

The interaction of copper atoms with nitric oxide radicals is described in terms of global, analytical potential energy surfaces derived from ab initio calculations published previously [1-3]. These surfaces are used here for wave packet calculations within the Multi-Configurational Time Dependent Hartree (MCTDH) program [4] to simulate the collision dynamics of Cu with NO. Results indicate the existence of a rather long lived intermediate complex. Reactions involving these species are important in atmospheric chemistry and catalysis [5], as well as in various biochemical reaction pathways [6]. Understanding the elementary steps in the collision process of these species is therefore relevant. NO dimer clustered on Cu atoms have been observed in infrared spectroscopy of matrix isolated CuNO [7]. CuNO and its cation have been observed in the gas phase by neutralization-re-ionization mass spectrometry [8].

In the present contribution we report on collisions at energies in the order of some tens of meV, at which NO-bond cleavage will hardly be possible. The problem is addressed fully quantum mechanically, however. The results allow us to predict that experiments involving ultra-fast laser spectroscopic techniques should now become feasible with metal nitrosyl complexes. Calculations will be carried out on the lowest adiabatic potential energy surface for this system.

2. Methods

The nuclear motion is described in terms of the time dependent wave function $\psi(r_d, r_v, \theta)$, where is r_d the length of the vector linking the center of mass of the NO molecule with the Cu atom, r_v is the length of the vector linking the N and O atoms and θ is the polar angle between the two aforementioned vectors. This function is determined as the solution of the time dependent Schrödinger equation with a Hamiltonian can be given in terms of an exact kinetic energy Hamiltonian T [9]. With this approach we can calculate states of well defined total angular momentum and parity. The potential energy operator is the global analytical representation for

the lowest adiabatic electronic state of the CuNO system derived in [3]. We use the MCTDH program [4] to determine the time dependent wave function and refer to the documentation of this code [4, 10, 11] for further details on the methods used. We just point out here that, to obtain converged results, an effective "MCTDH-Hamiltonian matrix" of rank 4400 was sufficient, whereas the rank of a conventional Hamiltonian matrix would be on the order 440 000.

3. Results

To validate our approach, we find that vibrational eigenstates are identical to the eigenstates obtained with an independent variational program to solve the time independent Schrödinger equation restricted to the equilibrium region [3] which agree well with experimental values obtained in matrix isolation [7]. Note, however, that in [7] the attribution of transition is erroneous [3]. On the basis of this good agreement for vibrational transitions we discuss a simulation of the collision process by inspection of the wave packet dynamics. We start with a situation where the initial state where electrons are in their lowest possible adiabatic state and the NO molecule is in the rotational and vibrational ground state. The state is a Gaussian superposition of incoming scattering waves in the r_d coordinate with an averaged kinetic energy of 100 meV.

Figure 1 shows snapshots of the reduced probability density of this state at different times of the evolution (axes give the x and y coordinates of the molecular plane in units of 100 pm). This wave packet is initially (t=0 fs) localized at a distance of 500 pm, well outside the half-circle marked by S in the figure. This half-circle indicates the region where Cu and NO interact strongly (see Figure 4 in [3]) and marks somewhat the region of definition of the CuNO complex. While localized in r_d, it is completely delocalized in θ, because we simulate here the collision dynamics for a rotationless NO molecule (j=0). After 260 fs, the wave packet has already penetrated almost completely the collision active region. We notice a splitting of the wave packet with an important localization of a portion of the wave packet in the vicinity of the potential minimum.
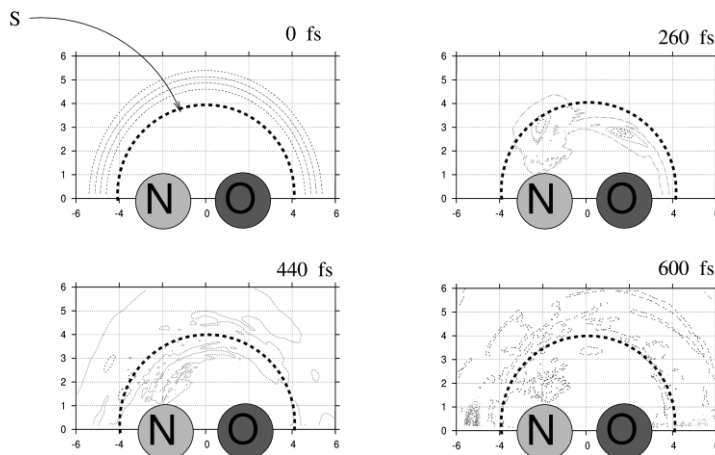
After 440 fs, the wave packet has started to move outside the collision region, while spreading out in the energetically accessible region. After 600 fs, the largest portion of the wave packet has left the collision region, moving outwards. A smaller portion remains in the region around the potential minimum, keeping a kind of "memory" of its location.

The figure allows to appreciate the rather long time interval for the existence of the complex, during which modern techniques could enable us to detect and analyze the complex, for instance via ultra-short spectroscopy coupled to molecular beams. Scattering matrix elements using the formula derived by Tannor and Weeks [12] show that the collisions lead to a very efficient tranfer of translational to internal rotational motion of the NO molecule.

4. Conclusions

The quantum dynamics of the scattering of Cu atoms with NO molecules has been calculated with the Heidelberg Multi-Configurational Time Dependent Hartree method. It has been shown, for the first time, that this method can be used to calculate in a realistic way the wave packet propagation, the spectroscopic and the scattering signature of a system involving a heavy element by determination of infrared bands and scattering probability distributions. The results indicate that the intermediate CuNO complex might exist in the gas phase, as a result of the collision, during a time interval of at least 200 to 300 fs. This time is sufficiently long to foresee the interaction of the complex with ultra-short or intense laser pulses in order to characterize spectroscopically its nature. In future applications of the present

methods, we plan to include several excited electronic states, the potential energy surfaces of which have already been determined from *ab initio* calculations [2].

Acknowledgments

References

[1] B. M. Krishna and R. Marquardt. In R. Marquardt, M. Lewerenz, O. Dutuit, editor, Proc. 18 Int. Symposium on Atomic and Surface Physics and Related Topics, L'ALpe d'Huez, France, pages 218–222, Innsbruck, (2012). Innsbruck University Press.

[2] B. M. Krishna and R. Marquardt, J. Chem. Phys., 136, 244303 (2012).

[3] Y. Cornaton, B. M. Krishna, and R. Marquardt, Mol. Phys., 111, 2263–2282 (2013).

[4] G. A. Worth, M. H. Beck, A. Jäckle, and H.-D. Meyer. The MCTDH Package, Version 8.2, (2000). H.-D. Meyer, Version 8.3 (2002), Version 8.4 (2007), Revision 8 (2012). See http://mctdh.uni-hd.de/.

[5] G. B. Richter-Addo and P. Legzdins. Metal Nitrosyls. Oxford University Press: New York, Oxford, 1992 edition, (1992).

[6] I. M. Wasser, S. de Vries, P. Moenne-Loccoz, I. Schröder, and K. D. Karlin, Chem. Rev., 102, 1201–1234 (2002).

[7] L. Krim, X. Wang, L. Manceron, and L. Andrews, J. Phys. Chem. A, 109, 10264–10272 (2005).

[8] Sülzle, D. and Schwarz, H. and Moock, K. H. and Terlouw, J. K., Int. J. Mass Spec. and Ion. Proc., 108, 269–272 (1991).

[9] J. Tennyson and B. T. Sutcliffe, J. Chem. Phys., 77, 4061–4072 (1982).

[10] M. H. Beck, A. Jäckle, G. A. Worth, and H.-D. Meyer, Phys. Rep., 324, 1 (2000).

[11] H.-D. Meyer, F. Gatti, and G. A. Worth. Multidimensional Quantum Dynamics. Wiley-VCH, Weinheim, (2009).

[12] D. J. Tannor and D. E. Weeks, J. Chem. Phys., **98**, 3884–3893 (1993).

Atmospheric pressure ion chemistry studied by Ion mobility-mass spectrometry

Štefan Matejčík, Martin Sabo

Department of Experimental Physics, Comenius University, mlynská dolina F2, 84248 Bratislava, Slovakia

1. Introduction

This work was motivated by the aim to understand the generation of negative and positive ions in air in CD sing Ion Mobility spectrometry – Mass Spectrometry (IMS-MS) technique. The knowledge obtained in this study we plan to apply for selective formation of the specific negative and positive ions. The CD discharge has a great potential to be used as ion source for IMS. The selectivity of the generation of positive and negative ions in CD increases the applicability of CD ion source for atmospheric pressure chemical ionisation (APCI). This results in improvement of the selectivity of the analytical methods (IMS and MS). The main application of the IMS-MS instruments is in analytical sciences; however we will demonstrate its application for fundamental sties in the field of ion-molecule reactions at atmospheric pressure.

The mass spectrometry studies of the negative and positive ions formed in corona discharge (CD) in air at atmospheric pressure were performed by several laboratories [1-5]. While in the case of positive CD the primary ions are quickly converted to stable $H_3O^+(H_2O)_n$ or $NO^+(H_2O)_n$ ions [1,2], the spectra of negative polarity are more complex. This is mainly due to sensitivity of negative CD to many parameters like discharge power, gas flow, gas composition, pressure, temperature, etc.. In negative CD in dry air different negative ions were reported NO_2^-, O_3^-, OH^-, CO_3^- and NO_3^- [3], CO_3^- and its water clusters [4] in ambient air. The time evolution of the ions (1 and 10 ms) and the effect of humidity were investigated by Nagato et al. [5]. The role of neutrals formed in CD gap in negative ions composition was elucidated by Ross and Bell [6]. They applied different gas flow conditions (flow directions, flow rates) through CD gap, what resulted in changes in negative ion composition from O_3^-, CO_3^- and NO_3^- (normal flow) to O_2^- and CO_4^- (reverse flow). We continue the study of the positive and negative ion chemistry associated with CD in order to improve and optimise new sorces of ions for IMS and IMS-MS.

2. Experiment

The Corona Discharge Ion Mobility Spectrometry orthogonal acceleration time of flight spectrometer (CD-IMS-oaTOF) instrument was developed at Comenius [7].

The IMS is operated at atmospheric pressure in positive and negative polarity. The detailed description of IMS was given in our earlier work [7].

The CD-IMS-oaTOF instrument was able to operate in three modes in single IMS mode, in single TOF mode when the SG of IMS was fully open and in the two-dimensional mode used when the both spectrometers works synchronically together. In order to obtain sufficient data was the operation time of CD-IMS-oaTOF in the two-dimensional mode in the range 5-10 minutes.

3. Results and discussions

The IMS and MS spectra of ions generated in CD at 800 ml/min of N_2 flow and 14 μA CD current are shown in the Figures 2a. The dominant reactant ion peak of IMS (8.08 ms reduced mobility 2.06 $cm^2V^{-1}s^{-1}$) was composed of $H_3O^+.(H_2O)_n$ ions (n=1,2,3) (m/z= 37, 55 and 73 Da in MS).
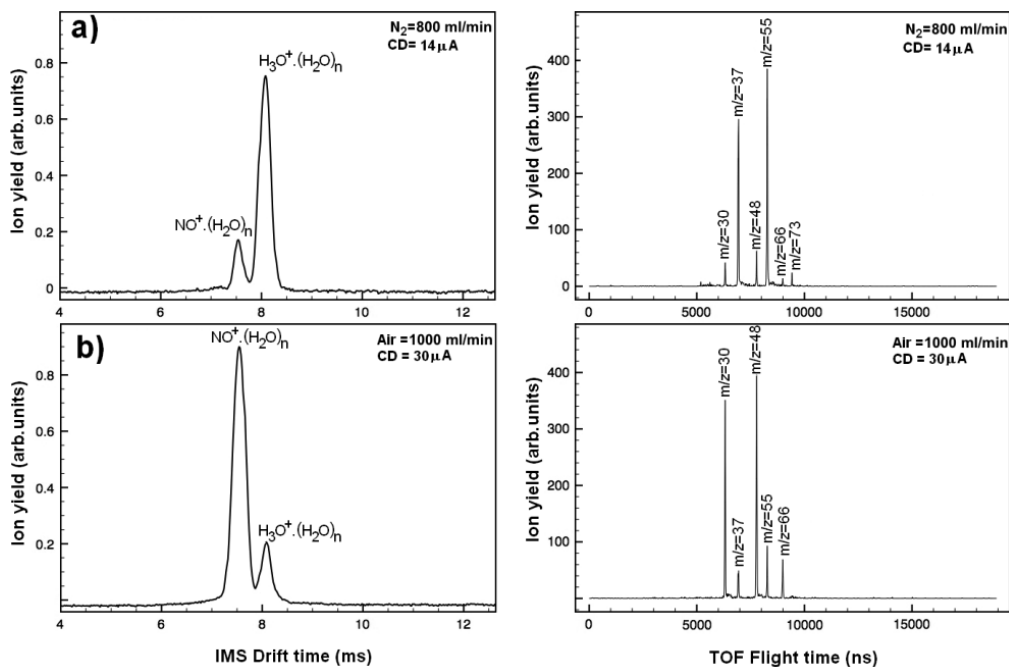
Figure 1: *IMS and MS spectra of positive ions formed in CD in N_2 and in air.*

The second reactant ion peak in the Figure 1a (7.54 ms, reduced mobility 2.21 $cm^2V^{-1}s^{-1}$) was composed of $NO^+.(H_2O)n$ (n=0,1,2) ions (m/z=30, 48 and 66 Da). The NO is formed in CD and the change of the feed gas from N_2 (5 ppm O_2) to air results in

increased formation of NO and consequently in increased NO^+ generation via processes:

$$O_2^+/N_2^+ + NO \rightarrow NO^+ + O_2/N_2 \qquad\qquad (1)$$
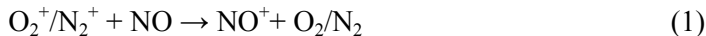
The high efficiency of NO generation in CD (Figure 1b) was additionally supported by special design of the CD including gas flow directions and flow rates, which is described in the paper [8].

The negative CD under standard flow conditions in air results in spectra depicted in the Figure 2.
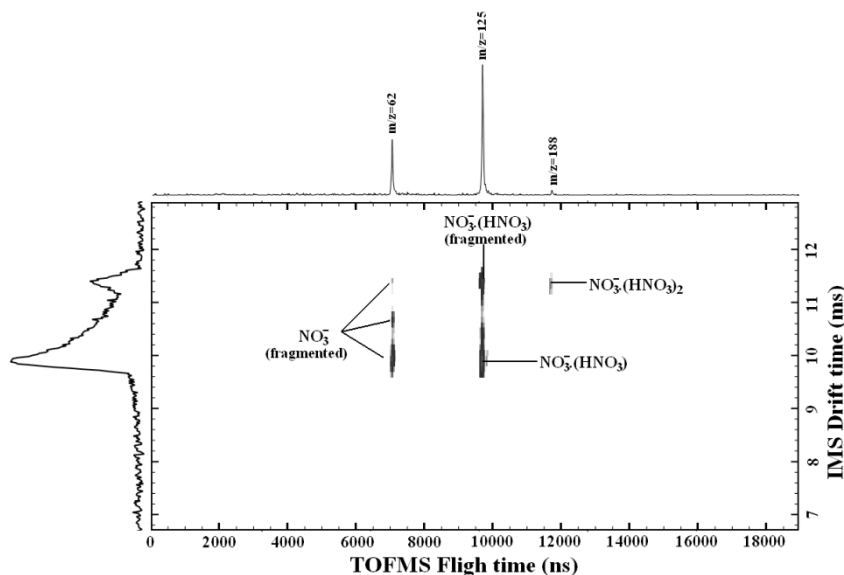
Figure 2: *Two dimensional IMS-MS spectrum of negative CD in air.*

In the Figure 2 a peak in IMS spectrum is located at (11.4 ms reduced mobility 1.75 $cm^2V^{-1}s^{-1}$). This IMS peak is composed of the ions with m/z 62, 125 and 188 Da. The m/z of 188 Da we assign to $NO_3^-.(HNO_3)_2$. The fragmentation of $NO_3^-.(HNO_3)_2$ occurs already in IMS drift tube and in IMS-MS interface. The peak in IMS (drift time 9.88 ms and reduced mobility 2.02 $cm^2V^{-1}s^{-1}$ at T=295K) has a significant tail, which is composed only of $NO_3^-.(HNO_3)$ and NO_3^-. The presence of the tail we elucidate by the dissociation of $NO_3^-.(HNO_3)_2$ in IMS drift tube, to its monomer $NO_3^-.(HNO_3)$ ions. We were able to determine the lifetime of the $NO_3^-.(HNO_3)_2$ for dissociation into $NO_3^-.(HNO_3)$ to 8.0±0.5 ms (under present experimental conditions (for following experimental conditions T=295K, p=1005 mbar, E from 588 to 242 V/cm).

4. Conclusions

IMS-MS technique is a powerful toll to study negative and positive ion formation in CD in air and air constituting gases. We have found ways to selectively generate different ions in CD in air using different discharge conditions, which give to the CD a broad application in analytical sciences for APCI.

Acknowledgments

References

[1] M.M.Shahin, J.Chem.Phys., 45 (1965) 2600.
[2] J.Pavlik, J.D.Skalný, Rapid Commun. Mass Spectrom, 11 (1997) 1687.
[3] B.Gravendeel, F.J.Hoog, J.Phys. B: At. Mol. Phys, 20 (1987), 6337.
[4] J.D.Skalny, T.Mikoviny, S.Matejcik, N.J.Mason, Int. J. Mass Spectrom, 233 (2004) 317.
[5] K.Nagato, Y.Matsui, T.Miyata, T.Yamauchi,. Int. J. Mass Spectrom, 248 (2006) 142.
[6] S.K.Ross, A.J.Bell., Int. J. Mass Spectrom., 218 (2002), L1.
[7] M.Sabo, J.Matuska, S.Matejcik, Talanta 85 (2011) 400.
[8] M. Sabo, S. Matejcik, Analyst 138 (2013) 6907

Fragmentation of complex biomolecular systems upon interaction with multiply charged ions

V. Vizcaino, J-C. Poully, A. Méry, S. Maclot, R. Delaunay, M. Capron, A. Domaracka, P. Rousseau, J. Rangama, J-Y. Chesnel, L. Adoui and B.A. Huber
Centre de recherche sur les ions, les matériaux et la photonique - CIMAP UMR6252 CEA/CNRS/ENSICAEN/Université de Caen Basse-Normandie.

Interactions of multiply charged ions with biologically relevant systems have been studied in a crossed-beam apparatus. Appearance sizes and mass distributions of q-fold charged clusters will be given and compared for different systems. Delayed evaporation in cytosine clusters will be discussed. Finally, a new experimental set-up allowing the study of size selected clusters will be presented.

The use of ion beams (protons or carbon ions) is increasingly employed in medicine for the treatment of cancer because unlike conventional radiotherapy it allows a proper localization of the energy deposition in the tissue and thus spares the surrounding healthy organs. Therefore, in recent years, many studies have focused on the interaction between multiply charged ions and small molecules of biological interest such as DNA bases or amino acids [1, 2]. These studies, conducted in the gas phase on isolated molecules, have allowed understanding the intrinsic properties of these biomolecules and the fundamental mechanisms involved at the molecular level. However, they are not representative of the complexity of interactions *in vivo* and do not take into account the influence of the environment on the stability of biomolecules. A first step to simulate the chemical environment of biomolecules is to study biomolecular clusters [3, 4].

Experiments on biomolecular clusters were performed with a crossed beam apparatus, a detailed description of this set-up can be found in Ref.[5]. Molecules are evaporated in a resistively heated oven and are being carried away by a buffer gas (helium) toward the condensation channel, kept at liquid nitrogen temperature, where they will aggregate. The collimated cluster beam then collides with a pulsed ion beam delivered by an ECR ion source. The cationic fragments are analyzed in mass-over-charge by a linear time-of-flight mass spectrometer. In order to increase the detection efficiency over a large mass range, the ions are post-accelerated towards a conversion plate kept at 25 kV and the secondary electrons produced by the impact on the plate are detected with a three-stage MCP detector.

The interaction with highly charged ions leads to the formation of a multiply charged cluster in an excited state. It will decay, dissipating the excess charge and energy (few to tens of eV) transferred during the collision, by a combination of evaporation, fission and intramolecular fragmentation. The latter process is observed only in a few cases; the intermolecular bonds (hydrogen bonds in the case of biomolecular systems) break preferably [4]. Below a critical size (n_c), the energetic barrier against fission disappears and the cluster can no longer accommodate the charges and breaks due to the Coulomb repulsion. Experimentally we observe appearance sizes (n_{app}) which are usually larger than the critical size of the system. In figure 1, we report the appearance sizes for q-fold charged clusters (q from 2 up to 5) for the DNA (or RNA) bases cytosine, adenine, thymine, uracil and amino acids α-alanine, α-aminobutyric acid and β-aminobutyric along with other systems.
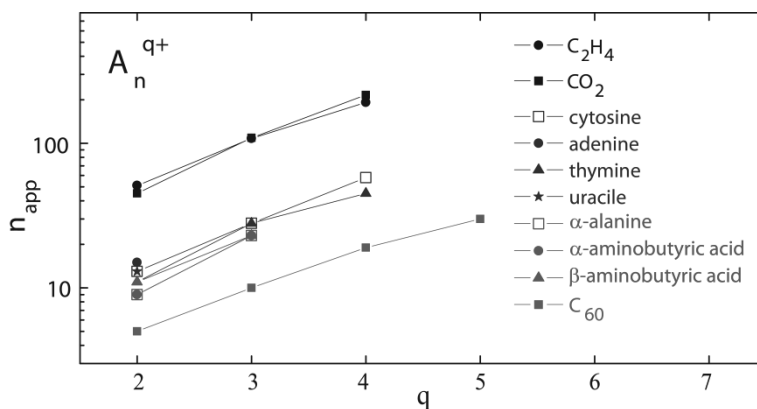
Figure 1: *Appearance size for multiply charged clusters. Values for C_2H_4 and CO_2 clusters are from electron impact ionization [6]. All the others systems were measured in Caen with low energy ions typically O^{6+} at 50 keV for DNA bases [3], He^+ at 11 keV for amino acids and Xe^{20+} at 400keV for C_{60} [7].*

A typical TOF spectrum of cytosine clusters after interaction with O^{6+} ions at 50keV is shown in figure 2. The measured appearance sizes of $(Cyt)_n^{q+}$ for q=2,3 and 4 are 13, 29 and 55, respectively. The spectrum presents a large background partly due to delayed evaporation processes. Indeed after ionization, energy redistribution and cluster dissociation occur within a few ns, but evaporative cooling still continues to occur within a few μs. Evaporation of one monomer from singly-, doubly- or triply-charged cytosine clusters in the first extraction region of the time-of-flight mass spectrometer can be seen experimentally by onsets in the spectra (see inset in figure 2).
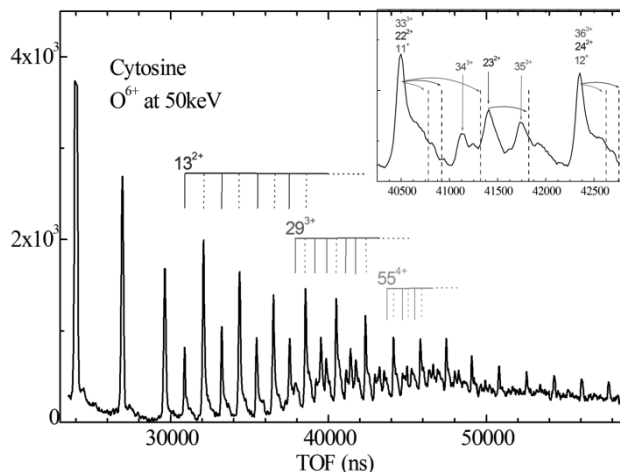
Figure 2: *Time-of-flight spectrum of the cationic products of the interaction of cytosine clusters with O^{6+} ions at 50keV. Inset: the dash lines correspond to the calculated delay for the loss of one monomer from a singly charged (red), a doubly charged (blue) and a triply charged (red) cluster.*

A new experimental set-up (see figure 3) is in the final stage of development, it will be dedicated to the study of size selected biomolecular clusters. The idea behind the development of such an apparatus is to determine the influence of the environment on the fragmentation of biomolecules upon interaction with multiply charged ions. Indeed, by controlling the number of water molecules attached to the system under study we will be able to quantify the so-called direct and indirect effects of ionizing radiation.

In this experimental set-up, the beam of biomolecular complex (nano-hydrated biomolecules) is formed by an electrospray ionization source, collimated in a funnel before being mass-selected by a quadrupole mass analyzer. In order to obtain a beam of sufficient density, the biomolecular ions are accumulated in a Paul trap before entering the interaction zone. The projectile ion beam is shaped by a quadrupole triplet in order to optimize the overlap between the two ion bunches. The fragments from the collision are analyzed by a time-of-flight mass spectrometer which can operate in both linear or reflectron modes.
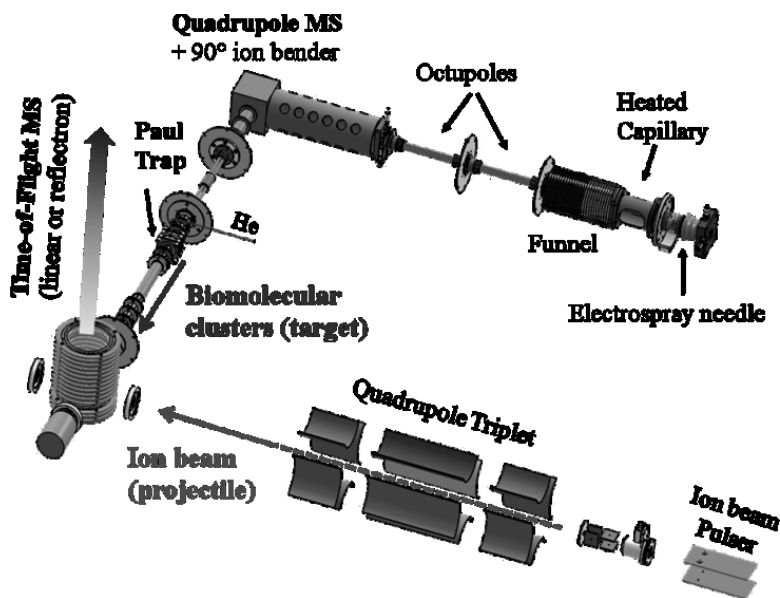
Figure 3: *Experimental set-up (PIBALE) for the study of size-selected biomolecular clusters.*

Acknowledgements

References

[1] Bari et al., J.Chem.Phys, **128,** 074306 (2008)
[2] Capron et al., Chem. Eur. J., **18,** 9321 – 9332 (2012)
[3] Schlathölter et al., ChemPhysChem, **7**, 2339-2345 (2006)
[4] Maclot et al., ChemPhysChem, **12**, 930-936 (2011)
[5] Bergen et al., Rev. Sci. Instrum. **70** 3244 (1999)
[6] Echt et al., Phys.Rev.A., **38,** 7 (1988)
[7] Manil et al., Phys.Rev.Lett., **91,** 215504 (2003)

The reactions of gas-phase dications and trications with neutral species: reactivity and dynamics

Stephen D. Price

Chemistry Department, University College London, 20 Gordon Street, London
WC1H 0AJ, UK.
s.d.price@ucl.ac.uk

There is increasing interest in the role of molecular dications (doubly-charged molecules) in both astrochemistry and the chemistry of planetary ionospheres.[1-7] Small molecular dications, such as N_2^{2+}, are highly energy-rich metastable species with lifetimes to dissociation ranging from femtoseconds to many seconds.[8] This talk will discuss the consequences of the bimolecular interactions of molecular and atomic dications, and trications, with other atoms and molecules.

Section of a coincidence spectrum recorded following collisions of N_2^{2+} with O_2 at 7.1 eV. The spectrum clearly shows two dissociative electron transfer reactions and two bond-forming reactions forming NO^+
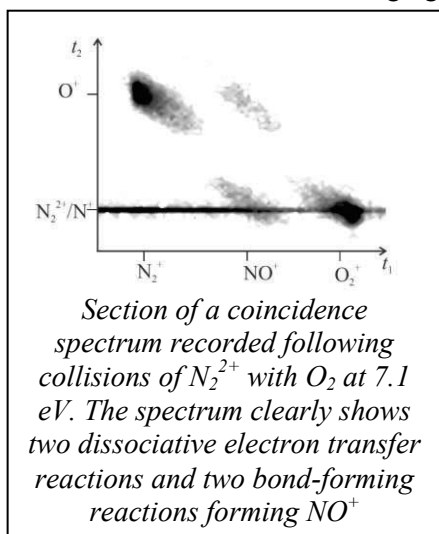
Recent laboratory developments have shown that molecular dications possess a rich and unusual bimolecular chemistry.[9] As well as the expected electron-transfer reactions, molecular dications exhibit extensive bond-forming reactivity in low-energy collisions with neutral molecules. These "chemical" reactions usually generate pairs of product monocations, often accompanied by neutral species:

$$N_2^{2+} + C_2H_2 \rightarrow N^+ + NC_2H^+ + H$$

The product monocations from these reactions possess considerable translational energies and can have markedly different reactivity to that of thermalised monocations in a given energized medium.

The reaction dynamics of these unusual reactions can be investigated by traditional mass spectrometry and by multi-parameter coincidence experiments.[10-16] The coincidence experiments allow a detailed investigation of the kinematics of these reactions revealing unusual reaction pathways, involving sometimes involving initial complexation with the neutral species.

$$N_2^{2+} + O_2 \rightarrow [N_2O_2]^{2+} \rightarrow N_2O^{2+} + O$$
$$N_2O^{2+} \rightarrow N_2^+ + O^+$$
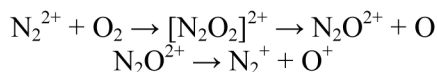
A discussion of the dynamics of dication reactions will be illustrated by recent experimental studies of the reactions of N_2^{2+} and O_2^{2+} with small organic molecules. In these experiments O_2^{2+} displays a quite remarkable range of bond-forming reactivity.

We will also discuss the extension of our multi-parameter coincidence experiments to investigate the reactivity of atomic and molecular trications (I^{3+}, Xe^{3+}, CS_2^{3+}) with small molecules. Despite the very high internal energy of the trication reactants, we see that bond-forming chemistry competes effectively with electron transfer reactions. A simple model will be presented to account for the bond-forming reactions we observe in these trication-neutral collisions.[17]
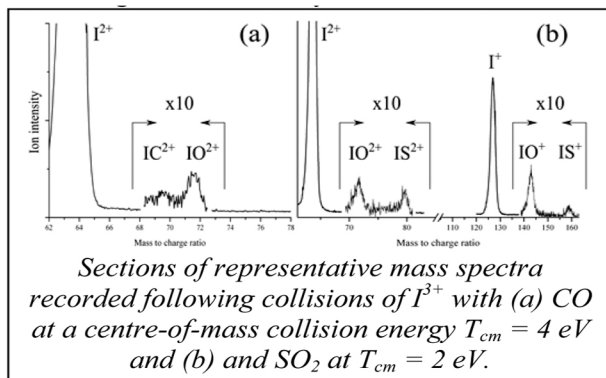
Sections of representative mass spectra recorded following collisions of I^{3+} with (a) CO at a centre-of-mass collision energy $T_{cm} = 4\ eV$ and (b) and SO_2 at $T_{cm} = 2\ eV$.

References

[1] O. Witasse, O. Dutuit, J. Lilensten, R. Thissen, J. Zabka, C. Alcaraz, P. L. Blelly, S. W. Bougher, S. Engel, L. H. Andersen, and K. Seiersen, Geophys. Res. Lett. **29,** 1263, (2002).

[2] C. Simon, J. Lilensten, O. Dutuit, R. Thissen, O. Witasse, C. Alcaraz, and H. Soldi-Lose, Ann. Geophys. 23, 781, (2005).

[3] J. Lilensten, O. Witasse, C. Simon, H. Solidi-Lose, O. Dutuit, R. Thissen, and C. Alcaraz, Geophys. Res. Lett. 32, L03203, (2005).

[4] J. Roithova and D. Schroder, J. Am. Chem. Soc. 128, 4208, (2006).

[5] G. Gronoff, J. Lilensten, C. Simon, O. Witasse, R. Thissen, O. Dutuit, and C. Alcaraz, Astron. Astrophys. 465, 641, (2007).

[6] O. Dutuit, N. Carrasco, R. Thissen, V. Vuitton, C. Alcaraz, P. Pernot, N. Balucani, P. Casavecchia, A. Canosa, S. Le Picard, J.-C. Loison, Z. Herman, J. Zabka, D. Ascenzi, P. Tosi, P. Franceschi, S. D. Price, and P. Lavvas, Astrophysical Journal Supplement Series **204,** (2013).

[7] R. Thissen, O. Witasse, O. Dutuit, C. S. Wedlund, G. Gronoff, and J. Lilensten, Phys.Chem.Chem.Phys. 13, 18264, (2011).

[8] D. Schroder and H. Schwarz, J. Phys. Chem. A 103, 7385, (1999).

[9]   S. D. Price, Int. J. Mass Spectrom. 260, 1, (2007).

[10] M. A. Parkes, J. F. Lockyear, D. Schroeder, J. Roithova, and S. D. Price, Phys.Chem.Chem.Phys. 13, 18386, (2011).

[11] J. F. Lockyear, C. L. Ricketts, M. A. Parkes, and S. D. Price, Chemical Science 2, 150, (2011).

[12] J. F. Lockyear, M. A. Parkes, and S. D. Price, Angewandte Chemie International Edition 50, 1322, (2011).

[13] D. Ascenzi, P. Tosi, J. Roithová, C. L. Ricketts, D. Schröder, J. F. Lockyear, M. A. Parkes, and S. D. Price, Phys. Chem. Chem. Phys 10, 7121 (2008).

[14] J. Roithova, C. L. Ricketts, D. Schroder, and S. D. Price, Angew. Chem. Int. Edit. 4**6,** 9316, (2007).

[15] D. Ascenzi, P. Franceschi, P. Tosi, D. Bassi, M. Kaczorowska, and J. N. Harvey, J.Chem.Phys. 118, 2159, (2003).

[16] D. Ascenzi, J. Roithova, D. Schroder, E. L. Zins, and C. Alcaraz, J. Phys. Chem. A 113, 11204, (2009).

[17] J. D. Fletcher, M. A. Parkes, and S. D. Price, Chemistry-a European Journal **19,** 10965, (2013).

How do we reconcile the observed and modeled HCNH$^+$ density in Titan's ionosphere?

<u>Véronique Vuitton</u>, Roland Thissen
Institut de Planétologie et d'Astrophysique de Grenoble,
Université Joseph Fourier / CNRS, Grenoble, France.

Stephen J. Klippenstein
Chemical Sciences and Engineering Division,
Argonne National Laboratory, Argonne, IL, USA.

Panayotis Lavvas
Groupe de Spectrométrie Moléculaire et Atmosphérique,
Université de Reims Champagne-Ardenne / CNRS, Reims, France.

Erik Vigren
Swedish Institute of Space Physics, Uppsala, Sweden.

Roger V. Yelle
Lunar & Planetary Laboratory, University of Arizona, Tucson, AZ, USA.

Titan harbors an ionosphere in which solar photons and associated photoelectrons ($h\nu/e_s^-$) dissociate and ionize the major neutral molecules, N_2 and CH_4. The subsequent formation of complex ions has been observed by the Ion and Neutral Mass Spectrometer (INMS) onboard the Cassini spacecraft. The chain of reactions leading to these more complex species has been extensively studied through photochemical modeling, which reproduces the general composition of the ionosphere, with peak densities near 1150 km dominated by $HCNH^+$, $C_2H_5^+$, and CH_5^+.

It is however, a recurrent problem amongst Titan ionospheric models (from either the Cravens [1, 2], Waite [3, 4] or Yelle [5, 6] groups) that they predict an $HCNH^+$ density that is typically 2-3 and up to 5 times higher than observed by INMS. $HCNH^+$ being the major ion, this issue is associated to the overestimation of electrons in models assuming local balance between photoionization and ion-electron recombination [7].

A flowchart highlighting our current understanding of the reactions producing and consuming $HCNH^+$ is presented in Figure 1. Primary ions (N_2^+, N^+, CH_4^+) react with CH_4 to form CH_5^+, and $C_2H_5^+$ via CH_3^+. CH_5^+ and $C_2H_5^+$ further give a proton to HCN to produce $HCNH^+$. The latter is mostly lost by dissociative recombination with thermal electrons (e_T^-) and proton transfer to neutrals having a higher proton affinity (C_4H_2, C_2H_3CN, etc.). These primary steps of the chemistry have been validated with dedicated laboratory experiments performed by our group, at room temperature and below ([8] and unpublished results). We and others [4] have extensively focused on the discrepancy between observed and modeled $HCNH^+$ densities. A summary of these studies is given below.
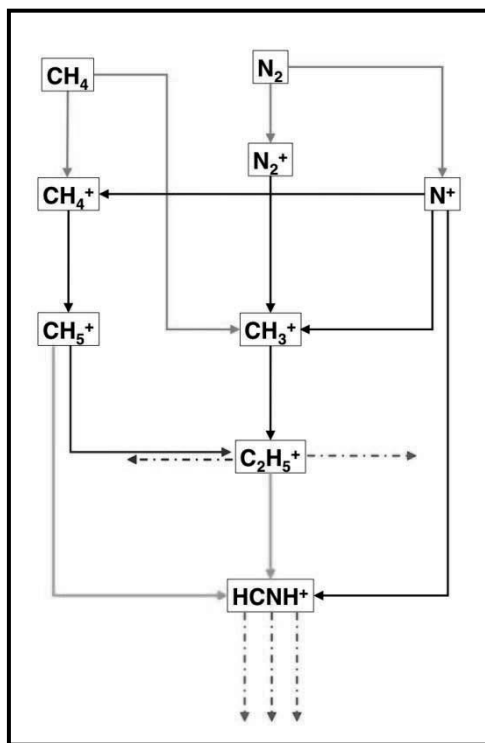
Figure 1: *Flowchart highlighting the very first steps of the ionospheric chemistry.*

Ionization ($h\nu/e_s^-$): orange. Ion-neutral reactions with CH_4 (black), C_2H_4 (blue), C_4H_2 (pink), HCN/HNC (cyan) and C_2H_3CN (red).
Ion-electron dissociative recombination (e_T^-): green.

1. <u>Primary ionization:</u> We have recently demonstrated that high-resolution cross-sections are necessary to accurately describe the photoionization of N_2 [9]. With these cross sections, the models can accurately reproduce the observed CH_3^+ and CH_4^+ densities but their impact on $HCNH^+$ is minor [3].

2. <u>Ion-molecule reactions:</u> Most of the reactions in Figure 1 have been extensively studied experimentally, and rate coefficients are well known, at least at room temperature [10] or can be reasonably assumed to be equal to the capture rate coefficient [5]. The temperature dependence of these rate coefficients is expected to be small and although branching ratios can exhibit a stronger dependency, the uncertainty on kinetic parameters associated to the low Titan temperature (150 K) cannot alone lead to a decrease of the $HCNH^+$ density by a factor of 2-3 ([11] and unpublished results).

3. <u>Electron recombination of $HCNH^+$:</u> Electron recombination is the major loss for $HCNH^+$. The electron recombination rate is dependent on both the electron density and temperature. Runs using different realistic sets of values for the electron density and temperature show that these parameters have some effect on the $HCNH^+$ density but cannot completely solve the problem. Both electron recombination rate constants available in the literature [12, 13] were also tested but none is fast enough to lead to a sufficient loss of $HCNH^+$ [4].

4. <u>Atmospheric parameters:</u> Another potential culprit for the model overestimation is the HCN atmospheric density, which is poorly constrained by INMS. However, while decreasing the HCN density has the desired effect of decreasing the $HCNH^+$ density, it does so at the expense of the CH_5^+ and $C_2H_5^+$ densities, which are as a consequence overestimated. Therefore, the HCN profile cannot be responsible for the $HCNH^+$ overestimation [4].

5. <u>Heavy species:</u> Large amounts of undetected heavy neutrals could lead to a significant loss of $HCNH^+$ through proton exchange reactions. However, the expected scale height of such species is incompatible with the large excess of $HCNH^+$ still observed at higher altitude. The positive - negative ion recombination rates and negative ion densities are too small to be competitive with ion - neutral reactions [4].

6. <u>Missing reactions of $HCNH^+$ with light species:</u> The reaction of $HCNH^+$ with H_2, CH_4, C_2H_2 or C_2H_4 would lead to enough destruction of $HCNH^+$ to reproduce the observations, were the rate coefficients close to 10^{-10} cm^3 s^{-1} [4]. This suggestion prompted some new experimental investigations, which confirm that the rates are much slower than required (typically $k < 5 \times 10^{-13}$ cm^3 s^{-1}) [14]. Theoretical calculations performed by one of us for $HCNH^+ + C_2H_4$ support those conclusions.

7. <u>Missing excited state of N^+</u>: The dissociative ionization of N_2 is known to lead to $N^+(^1D) + N(^4S)$ but so far, models only consider the production in the $N^+(^3P) + N(^2D)$ states [9]. The $N^+(^1D)$ state has a lifetime of 258 s [10] and its consideration in the calculations could in principal significantly impact the subsequent chemistry although in practice its effect is expected to be small [11].

8. <u>Different isomer of $[CH_2N^+]$</u>: The coexistence of two or more $[C H_2N^+]$ isomers in Titan's atmosphere could explain the observed discrepancy. Although the singlet linear $HCNH^+$ is the most stable form, four triplet isomers with stable geometries have been computed [15]. However, based on the reactions forming $[CH_2N^+]$ in the Titan models, linear $HCNH^+$ is likely the only isomeric form, in agreement with the observations in laboratory experiments [13, 14].

We showed that none of the above suggestions could satisfactorily solve the $HCNH^+$ problem. We hope that this presentation will trigger some suggestions of other missing processes that could be investigated.

References

[1] Cravens, T.E., et al., *Icarus*, 199, 174 (2009).
[2] Robertson, I.P., et al., *Planet. Space Sci.*, 57, 1834 (2009).
[3] Mandt, K.E., et al., *J. Geophys. Res.*, 117, #E10006 (2012).
[4] Westlake, J.H., et al., *J. Geophys. Res.*, 117, #E01003 (2012).
[5] Vuitton, V., R.V. Yelle, and M.J. McEwan, *Icarus*, 191, 722 (2007).
[6] Yelle, R.V., et al., *Faraday Discuss.*, 147, 31 (2010).
[7] Vigren, E., et al., *Icarus*, 223, 234 (2013).
[8] Thissen, R., et al., *J. Phys. Chem. A*, 113, 11211 (2009).
[9] Lavvas, P., et al., *Icarus*, 213, 233 (2011).
[10] Dutuit, O., et al., *Astrophys. J. Suppl. Ser.*, 204, #20 (2013).
[11] Carrasco, N., et al., *Planet. Space Sci.*, 56, 1644 (2008).
[12] McLain, J.L. and N.G. Adams, *Planet. Space Sci.*, 57, 1642 (2009).
[13] Semaniak, J., et al., *Astrophys. J. Suppl. Ser.*, 135, 275 (2001).
[14] Demarais, N.J., et al., *Struct. Chem.*, 10.1007/s11224 (2013).
[15] Holzmeier, F., et al., *J. Chem. Phys.*, 138, #214310 (2013).

High-Resolution Stark Spectroscopy of OH Containing Complexes in Helium Nanodroplets

Paul L. Raston[a,b], Tao Liang[a], <u>Gary E. Douberly</u>[a]

[a] *Department of Chemistry, University of Georgia, Athens, Georgia 30602, USA,*
douberly@uga.edu
[b] *School of Chemistry & Physics, The University of Adelaide, South Australia, 5005,*
paul.raston@adelaide.edu.au

The $X\,^2\Pi_{3/2}$ hydroxyl (OH) radical has been isolated in superfluid ^{4}He nanodroplets and probed with infrared (IR) laser depletion spectroscopy. From an analysis of the Stark spectrum of the $Q(3/2)$ transition, the Λ-doublet splittings are determined to be 0.198(3) and 0.369(2) cm^{-1} in the ground and first excited vibrational states, respectively. These splittings are 3.6 and 7.2 times larger than their respective gas phase values, which can be compared to the factor of 1.5 increase previously observed for NO by Havenith and co-workers [1]. A model is presented that assumes a realistic parity dependence of the rotor's effective moment of inertia and predicts a factor of 3.6 increase in the OH ground state (J=3/2) Λ-doubling when the B_0^e and B_0^f rotational constants differ by less than one percent.

We have also explored the low temperature (0.4 K) *in-situ* association reactions between OH and other small molecules, such as O_2, C_2H_2 and H_2O. Following the sequential pick-up and solvation of OH and O_2, the IR spectrum in the 3500-3700 cm^{-1} region reveals bands that are assigned to the ν_1 (OH stretch) fundamental and $\nu_1+\nu_6$ (OH stretch plus torsion) combination band of the covalently bound *trans*-HOOO isomer. Despite the characteristic low temperature and rapid cooling of helium droplets, there is no evidence for the formation of the previously predicted weakly bound OH-O_2 van der Waals complex, which implies the absence of a kinetically significant barrier in the entrance channel of the reaction. There is also no spectroscopic evidence for the formation of *cis*-HOOO, which is predicted by theory to be nearly isoenergetic to the *trans* isomer.

Stark spectroscopy of the *trans*-HOOO species provides vibrationally averaged dipole moment components that qualitatively disagree with predictions obtained from CCSD(T) computations at the equilibrium, planar geometry, indicating a floppy complex undergoing significant large-amplitude motion. A Hamiltonian in internal

bond-angle coordinates is derived to account for this large-amplitude motion, and the expectation values of the inertial dipole moment components are compared to those obtained from the Stark spectra, revealing a fundamental error in the underlying single-reference CCSD(T) potential energy surface.

The ro-vibrational a- (OH) and b-type (CH) stretching bands of the T-shaped OH-C_2H_2 complex reveal the effects of partially quenched electronic angular momentum. A model is presented, which accounts for this quenching phenomenon upon complex formation, along with a discussion of the expected He-solvation effects.

References

[1] K. von Haeften, A. Metzelthin, S. Rudolph, V. Staemmler, and M. Havenith, Phys. Rev. Lett. 95, 215301 (2005).

Ion mobility spectrometry: application to protein-ligand and metal-ligand complexes

Philippe Dugourd

Institut Lumière Matière, UMR5306 Université Lyon 1-CNRS, Université de Lyon 69622 Villeurbanne cedex, France

We developed a home-made 1 meter long drift tube coupled to a time-of-flight mass spectrometer. We will first use the competition between globular and helical structures for a transmembranar peptide issued from the M2 protein of the influenza virus to illustrate theoretical approaches developed to interpret experimental data. In a second series of examples, we will address the influence of formation of complexes on conformation. An unfolded to folded transition of a salivary intrinsically unstructured protein upon binding to tannins will be discussed. Clusters of tannins bound to the proteins have been identified, isolated and characterized. Finally, we will show how a global strategy for identification of structures and study of folding dynamics can include ion mobility spectrometry and gas phase spectroscopy. In particular, results on action-FRET will be displayed for the first time.
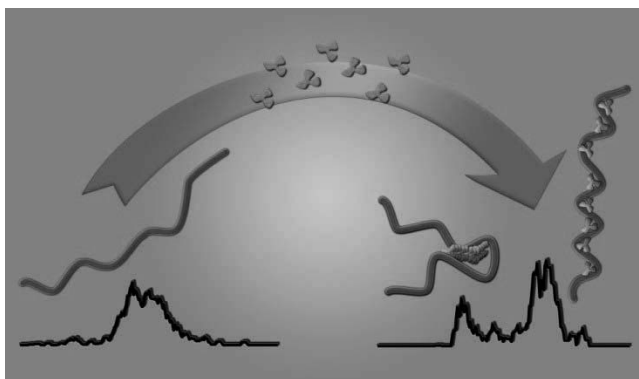
References

[1] B. Bellina, I. Compagnon, L. MacAleese, F. Chirot, J. Lemoine, P. Maître, M. Broyer, R. Antoine, A. Kulesza, R. Mitric, V. Bonacic-Koutecky and P.

Dugourd, *Binding motifs of silver in Prion octarepeat model peptides: a joint ion mobility, IR and UV spectroscopies, and theoretical approach.* Phys. Chem. Chem. Phys. 14, 11433-11440 (2012).

[2] F. Calvo, F. Chirot, F. Albrieux, J. Lemoine, Y. O. Tsybin, P. Pernot and P. Dugourd, *Statistical Analysis of Ion Mobility Spectrometry. II. Adaptively Biased Methods and Shape Correlations.* J. Am. Soc. Mass Spectrom. 23, 1279-1288 (2012).

[3] F. Canon, R. Ballivian, F. Chirot, R. Antoine, P. Sarni-Manchado, J. Lemoine and P. Dugourd. *Folding of a Salivary Intrinsically Disordered Protein upon Binding to Tannins.* J. Am. Chem. Soc. 133, 7847–7852 (2011).

[4] F. Albrieux, H. Ben Hamidane, F. Calvo, F. Chirot, Y. O. Tsybin, R. Antoine, J. Lemoine and P. Dugourd, *Structural Preferences of Gas-Phase M2TMP Monomers upon Sequence Variations.* J. Phys. Chem. A 115, 4711–4718 (2011).

Electron induced chemical reactions in water clusters

Martin K. Beyer

Institut für Ionenphysik und Angewandte Physik, Leopold-Franzens-Universität Innsbruck, Technikerstraße 25, 6020 Innsbruck, Austria, and Institut für Physikalische Chemie, Christian-Albrechts-Universität zu Kiel, Olshausenstraße 40, 24098 Kiel, Germany

Electrons solvated with water molecules in the gas phase not only exhibit interesting dynamics [1], but also a rich and multifaceted chemistry with small molecules. These fundamental chemical reactions can be studied by Fourier transform ion cyclotron resonance (FT-ICR) mass spectrometry [2].

Clusters of the composition $(H_2O)_n^{\bullet-}$, $n = 30\text{-}100$, provide an ideal medium to investigate one electron reductions. Several molecules have been found to undergo the first step of the Birch reduction, including acetonitrile [3], chlorobenzene [4], as well as di- and trifluorobenzene [5]. In these reactions, electron transfer to the incoming molecule is followed by proton transfer from the water cluster, reaction (1). A neutral, hydrogenated radical evaporates from the cluster, leaving behind $OH^-(H_2O)_m$. With the halobenzene molecules as reactants, however, Birch reduction competes with halogen abstraction, leading to formation of a hydrated halide ion, reaction (2).

$$(H_2O)_n^{\bullet-} + M \rightarrow OH^-(H_2O)_m + MH^\bullet + (n\text{-}m\text{-}1)\ H_2O \qquad (1)$$
$$(H_2O)_n^{\bullet-} + XR \rightarrow X^-(H_2O)_m + R^\bullet + (n\text{-}m)\ H_2O \qquad (2)$$
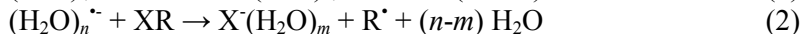
Electron induced bond cleavage is also observed with methyl mercaptane CH_3SH and dimethyldisulfide CH_3SSCH_3 [6]. The products, however, differ from the reactions with bulk hydrated electrons, presumably due to the reduced cage effect in gas phase clusters.

Many molecules, e.g. O_2 and CO_2, simply form hydrated radical anions. In these cases it is particularly interesting to analyze the thermochemistry of the reaction with nanocalorimetry [7]. These data in turn yield access to the hydration enthalpy of the radical anion in bulk solution.

Hydrated electrons are not only destructive. They may also induce oligomerization reactions, e.g. with acrylic acid, or the formation of five membered rings in the case

of methyl acrylate [8]. The complex reaction sequence of the latter reaction only became evident through the high mass resolution of the FT-ICR technique.

References

[1] R. M. Young, D. M. Neumark, Chem. Rev. 112, 5553-5577 (2012).

[2] O. P. Balaj, C.-K. Siu, I. Balteanu, M. K. Beyer, V. E. Bondybey, Int. J. Mass Spectrom. 238, 65-74 (2004).

[3] O. P. Balaj, I. Balteanu, B. S. Fox-Beyer, M. K. Beyer, V. E. Bondybey, Angew. Chem. Int. Ed. 42, 5516-5518 (2003).

[4] Y. Cao, R. F. Höckendorf, M. K. Beyer, Int. J. Mass Spectrom. 277, 206-209 (2008).

[5] R. F. Höckendorf, O. P. Balaj, M. K. Beyer, Phys. Chem. Chem. Phys. 13, 8924-8930 (2011).

[6] R. F. Höckendorf, Q. Hao, Z. Sun, B. S. Fox-Beyer, Y. Cao, O. P. Balaj, V. E. Bondybey, C.-K. Siu, M. K. Beyer, J. Phys. Chem. A, 116, 3824-3835 (2012).

[7] R. F. Höckendorf, C. van der Linde, O. P. Balaj, M. K. Beyer, Phys. Chem. Chem. Phys. 12, 3772-3779 (2010).

[8] K. Philip Jäger, Robert F. Höckendorf, Martin K. Beyer, Int. J. Mass Spectrom. 330/332, 246-253 (2012).

What are chiral molecules good for?

Jürgen Stohner

Zürich University of Applied Science (ZHAW), Institute of Chemistry and Biological Chemistry (ICBC), Campus Reidbach RC E0.40, Einsiedlerstrasse 31, CH 8820 Wädenswil, Switzerland,
Email: sthj@zhaw.ch

According to IUPAC, a chiral molecule contains an atom, which holds a set of ligands in such a spatial arrangement, which is not superimposable on its mirror image [1]; this definition is a generalized extension to the asymmetric carbon atom. Homo-chirality in Nature prefers *L*- over *D*-amino acids and *L*- over *D*-sugars [2]. Examining protein databases to look for post-translational modifications in proteins revealed that from the 187941074 amino acids documented in the database, only 837 *D*-isomers were found among which about 79 % were alanines [3]. One can imagine that far more chiral than non-chiral molecules exist. Chiral molecules are very important in pharmaceutical research. In order to fulfill the FDA's requirements for admission of drugs in the US, specifications for the final pharmaceutical product should assure identity, strength, quality, and purity from a stereo-chemical viewpoint – being a lesson learned from the contergan (thalidomide) case in the 1960's. Chromatographic separation of enantiomers proved important to investigate the teratogenic potential of thalidomide [4].

We focus on the role of chiral molecules at the border between chemistry and physics, also in relation to the current attempts to measure parity violating effects in molecular spectroscopy [5,6]. Parity violation in particle physics was first predicted and shortly thereafter experimentally verified by various research groups [7-9]. It was realized with delay that parity violation has an immediate consequence in chemistry, namely that it introduces a tiny energy difference between enantiomers isolated in the gas phase [10,11]. This implies that the heat of reaction for inter-conversion between enantiomers is different from zero, although very small, e.g. $\Delta_r H^0 \approx 10^{-14}$ kJ/mol in case of CHBrClF [12,13]. The energy difference between two enantiomers results in slightly different spectra with small shifts, independent of the spectral region considered. Various early attempts to measure those shifts in NMR [14] and Mössbauer [15] spectra have been reported, however, none of those with success. Optical spectroscopy in the infrared (and microwave) region are considered to be more suited for measuring frequency shifts because the molecular

system can be investigated under nearly isolated conditions; recent reviews summarize our current understanding of the role of molecular parity violation [1,2]. We have shown, however, that the interpretation of line shifts require a deep understanding of the high-resolution spectroscopy, including for example the influence of nuclear spin on molecular rotation [16].

Chiral methane derivatives are discussed in relation to efforts for experimental proofs of parity violation in molecules [1,2,17]. When a spectroscopic route is pursued [1,2], the separation of the target compound into its enantiomers is mandatory. In the past, the separation was achieved by fractional crystallization [17] – this method was introduced at the beginning of stereochemistry when Louis Pasteur separated large crystals of sodium ammonium tartrate using tweezers and a magnifying glass in 1848 [18].

Chromatographic separation of enantiomers is very difficult when large quantities (a few gram) are involved. While a separation on an analytical scale (a few microgram) is possible by using chiral stationary phases, there is no guarantee that a separation can be achieved by up-scaling using the same chiral column material. The search for column material, which facilitates such separation is of utmost importance but very difficult. We report our achievements in this respect [19].

Most recently, CHBrClF has been used to demonstrate the capability of gas-phase Coulomb explosion imaging (CEI) for the direct determination of the spatial atomic arrangement of molecules in the gas phase [20]. Next, the enantio-enrichment of *R*- and *S*-CHBrClF in large quantities is needed to demonstrate that COLTRIMS-CEI ("cold target recoil ion momentum spectroscopy") can be used to determine the absolute configuration in a direct manner under isolated conditions. We will report our most recent achievements towards this goal [21].

References

[1]   G. P. Moss, Pure & Appl. Chem. 68, 2193 (1996).
[2]   M. Quack, Angew. Chem. Int. Ed. 41, 4618 (2002).
[3]   G. A. Khoury, R. C. Baliban and C. A. Floudas, Scientific Reports 90, 1 (2011).
[4]   G. Blaschke, H. P. Kraft, K. Fickentscher and F. Köhler, Arzneimittelforschung 29, 1640 (1979).
[5]   M. Quack and J. Stohner, Chimia 59, 530 (2005).
[6]   M. Quack, J. Stohner, and M. Willeke, *Annu. Rev. Phys. Chem.* **59**, 741 (2008).

[7] C. S. Wu, E. Ambler, R. W. Hayward, D. D. Hoppes, and R. P. Hudson, Phys. Rev. 105, 1413 (1957).

[8] R. L. Garwin, L. M. Lederman, and M. Weinrich, Phys. Rev. 105, 1415 (1957).

[9] J. I. Friedman and V. L. Telegdi, *Phys. Rev.* **105**, 1681 (1957).

[10] Y. Yamagata, J. *Theoret. Biol*. **11**, 495 (1966).

[11] D. Rein*, J. Mol. Evol*. **4**, 15 (1974).

[12] M. Quack and J. Stohner, *Chirality* **13**, 745 (2001).

[13] M. Quack and J. Stohner, *Phys. Rev. Lett*. **84**, 3807 (2000).

[14] [14] A. Barra, J. Robert, and L. Wiesenfeld, *Phys. Lett. A* **115**, 443 (1986).

[15] A. Lahamer, S. Mahurin, R. Compton, D. House, J. Laerdahl, M. Lein, and P. Schwerdtfeger, *Phys. Rev. Lett*. **85**, 4470 (2000).

[16] F. Hobi, R. Berger and J. Stohner, Mol. Phys. 111, 2345 (2013).

[17] B. Darquié, C. Stoeffler, A. Shelkovnikov, C. Daussy, A. Amy-Klein, C. Chardonnet, S. Zrig, L. Guy, J. Crassous, P. Soulard, P. Asselin, T. R. Huet, P. Schwerdtfeger, R. Bast and T. Saue, Chirality 22, 870 (2010).

[18] L. Pasteur, C. R. Acad. Sci. Paris 26, 535 (1848).

[19] B. Spenger, MSc Thesis, ZHAW Wädenswil (2013).

[20] M. Pitzer, M. Kunitski, A. S. Johnson, T. Jahnke, H. Sann, F. Sturm, L. Ph. H. Schmidt, H. Schmidt-Böcking, R. Dörner, J. Stohner, J. Kiedrowski, M. Reggelin, S. Marquardt, A. Schiesser, R. Berger and M. S. Schöffler, Science 341, 1096 (2013).

[21] M. Mazenauer, *MSc Thesis*, ZHAW Wädenswil; in preparation.

Hot Topic Papers

Two-photon excitation by polarization shaped laser pulses for improved anisotropy contrast

Albrecht Lindinger

Institut für Experimentalphysik, FUB, Arnimallee14, D-14195Berlin, Germany e-mail: lindin@physik.fu-berlin.de

Polarization-shaped pulses are applied in order to improve the two-photon excited fluorescence contrast between two dyes by taking advantage of their molecular fluorescence anisotropy. This is reported for rhodamine B (RhoB) and stilbene 3 (Sti3) in glycerol through altering their fluorescence contrast by phase-shaping of perpendicular polarization directions.

1. Introduction

Fluorescence spectroscopy by multi-photon excitation enables to exploit nonlinear and interference effects [1]. This allows particularly for three-dimensional imaging by two-photon microscopy e.g. for conducting cancer diagnosis [2]. Polarization anisotropy can moreover provide information about molecular orientation, aggregation, and rotational diffusion, which is not accessible by other observables [3].

Recently it has been demonstrated that phase-shaped laser pulses can be used for selective two-photon excitation which yields higher contrasts than with spectral filters [4]. Not only shaping of phase and amplitude but also full control including polarization can be performed [5,6].

Here the selective excitation of two fluorescent dyes in glycerol by polarization-shaped laser pulses is reported. The pulses consist of two orthogonal linearly polarized sub pulses, where the phase of the horizontally polarized sub pulse is optimized to excite one dye while the phase of the vertically polarized sub pulse is optimized for the other dye. Due to fluorescence anisotropy the contrast between both fluorescence signals can be altered by using a polarizer before the detector. This method can be applied to improve imaging in medicine and biology.

2. Experiment

The laser pulses are delivered by a regenerative amplifier (RegA 9050, Coherent) with a repetition rate of 284 kHz. The FWHM was set to 24.5 nm at a central wavelength of 805 nm. The pulses were shaped by a spatial light modulator (SLM-640, CRi) having two liquid crystal arrays with optical axes at ±45° in a 4f-setup, consisting of two diffraction gratings of 1200 lines/mm and two cylindrical lenses of

250 mm focal length. The two arrays are used to generate two perpendicular linear polarized independently shaped pulses. One half-wave plate (HWP) is issued to compensate for different reflectivity in horizontal and vertical polarization. Another HWP is placed after the SLM-640 to rotate the polarization from +45° and −45° to 0° and 90°. This method of polarization shaping and its capabilities is described in ref. [7]. The shaped pulses with pulse energies up to 400 nJ are focused with a f = 50 cm lens into a cuvette filled with the dye solution. The fluorescence-signal is collected by two lenses which focus the light on a spectrometer behind a polarizer. A third HWP is used to measure the anisotropy. The pulses shapes are detected by recording cross-correlation traces for 10 different positions of the third HWP [8]. Polarization and anisotropy are calculated from cross-correlation traces and spectra, respectively. The dye concentration was 4 mM for Sti3 and 0.04 mM for RhoB.

Both dyes show two-photon absorption around 805 nm with different spectral slopes for Sti3 and RhoB. This enables to influence the fluorescence contrast by phase-shaping. The dye emission was distinguished with a spectrometer and both show high polarization anisotropy in glycerol. While the emission of RhoB has the same polarization for all wavelengths, Sti3 has two overlapping emission bands with perpendicular polarization [9,10]. This leads to a leap of the orientation curve around 460 nm. For the RhoB fluorescence and the longer wavelengths of the Sti3 fluorescence the principal axis of the polarization ellipse is parallel to the polarization of the exciting laser pulses. The anisotropy of Sti3 is matched to that of RhoB by selecting the range 520-540 nm. This condition is applied for polarization-shaping.

3. Theory

The fluorophore molecules are randomly oriented in a liquid. Most of the photo-excited molecules have transition dipole moments oriented close to the irradiating light polarization. The fluorescence polarization direction is in most cases parallel to the transition dipole moment, if the molecules do not lose their orientation by rotation. Anisotropy is defined as

$$a = \frac{I_{\parallel} - I_{\perp}}{I_{\parallel} + 2I_{\perp}} \qquad (1)$$

with the intensities $I_{\parallel}$ and $I_{\perp}$ being the two components of the fluorescence signal polarized parallel and perpendicular to the exciting light. $I_{\parallel}$ and $I_{\perp}$ itself are composed of the fluorescence components by the horizontally and vertically polarized part of the laser pulse.

The contrast between the fluorescence signals (I_1, I_2) of two dyes is

$$k(I_1, I_2) = \frac{I_1 - I_2}{I_1 + I_2} \,. \tag{2}$$

The contrast depends on polarization orientation and anisotropy of the fluorophores. The contrasts parallel and perpendicular to the polarization direction are $k_\parallel$ and $k_\perp$. The goal is to achieve a large difference

$$\Delta k(I_1, I_2) = \left| k_\parallel(I_1, I_2) - k_\perp(I_1, I_2) \right|. \tag{3}$$

This value is dependent on the fluorophores and the applied laser pulses.

4. Results
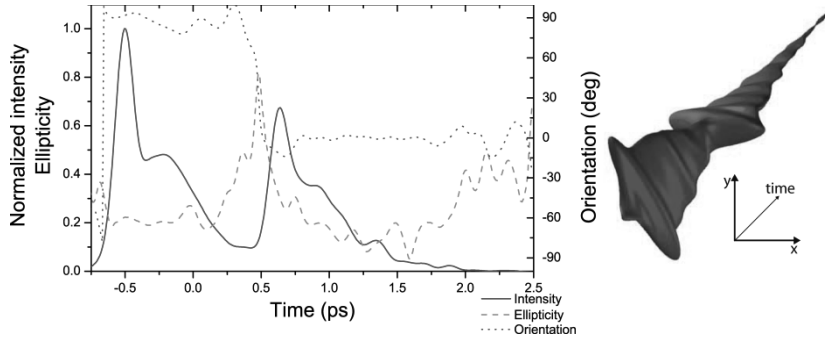
Figure 1: *Pulse shape to excite Sti3 in horizontal and RhoB in vertical polarization direction. On the left, intensity (solid line), ellipticity (dashed), and orientation (dotted) is displayed. A 3-dimensional pulse representation is shown right hand.*

To find pulse shapes leading to a high contrast, phases of the form

$$\varphi(\lambda) = A\left(\frac{c}{\lambda} - \frac{c}{\lambda_0}\right)^3 \tag{4}$$

were written on the modulator for different wavelengths λ_0. For each λ_0 the contrast k was calculated by taking the integrated intensities of the RhoB and Sti3 spectra. This was done separately for both modulator arrays. Due to the shape of the absorption curves the Sti3 fluorescence is higher for shorter wavelengths λ_0 whereas the RhoB fluorescence increases for longer λ_0. The maximal contrast difference, a measure for improved selectivity, is 0.3. The parameters used for polarization-shaping are A = $5 \cdot 10^5$ fs^3, $\lambda_0 = 792$ nm for a horizontally polarized sub pulse to efficiently excite Sti3 and $\lambda_0 = 816$ nm for a vertically polarized sub pulse to excite RhoB. These parameters were chosen to receive high contrast and similar intensities in both polarization directions. The temporal shape of this pulse measured by cross-correlation is shown in Fig. 1. Its emission spectra were recorded for different polarization angles.

For each direction the signal was integrated over the right part of the Sti3 spectrum (520–540 nm) and the whole RhoB spectrum (560–650 nm). The signals were normalized by dividing by the maximal value before calculating the contrast. The contrasts are shown in Fig. 2 in comparison to the contrasts of a linear polarized pulse. While the contrast of the linear pulse stays almost constant for all angles the contrast of the polarization-shaped pulse varies from −0.02 to 0.15. This exemplifies the improvement of using polarization shaped laser pulses for two-photon fluorescence.
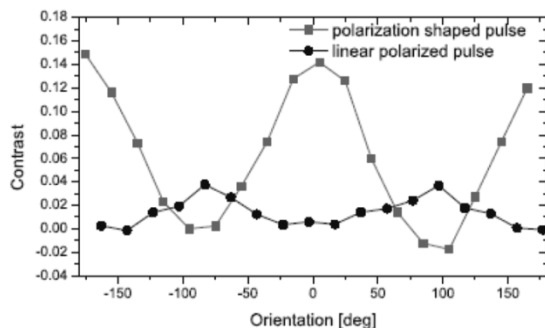
Fig. 2: Contrast between the 520–540 nm part of the Sti3 and the RhoB spectrum for the polarization shaped pulse from Fig. 1 (red squares) and a linear polarized pulse (black circles).

5. Conclusion

Improved fluorescence signal separation for two dyes with similar anisotropy was demonstrated by using polarization-shaped pulses. This method could be applied for imaging in biology and medicine.

References

[1]   V.V. Lozovoy, I. Pastirk, K.A. Walowicz, M. Dantus, JCP **118,** 3187 (2003)
[2]   S. Perry, R. Burke, E. Brown, Ann. Biomed. Eng. **40,** 277 (2012)
[3]   A.H.A. Clayton, Q.S. Hanley, D.J. Arndt-Jovin, V. Subramaniam, T.M. Jovin, Biophys. J. **83,** 1631 (2002)
[4]   J.P. Ogilvie, D. D´ebarre, X. Solinas, J.-L. Martin, E. Beaurepaire, M. Joffre, Opt. Express **14,** 759 (2006)
[5]   F. Weise, A. Lindinger, Opt. Lett. **34,** 1258 (2009)
[6]   F. Weise, G. Achazi, A. Lindinger, PCCP **13,** 8621 (2011)
[7]   M. Pawłowska, A. Patas, G. Achazi, N. Rahmat, F. Weise, A. Lindinger, J. Opt. Soc. Am. B **29,** 833 (2012)
[8]   M. Plewicki, F. Weise, S.M. Weber, A. Lindinger, AO **45,** 8354 (2006)
[9]   A.J.W.G. Visser, K. Vos, A. Van Hoek, J.S. Santema, JPC **92,** 759 (1988)
[10] N. Sanz, A. Ibanez, Y. Morel, P.L. Baldeck, APL **78,** 2569 (2001)

Wave packet dynamics of the gas phase collision reaction of chloride and methyl iodine

Markus Kowalewski
Division of Scientific Computing, Uppsala University, Uppsala, Sweden
Regina de Vivie-Riedle
Department of Chemistry, Ludwig-Maximilians University, München, Germany

1. Introduction

The bimolecular substitution reaction of chloride and methyl iodine belongs to a fundamental class of chemical reactions. In solution it is a very well understood reaction serving as an essential everyday tool in organic and inorganic synthesis. In contrast to the behaviour in solution the reaction shows many facets in the gas phase which offer the possibility to distinguish solvent effects from the intrinsic dynamics. The gas phase reaction has been investigated experimentally in a crossed beam experiment [1] as well as by on-the-fly trajectory calculations [2].

In this contribution we employ quantum dynamical wave packet calculations to study the S_N2 reaction. Bond breaking and formation occurs on the subpicosecond time scale and the associated energy redistribution among the internal molecular and translational degrees of freedom is followed in detail. We inspect the dominant reaction mechanism – the so called Walden inversion where the nucleophile attacks from the backside under the inversion of the CH_3 group. We use specially designed reactive coordinates which allow for an efficient description of the reaction, including the role of the spectator mode (CH_3 umbrella motion). It is known from experiments [1] and theoretical studies [2] that in this direct rebound mechanism the reactivity is suppressed even though there is no net barrier. The quantum dynamical calculations show that the reaction is not sufficiently characterized by the stationary points on the potential energy surface (PES) but by its dynamical properties.

2. Theoretical approach

For the quantum dynamical description of the reaction to be possible a set of suitable reactive coordinates has to be chosen. A full dimensional description would involve 15 degrees which is not treatable by a direct spatial discretization. A collinear geometry as depicted in Fig. 1 is chosen which implies a strict C_{3v} symmetry. For the collision of the chloride and the methyl iodine the most important coordinates are the

iodine-carbon distance (r_{CI}) and the chloride-carbon distance (r_{CCl}). During the reaction the angle of the H-atoms in the CH3 group (Θ) also changes (umbrella motion). With this set of coordinates a quantum dynamical calculation on a regular spatial grid would already be possible but not very efficient. This choice would also include regions on the potential energy surface which are of no relevance at collision energies below 3.5 eV. The molecular coordinates r_{CI}, r_{CCl}, and Θ are thus expressed as functions of a set of new reactive coordinates called q_1, q_2, and q_3 by a unique transformation. The coordinate q_1 represents the intrinsic reaction coordinate (IRC). The coordinate q_2 describes a parallel shift of the IRC path in the r_{CI}-r_{CCl} plane. The third coordinate coordinate q_3 is related to a parallel shift of the IRC path along Θ. To carry out the wave packet calculations the time dependent Schrodinger equation is solved numerically on a spatial grid. The IRC path and the involved PES is determined in a quantum chemical calculation (MP2/ECP46MWB/aug-cc-pVDZ).
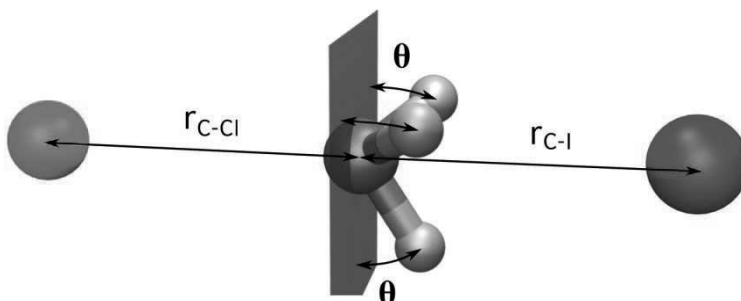
Figure 1: *The geometry for the gas phase collinear collision reaction of methyl iodine and chlorine. The figure shows the choice of coordinates which are of major importance for the reaction: The CCl and the CI bond are directly involved in the bond formation and bond cleavage process. The angle of the Hydrogen atoms Θ is called umbrella motion. It follows the reaction and undergoes and inversion.*

3. Results

In previous experiments a suppressed direct reaction has been observed [1] for relative energies below 0.5 eV. With the model explained in Sec. 2 it is possible to observe the direct collision dynamics. Processes which are due to rotation or the energy redistribution in internal degrees of freedom other than the CI bond are not included. Under experimental conditions those excluded effects lead to trapping in the anion-dipole complex and increase in the overall reaction probability but on a much longer time scale which is dominated by the rotation of the complex. The presented reaction probabilities have to be considered as a relative measure.

In Fig. 2 the reaction probabilities for different relative energies are shown. Even though there is no net barrier in the system about 0.55 eV is required to obtain a 50 % reaction probability. Experimental results show a similar qualitative trend. For smaller energies the major part of the wave packet is reflected back since the coupling between the CCl bond and the CI bond is not sufficient. To study the influence of the umbrella mode on the reaction, this mode can be included in the model as active coordinate (3D) or as a relaxed coordinate (2D). Comparison of the reaction probabilities of both models against each other shows that the reaction probabilities are shifted to smaller relative energies. However no fundamental difference in the mechanisms could be found. It can be concluded that the umbrella mode serves as a correction to the quantitative description.

Moreover from the analysis of the propagated wave packets an intuitive concept of a dynamical barrier can be derived. By looking at the time dependent position expectation values of the transmitted wave packet it becomes clear that the major part of the wave packet has to overcome a significant barrier on the multi-dimensional PES. We define the dynamic barrier as the maximum of the projection of the wave packet path onto the potential. The height of the dynamic barrier scales linear with the relative collision energy. The dynamic barrier reflects the dynamical reaction path and adapts the familiar concepts of stationary points on the PES like a transition state to dynamics.
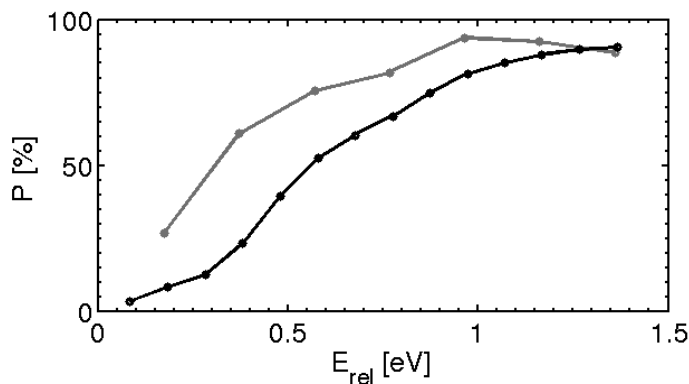
Figure 2: Calculated relative reaction probabilities for the direct rebound mechanism versus relative energy. A main feature of the reaction is the suppressed reactivity of the reaction. This feature is qualitatively reproduced in the 2D model of the direct reaction (black, solid line). The comparison with the 3D model shows the influence of the spectator mode (grey, solid line): The reactivity is slightly increased (shifted by ≈ -0.2 eV).

4. Conclusion

We have shown wave packet calculations in a reduced dimensionality model which resolves the direct rebound mechanism and reproduces its main features. A novel concept for the representation of the direct usage of the reaction path and its parallel shifts allows for a efficient description on a spatial grid covering a limited energy range of interest on the PES.

References

[1] J. Mikosch, S. Trippel, C. Eichhorn, R. Otto, U. Lourderaj, J. X. Zhang, W. L. Hase, M. Weidemüller, and R. Wester, *Science* **319**, 183 (2008).
[2] J. Zhang, U. Lourderaj, R. Sun, J. Mikosch, R. Wester, and W. L. Hase, *J. Chem. Phys*. **138**, 114309 (2013).

Interaction of Be surfaces with fusion relevant seeding impurity and fueling ions

K. Dobes, F. Aumayr

Institute of Applied Physics, TU Wien, Association EURATOM-ÖAW, Vienna, Austria

M. Köppen, Ch. Linsmeier

Institute of Energy and Climate Research - Plasma Physics, Forschungszentrum Jülich GmbH, Association EURATOM-FZJ, 52425 Jülich, Germany

M. Oberkofler, T. Höschen

Max-Planck-Institut für Plasmaphysik, EURATOM Association, 85748 Garching, Germany

C. P. Lungu, C. Porosnicu

National Institute for Laser, Plasma and Radiation Physics, Bucharest, Romania

1. Introduction

The international experimental fusion reactor ITER is being built in the south of France. Its aim is to demonstrate the usability of fusion for commercial energy production. ITER will be the first fusion machine to ever produce net energy, with a goal of delivering ten times the energy it consumes.

The interaction of a fusion plasma with the walls of its containing vessel will however constitute one of the key challenges in the successful realization of a future fusion power plant. A profound knowledge about sputtering yields of plasma facing components under the impact of fusion relevant ion species is hence desired. The evolution of plasma facing materials like beryllium in the environment of a burning fusion plasma, especially also the mixing of materials, is of considerable interest. In addition, also the retention of hydrogen isotopes in plasma facing components is of major concern. Particularly the build-up of a tritium inventory within the plasma vessel imposes operational limits due to safety considerations.

ASDEX Upgrade was the first fusion machine to operate with a full tungsten wall [1]. In order to reduce the power loads to the divertor target plates at the bottom of the machine to acceptable values, radiation cooling is essential [2]. With the elimination of carbon as a plasma facing material in an all-metal wall fusion device however, radiation cooling from intrinsic impurities does no longer suffice and has to be replaced by the seeding of additional impurities [2]. In ASDEX upgrade nitrogen

seeding with feedback control has successfully matured into a standard operational scenario [1].

In this work we present detailed studies of the interaction of N as well as deuterium ions with a Be surface. On the one hand we investigated transient surface conditions, where one can observe the build-up of a surface layer containing N and D respectively. In addition we also studied steady state conditions, where the formation and the erosion of this modified surface layer is in dynamic equilibrium.

2. Experimental setup

We investigated total sputtering yields of BE surfaces at IPP Garching using a highly sensitive quartz crystal microbalance (QCM) technique developed at TU Wien [3-4]. The centerpiece of the setup is a stress compensated (SC) cut quartz crystal, which is driven at its thickness shear mode in series resonance at a resonance frequency of about 6 MHz. One side of the quartz crystal is coated with a 500 nm thick Be layer. The Be surfaces are fabricated by thermionic vacuum arc deposition at the National Institute of Laser, Plasma and Radiation Physics in Bucharest [5]. They were transferred in air before being installed in a vacuum chamber for sputtering yield investigations. The Be samples used in our studies thus exhibit a native oxide layer on the surface.

Total mass changes of the target film are determined from a change in resonance frequency of the quartz crystal according to the relation $\Delta f/f = -\Delta m/m$ [6]. In our experiments the sputtering yield is derived from the slope of a fit to the frequency-change curve with fluence.

In order to minimize influences of temperature changes during ion bombardment on the resonance frequency of the quartz crystal, measurements were always conducted at 192°C, which is a temperature where the resonance frequency of the quartz is least sensitive to temperature fluctuations. A sophisticated electronics permits the detection of mass changes of as small as 0.2 amu/ion·nA/cm^2 [3], corresponding to mass changes of approximately $5 \cdot 10^{-5}$ Be monolayers per second.

A schematics of the experimental setup can be found in figure 1. The quartz is mounted on a sample holder in a UHV chamber at a base pressure of approximately $1 \cdot 10^{-9}$ mbar. It is equipped with a faraday cup for frequent ion current density determination in between surface sputtering.
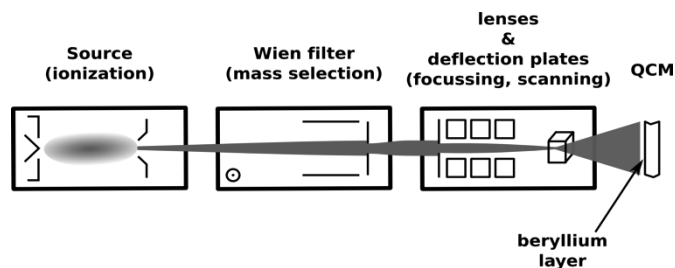
Figure 3 Schematic of the experimental setup (not to be scaled)

The N_2^+ as well as D_2^+ ions used in our studies were produced in an electron impact ion source (SPECS IQE 12/38). The source is equipped with a Wien filter, which is used to select a specific mass from the extracted ion beam. By means of two lenses and a pair of deflection plates, the extracted ion beam is guided and focused onto the sample position in the experimental chamber. By applying AC voltages of different frequency to the deflection plates, the beam is rapidly scanned over the whole active area of the crystal in order to guarantee an accurate determination of the ion current and to avoid mechanical stress due to non uniform mass removal.

3. Results

In-situ and in-real-time investigations of the total sputtering yield of Be surfaces under N_2^+ and D_2^+ ion impact respectively were conducted under controlled laboratory conditions. In particular the evolution of the mass change per incident projectile, as a function of the applied cumulative ion fluence was determined for both ion species.

When bombarding a virgin Be sample by 5 keV N_2^+ ions (corresponding to. 2.5 keV per N constituent), one finds that the observed rate of mass change depends strongly on the applied ion fluence (at constant flux). This is most significant for very low fluences. The interaction of the N projectiles and the Be surface is first dominated by a high net erosion. This fast mass loss can most likely be attributed to the removal of loosely bound adsorbates. It is followed by a net mass increase due to dominant N implantation. After some 10^{17} N per cm^2 have been applied to the surface, equilibrium surface conditions are established, i.e. the net mass change per impinging ion is furthermore independent from the ion fluence. In steady-state a net mass decrease is observed. This behavior can be ascribed to the formation of a Be nitride surface layer within the ion penetration range as it has been observed in recent studies [7].

Subsequently, sputtering yields of the so-formed Be nitride layer under steady state conditions, i.e. were the formation and the erosion of the modified surface layer is in dynamic equilibrium, were in investigated for different N_2 projectile energies.

In a similar way experiments using D_2^+ ions were conducted. The evolution of the mass change per incident D projectile was determined for both, a previously N saturated Be nitride surface as well as a virgin Be sample. In both cases for low D fluences again a regime of net mass increase is observed, as a result of dominant D implantation. Steady state surface conditions are reached after an accumulated ion fluence of more than 10^{18} D per cm^2. For the virgin Be surface approximately twice the fluence is needed to reach steady state as in the case of the Be nitride surface.

References

[1] A. Kallenbach, R. Dux, J.C. Fuchs et al., Plasma Phys. Control. Fusion **52** (2010), 055002

[2] J. Rapp, G.F. Matthews, P. Monier-Garbet et al., J. Nucl. Mat. **337 – 339** (2005), 826

[3] G. Hayderer, M. Schmid, P. Varga, HP. Winter and F. Aumayr, Rev. Sci. Instrum. **70** (1999), 3696

[4] A. Golczewski, K. Dobes, G. Wachter, M. Schmid and F. Aumayr, Nucl. Instrum. and Meth. B **267** (2009), 695

[5] C. P Lungu, I Mustata, V. Zaroschi, A. M. Lungu, P. Chiru, M. Rubel, P. Coad and G.F. Matthews, Phys. Scr. **T 128** (2007), 157

[6] G. Sauerbrey, Z. Phys. **155** (1959) 206

[7] M. Oberkofler and Ch. Linsmeier, Nucl Fusion **50** (2010), 125001

Surface scattering of oriented and velocity controlled diatomic molecules

Nils Bartels, Kai Golibrzuch, Christof Bartels, Fabian Grätz, Daniel P. Engelhart, Tim Schäfer

Institute of Physical Chemistry, Georg-August University of Göttingen, Tammannstraße 6, 37077 Göttingen, Germany

Chen Li, Daniel J. Auerbach, Alec M. Wodtke

Department of Dynamics at Surfaces, Max Planck Institute for Biophysical Chemistry, Am Faßberg 11, 37077 Göttingen, Germany

1. Introduction

How molecules point in space—that is, their spatial orientation—determines how they interact with their environment. Exchange of energy, photons, and particles as well as chemical reactions are all elementary processes that depend on orientation. Electron transfer reactions are of particular interest because of their importance in a remarkably wide range of phenomena.

In this work, we examine electron transfer reactions at surfaces, which control the change of oxidation state in surface chemistry, a critical factor understanding catalytic activity and selectivity.

Two different approaches are presented. In a first experiment we studied the incidence translational energy dependence of steric effects in electronically non-adiabatic collisions of $NO(v = 3)$ molecules with a Au(111) surface.[1] We employed a recently developed technique to orient beams of vibrationally excited NO molecules at incidence energies of translation between 0.08 and 0.89 eV.[2]

We find a strong orientation dependence for vibrational relaxation of a diatomic molecule colliding with a metal surface, an energy transfer process driven by electron transfer. These observations represent a challenge to modern theories of surface chemistry.

In a second approach we investigated the relaxation mechanism of electronically excited molecules at surfaces. For this, we combined a Stark decelerator with a molecular beam-surface scattering setup and investigated the quenching of metastable CO* ($a^3\Pi$) at a clean Au(111) surface.[3] We further studied the effect of

surface coverage on the relaxation process and found a strong correlation between the coverage and the emission of surface electrons.

2. Experimental

The results presented here have been produced on two different experimental setups. Steric dependence studies of the vibrational relaxation probability of NO($v = 3$) in collisions with a Au(111) surface have been performed on a typical molecular beam surface scattering apparatus equipped with a high voltage orientation electrode shown in Fig. 1.
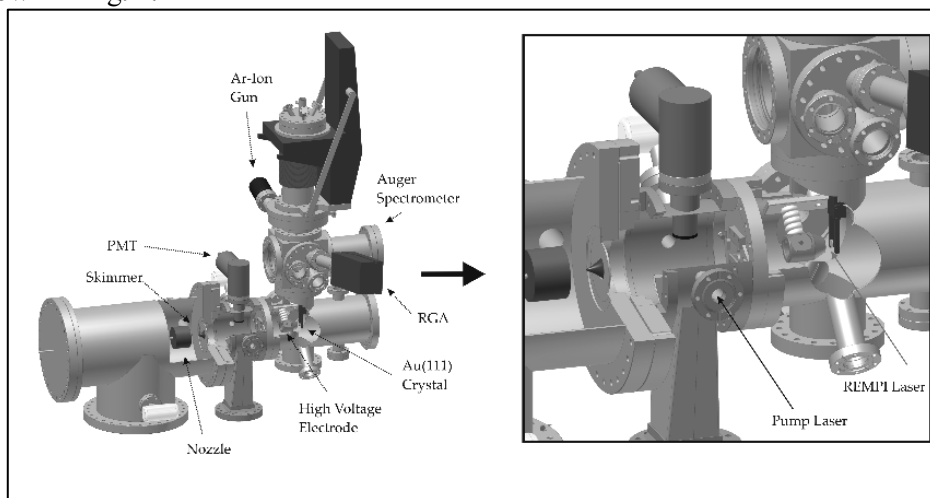
Figure 4: *Experimental setup of the orientation experiments. The molecular beam originates at the nozzle on the left side of the experiment. The high voltage electrode is mounted close to the surface enabling orientation of NO molecules employing the linear Stark effect.*

Measurements on electronically excited CO have been carried out on a UHV surface scattering chamber combined with a Stark decelerator as depicted in Fig. 2. A decelerated molecular beam pulse of metastable CO molecules is scattered from a Au(111) surface. The surface can be temperature controlled between 25 K and 1000 K and the chamber is equipped with a temperature programmed desorption (TPD) device. This allows a controlled coverage of the surface with a variety of different adsorbates.
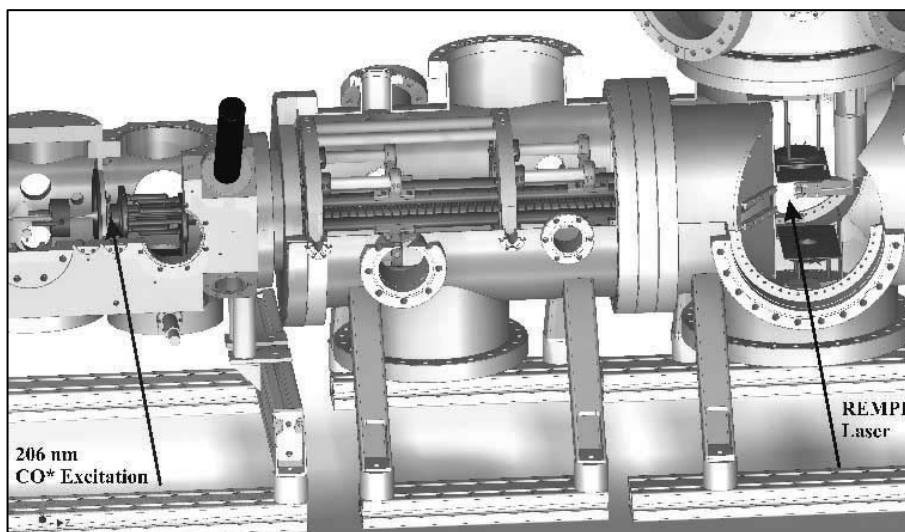
Figure 5: Cutout of the experimental apparatus of the metastable CO experiment. The molecular beam is produced at the nozzle (red) and passes hexapole (green) and decelerator (orange) before entering the UHV chamber. The Au(111) surface is mounted to a movable sample holder (orange) and can be temperature controlled between 25 K and 1000 K.

3. Results

Both studies investigated the influence of the scattered molecules' incidence conditions on the relaxation process.

The results obtained by scattering vibrationally excited NO from Au(111) clearly suggest a relaxation mechanism that strongly depends on the orientation of the colliding molecules: The survival probability of NO($v = 3$) is drastically reduced when the NO molecule hits the surface with the N-atom first. See Fig. 3.

In contrast, the influence of the CO* molecule's incidence conditions on the relaxation mechanism in metastable quenching on Au(111) is much weaker. No incidence translational energy dependence could be observed. However, the composition of the surface drastically affects the electron emission during the quenching process. Even a monolayer of an adsorbed rare gas can increase the electron emission yield by a factor of ~3.5.
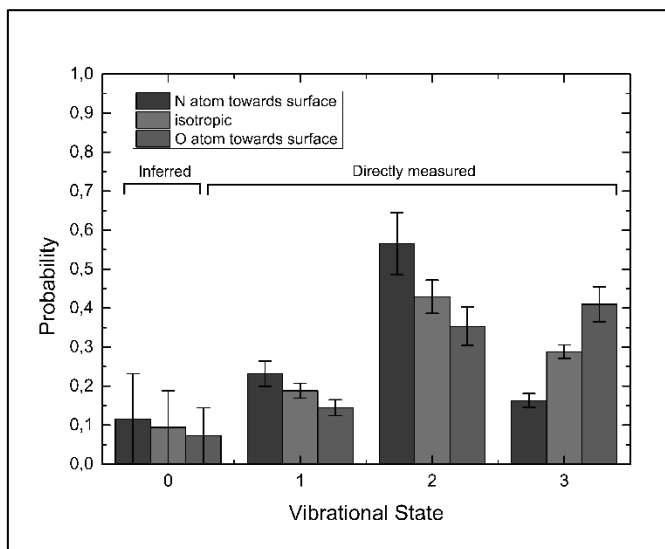
Figure 6: *Vibrational state distributions of: 1) scattered unoriented NO(v=3) (green bars), 2) NO(v=3) with an incidence orientation of O-atoms pointing towards the surface (red bars), and 3) NO(v=3) scattered with an incidence orientation of the N-atoms pointing towards the surface (blue bars) from a Au(111) surface.*

4. References

[1] Bartels, N.; Golibrzuch, K.; Bartels, C.; Chen, L.; Auerbach, D. J.; Wodtke, A. M.; Schäfer, T., Observation of orientation-dependent electron transfer in molecule–surface collisions. *Proceedings of the National Academy of Sciences* **2013**.

[2] Schäfer, T.; Bartels, N.; Hocke, N.; Yang, X.; Wodtke, A. M., Orienting polar molecules without hexapoles: Optical state selection with adiabatic orientation. *Chemical Physics Letters* **2012,** *535* (0), 1-11.

[3] Gratz, F.; Engelhart, D. P.; Wagner, R. J. V.; Haak, H.; Meijer, G.; Wodtke, A. M.; Schafer, T., Vibrational enhancement of electron emission in CO (a3Π) quenching at a clean metal surface. *Physical Chemistry Chemical Physics* **2013,** *15* (36), 14951-14955.

Vibrationally Promoted Chemisorption of Water on Ni(111)

P. Morten Hundt, Maarten E. van Reijzen, and Rainer D. Beck
Group for Gas-Surface Dynamics,
Labaratoire de Chimie Physique Moléculaire
Ecole Polytechnique Fédéral de Lausanne, Switzerland

The dissociation of water on transition-metal surfaces plays a major role in heterogeneous catalytic reactions, like steam reforming or the water-gas-shift reaction. Despite this importance no experimental studies on the dynamics of the dissociative chemisorption of water on metal surfaces have been reported. However, ab-initio work of several groups predicts vibrational activation of the dissociative chemisorption of water on Cu(111) surfaces[1-4].

In our study, we combine a molecular beam/surface science apparatus with powerful continuous wave (cw) infrared lasers to investigate the influence of selective vibrational excitation on the chemisorption of D_2O on a Ni(111) single crystal surface. A molecular beam of water with well defined speed is sent to the solid surface. Before the collision the water molecules are excited to specific rovibrational states with one quantum or two quanta of O-D stretch by double-resonance laser excitation. Auger electron spectroscopy is used to quantify the dissociative chemisorption probabilities at a surface temperature above the desorption temperature of molecular water. The dissociation probability of water on Ni(111) is greatly increased if the molecules are prepared in v=2 by rovibrational excitation. To the best of our knowledge, we present the first experimental proof of vibrational enhancement of water dissociation on a metal surface.

The results of this study will help to clarify the role of vibrational energy transfer in the dissociation of water on metal surfaces and will serve as a stringent test for theoretical studies and hence contribute to a detailed predictive understanding of the mentioned processes.

References

[1] Jiang, B.; Li, J.; Xie, D.; Guo, H. *J. Chem. Phys.* **2013**, *138*.
[2] Jiang, B.; Ren, X.; Xie, D.; Guo, H. *Proceedings of the National Academy of Sciences of the United States of America* **2012**, *109*, 10224.
[3] Jiang, B.; Xie, D.; Guo, H. *Chemical Science* **2013**, *4*, 503.
[4] Mondal, A.; Seenivasan, H.; Tiwari, A. K. *J. Chem. Phys.* **2012**, *137*.

Cation reactions in electron-initiated chemistry

Esther Böhler, Jonas Warneke, Petra Swiderek

Universität Bremen, Fachbereich 2 (Chemie/Biologie), Institute of Applied and Physical Chemistry, Leobener Straße / NW 2, Postfach 330440, 28334 Bremen, Germany

1. Introduction

Electron attachment and the consequent formation of anions have been and remain at the focus of interest in the field of electron-initiated chemistry. Such resonant processes occur at well-defined incident electron energies and are thus easily recognized among the different electron-molecule interaction mechanisms [1,2]. Also, dissociative electron attachment (DEA) can be highly selective, i.e., lead to rupture of specific bonds within a molecule [3]. However, electron impact ionization near threshold where formation of the intact molecular radical cation dominates or the number of fragmentation channels is still limited can also initiate well-defined reactions. This is even highly appealing because the intact radical cation is the largest possible reactive species and thus can induce syntheses that may be classified as *atom-efficient* and are relevant to areas as diverse as surface functionalisation and astrochemistry [4]. This contribution reviews typical radical cation reactions as known from organic chemistry [5] and their relevance to the study of electron-initiated chemistry in the condensed phase [4].

2. Radical cation chemistry – an overview

The reactivity of radical cations has been reviewed previously from the perspective of organic synthetic chemistry [5]. Radical cations in their ground states are formed near the ionization threshold by removal of an electron from the HOMO of closed-shell molecules which may have σ-, π-, or non-bonding (n) character and defines the site within the molecule from which the charge is removed, the so-called electrophore. Typically, ionization from π and n orbitals can produce an intact molecular radical cation and is thus of interest for synthesis while ionization from a σ orbital leads to dissociation of the respective bond.

Besides bond dissociation, radical cations undergo different types of reactions relevant to electron-initiated synthesis (Fig. 1). Of particular interest are cycloadditions and the addition of the radical cation to a nucleophil as these can couple a given reactant to a variety of other molecules. Recombination of the radical cation with another radical is likely if concurrent ionization processes lead to both

the intact molecular radical cation and a cation and radical pair. Recombination of the radical cation with the molecular radical anion $[M]^{\bullet-}$, however, is unlikely as the latter is usually formed only at near-thermal E_0 and thus considerably below the threshold for ionization and consequent formation of $[M]^{\bullet+}$. It would require the low-energy secondary electron released upon ionization to be trapped by an adjacent molecule yielding $[M]^{\bullet-}$.

A particular property of organic radical cations is their strong acidity. This can lead to proton transfer in the condensed phase and should also be considered when explaining the outcome of an electron-induced reaction.

Generation of radical cation:

◯-A-B $\xrightarrow{-e^-}$ ⊕-A-B

Decay of the radical cation:

⊕-A-B ⟶ ⊙-A + B⁺ or ⊕-A + B•   Dissociation

⊕-A-H ⟶ ⊙-A + H⁺   Deprotonation

⊕-A-B ⟶ ⊕-B-A   Rearrangement

⊕-A-B $\xrightarrow[or +e^-]{-e^-}$ ⊕-A-B or ◯-A-B   Electron transfer
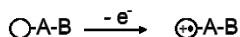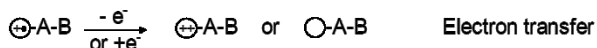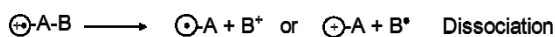
Reaction with closed-shell molecules:

⊕-A-B + Nu ⟶ Nu-⊙-A-B⁺   Attack of nucleophil

⊕-A-B + C-D ⟶ Cyclic product   Cycloaddition

⊕-A-H + Nu ⟶ ⊙-A + H-Nu⁺   Proton transfer

Reaction with second reactive intermediate:

⊕-A-B + R• ⟶ R-⊕-A-B   Radical attack

2⊕-A-B ⟶ (◯-A-B)²⁺   Dimerization

⊕-A-B + RA⁻• ⟶ RA-◯-A-B   Reaction with radical anion

Figure 1: *Schematic of typical reactions of radical cations. The circle refers to an electrophore of either π- or non-bonding character.*

3. Chemical synthesis initiated by electron impact ionization [4]

An example for a reaction of an intact molecular radical cation with a nucleophil is the formation of ethylamine ($C_2H_5NH_2$) in condensed mixtures of ethylene (C_2H_4) and ammonia (NH_3). The reaction is driven by strong Coulomb forces between

adjacent molecules arising after ionization (Fig. 2). Here, because of similar ionization thresholds, both reactants can acts as either the radical cation or the nucleophil. The stable neutral product then results upon neutralization of the ethylamine radical cation by recombination with thermalized electrons present in the molecular layer during electron exposure:
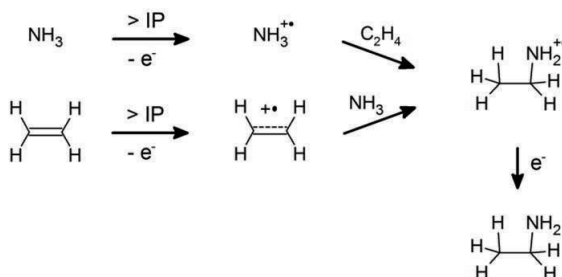
Figure 2: *Radical cation reaction with a nucleophil explaining the electron-induced formation of ethylamine from ethylene and ammonia.*

Proton transfer resulting from the strong acidity of radical cations can also explain the formation of specific products. As an example, 2-propanol was detected following electron exposure onto condensed layers of acetaldehyde (Fig. 3). Here, ionization leads to proton transfer to an adjacent acetaldehyde and dissociation of the remaining $[H_3CCO]^{\bullet}$ fragment to CO and a CH_3 radical. The radical can then add to the protonated acetaldehyde yielding the 2-propanol radical cation. Neutralization by thermalized electrons then again yields the final product.
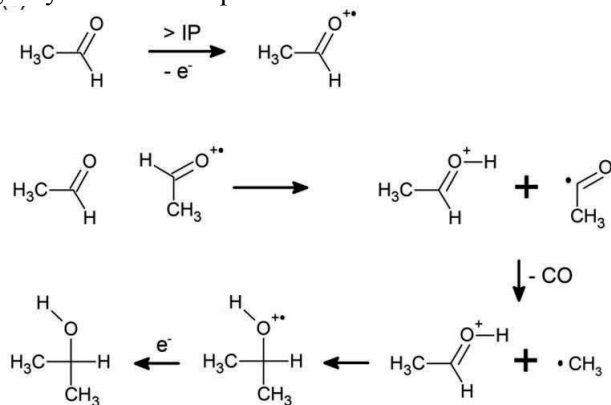
Figure 3: *Proton transfer reaction explaining the electron-induced formation of 2-propanol from acetaldehyde in condensed molecular layers.*

Finally, electron-impact ionization of hexamethyldisiloxane (HMDSO, $(CH_3)_3SiOSi(CH_3)_3$) yields [HMDSO-CH_3]$^+$ as dominant fragment at least within the first 10 eV above the ionization threshold. The undercoordinated cationic Si site of [HMDSO-CH_3]$^+$ can react with further HMDSO to form an intermediate with trivalent and positively charged oxygen which eliminates tetramethylsilane ($Si(CH_3)_4$) to yield a longer linear siloxane cation (Fig. 4).
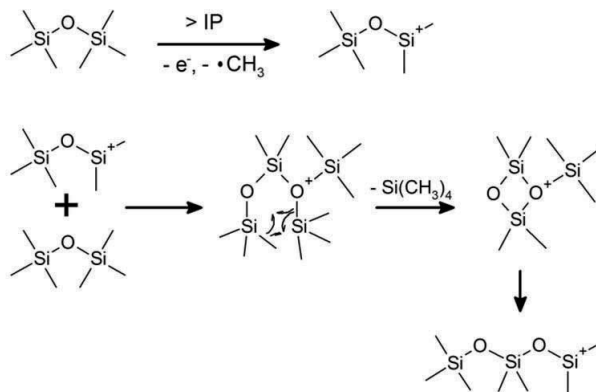
Figure 4: *Cation reaction explaining the electron-induced formation of larger siloxanes from HMDSO.*

References

[1] C.R. Arumainayagam, H.-L. Lee, R.B. Nelson, D.R. Haines and RP. Gunawardane, *Surf. Sci. Rep.*, 2010, **65**, 1-44.

[2] I. Bald, J. Langer, P. Tegeder and O. Ingólfsson, *Int. J. Mass Spectrom.*, 2008, **277**, 4-25.

[3] P. Swiderek, *Angew. Chem. Int. Ed.*, 2006, **45**, 4056-4059; and references cited therein.

[4] E. Böhler, J. Warneke, P. Swiderek, *Chem. Soc. Rev.*; DOI:10.1039/C3CS60180C.

[5] M. Schmittel and A. Burghart, *Angew. Chem. Int. Ed.*, 1997, **36**, 2550-2589.

Metastable hydrogen atoms from H_2 molecules: towards the realization of "twin" atoms

Aline Medina[1,2], G Rahmat[1], R Cireasa[1,3], A. Trimeche[1], A. Cournol[1], N Vanhaecke[1], Ginette Jalbert[1,2], <u>F Zappa</u>[4*], C R de Carvalho[1,2], R F Nascimento[2,5], Ioan F Schneider[1], N V de Castro Faria[1,2] and J Robert[1]

1. Laboratoire Aimé Cotton CNRS, Univ Paris Sud 11, 91405 Orsay Cedex, France
2. Instituto de Física, UFRJ, Cx. Postal 68528, Rio de Janeiro, RJ 21941-972, Brazil
3. Laboratoire de physique des solides, CNRS/Université Paris-Sud, Orsay, France
4. Departamento de Física, UFJF. Campus Universitário, Juiz de Fora, MG, 36036-900, Brazil
5. CEFET/RJ - Campus Petrópolis

* fabio.zappa@ice.ufjf.br

The dissociation of diatomic molecules is an important topic for different areas of research, like chemistry and astrophysics and quantum information. Particularly, it is a possible means of obtaining the so called "twin atoms", that will share some coherence between them because they are linked to the same molecular state. Detection of their spin coherence may allow such basic quantum mechanics tests in the same way that it is done for twin photons[1]. For instance, this has been pursued with the use of van der Waals molecules such as Hg_2 [2]

The superexited states of the H_2 molecules have been shown to be good candidates to perform twin photons experiments, using the dissociation in twin H(2p) atoms with subsequent emission of correlated Lyman-α photons [3]. Since spin analysis of H(2s) atom can be achieved through the use of Stern Gerlach interferometry [4], it is legitimate to investigate the dissociation of superexited states of the H_2 molecule in pairs of twin spin-polarized H(2s) atoms.

We present the first step of this study where we have revisited the dissociation of H_2 molecules excited by electron impact. The electron beam is produced by a high intensity, pulsed electron gun, and can have energies ranging between 30 to 200 eV. A cold H_2 molecular beam is obtained by supersonic expansion through a Campargue nozzle, in order to keep internal degrees of freedom at a low temperature and to obtain a high intensity flux. We have addressed dissociation by electron impact, rather than by photodissociation, in order to avoid limitations imposed by the selection rules governing the radiative transitions, encountered in previous experiments. With one detector, placed several centimeters away from the collision centre, one can analyse the neutral fragments as a function of

their time-of-flight (TOF) through Lyman-α detection. Measurements with two detectors show evidence of coincidence of pairs of H(2s).

Acknowledgments

References

[1] Fano U, Rev. Mod. Phys. 55, 855 (1983).
[2] Fry E S , Walther T, and Li S, Phys. Rev. A 52, 4381 (1995)
[3] T. Tanabe, T. Odagiri, M. Nakano, I. H. Suzuki, and N. Kouchi, Phys. Rev. Lett 103, 173002 (2009).
[4] S. Nic Chormaic, V. Wiedemann, Ch. Miniatura, J. Robert, S. Le Boiteux, V. Lorent, 0. Gorceix, S. Feron, J. Reinhardt, and J. Baudon, J. Phys. B 26, 1271 (1993).

Molecular dynamics probed with free electrons: dissociation mediated by π*/σ* mixing

J. Fedor, R. Janečková, O. May

Department of Chemistry, University of Fribourg, Chemin du Musée 9, CH-1700 Fribourg

A standard way of probing nuclear motion in molecules is by a time-resolved ultrafast spectroscopy. Resonant electron scattering on molecules provides and alternative tool of obtaining the dynamical information – it is encoded in cross sections for individual scattering channels. This results from the fact that a typical lifetime of an electron-molecule compound state (transient negative ion, resonance) with respect to electron autodetachment is in the order of picoseconds - timescale directly comparable with the timescale of intra-molecular motion. The resonant potential surface is often dissociative and the geometry distortion prior to the electron detachment leads to the vibrational excitation of the molecule. If the geometry distortion goes beyond the crossing point where the electron starts to be bound the detachment channel is suppressed and the resonance decays via producing negative ion and neutral radical. This channel is called dissociative electron attachment (DEA). The individual VE and DEA cross section thus reflect the position of atomic nuclei in the various stages of molecular dissociation.

In this contribution, we focus on small molecules where the incoming electron is captured into a vacant π* orbital of the target molecule and where the dissociation is provided by the symmetry lowering of the transient negative ion (π*/σ* mixing mediated by vibronic coupling). A prototype molecule for such behavior is acetylene C_2H_2, where the dissociating hydrogen atom follows an out of line trajectory. Replacing one hydrogen by a methyl group (methylacetylene) provides three more possibilities for an abstraction site and opens an intra-molecular competition between symmetry and proximity: the abstraction of acetylenic hydrogen has to be mediated by vibronic coupling, whereas abstraction of methyl group hydrogens is allowed without such symmetry lowering. However, the later ones are spatially further from the resonance centered on the C≡C bond. The experiments with partially deuterated methylacetylene show, that it is the acetylenic C-H bond which is dissociative which indicates a strong effectivity of vibronic coupling.

An interesting situation arises in formic acid HCOOH where where two dissociation mechanisms are a priori possible: the one mediated by π*/σ* mixing or the one where direct dissociation proceeds following electron attachment into σ*(OH)

orbital. Experiments with isotopically substituted isomers shown that the second process is actually operative here [3].
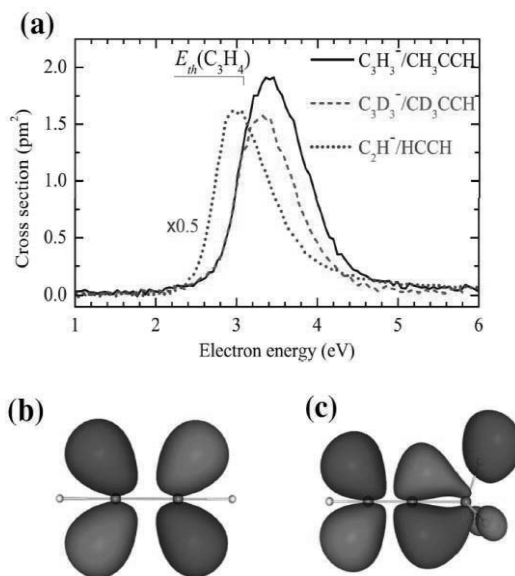
Figure 1. *DEA cross sections for the abstraction of an H atom in acetylene (multiplied by one half), methylacetylene and partially deuterated methylacetylene.* ***(b)*** *and* ***(c)*** *The lowest unoccupied* π^* *orbitals of acetylene and methylacetylene, respectively, demonstrating the symmetry character of the resonant wavefunction.*

References

[1] O. May, J. Fedor, M. Allan, *Phys. Rev. A* **80**, 012706 (2009)
[2] R. Janečková, O. May, J. Fedor, *Phys. Rev. A* **86**, 052702 (2012)
[3] R. Janečková, D. Kubala, O. May, J. Fedor, M. Allan, *Phys. Rev. Lett.*, in print

Combining ion mobility, cold ion spectroscopy and mass spectrometry for investigations of gas-phase peptides

Thomas R. Rizzo

Ecole Polytechnique Fédérale de Lausanne, Laboratoire de chimie physique moléculaire, CH H1 621, Station 6, CH-1015 Lausanne, Switzerland

Over the last several years, we have used cold, linear RF-ion traps to measure electronic and vibrational spectra of large biomolecular ions produced in the gas phase by electrospray [1]. In these experiments, we monitor the absorption of IR or UV radiation by action spectroscopy, in which we detect fragment ions generated upon UV excitation using an analyzing quadrupole. While helium buffer-gas cooling to ~10 K removes the spectral complexity arising from thermally populated vibrational states and narrows the rotational state distribution, the spectra of large molecules can still exhibit considerable complexity arising from the distribution of conformational states trapped at low temperatures. These kinetically trapped conformations, which will not relax upon further cooling, may contain memory of the conformation of the molecules in solution.

To further simplify the complex spectra of large molecules, we would like to separate different conformational states of the molecules before injecting them into a cold ion trap. Our first approach has been to use Field Asymmetric Ion Mobility Spectrometry (FAIMS) for conformational preselection, which separates ions on the basis of the difference in their mobility at high and low electric fields. Applying this approach to the 9-amino acid peptide Bradykinin, we have shown that after conformational selection, we can cool and trap molecules without extensive conformational scrambling [2], although the resolution in distinguishing conformations was limited.

To be able to increase our ability to resolve conformational states before injecting them into our trap, in collaboration with David Clemmer's group we have recently added to our cold-ion spectrometer a stage of drift-tube ion mobility separation [3], which allows us to sort molecules according to their orientationally averaged cross section. At the same time we have designed a cold, planar RF ion trap that is directly coupled to a time-of-flight mass spectrometer, which we use after ion-mobility separation. The combination of these techniques should allow us to further simplify the spectra of large, complex molecules as well as investigate of correlation between gas-phase and solution-phase structures.

References

[1] T.R. Rizzo, J.A. Stearns, and O.V. Boyarkin, Int. Rev. Phys. Chem. **28**, 481(2009).

[2] G. Papadopoulos, A. Svendsen, O. V. Boyarkin, and T. R. Rizzo, J. Am. Soc. Mass Spectrom. **23**, 1173 (2012).

[3] B.C. Bohrer, S.I. Mererbloom, S.L. Koeniger, A.E. Hilderbrand, and D.E. Clemmer, Ann. Rev. Anal. Chem **1**, 293 (2008).

A Novel Method to Measure Electronic Spectra of Cold Molecular Ions

S. Chakrabarty, M. Holz, E.K. Campbell, A. Banerjee, D.Gerlich and J.P. Maier
Department of Chemistry, University of Basel, Klingelbergstrasse 80, CH-4056 Basel, Switzerland

j.p.maier@unibas.ch

A universal method has been developed for measuring spectra of molecular ions in a 22-pole radio frequency trap at 5 K. It is based on laser induced inhibition of complex growth. The first successful measurements have been demonstrated on the A $^2\Pi_u$ - X $^2\Sigma_g^+$ electronic transition with some thousand N_2^+ ions, helium densities of 10^{15} cm^{-3} and storage times of 1 s. The reduction of the number of N_2^+-He complexes is the result of an interplay between excitation, radiative and collisional cooling, ternary association and collision induced dissociation. The electronic spectrum of N_2^+ could be recorded in spite of a ternary rate coefficient of only 10^{-31} cm^6 s^{-1} for N_2^+-He formation.

The technique is universal, because complexation of ions with helium can be impeded over a wide wavelength range. Depending on the molecule and the detailed kinetics of interest, the experimental parameters have to be adjusted: laser power, temperature, density and storage and interaction time, leading up to 10^{10} collisions. In the case of larger ions, internal conversion following electronic excitation forms "hot" ions, reducing the attachment of helium and thus making the method applicable.

Molecular Dynamics Simulations of CO_2 Formation in Interstellar ices

M. C. van Hemert[1], C. Arasa[1], E.F. van Dishoeck[2], and G. J. Kroes[1]

[1] *Gorlaeus Laboratories, Leiden Institute of Chemistry, Leiden University, P. O. Box 9502, 2300RA Leiden, The Netherlands*
[2] *Leiden Observatory, Leiden University, P. O. Box 9513, 2300RA Leiden, The Netherlands*

CO_2 ice is one of the most abundant components in ice-coated interstellar dust grains, besides H_2O and CO. Yet, the most favorable path to CO_2 ice is still not fully clear. Among the three possible routes,

$$HCO + O \rightarrow CO_2 + H, \quad CO + OH \rightarrow CO_2 + H \quad \text{and} \quad CO + O \rightarrow CO_2 ,$$
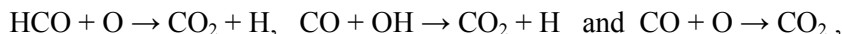
the one where a CO molecule reacts with an OH radical is the obvious one when the OH radicals are produced by photodissociation of water molecules.

Molecular dynamics calculations on different kinds of $CO–H_2O$ ice systems have been performed at 10 K in order to demonstrate that the reaction between CO and an OH radical resulting from H_2O photodissociation through the first excited state is a possible and plausible route to form CO_2 ice.
Our calculations [1], which take into account different ice surface models, suggest that there is another product with a much higher formation probability ($(3.00\pm0.07)\times10^{-2}$), which is the HOCO complex, whereas the formation of CO_2 has a probability of only $(3.6\pm0.7)\times10^{-4}$. The initial location of the CO is key to obtain reaction and form CO_2: the CO needs to be located deep into the ice. The HOCO complex becomes trapped in the cold ice surface in the trans-HOCO minimum because it quickly loses its internal energy to the surrounding ice, preventing further reaction to $H + CO_2$.

Several laboratory experiments have been carried out recently [2] and they confirm that CO_2 can also be formed through other, different routes. Here we compare our theoretical results with the data available from experiments studying the formation of CO_2 through a similar pathway as ours, even though the initial conditions were not exactly the same [3].

Our results show that also the HCO van der Waals complex can be formed, but now through the interaction of a CO molecule with an H atom that is also formed as a product of H_2O photodissociation. Thus, the H + CO reaction can be a possible route to form HCO ice and, provided there is a source of atomic oxygen, also to form CO_2 ice.

Finally it is realized that the bombardment of water molecules with energetic H atoms resulting from the photodissociation process, provides an additional source of OH radicals through the

$H_2O + H \rightarrow OH + H_2$ reaction. This channel was not taken into account in our MD simulations since all water molecules but the dissociating one were treated as rigid rotors. The secondary OH radicals have a translational and rovibrational energy distribution that differs from the primary ones.

Furthermore yet another OH radical may react with a trapped HOCO radical and still lead to the formation of CO_2 (and H_2O). It was shown that in gasphase the reaction has a high probability.[4] This route would bring theoretical and experimental formation rates in agreement and is subject of current investigation.

In our original calculations [1] for the OH CO interaction the LTSH potential energy surface [5] was used. Recently it was found that a newer potential energy surface [6] gives rather different outcomes for the enhancement of the gas phase reactive cross section by OH vibrational excitation. Also these effects on our model will be discussed.

References

[1] C. Arasa , M.C. van Hemert, E.F. van Dishoeck EF, G.J. Kroes, J. Phys. Chem. A. 117 (2013) 7064.
[2] C.J. Bennett, C.S. Jamieson, R.I. Kaiser, Phys. Chem.Chem. Phys. 11 (2009) 4210.
[3] N. Watanabe, A. Kouchi, Astrophys. J., 567 (2002) 651.
[4] H.G. Yu, J.T. Muckerman, J.S. Fransisco, J. Phys. Chem. 109 (2005) 5230.
[5] M.J. Lakin, D. Troya, G. Schatz, L.B.A Harding, J. Chem. Phys. 119 (2003) 5848.
[6] J.Li, Y. Wang, B. Jiang, J.Ma, R. Dawes,D.Xie, J.M. Bowman, H. Guo, J. Chem. Phys. 136 (2012) 041103.

Rotational and Rovibrational Spectroscopy at 4K: Laser Induced Inhibition of Complex Growth

Oskar Asvany, Pavol Jusko, Alexander Stoffels, Lars Kluge, Sandra Brünken, and Stephan Schlemmer

I. Physikalisches Institut, Universität zu Köln, Zülpicher Strasse 77, 50937 Köln, Germany

1. Introduction

To disentangle spectra of complex or fluxional ionic molecular species mass-selection and cooling of the ions is essential. This is fulfilled in low-temperature ion trapping experiments in which a multipolar ion trap (22-pole trap) guarantees relaxation to low temperatures. Due to the low number of trapped ions (~10000), some sort of action spectroscopy has to be applied, laser induced reactions (LIR) being the main workhorse in our group.

As an alternative pathway, at temperatures below 10 K attachment of helium atoms to the stored ionic species can be exploited for spectroscopy. While traditionally tagging of ionic species with rare gas atoms enables predissociation IR spectroscopy of the complex, narrow-band excitation of the naked species prior to tagging can hinder or slow down the attachment process. This has been termed 'laser induced inhibition of complex growth', LIICG, and successfully tested in our laboratory on different ionic species. Advantages of LIICG are operation at the lowest temperatures obtainable with commercial cryogenic refrigerators (4K) and in particular its general applicability to any ion.

LIICG has been demonstrated so far in our group for the rotational spectroscopy of HCO^+ and CO^+, the rovibrational IR spectroscopy of CH_5^+ [1] and CD_2H^+, as well as the electronic spectroscopy of N_2^+ in the group of John Maier in Basel [2]. In this contribution, we shall mainly concentrate on the rovibrational spectroscopy of CD_2H^+. The very high resolution and accuracy obtained by the combination of low temperature, narrow-band IR radiation and calibration by a frequency comb [3] allows predictions of rotational transitions with microwave accuracy.

2. Experimental details

For the measurements two recently completed tandem mass spectrometric 4K 22-pole ion trap machines have been used, one of them described in detail in [1] and sketched in the figure below. For the spectroscopy of ionic species A^+, a precursor gas is ionized in a storage ion source, the generated A^+ ions mass-selected in a first quadrupole mass

spectrometer, and about 10000 of them injected into the 3.7 K 22-pole trap constantly filled with about 10^{14} cm^{-3} helium. Within a trapping time on the order of 500 ms up to several 1000 A$^+$-He species can be generated. This attachment is then hindered by the exciting mm-wave radiation (multiplier chain) or IR radiation (1W 3μm OPO) entering the machine through appropriate windows (diamond or CaF$_2$) and traversing the trap. To obtain a spectrum, the second quadrupole mass spectrometer is adjusted to the mass of A$^+$-He, and the resulting counts recorded as a function of radiation frequency.

COLTRAP
Cologne Ion Trap
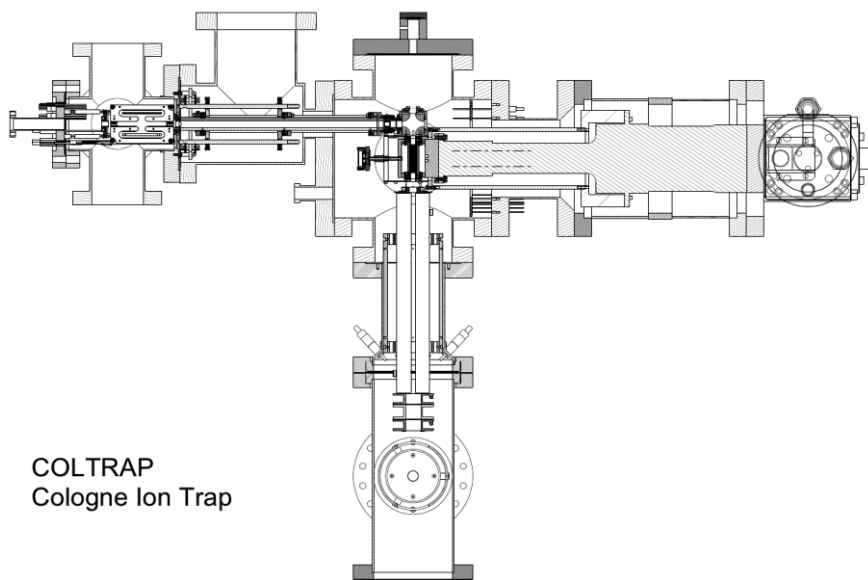
3. rotational LIICG-spectroscopy of CO$^+$ and HCO$^+$

As a test case for rotational LIICG spectroscopy the well-documented transitions N_J $=0_{1/2} - 1_{3/2}$ of CO$^+$ at 118.1 GHz and J=0-1 of HCO$^+$ at 89.2GHz have been detected. The decrease of A$^+$-He counts observed on resonance is on the order of 5%, requiring complete kinetic modeling for a full understanding. At the moment, the width of the lines is dominated by pressure broadening. Investigation of unknown rotational transitions (e.g. CD$_2$H$^+$, see below) will follow.

4. vibrational LIICG-spectroscopy of CD$_2$H$^+$

CD$_3$H precursor gas (Cambridge Isotope Laboratories, Inc.: Methane D3, 98%) has been used for the production of CD$_2$H$^+$. CD$_2$H$^+$ is a planar asymmetric top with C$_{2V}$ symmetry, and the spectroscopy of its ν_1 band centered around 3066 cm^{-1} was

pioneered by Oka 20 years ago in a discharge tube [4]. Due to the low temperature conditions of LIICG only about 16 lines from the lowest J=0,1,2 states could be detected, the transition $1_{01} \leftarrow 1_{10}$ for the first time. The figure below shows a stick spectrum of the measured lines together with a detailed view of the band center $1_{11} \leftarrow 0_{00}$. Its center frequency has been determined in this work to $(3066.112466 \pm 0.000013)$ cm^{-1} by multiple measurements with a frequency comb [3]. Both the width of the measured lines as well as the rotational population indicates that the ions have a temperature below 12K, as also found in the case of CH_5^+ [1].
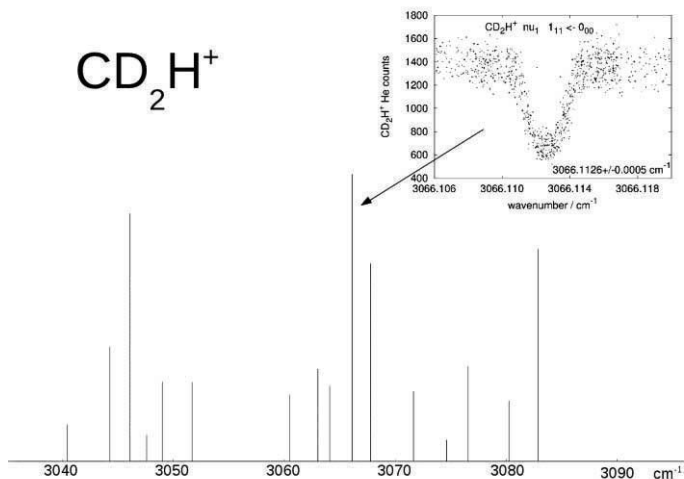
5. Outlook and Summary

To access higher J-states, LIR of CD_2H^+ at elevated temperatures will be applied. As in the case of CH_2D^+ [5], the high signal-to-noise ratio of LIR enables accurate IR measurements yielding rotational predictions with sub-MHz accuracy. These rotational transition frequencies can then be confirmed and refined by applying rotational LIICG as demonstrated for CO^+ and HCO^+. After the tentative detection of CH_2D^+ in space [6], this makes a search of interstellar CD_2H^+ feasible in the future.

The apparent general applicability of LIICG to any bare cation and to any sort of spectroscopy (rot/rovib/electronic) opens up many new pathways. In particular, LIICG makes rotational spectroscopy of mass-selected cold cationic species feasible, which is

not possible in discharge experiments. The application of LIICG to anions will be tested in the future.

References

[1] O. Asvany, S. Brünken, L. Kluge, and S. Schlemmer, *Appl. Phys. B.* 2013**,** doi:10.1007/s00340-013-5684-y
[2] S. Chakrabarty at al., *J. Phys. Chem. Lett.*, submitted
[3] O. Asvany, J. Krieg, and S. Schlemmer, *Rev. Sci. Instr.* 2012, **83, 093110**
[4] M.F. Jagod, M. Rösslein, C.M. Gabrys, and T. Oka, *J. Mol. Spectrosc.* 1992, **153, 666**
[5] S. Gärtner et al., *J. Phys. Chem. A* 2013, **117, 9975**
[6] E. Roueff et al., *J. Phys. Chem. A* 2013, **117, 9959**

Ion-molecule reactions of relevance for astrochemistry

Daniela Ascenzi, Linda Giacomozzi, Estefania Lopez-Marne, Paolo Tosi
Department of Physics, University of Trento, Via Sommarive 14, I-38123, Povo, Trento, Italy

Miroslav Polášek, Jan Žabka
J. Heyrovský Institute of Physical Chemistry, Academy of Science of the Czech Republic, Prague, Czech Republic

Christian Alcaraz
Lab. Chimie Physique, CNRS-Univ. Paris-Sud, Orsay Cedex & Synchrotron SOLEIL, Saint-Aubin, France

Emilie-Laure Zins
Laboratoire de Dynamique, Interactions et Réactivité, CNRS/UPMC, Place Jussieu 75252 Paris, France

1. Introduction

Astronomical observations and space missions to planets within our Solar System have shown that the interstellar medium (ISM) as well as the atmosphere of some satellites (e.g. Saturn's moon Titan) host a large variety of molecules with an increasing degree of complexity [1] and the characterization of their formation mechanisms can help to understand the formation of solar systems. In addition to the heterogeneous chemistry occurring on the surface of ice grains in molecular clouds, gas-phase chemistry can play an important role in "post-processing" the organic material liberated from the grains, especially when highly reactive species such as ions are involved. Ions, as well as excited species, can form in some particularly hot regions of the ISM as well as in the ionosphere of planets.

In the past we have investigated the formation mechanisms of aromatic, polycyclic aromatic and carbon ring chains by studying ion-molecule association reactions leading to the formation of new C-C bond between phenyl, ethyl, naphthyl and biphenyl cations with neutral arenes [2]. In this contribution we describe recent results on two different topics:
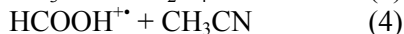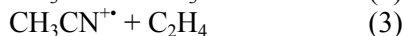
a) reactions of radical cations with neutrals of relevance for the formation of species containing C, H, N and O atoms in the ISM

b) reactions of unsaturated nitrile cations with other nitriles, of relevance for the synthesis of CN containing species in Titan's atmosphere.

2. Experimental approach and results

Ion-molecule reactivity is investigated using tandem mass spectrometric techniques, and different types of ion sources are used to control the amount of internal excitation during production of the molecular ions. Branching ratios of ionic products and absolute values of reactive cross sections as a function of the collision energy can be measured. In some cases photoionization via synchrotron radiation is used to generate cations with a known amount of internal energy and measure their reactivity using the "reactive monitoring" technique [3].

a) Reactions of ions with neutrals of relevance for the formation of C, H, N and O containing species

Several organic compounds have been detected in the ISM, among them unsaturated hydrocarbons, carboxylic acids, aldehydes, ketones, alcohols, nitriles and cyanides. Reactions between ions and neutrals containing C, H, O and N atoms are of paramount importance in the context of exobiology, since they may lead to the synthesis of prebiotic building blocks and hence biomolecules. We have focussed our attention on reactions involving radical cations of the simplest carboxylic acids detected in the ISM ($HCOOH$ and CH_3COOH) and the simplest nitrile (CH_3CN) reacting with the corresponding neutrals and the smallest unsaturated hydrocarbon (C_2H_4). In particular we have investigated the following reactions:

$CH_3CN^{+\bullet} + HCOOH$ (1)
$CH_3CN^{+\bullet} + CH_3COOH$ (2)
$CH_3CN^{+\bullet} + C_2H_4$ (3)
$HCOOH^{+\bullet} + CH_3CN$ (4)
$CH_3COOH^{+\bullet} + CH_3CN$ (5)

Since $CH_3CN^{+\bullet}$ is known to easily isomerize to $CH_2CNH^{+\bullet}$ upon ionization [4] reactions of the latter cation with $HCOOH$ and CH_3COOH have also been investigated by producing $CH_2CNH^{+\bullet}$ via dissociative ionisation of butyronitrile, C_3H_7CN. The main product channels for reactions (1)-(2) and (4)-(5) are due to proton and electron transfer, while for reaction (3) the formation of an adduct ion, as well as the loss of H_2 from the adduct is observed, as shown in Figure 1. In the same figure the difference in reactivity of $CH_3CN^{+\bullet}/ CH_2CNH^{+\bullet}$ with respect to proton and electron transfer is observed and it can be used to estimate the amount of isomerization of the $C_2H_3N^{+\bullet}$ radical cation.

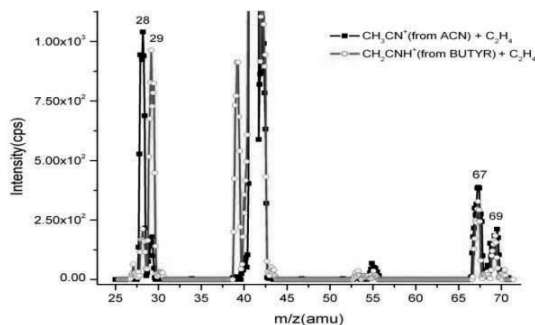***Figure 1:*** *Mass spectrum of the reaction of CH₃CN⁺·/ CH₂CNH⁺· (from acetonitrile or butyronitrile) with C₂H₄. The pressure of ethylene in the scattering cell is 6x10⁻⁵mbar, as measured by a spinning rotor gauge, and the collision energy is in the range 0.2-0.3 eV in the CM.*

b) **Reactions of nitrile cations of relevance for Titan atmosphere**
Motivation for this study stems from the observation of nitriles in Titan atmosphere, both as neutral and ionic species. In particular an ion of molecular formula $C_4H_5NH^+$ has been detected in Titan's ionosphere during the Cassini-Huygens mission and it has been assigned as the protonated form of C_4H_5N nitriles [5]. Several isomers exist for C_4H_5N, namely crotonitrile, allylcyanide, pyrrole, methacrylonitrile and cyclopropyl cyanide [6]. We have generated the protonated species $C_4H_5NH^+$ from different neutral isomers and we have investigated their reactivity with the corresponding neutrals as well as with the smallest of nitriles CH_3CN. In the case of unsaturated non cyclic nitriles the protonated species easily form proton bound dimers with their neutrals as well as with CH_3CN. Interestingly in the case of crotonitrile the proton bound dimer $[(C_4H_5N)_2H]^+$ shows the loss of an HCN molecule to give an ion of molecular formula $C_7H_{10}N^+$ that may represent a possible pathway through which small nitriles can grow into larger species. Hence this reactive channel can contribute to explain the existence of large N-containing unsaturated hydrocarbons on Titan. More detailed results will be presented at the meeting.

References

[1] UMIST database for Astrochemistry, http://www.udfa.net; V. Vuitton, et al. "Chemistry of Titan's atmosphere," in *Titan: Surface, Atmosphere and*

Magnetosphere, ed. by I. Mueller-Wodarg et al. Cambridge University Press, 2012.

[2] D. Ascenzi, et al. *J. Phys. Chem. A*, **111** 12513 (2007); J. Zabka, et al. *J. Phys. Chem. A*, **113** 11153 (2009); D. Ascenzi et al. *J. Chem. Phys.* **133** 184308 (2010); J. Aysina, et al. *J. Chem. Phys.* **138** 204310 (2013).

[3] C.J. Shaffer, et al. *Int. J. Mass Spectrom.* **17** 336 (2013) and references therein.

[4] J.C. Choe, *Int. J. Mass Spectrom.* **235** 15 (2004); C. Mair, et al. *Int. J. Mass Spectrom.* **223–224** 279 (2003); G. de Petris, et al. *J. Phys. Chem. A*, **109** 4425 (2005).

[5] V. Vuitton, et al. *Icarus*, **191** 722 (2007).

[6] M.W.E.M. van Tilborg, et al. *Int. J. Mass Spectrom. Ion Proc.*, **54** 299 (1983).

Ion trap study of O⁻ + H₂ interaction at low temperatures

Š. Roučka, P. JuskoD. Mulin, I. Zymak,, R. Plašil, J. Glosík
Charles University in Prague, Faculty of Mathematics and Physics, Department of Surface and Plasma Science, V Holešovičkách 2, 18000, Prague, Czech Republic

1. Introduction

The reaction between O⁻ and H_2 has two exothermic channels that are relevant at low temperatures. Those are the associative detachment

$$O^- + H_2 \xrightarrow{k_1} H_2O + e^-$$

(1)

and hydrogen atom transfer

$$O^- + H_2 \xrightarrow{k_2} OH^- + H.$$

(2)

These reactions have been studied before using drift tube, flowing afterglow, tandem mass spectrometer, and ion trap instruments (McFarland et al. 1973, Viggiano et al. 1991, Jusko et al. 2013) at temperatures above 300 K (176 K by Viggiano (1991)). The energy partitioning in reaction (1) has recently been studied using an electron spectrometer capable of measuring the energy distribution of the detached electrons (Jusko et al. 2013). This abstract presents the results of our recent experimental work extending the measurements of the rate coefficients down to 10 K.

2. Experimental

The experiment was conducted using the ion trapping technique. Our setup is based on the 22-pole radiofrequency ion trap (Gerlich, Horning 1992). The O⁻ ions are produced in a storage ion source (Gerlich 1992) by the electron bombardment of N_2O precursor gas. The O⁻ ions are precooled in the storage ion source approximately to the room temperature. After mass selection using a quadrupole mass filter, the ions are injected into the 22-pole trap. The temperature of the trap is variable in the range 10-300 K. The ions are thermalized to the trap temperature by buffer gas cooling with helium. The reactant H_2 is leaked directly into the trap and the absolute density of the reactant is calibrated using a spinning rotor gauge. After a certain trapping time, the stored ions are extracted from the trap, mass analyzed using a second quadrupole mass filter, and detected using a microchannel plate detector. A standard procedure for studying the ion molecule reactions in the trap consists of repeatedly

trapping and extracting the ions with various trapping times. This way the time evolution of ion numbers can be obtained.

3. Results and discussion

In case of the reactions (1) and (2), we can observe the decrease of the of O^- count (N_O) due to both reactions and an increase of the OH^- count (N_{OH}) due to reaction (2). The time evolution of the ion counts is governed by the following differential equations

$$\frac{dN_O}{dt} = -(k_1 + k_2)[H_2]N_O, \quad \frac{dN_{OH}}{dt} = k_2[H_2]N_O, \tag{3}$$

where $[H_2]$ indicates the number density of the reactant. These equations can be solved analytically and the measured data are analyzed by least squares fitting with the analytical solutions. An example of the measured data with the analytical fits is shown in the figure 1. By measuring at various trap temperatures, we were able to obtain the temperature dependence of rate coefficients of reactions (1) and (2) in the temperature range 10–300 K. Our results in comparison with previous work of McFarland et al. (1973), Viggiano et al. (1991), and Moruzzi et al. (1968) are shown in figure 2. We can observe that the rate coefficient of reaction (1) is comparable to the Langevin reaction rate coefficient ($k=1.56\times10^{-9}$ cm^{3}s^{-1}) in the temperature range of our measurement. However, a distinct maximum of the rate coefficient is present at temperature approximately 40 K. This unexpected maximum indicates a specific shape of the potential energy surface of the $O^- - H_2$ system. Theoretical studies of this system in collaboration with the Institute of Theoretical Physics of Charles University in Prague are in progress in order to fully understand the origin of the observed behavior. Also the isotopic effect of exchanging H_2/D_2 has been studied in our laboratory and is being prepared for publication.
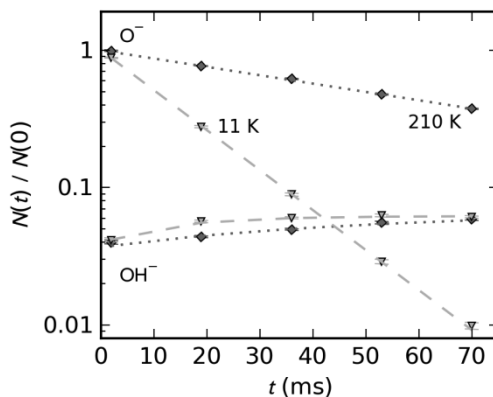
***Figure 1**: The measured numbers of trapped O⁻ and OH⁻ as a function of the trapping time. Data obtained at two trap temperatures are shown and the corresponding fits with analytical curves are indicated by the dashed and dotted lines. The differences between the data at two temperatures are mainly due to different H_2 number densities in the trap.*
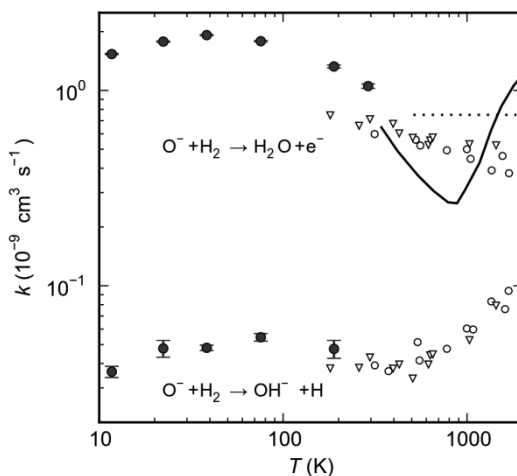
***Figure 2**: Temperature dependence of the reaction rate coefficients of reactions (1) and (2). The filled circles indicate the data obtained in this work. The results of previous measurements by Viggiano et al. (1991) and McFarland et al. (1973) are indicated by the hollow triangles and circles respectively. The dotted and solid lines indicate the rate coefficient of reaction (1) reported by Moruzzi et al. (1968) and Mauer & Schulz (1973) respectively.*

Acknowledgement

References

[1] Gerlich, D., *Adv. Chem. Phys.,* **82** (1992)

[2] Gerlich, D. & Horning, S., *Chemical Reviews,* **92**, 1509-1539 (1992)

[3] Jusko, P.; Roučka, v. S.; Plašil, R. & Glosík, J., *Int. J. Mass Spectrom.,* **352**, 19–28 (2013)

[4] Mauer, J. L. & Schulz, G. J., *Phys. Rev. A,* **7**, 593-605 (1973)

[5] McFarland, M.; Albritton, D. L.; Fehsenfeld, F. C.; Ferguson, E. E. & Schmeltekopf, A. L., *J. Chem. Phys.,* **59**, 6629-6635 (1973)

[6] Moruzzi, J. L.; J. W. Ekin, J. & Phelps, A. V., *J. Chem. Phys.,* **48**, 3070-3076 (1968)

[7] Viggiano, A. A.; Morris, R. A.; Deakyne, C. A.; Dale, F. & Paulson, J. F., *J. Phys. Chem.,* **95**, 3644-3647 (1991)

Dynamic two-dimensional mapping of gaseous combustion and pyrolysis product concentrations in solid-fuel combustion: Looking into a burning cigarette

R. Zimmermann[1], R. Hertz-Schünemann[1], S. Ehlert[1], C. Liu[2], K. McAdam[2], R. R. Baker[2†], S.Coburn[2], T. Streibel[1]

[1]*Joint Mass Spectrometry Centre of University of Rostock, Chair of Analytical Chemistry, Rostock, Germany,*
* Correspondence to: ralf.zimmermann@uni-rostock.de
[2]*GR&D, BAT Ltd, Southampton, UK*
†Deceased.

Combustion and pyrolysis are extremely complex and dynamic chemical processes, that are by far not fully understood. This is in particular true when complex condensed-phase fuels (such as liquid petrochemical fractions) or solid fuels (such as biomass) and transient combustion processes are considered. The gas phase chemistry of solid fuel combustion in the fuel's voids and pores is extremely difficult to address by conventional analytical methods. In the last years photo ionisation mass spectrometry (PIMS) was established as a fast on-line analytical technique to analyse the chemical signature of highly dynamic combustion and pyrolysis processes in cigarettes during puffing [1]. Recently a new combination of PIMS (laser based single photon ionisation, 118 nm) and a capillary microprobe sampling system (μ-probe) was developed, allowing direct examination of the composition of organic vapours even in the centre of the cigarette's combustion zone [2]. This μ-probe-PIMS approach was then further developed to a spatial and temporal resolved mapping method. For this, repetitive smoking experiments with a reproducible smoke machine and standard reference cigarettes were done. Different sampling positions in the cigarette tip were multiply addressed by μ-probe PIMS measurements. The time resolved PIMS sequences were later combined to spatially resolved, time-dependent "maps" for the different compounds. This new technique for dynamic mapping was used to measure quantitative distributions of nitrogen monoxide, benzene and oxygen in the burning tip of a cigarette during a 2 second lasting puff (with up to 100 ms time resolution). The different formation and destruction zones of the investigated compounds in the reaction region and their dynamic changes were observed during the puff, and space-resolved kinetic data was obtained. For example, the classical formation and destruction mechanisms of NO during the puff (fuel-NO formation and re-burn in hydrocarbon rich zones) could be observed in a space- and time-resolved manner. The μ-probe-PIMS mapping

technology can be applied for comprehensive chemical studies on various combustion or pyrolysis systems as well as on model systems for catalytic processes or any other heterogenic processes at the gas/solid or gas/liquid boundary layer and thus is of large interest for fundamental and applied research.

References

[1] T. Adam, J. McAughey, C. Mocker, C. McGrath, and R. Zimmermann, Analytica Chimica Acta 657 (2010) 36-44.
[2] R. Hertz, T. Streibel, C. Liu, K. McAdam, R. Zimmermann, Analytica Chimica Acta, 714 (2012) 104-113

Inelastic Hydrogen Atom Scattering: A new tool to investigate energy conversion processes at surfaces

Oliver Bünermann, Hongyan Jiang, Yvonne Dorenkamp, and
Alec Wodtke
*Georg-August-Universität Göttingen,, Institut für Physikalische Chemie,
Tammannstr. 6, 37077 Göttingen, Germany*

Obtaining an atomic-level understanding of the dynamics of energy conversion at surfaces remains a richly complex and challenging area of modern research in physical chemistry. A general strategy to this field follows the lessons of gas-phase bimolecular chemical dynamics, where simple model systems are studied experimentally with great care while theoretical simulations are developed.

One of the simplest systems to think of is Hydrogen atom scattering from a single crystalline surface. A new apparatus to experimentally investigate this model system with extraordinary precision is presented. Laser photolysis of Hydrogen Iodide is employed to produce a monochromatic Hydrogen atom beam with well-defined initial directions. Kinetic energies between 100 meV and 6 eV can be produced by tuning the wavelength of the photolysis laser. The final kinetic energy and scattering angle are measured with extraordinary resolution employing Rydberg Atom Tagging. Both techniques are adopted and combined with a state of the art surface scattering machine, introducing an entirely new approach to surface analysis. High control of experimental parameters as well as angular and energy resolved detection give a very detailed picture of the scattering process.

Recently, first experiments scattering Hydrogen atoms from an Au(111) surface were performed. Kinetic energy loss spectra were recorded for various polar and azimuthal incident and scattering angles. The time-of-flight spectra clearly show two different components: The first component is characterized by small kinetic energy loss and narrow energy spread, the second by large kinetic energy loss and wide energy spread. Both show different dependencies on the incident and scattering angles. The experimental results are compared to high level theoretical calculations and the importance of electronically non-adiabatic processes and penetrating collisions is discussed.

Benzene Dication

Jana Roithová, Juraj Jašík

Faculty of Science, Department of Organic Chemistry, Charles University in Prague, Hlavova 2030/8, CZ-128 43 Prague 2, Czech Republic

Dieter Gerlich

Department of Physics, University of Technology, 09107 Chemnitz (Germany)

Structure of benzene dication represents a puzzle. While the double ionization of benzene leads to the classical six-membered ring structure, it has been suggested that upon ionization rearrangements to more stable structures take place.[1] Theoretically, several structures have been proposed.[2] We have investigated the structure of doubly ionized benzene by infrared predissociation spectroscopy of helium-tagged complexes.[3] It is shown that part of the generated dications $C_6H_6^{2+}$ retain the six-membered ring structure while the other part undergoes a rearrangement to the most stable pyramidal structure with a C_5H_5 base and CH at the apex. Using isomer selective heating by a CO_2 laser, complexes with the classical six-membered ring structure have been destroyed and the pure IRPD spectrum of the pyramidal dication obtained.

Acknowledgement

References

[1] J. H. D. Eland*, Chem. Phys.* **2008,** *345*, 82.
[2] K. Krogh-Jespersen, *J. Am. Chem. Soc.* **1991,** *113*, 417.
[3] J. Jašík, J. Žabka, J. Roithová, D. Gerlich, *Int. J. Mass Spectrom.* **2013**, on line, DOI: 10.1016/j.ijms.2013.06.007.

Prompt atom knockout in PAH$^+$+He collisions

H. Zettergren, M. H. Stockett, J. D. Alexander, T. Chen,
M. Gatchell, N. Haag, A. Johansson, H. A. B. Johansson,
K. Kulyk, S. Rosén, H. T. Schmidt, and H. Cederquist.
Department of Physics, Stockholm University, SE-106 91 Stockholm, Sweden.

P. Rousseau, L. Adoui, and B. A. Huber
Centre de Recherche sur les Ions, les Matériaux et la Photonique (CIMAP), CEA-CNRS-ENSICAEN, F-14070 Caen Cedex 05, France.
Université de Caen Basse-Normandie, F-14032 Caen, France.

U. Berzins
Institute of Atomic Physics and Spectroscopy, University of Latvia, Riga, LV-1586, Latvia

K. Stochkel and P. Hvelplund
Department of Physics and Astronomy, Aarhus University, DK-8000 Aarhus C, Denmark

Polycyclic Aromatic Hydrocarbons (PAHs) consist of fused aromatic carbon rings (C_nH_m). When internally heated, they may get rid of their excess energy by emission of photons, electrons, or by fragmentation. The latter normally proceeds through the emission of H-atoms or C_2H_2 molecules, rather than CH_x-loss (x=0,1,…). This is well understood based on very large differences in dissociation energies – about 11-17 eV for the latter processes and about 5-7 eV for emission of H or C_2H_2.

In this work [1], we show that CH_x-loss is a prominent decay pathway in 110 eV center of mass energy PAH$^+$ + He collisions. This is due to prompt atom knockout processes in billiard-ball-like nuclear interactions. We demonstrate that such processes become increasingly more important with PAH size (cf. Fig. 1) and lead to the formation of defect structures with highly reactive sites related to those found in graphene [2-4]. Prompt knockout processes may thus open up different routes to the formation of larger molecules compared to statistical fragmentation processes which favor the fragmentation channels with the lowest dissociation energies. This was recently demonstrated in collisions between He^{2+} ions and clusters of C_{60} molecules, where single carbon knockout from one C_{60} molecule led to the formation of dumbbell-shaped C_{119}^+ in C_{59}^+ + C_{60} bond-forming reactions [5].
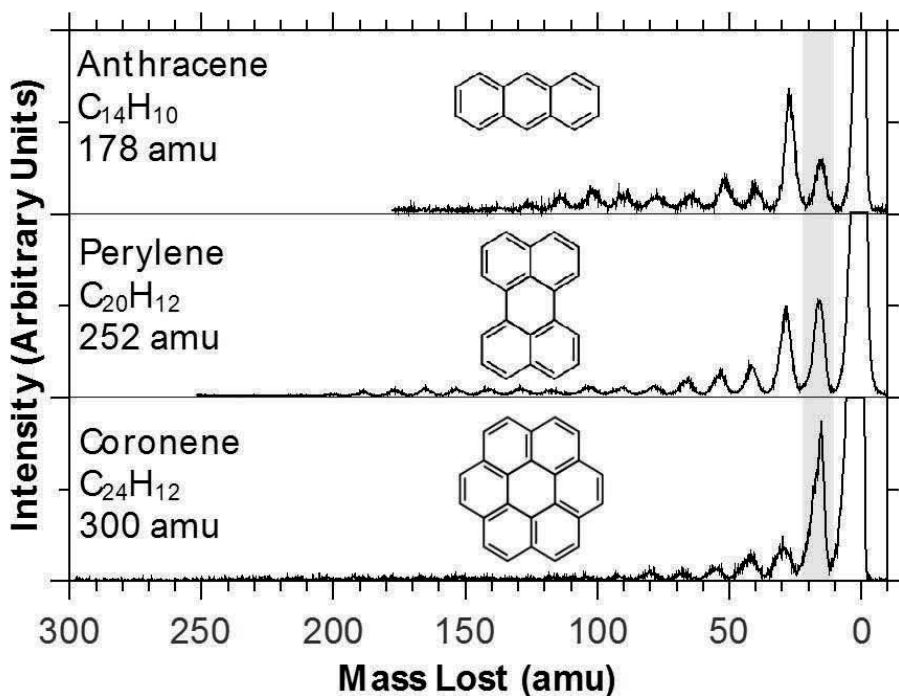
Figure 1: *Mass loss spectra for PAH$^+$ + He collisions at 110 eV center-of-mass energy. The CH$_x$-loss peak (highlighted in gray) is due to prompt carbon atom knockout processes and becomes more prominent with increasing mass of the PAH$^+$ parent ion. The spectra are normalized to the total integrated intensity of the carbon loss fragments.*

References

[1] M. Stockett *et al*, to be submitted
[2] J. C. Meyer *et al*, Phys. Rev. Lett., 108, 196102 (2012)
[3] A. V. Krasheninnikov *et al,* Phys Rev. B 81, 153401 (2010)
[4] P. A. Denis and F. Iribarne, J. Phys. Chem. C 117, 19048 (2013)
[5] H. Zettergren *et al*, Phys. Rev. Lett., 110, 185501 (2013)

FT-ICR studies of anionic reactions for the chemistry of planetary ionospheres

C. Romanzin, E. Louarn, J. Lemaire, <u>C. Alcaraz</u>
Lab. de Chimie Physique, Bât 350, UMR 8000 CNRS - Université Paris-Sud 11,
91405 Orsay, France

J. Žabka and M. Polášek
J. Heyrovsky Institute of Physical Chemistry of the ASCR, v. v. i. Dolejškova 2155/3,
182 23 Prague 8, Czech Republic

J.-C. Guillemin
Ecole Nationale Supérieure de Chimie de Rennes, UMR CNRS 6226, 11, Allée de
Beaulieu, 35708 Rennes Cedex 7, France

Titan, Saturn's largest moon, exhibits a dense atmosphere characterized by a thick orange haze and mainly composed of molecular nitrogen and methane as well as numerous other organic compounds such as nitriles. The chemistry taking place in its atmosphere is complex and still not completely understood. Yet, results from the Cassini-Huygens mission have shown that ionospheric chemistry must play a more important role than previously thought. The discovery of CN^-, C_3N^- and C_5N^- together a large amount of heavy cations and anions in the upper atmosphere [1-3] came indeed as a surprise and suggests that they contribute to the formation of aerosols particles.

In this context, we have undertaken experimental investigations of ion-molecule reactions involving small anions such as CN^-, C_3N^- and C_5N^- in a common effort between several French and Czech groups [4-7].

In the last SASP meeting, we have presented the study of the $CN^- + HC_3N$ reaction in a tandem mass spectrometer as a function of the HC_3N target pressure in order to explore different collisional conditions. The primary and secondary reactions with HC_3N are found to be extremely efficient, resulting in anionic products of rapidly growing size. A detailed mechanism for the growth of these species has been proposed and its relevance to the growth of heavy anions in Titan's ionosphere discussed [4].

Our objective is now to precisely caracterize each step of this mecanism by studying the reactions in a single collision regime and by measuring rate constant and absolute reaction cross section as a function of temperature and collision energy.

Rate constant of the $CN^- + HC_3N$ reaction has been measured as a function of temperature from 300 K down to 49 K [5,6] in the french group of S. Le Picard et al at the University of Rennes 1. Low temperature measurements have been achieved with the help of the CRESU technique [6].

In this contribution, we will present a FT-ICR study at 300 K [7] done at Orsay with the MICRA setup [8] of the following reactions:
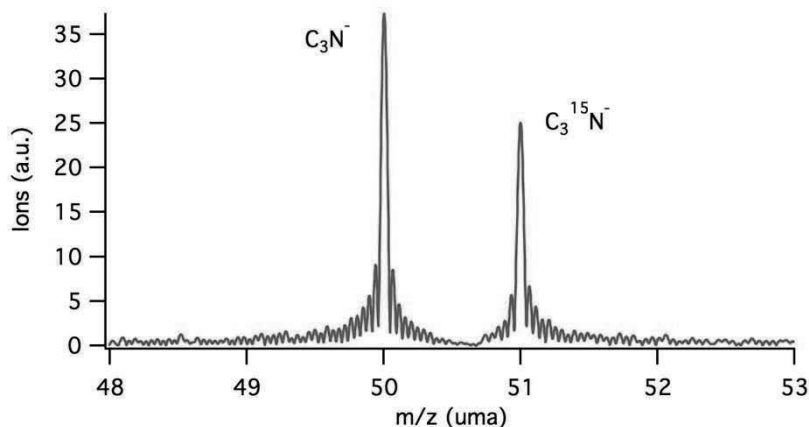
$$
\begin{array}{lll}
CN^- & + & HC_3N \\
C_3N^- & + & HC_3N \\
C_3N^- & + & HC_3{}^{15}N \\
C_3{}^{15}N^- & + & HC_3N
\end{array}
$$
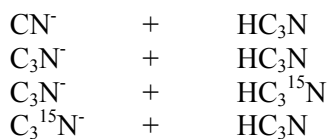
Figure 1: *Mass spectrum of the C_3N^- parent and $C_3{}^{15}N^-$ product anions resulting from the proton transfer channel in the $C_3N^- + HC_3{}^{15}N$ reaction*

CN^- and C_3N^- parent ions have been produced by dissociative electron attachment on $BrCN$ and BrC_3N respectively. After ejection of the electrons, pulses of increasing length of cyanoacetylene target gas were injected to probe the kinetics of the reactions and derive their rate constant at 300 K. Several mecanisms, included fast proton transfer as in illustrated in Figure 1, have been identified and will be discussed at the conference.

Further studies are planned on the CERISES setup [9] at Orsay to caracterize the reaction mecanism by measuring the absolute reaction cross section and product velocity distributions as a function of collision energy.

Acknowledgments

References

[1] A.J. Coates, F.J. Crary, G.R. Lewis, D.T. Young, J.H. Waite, E.C. Sittler, "*Discovery of heavy negative ions in Titan's ionosphere*", Geophys. Res. Lett. **34**(22) (2007).

[2] A.J. Coates, A. Wellbrock, G.R. Lewis, G.H. Jones, D.T. Young, F.J. Crary, J.H. Waite, R.E. Johnson, T.W. Hill, E.C. Sittler, "*Negative ions at Titan and Enceladus: recent results*", Farad. Discuss.**147**, 293-305 (2010).

[3] V. Vuitton, P. Lavvas, R.V. Yelle, M. Galand, A. Wellbrock, G.R. Lewis, A.J. Coates, J.E. Wahlund, "*Negative ion chemistry in Titan's upper atmosphere*", Planet. Space Sci. **57**(13), 1558-72 (2009).

[4] J. Žabka, M. Polášek, C. Romanzin, C. Alcaraz, "*Anion Chemistry on Titan: A possible route to large N-bearing hydrocarbons*", Icarus **219**(1), 161-167 (2012)

[5] S. Carles, F.A., C. Monnerie, J.-C. Guillemin, J.-L. Le Garrec, *Kinetic studies at room temperature of the cyanide anion CN- with cyanoacetylene(HC3N) reaction.* Icarus, **211**(1), 901-905 (2011).

[6] L. Biennier, S. Carles, D. Cordier, J.-C. Guillemin, S.D. Le Picard, and A. Faure, *Low temperature reaction kinetics of CN^- + HC_3N and implications for the growth of anions in Titan's atmosphere*. Icarus **227**, 123-131 (2013).

[7] C. Romanzin, C. Alcaraz, E. Louarn, J. Lemaire, J.-C. Guillemin, J. Žabka, and M. Polášek (in preparation)

[8] G. Mauclaire, J. Lemaire, P. Boissel, G. Bellec, and M. Heninger, *MICRA: a compact permanent magnet Fourier transform ion cyclotron resonance mass spectrometer*. Europ. J. Mass Spectrom. **10**(2), 155-162 (2004).

[9] C. Alcaraz, C. Nicolas, R. Thissen, J. Zabka, and O. Dutuit, $^{15}N^+$ + CD_4 and O^+ + $^{13}CO_2$ *state-selected ion-molecule reactions relevant to the chemistry of planetary ionospheres*. J.Phys.Chem.A **108**(45), 9998-10009 (2004).

Synchrotron based FTIR spectroscopy of the chiral molecules CDBrClF and CHBrIF

S. Albert[a,b], S. Bauerecker[a], K. Keppler[a], Ph. Lerch[b] and M. Quack[a]

[a]Physical Chemistry, ETH Zurich, CH-8093 Zürich, Switzerland,
[b]Swiss Light Source, Paul-Scherrer-Institute, CH-5232 Villigen, Switzerland

1. Introduction

High resolution spectroscopy from the microwave through the infrared and optical region of chiral molecules are of fundamental interest [1,2]. Due to parity violation the two enantiomers of a chiral molecule have slightly different ground state energies and also slightly different spectra expressed as line shifts in the spectrum [3–5]. One of the great challenges of modern high resolution spectroscopy is the experimental detection of either the parity violating ground state energy difference $\Delta_{PV}E$ of the two enantiomers [15] or relative line shifts in their spectra which are predicted to be in the mHz to Hz regime [5,12]. In particular, the infrared region is a promising spectral range to detect such line shifts. Two important conditions are required for a successful experiment. On one hand ultra-high resolution devices must be available in the spectral region of interest and on the other hand the spectrum of the chiral molecules must be well understood in this spectral region. The infrared region fulfills these conditions. As ultra-high resolution devices such as CO_2-lasers [6] and frequency combs are available. Thanks to new FTIR technology [7, 8], the synchrotron sources [9] and highly resolving interferometers [2,7-10], the IR spectra of simple chiral molecules can now be completely resolved and analysed in broad spectral ranges say, 100 to 2000 cm^{-1}. The understanding of the chiral molecule's spectrum is the first essential step in the experimental detection of parity violation. Here we present an analysis of the infrared spectra of the chiral molecules CDBrClF, the deuterated isotopomer of CHBrClF [11], and CHBrIF [16]. Parity violating line shifts in the spectra of these molecules have already been calculated and they are in the range of a mHz and smaller [12,13].

2. Analysis of the FTIR spectra

The FTIR spectra of CDBrClF and CHBrIF have been measured with our FTIR setups at the SLS using synchrotron radiation and at ETH Zurich in the range 620 to 2200 cm^{-1}. The spectra of the two major isotopomers CD^{79}Br^{35}ClF and CD^{81}Br^{35}ClF have been analysed within the v_5 (CCl-stretching), v_4 (CF-stretching) and v_3 (CDF-bending) regions and the CH^{79}BrIF and CH^{81}BrIF spectra within the v_4 (CF-

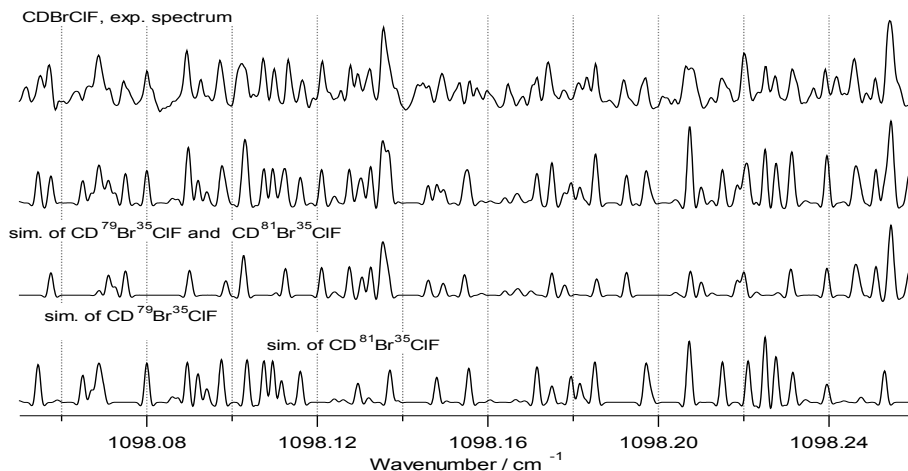stretching) and $2v_4$ region using Watson´s Hamiltonian [14]. Figure 1 shows a comparison of

Figure 1: *R branch range of the v_4 fundamental of CDBrClF centered at 1082.8116 $cm^{-1}(CD^{79}Br^{35}ClF)$ and at 1082.7963 cm^{-1} ($CD^{81}Br^{35}ClF$). The upper trace displays the spectrum recorded with the synchrotron source and the second trace shows the simulated sum spectrum of $CD^{79}Br^{35}ClF$ and $CD^{81}Br^{35}ClF$ (sum of the two lowest traces).*

the measured and simulated spectra of the CF-stretching region of CDBrClF around 1098 cm^{-1}. Figure 2 shows a comparison of the measured and simulated spectra of the CF overtone stretching region of CHBrIF around 2089 cm^{-1}.

The present analysis provides the basis for future experimental tests of parity violation in CDBrClF and CHBrIF using spectroscopy at ultra- high resolution. In this context we have already derived some coincidences with CO_2 laser lines. In particular, due to the analysis of the first overtone spectra of the CF-stretching overtone of CHBrIF at 2089 cm^{-1} one may conduct Doppler free CO_2 laser quasi resonant two photon spectroscopy. Considering our analysis we recommend *a*-type lines for ultra-high resolution experiments. While in the long run quantitative measurements of parity violation in lighter molecules are important for reasons discussed in [3-5], CHBrIF may still be very useful as an important experimental starting point because CO_2 laser- [6] and submillimeter wave spectroscopy can be conducted on this molecule.
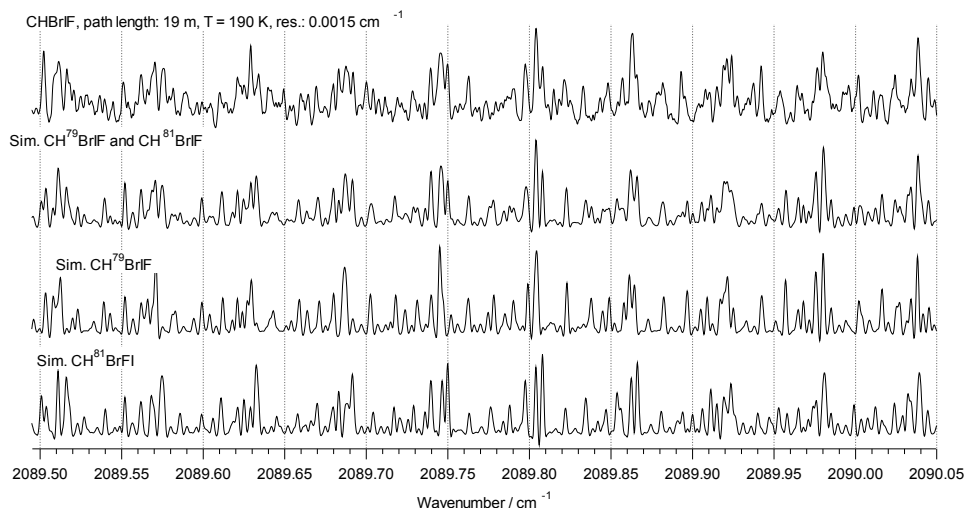
CHBrIF, path length: 19 m, T = 190 K, res.: 0.0015 cm^{-1}

Sim. CH^{79}BrIF and CH^{81}BrIF

Sim. CH^{79}BrIF

Sim. CH^{81}BrFI

2089.50   2089.55   2089.60   2089.65   2089.70   2089.75   2089.80   2089.85   2089.90   2089.95   2090.00   2090.05

Wavenumber / cm^{-1}

Figure 2: *R branch range of the 2v$_4$ fundamental of CHBrIF centered at 2103.7572 cm^{-1}(CH^{79}BrIF) and at 2103.6597 cm^{-1}(CH^{81}BrIF). The upper trace displays the spectrum recorded with the globar source and the second trace shows the simulated sum spectrum of CH^{79}BrIF and CH^{81}BrIF at 180 K (sum of the two lowest traces).*

References

[1] F. Merkt and M. Quack. Molecular quantum mechanics and molecular spectra, molecular symmetry, and interaction of matter with radiation, in Handbook of High-Resolution Spectroscopy, Vol. 1, (Eds. M Quack and F Merkt), Wiley, Chichester (2011), 1-55.

[2] S. Albert and M. Quack, ChemPhysChem., 8, 1271 – 1281 (2007).

[3] M. Quack, Angew. Chem. Intl. Ed. (Engl.), 41, 4618–4630 (2002).

[4] M. Quack, Fundamental symmetries and symmetry violations from high resolution spectroscopy, in Handbook of High-Resolution Spectroscopy, Vol. 1, (Eds. M Quack and F Merkt), Wiley, Chichester (2011), 965-1021.

[5] M. Quack, J. Stohner, and M. Willeke, Annu. Rev. Phys. Chem., 59, 741 – 769 (2008).

[6] C. Daussy, T. Marrel, A. Amy-Klein, C.T. Nguyen, C.J. Borde and C. Chardonnet, Phys. Rev. Lett., 83, 1554–1557 (1999).

[7] S. Albert, K. K. Albert and M. Quack, High Resolution Fourier Transform Infrared Spectroscopy, in Handbook of High-Resolution Spectroscopy, Vol. 2, (Eds. M Quack and F Merkt), Wiley, Chichester (2011), 965-1021.

[8]   S. Albert, P. Lerch, R. Prentner, and M. Quack, Angew. Chem. Intl. Ed. (Engl.), 52, 346–349 (2013).

[9]   S. Albert, K. K. Albert, P. Lerch, and M. Quack, Faraday Discussions, **150**, 71–99 (2011).

[10] S. Albert, K. K. Albert, and M. Quack, TOPS, 84, 177 – 180 (2003).

[11] A. Bauder, A. Beil, D. Luckhaus, F. Müler, and M. Quack, J. Chem. Phys., 106, 7558– 7570 (1997).

[12] M. Quack and J. Stohner, Phys. Rev. Lett., 84, 3807 (2000), M. Quack and J. Stohner. *J. Chem. Phys.*, 119, 11228 (2003).

[13] J.K. Laerdahl, P. Schwerdtfeger and H.M. Quiney, Phys. Rev. Lett.,

[14] 84, 3811 (2000).

[15] D. Luckhaus and M. Quack, Mol. Phys., 68, 745 (1989).

[16] M. Quack, Chem. Phys. Lett. **132**, 147 (1986).

[17] S. Albert, K.K. Albert, S. Bauerecker and M. Quack, Proceedings of the 16th SASP 2008, ISBN 978-3-902571-31-1, R.D. Beck, M. Drabbels and T.R. Rizzo (Eds), Innsbruck University press, pp. 79-82 (2008)

Molecular surface dynamics by inelastic electron tunneling: rotors and unidirectional motion

Tibor Kudernac, Nopporn Ruangsupapichat, Beatriz Macia, Nathalie Katsonis,
Syuzanna R. Harutyunyan, Ben L. Feringa
Stratingh Institute for Chemistry, University of Groningen, Netherlands;

Manfred Parschau and Karl-Heinz Ernst
*Empa, Swiss Federal Laboratories for Materials Science and Technology,
Dübendorf, Switzerland*

Propelling single molecules in a controlled manner along an unmodified surface remains extremely challenging because it requires molecules that can use light, chemical or electrical energy to modulate their interaction with the surface in a way that generates motion. Biomolecular motors, such as the protein kinesin or the F1-ATPase, function as linear walkers or rotary motors. Kinesin, for example, walks on tracks, so-called microtubules, which determine direction and induce uni-directionality. In order to mimic these biological motors, chemists strived for synthesis of molecules that can show unidirectional motion. One successful approach was the use of ratchet-style unidirectional rotors based on overcrowded helical systems [1,2]. Based on such concepts, a molecule has been synthesized that includes

four unidirectional rotors connected via a chassis. Depending on the stereochemistry of these rotors, either all rotors turn into the same direction when the molecule is attached to a surface or the rotors work in part against each other.
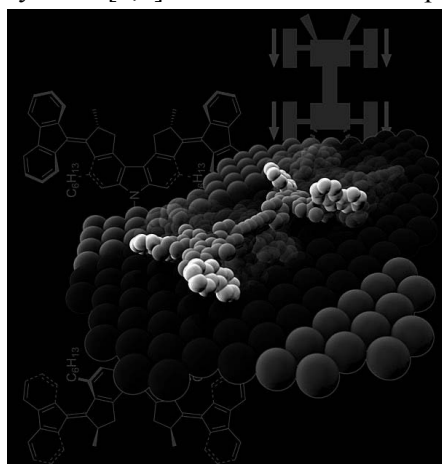
Figure 1. *Sketch of a molecule with four unidirectional rotors. After electronic excitation with tunneling electrons from an STM tip, concerted rotation of the rotors may lead to linear translation on a surface.*

We show that excitation with inelastically tunneling electrons emanating from the tip of a scanning tunneling microscope (STM) very efficiently excites the rotors and leads to linear movement of the molecule on the surface for the right isomer [3]. This

requires a transient electron attachment into the LUMO, while vibronic excitation of the motor axles lead to reversible rearrangement without movement. We will discuss possible mechanisms and implication for further research and design of nanotechnological devices.

References

[1] Kelly et al. *Nature* **1999**, *401*, 150.
[2] Koumura, et al. *Nature* **1999**, *401*, 152.
[3] Kudernac et al. *Nature* **2011**, *479*, 208.

Elucidating the Building and Breaking of Hydrogen Bonds:Two color delay dependent IR probing of torsional isomerization in a [AgL$_1$L$_2$]$^+$ complex

Maximilian Gaffga, Johannes I. Lang, Fabian Menges and <u>Gereon Niedner-Schatteburg</u>
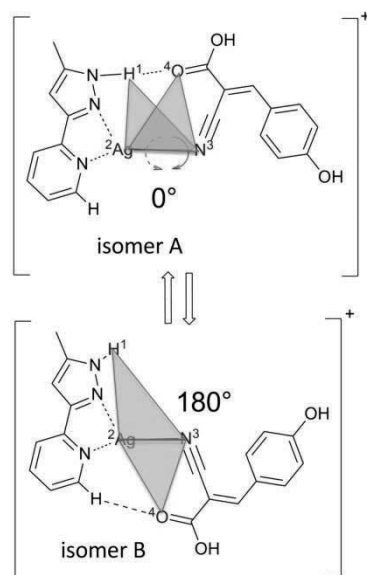
Fachbereich Chemie und Forschungszentrum OPTIMAS,
Technische Universität Kaiserslautern, 67663 Kaiserslautern, Germany

1. Motivation

Dynamical hydrogen bonding is ubiquitous. Building and breaking bonds conceptually involves approach and withdrawal of acceptor and donor. While this suggests a one dimensional picture to the naïve it is mandatory to elucidate full phase space e.g. in the framework of normal modes. Most often, it is out of reach to cover full dimensionality, in particular due to the prevailing anharmonicities that may render a scaled harmonic approach meaningless, as found e.g. in ionic systems with highly mobile protons [1-3]. However, it is sometimes conceivable – and doable – to identify reasonable constraints and invoke reduced dimensionality approaches [4]. Motion perpendicular to a hydrogen bond axis inevitably comes to mind. Such motifs of sideways migration certainly prevail in transport processes and rearrangements under high steric constraints, such as in zeolite pores, in trans membrane channels, or upon folding/unfolding of proteins under solvation.

Scheme 1: *Definition of the dihedral angle that describes the torsional isomerization in the [AgL$_1$L$_2$]$^+$ complex. Note, that isomer A stabilizes through a NH---O hydrogen bond and isomer B through a CH---O hydrogen bond.*

2. System to study and methods to apply

We have recently studied complexes of multiple silver ions that spontaneously coordinate with nucleobase mimicking ligands in solution [6].

These complexes showed to stiffen through arrangement of the two metal centers and the two ligands in a pairwise η_2 coordination. Here, we investigate the more flexible arrangement of a single Ag^+ center with two suitable ligands, α-Cyano-4-hydroxycinnamic acid (HCCA = L_1) and 2-(5-methyl-1H-pyrazol-3-yl)pyridine (MPP = L_2), one each. The resulting $[AgL_1L_2]^+$ complex is depicted in Scheme 1, which reveals a possible torsional isomerization. Investigation of these complexes arises through application of infrared induced multiple photon dissociation (IR-MPD, also known as action spectroscopy) while keeping the complexes stored as isolated ions in an ion trap that serves for mass selection and analysis in parallel.

3. Findings in short

The recorded IR-MPD spectra reveal well discernible bands, which we assign to the stretching vibrations of NH and OH oscillators in both ligands (Fig. 1). Redshifts and enhancements arise from application of a second, attenuated IR_{fix} pulse at resonance to some of these bands (ν_{PhOH}). Most notably, it very much depends on the time delay between the IR_{scan} and IR_{fix} pulses whether there is a hydrogen bound NH stretching band around 3410 cm^{-1} or not.
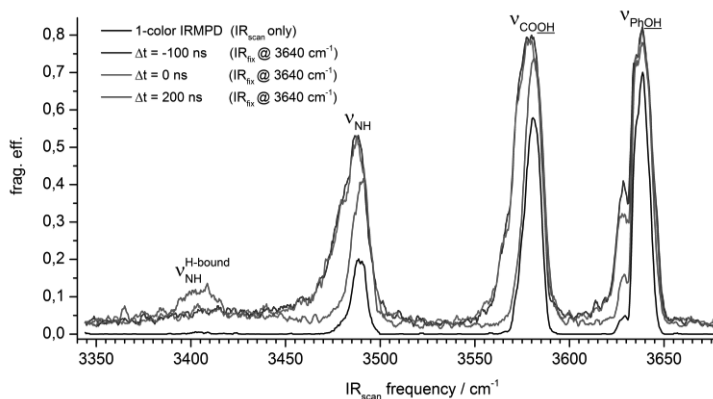

Figure 1: Details from the infrared spectra of stretching vibrations in $[AgL_1L_2]^+$. Two color pump probe spectra reveal a delay dependent heating and / or isomerization.

Interpretation of these and further findings arises in conjunction with *ab initio* calculations (Fig.2). Isomers A and B are well confirmed through the change of total energy (bottom) by the dihedral angle (Scheme 1). There are considerable frequency red shifts (middle) upon hydrogen bonding, and significant IR intensity increases (top). The significance of the CH---O hydrogen bond is clearly revealed, while the

acidic proton in the CH site of the pyridine heterocycle would have been overlooked easily, e.g. in a first guess of possible $[AgL_1L_2]^+$ structures.

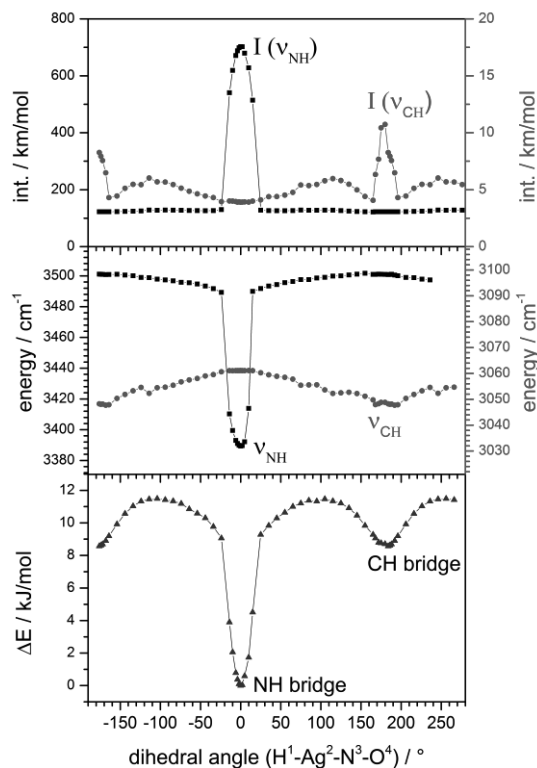***Figure 2:*** *Total energy of torsional twisting in $[AgL_1L_2]^+$ (bottom), frequencies of hydrogen bonding vibrations (middle) and their IR intensities (top) by DFT calculations at the B3LYP/cc-pVTZ level. Formation and breaking of the hydrogen bonds by torsional isomerization fingerprints in all three diagrams. Note, that the angular width of the strong NH---O bond is narrow, while that of the weaker CH---O bond is much wider.*

4. Summary and outlook

This study confirms the multi dimensional character of hydrogen bond formation and of their breaking. It further elucidates how weak bonds come into play to stabilize conformers off the global minimum structure. The importance of torsional rearrangements becomes clear once more by the gained picture, as was e.g. similarly unravelled in a previous study on ligand torsion in a Ru complex that precedes and enables activation of the catalytic center in a somewhat surprising way [6]. Our studies benefit from two color IR pulse probing as a valuable tool for such investigations. Obviously, the present work in progress awaits swift extension and subsequently enhanced modelling to do.

5. Invitation

Despite the extended presentation of the current findings in this abstract the attendees of SASP 2014 are cordially invited to a tour through this topic in the course of the evening poster sessions.

Acknowledgement

References

[1] J. M. Headrick, E. G. Diken, R. S. Walters, N. I. Hammer, R. A. Christie, J. Cui, E. M. Myshakin, M. A. Duncan, M. A. Johnson, K. D. Jordan, *Science* **2005**, *308*, 1765; N. I. Hammer, E. G. Diken, J. R. Roscioli, M. A. Johnson, E. M. Myshakin, K. D. Jordan, A. B. McCoy, X. Huang, J. M. Bowman, S. Carter, *J. Chem. Phys.* **2005**, *122*; J. R. Roscioli, L. R. McCunn, M. A. Johnson, *Science* **2007**, *316*, 249.

[2] O. Vendrell, F. Gatti, H.-D. Meyer, *Angew. Chem. Int. Ed.* **2007**, *46*, 6918.; *J. Chem. Phys.* **2007**, *127*, 184303; *ibid.* **2009**, *131*, 034308

[3] G. Niedner-Schatteburg, *Angew. Chem. Int. Ed.* **2008**, *47*, 1008

[4] K. Giese, M. Petkovic, H. Naundorf, O. Kuhn, *Physics Reports* **2006**, *430*, 211

[5] Y. Nosenko, F. Menges, C. Riehn, G. Niedner-Schatteburg
Phys. Chem. Chem. Phys. **2013**, *15*, 8171

[6] L. T. Ghoochany, C. Kerner, S. Farsadpour, F. Menges, Y. Sun, G. Niedner-Schatteburg, and W. R.Thiel, *Europ. J. Inorg. Chem.* **2013**, *24*, 4305-4317

Contributed Papers

Posters

Applications of Selective Reagent Ionisation-Time-of-Flight-Mass Spectrometry (SRI-ToF-MS) for increased selectivity in the detection of designer drugs

Matteo Lanza, Kostiantyn Breiev, Tilmann D. Märk
Ionicon Analytik GmbH., Innsbruck (Austria)
Institut für Ionenphysik und Angewandte Physik, Leopold-Franzens Universität Innsbruck, Innsbruck (Austria)
matteo.lanza@ionicon.com

Simone Jürschik, Philipp Sulzer, Alfons Jordan, Eugen Hartungen, Gernot Hanel, Lukas Märk
Ionicon Analytik GmbH., Innsbruck (Austria)

W. Joe Acton
Ionicon Analytik GmbH., Innsbruck (Austria)
Lancaster Environment Centre, Lancaster (UK)

Chris A. Mayhew
School of Physics and Astronomy, University of Birmingham, Birmingham (UK)

The abuse of drugs is an increasingly important issue affecting today's society. Although many drug species are controlled by law, a new market for "legal" highs, which are not yet controlled by drug legislation, has emerged. The use of these chemicals as substitutes for prohibited drugs has increased, especially among those who are interested in experiencing a high without committing a criminal act [1].

As new psychoactive substances (NPS) regularly enter the market, analytical methods capable of providing rapid detection and identification are needed. Rapid identification is of particular importance for example in medical applications, in cases of subjects who have taken an unidentified drug and require urgent medical treatment.
Selective Reagent Ionisation -Time-of-Flight- Mass-Spectrometry (SRI-ToF-MS) has the capability to detect trace compounds with high sensitivity (single digit pptv detection limits), in real time (instrumental response within 100 ms) and, because of high mass resolution (up to 8000 m/Δm), with a high level of confidence in

identification (low rate of false positives) [2]. Selectivity may be further improved by using the dependence of the product ion branching ratios as a function of reduced electric field (*E/N*), but this is not always the case, especially for isomers. For example, Figure 1 presents the product ion branching ratios as a function of *E/N* for 4-methylethylcathinone (4-MEC) and N-ethylbuphedrone resulting from the reaction of these compounds with H_3O^+. It can be seen that there are no significant differences. However, in addition to changing *E/N* we can also change the reagent ion, using the recently developed Switchable Reagent Ion Technology, developed by Ionicon Analytik GmbH [3, 4], which may alter the ion-molecule chemistry in such a way that different product ions are produced for different isomers, thereby allowing improved discrimination.
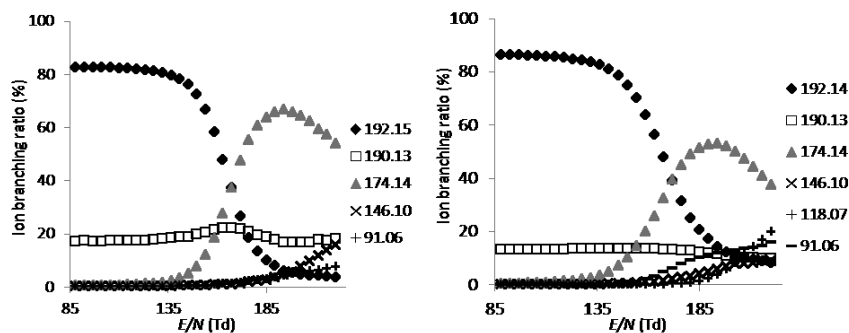

Figure 1: *Product ion branching ratios of 4-MEC (left) and NEB (right) resulting from proton transfer using H_3O^+ as the reagent ion.*

In Fig. 2 the most abundant product ions resulting from reactions of the two isomers mentioned above with NO^+ are shown. In contrast to H_3O^+ chemistry where identical product ions are observed for both isomers, in the case of NO^+ chemistry, a distinct product ion is observed at *m/z* 72.08 for 4-MEC and at *m/z* 86.10 for NEB, *i.e.* the two isomers can be discriminated [5]. In a real-life scenario a SRI-MS detector could at first measure the product ion ratios in H_3O^+ mode to identify that the substance is either 4-MEC or NEB (or both) and subsequently unambiguously identify the isomers present by switching to NO^+ as the reagent ion. We have demonstrated in earlier work that switching can be done within seconds [6].
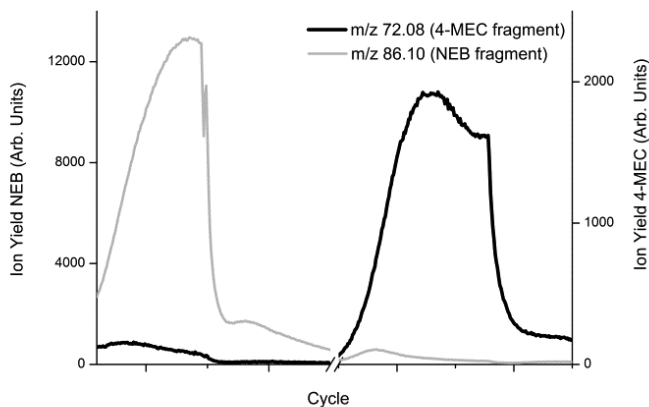
Figure 2: Measurement of the dynamic headspace in a vial containing NEB powder and subsequently a second vial containing 4-MEC powder using NO$^+$ as the reagent ion.

In addition to the study mentioned above, a detailed investigation of the reactions of H_3O^+, NO^+, O_2^+ and Kr^+ with a number of NPS (e.g. 4-fluoroamphetamine, methiopropamine, 4-methylethcathinone, N-ethylbuphedrone, 5-MeO-DALT, dimethocaine and nitracaine) as a function of E/N with a high mass resolution SRI-ToF-MS instrument will be presented.

Acknowledgement

References

[1] B. Werse, C. Morgenstern, *Drugs and Alcohol Today*, 12/4 (2012) 222 – 231.
[2] A. Jordan, S. Haidacher, G. Hanel, E. Hartungen, L. Märk, H. Seehauser, R. Schottkowsky, P. Sulzer, and T.D. Märk, *International Journal of Mass Spectrometry* 286 (2009) 122–128.

[3] A. Jordan, S. Haidacher, G. Hanel, E. Hartungen, J. Herbig, L. Märk, R. Schottkowsky, H. Seehauser, P. Sulzer, and T.D. Märk, *International Journal of Mass Spectrometry* 286 (2009), 32–38.

[4] P. Sulzer, A. Edtbauer, E. Hartungen, S. Jürschik, A. Jordan, G. Hanel, S. Feil, S. Jaksch, L. Märk, T.D. Märk, *International Journal of Mass Spectrometry* 321-322 (2012) 66–70.

[5] M. Lanza, W. J. Acton, P. Sulzer, S. Jürschik, A. Jordan, E. Hartungen, G. Hanel, L. Märk, C. A. Mayhew, T. D. Märk, *Journal of Mass Spectrometry* 48 (2013) 1015–1018.

[6] P. Sulzer, B. Agarwal, S. Jürschik, M. Lanza, A. Jordan, E. Hartungen, G. Hanel, L. Märk, T. D. Märk, R. González-Méndez, P. Watts, C. A. Mayhew, *International   Journal   of   Mass   Spectrometry*   (2013), http://dx.doi.org/10.1016/j.ijms.2013.05.004

Phase transition of water clusters

Isabelle Braud, Julien Boulon, Sébastien Zamith, Pierre Labastie and Jean-Marc L'Hermite

Université de Toulouse, UPS, Laboratoire Collisions Agrégats Réactivité, IRSAMC and CNRS, UMR 5589, F-31062 Toulouse, France

Since the pioneering work by Haberland and coworkers on the phase transitions in sodium clusters [1], a number of other cluster species have been shown to exhibit a first order phase transition. Metallic clusters in particular (aluminium, tin, gallium, sodium, etc) have been studied extensively with this respect (see for example [2]).

It is only very recently that phase transitions in molecular cluster have been experimentally studied. The temperature dependence of the heat capacity of both negatively $(H_2O)_n^-$ [3], $(H_2O)_{n-1}OH^-$ [4] and positively $(H_2O)_nH^+$ [5] charged water clusters has been reported. These clusters have been shown to undergo a phase transition prior to evaporation.

In the present study we report the measurement of heat capacities of mass selected protonated $(H_2O)_nH^+$ and deprotonated $(H_2O)_{n-1}OH^-$ water clusters as a function of temperature in the size range n = 20–118. We have found that they undergo a phase transition in the range 110–130 K. For both protonated and deprotonated water clusters the size dependent transition temperatures are strongly correlated with the dissociation energies around the shell closure at n = 55. Furthermore, the evolution of the transition temperature with size shows two different regimes, namely below and above n=35. This is interpreted as an overall structural change around the size n=35.

References

[1] M. Schmidt, R. Kusche, B. von Issendorff, H. Haberland, Nature 393, 238 (1998).
[2] A. Aguado and M.F. Jarrold, Annu. Rev. Phys. Chem. 62, 151 (2011)
[3] C. Hock, M. Schmidt, R. Kuhnen, C. Bartels, L. Ma, H. Haberland, B. v.Issendorff, Phys. Rev. Lett. 103, 073401 (2009)
[4] S. Zamith, P. Labastie, J.-M. L'Hermite, J. Chem. Phys. 138, 034304 (2013)
[5] M. Schmidt and B. von Issendorff, J. Chem. Phys. 136, 164307 (2012)

Investigations on the sensitivity and selectivity for the detection of the explosive picric acid using switchable reagent ion soft chemical ionisation mass spectrometry

Ramón González-Méndez, Peter Watts, Chris A. Mayhew
School of Physics and Astronomy, University of Birmingham, Edgbaston, Birmingham, B15 2TT, UK

Bishu Agarwal[a,b], Matteo Lanza[a], Philipp Sulzer[a], Tilmann D. Märk[a,b]
[a]Ionicon Analytik Gesellschaft m.b.H., Eduard-Bodem-Gasse 3, A-6020 Innsbruck, Austria. [b]Institut für Ionenphysik und Angewandte Physik, Leopold Franzens Universität Innsbruck, Technikerstr. 25, A-6020 Innsbruck, Austria

Using proton transfer reaction - time of flight - mass spectrometric instrumentation with a switchable reagent ion source (Ionicon Analytik GmbH, Austria)[1], the reactions of NO^+, H_3O^+, O_2^+ and Kr^+ with the trinitroaromatic compound picric acid (2,4,6 trinitrophenol, $C_6H_3N_3O_7$, PiA) have been investigated. NO^+ is found to react via three body association to form a simple adduct ion $PiA.NO^+$. A third body is crucial for the adduct formation because for the adduct to be stable the excess energy must be removed by a collisional process. However, it needs to be appreciated that the formation of the adduct rapidly decreases with increasing reduced electric field (E/N) in the drift tube because of collisional dissociation rather than collisional stabilisation.
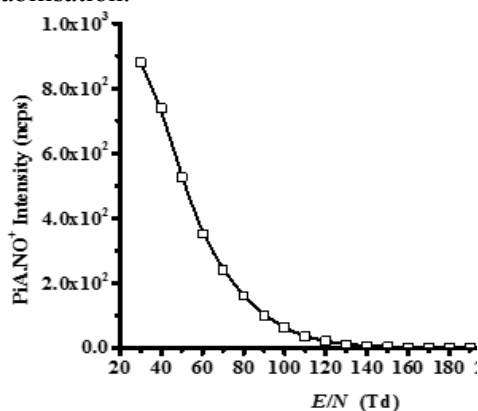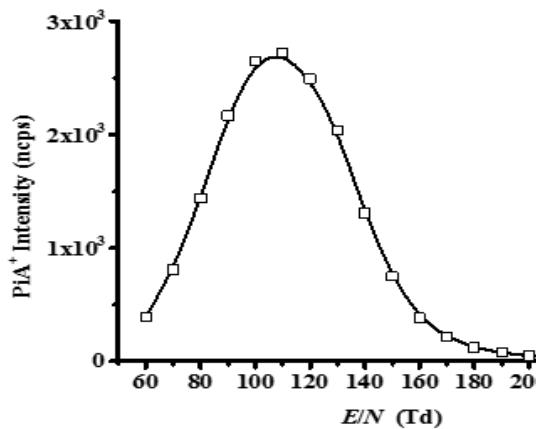

Normalised signal intensity of $PiA.NO^+$ as function of E/N
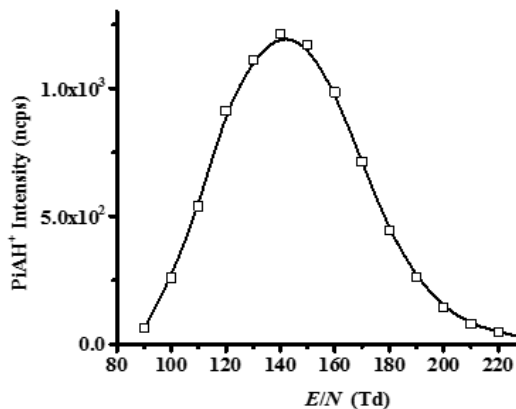
Normalised signal intensity of $PiA.H^+$ as function of E/N (with H_3O^+)
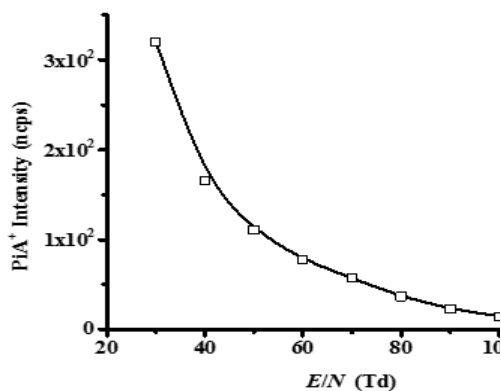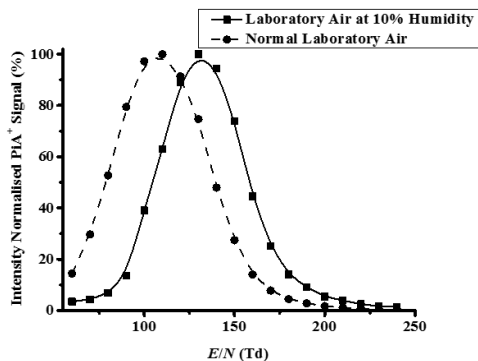
Normalised signal intensity of PiA⁺ as function of E/N (with Kr⁺)

Normalised signal intensity of PiA⁺ as function of E/N (with O₂⁺)

H_3O^+ reacts with picric acid via non-dissociative proton transfer only resulting in PiAH$^+$. Both O_2^+ and Kr$^+$ are found to react with picric acid by non-dissociative charge (electron) transfer to produce PiA$^+$.

Remarkably, for the reagent ions H_3O^+ and O_2^+ we find that the detection sensitivity of picric acid shows a similar dependence on *E/N* (although over a different *E/N* range), namely that when operating the drift tube with humid air the intensity of the PiAH$^+$ and PiA$^+$ ions start low at low drift tube voltages and increase as the drift tube voltage (and hence *E/N*) is increased, reaching a peak intensity at a given voltage (which is humidity dependent) and then decreasing.

Variation in relative ion signal intensities for normalised PiA⁺ as a function of E/N recorded using normal laboratory air compared to using laboratory air at 10% humidity as a carrier gas

The actual final product ion in a humid reaction system when either $PiAH^+$ or PiA^+ are the product ions is highly dependent on the *E/N* used, because once $PiAH^+.H_2O$ and $PiA^+.H_2O$ are able to be formed, secondary ion reactions with water lead to a product ion that no longer contains picric acid. As for protonated TNT and TNB[2], the behaviour of the intensity of protonated picric acid parent as *E/N* is changed by rapidly changing the drift tube voltage can be used as a powerful discriminatory analytical probe to detect picric acid. This coupled with switching from water to oxygen chemistry, which can be done within seconds, followed again by changing *E/N* provides an analytical procedure for the unambiguous detection of picric acid. An important message from this work is that by exploiting ion-molecule chemistry occurring in the drift tube of a PTR-MS it is possible to overcome a limitation of all one dimensional mass spectrometric analytical techniques: a nominal *m/z* value does not necessarily provide a unique indicator for the identity of an analyte in a complex chemical environment, *i.e.* isomeric (and isobaric if high resolution mass spectrometers are not used) compounds cannot usually be distinguished. Therefore special procedures need to be adopted to achieve a high level of confidence in the assignment of chemicals in what could well be complex chemical environments (*e.g.* airports), where these procedures need to be rapid if they are to be of any use in security areas where rapid turnarounds are required. Rapid switching of reagent ions is one way to achieve this[3]. This alters the ion chemistry and hence the *m/z* of the product ion(s) detected.

References

[1] http://www.ptrms.com (last accessed October 2013).
[2] P. Sulzer, F. Petersson, B. Agarwal, K. H. Becker, S. Jürschik, T. D. Märk, D. Perry, P. Watts, and C. A. Mayhew. Analytical Chemistry 84 (2012) 4161-4166.
[3] P. Sulzer, L. Märk, M. Lanza, S. Jürschik, B. Agarwal, T. D. Märk, Ramón. González-Méndez, P. Watts, and C. A. Mayhew. Int. J. Mass Spectrom. (Accepted May 2013).

Microplasmas: Where Science meets Engineering

Kurt H. Becker

Dept. of Applied Physics and Dept. of Mechanical Engineering, New York University Polytechnic Institute, Brooklyn, NJ 11201 USA

Abstract: We discuss the basic properties of high-pressure (micro)plasmas and presents a few examples of biologicala and (bio)medical, applications of microplasmas. The importance of plasma-surface interactions and the plasma chemistry in all these applications will be highlighted.

1. Introduction

Systematic studies of atmospheric-pressure plasmas in the 1980s showed that non-equilibrium plasma conditions with electron energies much higher than those of heavy particles, and properties similar to low-pressure glow discharges, can exist also at atmospheric pressure. However, self-sustained diffuse discharges tend to be unstable at high pressure due to their susceptibility to filamentation and the transition to an arc, which limits their practical utility. Among the most frequently employed approaches to achieve stabilization are (1) pulsed excitation, which essentially extinguishes the glow phase of the plasma before a transition into an arc occurs and (2) confining the plasma in a cavity, where at least one dimension is below ~1 mm, so-called microplasma.

One factor that contributes to the stabilization of microplasmas has to do with "pd scaling". The voltage required to ignite a discharge depends on the product of pressure "p" and electrode separation "d" (commonly referred to as the Paschen curve). If one increases the pressure for a fixed value of "d", the required breakdown voltage increases. At atmospheric pressure, breakdown voltages in the kV range are required. The high breakdown voltage leads to a high current density after ignition, particularly in the cathode fall of the discharge. This is the source of discharge instabilities in the cathode fall region, which quickly lead to the formation of an undesirable arc. As a consequence of "pd scaling", the breakdown voltage can be kept low, if the electrode separation "d" is reduced when the pressure "p" is increased. At atmospheric pressure, d-values below 1 mm are required to be near the minimum in the Paschen curve for essentially all gases. Another factor that at least in part contributes to the stability of high-pressure microplasmas are the high losses of charge carriers to the surrounding walls.

2. Selected Biological Applications of Microplasmas

The application of microplasmas in biology can be traced back to the mid-1990s [2]. Work concentrated primarily on bacteria removal from surfaces. More recently, microplasmas have also been utilized in biomedicine and medicine, as a promising method to – among other things - disinfect root canals, coagulate blood, and heal chronicle wounds.

In terms of the evaluation of the microplasma inactivation efficacy, two different methods are used. First, the D-value (or decimal reduction time), refers to the time required to reduce the concentration of microorganisms to 10% of its original value. Typically, in a bacteria survivor plot, the concentration of surviving microorganisms is shown as a function of plasma treatment time on a semi-logarithmic scale. The D-value can be determined by reading a one-log reduction assuming the plasma action can be described by a single exponential decay. Second, the inactivation rate (or inactivation factor) evaluates the percent difference between the microorganism population of the treated samples and that of an untreated control group. The inactivation rate can be calculated by using $|CFU_{control}-CFU_{treated}|/CFU_{control}\times100\%$, where CFU stands for "colony forming unit".
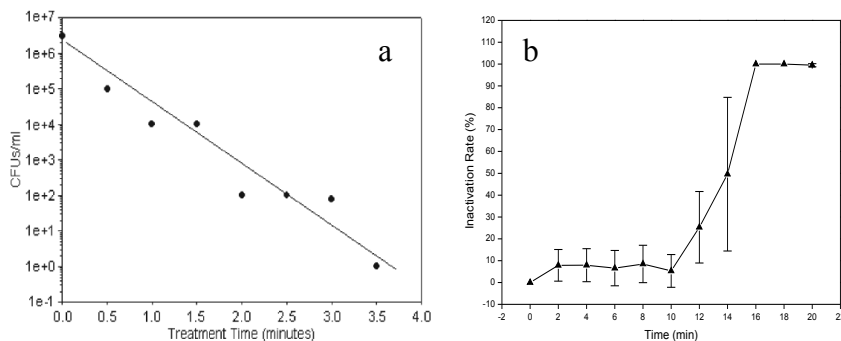

Figure 1: Example of (a) a semi-logarithmic survivor curve of E. coli on Luria-Bertani broth exposed to a He/air plasma and (b) the inactivation rate of S. aureus in water vs. treatment time (figures courtesy of W. Zhu and J. Zhang)

Inactivation rates, as a function of plasma treatment time, directly reflect the inactivation effectiveness. Fig. 1 shows 2 inactivation efficacy graphs.
Both methods involve plating and counting colony forming units in comparison to a control group. However, bacteria may exist in a state, in which they are alive (viable), but they are not culturable (they do not form colonies). Viable bacteria may

be revived and continue to form colonies when the conditions are appropriate. Thus, a statement of "inactivation" should be supported by either a "Live/Dead® BacLight™ bacterial viability test", Scanning Electron Microscope pictures, or a DNA stain test.

3. Inactivation of prokaryotic microorganisms in air and water

We carried out plasma inactivation experiments with both Gram-positive and Gram-negative bacteria. Fig. 2 shows the inactivation of Gram-negative *Escherichai coli* (*E. coli*) and Gram-positive *Micrococcus luteus* (*M. luteus*) by an atmospheric-pressure air microplasma jet. The 2×2 cm^2 squares in the center of each Petri dish mark the area directly treated by the plasma ("treated area"). The Petri dish was moved under the spatially fixed plasma jet with a constant speed of 4 mm/s along preset gridlines within the squares. Each complete travel cycle of the gridlines corresponds to a treatment time of 30 seconds.
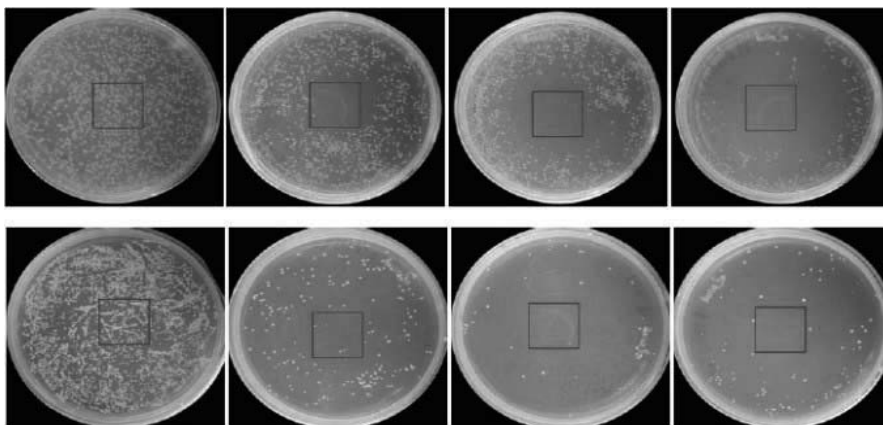

Figure 2: *Inactivation of E. Coli (bottom row) and M. luteus (top row), each treated for 0s (control) 30 s, 60 s, and 90 s, respectively, from left to right (figure courtesy of W. Zhu and J. Zhang)*

However, during each treatment cycle, any given area part of the treated area is only directly exposed to the plasma for about 0.5 s In both cases, nearly all bacteria in the "treated area" are inactivated within 30 s. Bacteria in the outer untreated area of teh Petri dish are also inactivated, but with longer treatment time, confirming the notion og a lateral transport of long-lived reactive plasma species. The inactivation of *M. luteus* follows a more diffused pattern, progressing radially out from the treated area

on the Petri dish, while the inactivation of *E. coli* appears to be more uniform across the whole Petri dish.

Under external stress (e.g. lack of nutrients), some Gram-positive bacteria enter a dormant state by forming endospores. Endospores are more difficult to inactivate due to the multiple coatings and layers surrounding the genetic core. *Bacillus subtilis* (*B. subtilis*) endospores were treated with a microplasma jet following the same method mentioned above. The endospores in the treated area were reduced to below 10% only after a 90 s total treatment (3 cycles of 30 s of plasma treatment), while the spore count in the untreated area remained at above 60%.

Over 100 different types of bacteria, protozoa and viruses are known to exist in contaminated water. These microorganisms are responsible for various serious illnesses such as kidney failure and degenerative heart disease. Both vegetative bacteria and bacterial endospores are also effectively inactivated by microplasmas directly in water.

Other applications will also be presented and discussed in the presentation such as the inavtivation of bacerial biofilms, eukaryotic microorganisms (fungi) and fungal biofilms, and the inactivation of microorganisms in water and aqueous solutions.

References

[1] E.E. Kunhardt, IEEE Trans. Plasma Sci. <u>28</u> (2000) 1 and references therein to earlier work
[2] M. Laroussi, IEEE Trans. Plasma Sci. <u>24</u> (1996) 1188

Reactivity of Hydrated Monovalent First Row Transition Metal Ions $M^+(H_2O)_n$, M = Cr, Mn, Fe, Ni, Co, Cu and Zn toward Acetonitrile

I. Herber

Institut für Physikalische Chemie, Christian-Albrechts-Universität zu Kiel, Olshausenstraße 40, 24098 Kiel, Germany

M. K. Beyer

Institut für Ionenphysik und Angewandte Physik, Leopold-Franzens-Universität Innsbruck, Technikerstraße 25 6020 Innsbruck, Austria

Hydrated singly charged metal ions $M^+(H_2O)_n$ in the gas phase can be considered as a model system for aqueous solutions of transient species. They have been studied in detail over the last two decades by a combination of experiment and theory [1]. The investigation of the reactions of $M^+(H_2O)_n$ (M = V, Cr, Mn, Fe, Co, Ni, Cu and Zn) with NO shows the oxidation of zinc and iron by forming $[MOH(H_2O)_n]^+$ [2]. The reaction of magnesium with acetonitrile, CH_3CN, also revealed the formation of hydroxide species, $[MgOH(H_2O)_n]^+$ [3].

In the present study, reactions of $M^+(H_2O)_n$ (M = Cr, Mn, Fe, Ni, Co and Zn; n < 40) with CH_3CN were studied by Fourier transform ion cyclotron resonance (FT-ICR) mass spectrometry in the gas phase. $M^+(H_2O)_n$ ions were generated in an external laser vaporisation source. Uptake of CH_3CN was observed for all metal ions. By analysing the kinetics the reaction rate constants were determined. The number of CH_3CN molecules taken up depends on the metal ion and the pressure used for CH_3CN. However, the final product $M^+(ACN)_n$, n = 2, 3 is independent of the concentration of acetonitrile. During the reactions the uptake of more than three molecules acetonitrile, with size dependence, was observed. In contrast to the reactions with NO, oxidation is observed only for zinc, with concomitant reduction of acetonitrile to form the CH_3CHN or CH_3CNH radicals. After a reaction delay of 200s three more CH_3CN molecules are taken up, in subsequent reaction steps, to form $[ZnOH(CH_3CN)_3]^+$, the same final product that was observed with hydrated magnesium [3]. However, while in the reactions of $Mg^+(H_2O)_n$ with CH_3CN, the first reaction step inevitably leads to elimination of CH_3CHN or CH_3CNH, in the case of

$Zn^+(H_2O)_n$, uptake of CH_3CN proceeds, and oxidation may take place with any number of acetonitrile molecules in the cluster.

By counting the number of evaporating water molecules during the reaction of the metal ions with acetonitrile we determine the reaction enthalpy. However, nanocalorimetry worked only for the first and sometimes for the second uptake of acetonitrile, since the rates of subsequent reaction steps are size dependent.

References

[1] a) M. A. Duncan, Annu. Rev. Phys. Chem. **48**, 69 (1997); b) A. Irigoras, O. Elizalde, I. Silanes, E. Fowler, J. M. Ugalde, J. Am. Chem. Soc. **122**, 114 (2000).
[2] C. van der Linde, R. F. Höckendorf, O. P. Balaj, M. K. Beyer, Chem. Eur. J. **19**, 3741 (2013).
[3] T.-W. Lam, C. van der Linde, A. Akhgarnusch, Q. Hao, M. K. Beyer, C.-K. Siu, ChemPlusChem **78**, 1040 (2013).

Using Kr$^+$ as Reagent Ions in a Selective-Reagent-Ionization – Mass Spectrometry (SRI-MS) Instrument

Kostiantyn Breiev, Matteo Lanza, Tilmann D. Märk
IONICON Analytik GmbH., Innsbruck (Austria)
Institut für Ionenphysik und Angewandte Physik, Leopold-Franzens Universität Innsbruck, Innsbruck (Austria)
kostiantyn.breiev@ionicon.com

Achim Edtbauer, Simone Jürschik, Philipp Sulzer, Jens Herbig, Alfons Jordan, Eugen Hartungen, Gernot Hanel, Lukas Märk
IONICON Analytik GmbH., Innsbruck (Austria)

W. Joe Acton
Lancaster Environment Centre, Lancaster University, Lancaster (UK)

Proton-Transfer-Reaction Mass Spectrometry (PTR-MS) possesses a large variety of advantages, such as high reagent ion yields and thus high sensitivity and low detection limits, response times in the 100 ms regime and online quantification [1]. Furthermore, the total energy transfer in PTR ionization is low, non-dissociative charge transfer dominates and relatively simple mass spectra are obtained, with the main product ion usually being the protonated parent molecule. In contrast to Selected-Ion Flow-Tube Mass Spectrometry (SIFT-MS) [2] in PTR-MS no mass filter is employed between the ion source and the reaction region, which results in significantly higher reagent ion yields and therefore overall instrumental sensitivity. However, original PTR-MS instruments were limited to H_3O^+ as reagent ions, whereas in SIFT-MS instruments the reagent ions can be selected between H_3O^+, NO^+ and O_2^+. Additional reagent ions provide important advantages, such as increased selectivity and a broader range of detectable substance classes.

Recently advanced PTR-MS instruments have been introduced, which are called Selective-Reagent-Ionization Mass Spectrometry (SRI-MS) instruments [3,4]. SRI-MS enables the use of H_3O^+, NO^+, O_2^+, Kr^+ and Xe^+, respectively, as reagent ions. It has been shown that with such a setup several isomeric compounds can be easily separated [3,5] and even inorganic molecules can be detected [4]. However, so far no data has been published dealing with real-life applications of inorganic compound quantification.

Here we will present detailed calculations on the ideal operating conditions of SRI-MS in Kr$^+$ mode. These operating conditions are subsequently applied to common

fields of application, where so far PTR-MS has been widely used but was limited to the quantification of Volatile Organic Compounds (VOCs). Fig. 1 displays one example of the analysis of indoor air in our laboratory. It is neither possible to ionize O_2, nor CO_2 with H_3O^+, NO^+ or O_2^+. With Kr^+ as reagent ions simple charge transfer reactions occur, leading to O_2^+ and CO_2^+. It is well known from literature that indoor air typically contains about 20% oxygen and about 750 ppmv carbon dioxide [6]. Comparing these values with the results of our measurement in Fig. 1 indicates a very high level of accuracy in quantification, with 20.8% oxygen and 770 ppmv carbon dioxide.
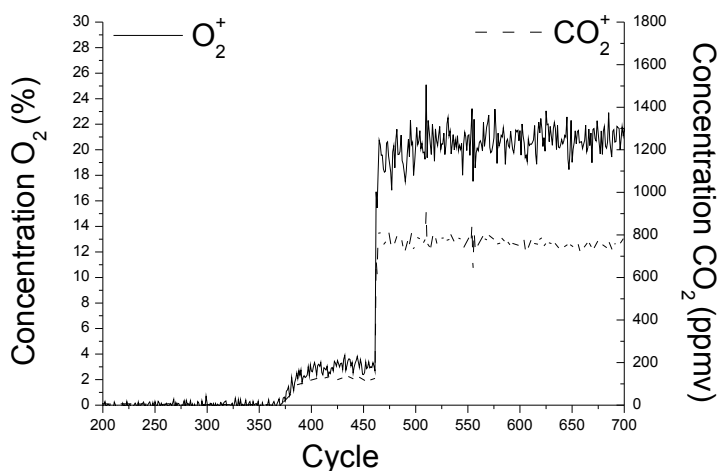

Figure 3*: SRI-MS analysis of O_2 (left y-axis) and CO_2 (right y-axis) concentrations in laboratory air (starting at about cycle no 470) utilizing Kr^+ as reagent ions*

As a second important field of application we will present results on engine exhaust analyses. Again, several PTR-MS studies on VOCs in car exhaust have been published, but for the detection and quantification of compounds with lower proton affinities than water, additional analytical equipment was necessary. Utilizing SRI-MS in Kr^+ mode we compare the CO and CH_4 concentrations of two cars (diesel and gasoline) and find that the CO as well as the CH_4 concentrations are both significantly (factor 2-3) lower for the diesel engine.

In summary we conclude that an SRI-MS instrument, operated in the way presented here, makes PTR-MS much more versatile and virtually the only instrument necessary. All advantages are preserved when operated in H_3O^+ mode, but the

instrument can easily be switched to O_2^+, NO^+ or Kr^+ chemistry if higher selectivity [5] and/or the quantification of additional substance classes are needed.

Acknowledgement

References

[1] W. Lindinger, A. Hansel and A. Jordan, On-line monitoring of volatile organic compounds at pptv levels by means of Proton-Transfer-Reaction Mass-Spectrometry (PTR-MS): Medical applications, food control and environmental research, Review paper, *Int. J. Mass Spectrom. Ion Proc.* 173, 191-241 (1998).

[2] D. Smith, P. Spanel, Selected ion flow tube mass spectrometry (SIFT-MS) for on-line trace gas analysis, *Mass Spectrometry Reviews* 24 (2005) 661 - 700.

[3] A. Jordan, S. Haidacher, G. Hanel, E. Hartungen, J. Herbig, L. Märk, R. Schottkowsky, H. Seehauser, P. Sulzer, T.D. Märk, An online ultra-high sensitivity proton-transfer-reaction mass-spectrometer combined with switchable reagent ion capability (PTR+SRI-MS), *International Journal of Mass Spectrometry* 286 (2009), 32-38.

[4] P. Sulzer, A. Edtbauer, E. Hartungen, S. Jürschik, A. Jordan, G. Hanel, S. Feil, S. Jaksch, L. Märk, T. D. Märk: From conventional Proton-Transfer-Reaction Mass Spectrometry (PTR-MS) to universal trace gas analysis, *International Journal of Mass Spectrometry* 321-322 (2012) 66-70.

[5] M. Lanza, W.J. Acton, S. Jürschik, P. Sulzer, K. Breiev, A. Jordan, E. Hartungen, G. Hanel, L. Märk, C.A. Mayhew, and T.D. Märk: Distinguishing two isomeric mephedrone substitutes with selective-reagent-ionization mass spectrometry (SRI-MS), *Journal of Mass Spectrometry* 48 (2013) 1015-1018.

[6] D. Norback, I. Michel, J. Widstrom, Indoor air quality and personal factors related to the sick building syndrome, *Scand J Work Environ Health* 1990;16(2):121-128.

Simulations of C_{60} aggregates decorated with small molecules

Alexander Kaiser, Andreas Mauracher, Paul Scheier, Michael Probst
Institut für Ionenphysik und Angewandte Physik, University of Innsbruck,
Technikerstrasse 25, A-6020 Innsbruck, Austria

Olof Echt
Department of Physics, University of New Hampshire, Durham, NH 03824, USA

Frank Hagelberg
Department of Physics and Astronomy, East Tennessee State University, Johnson City, TN 37614, USA

The adsorption of molecules on the outer side of fullerenes is a model reaction that allows testing adsorption features of more extended carbonaceous materials. Complexes with different adsorbates such as He, H_2, CH_4, C_2H_4 and CO_2 have been measured by mass spectrometry in the labs of the University of Innsbruck. We complemented the experimental results with molecular dynamics simulations based on ab initio potential energy surfaces. We studied adsorption capacities and energies as well as the molecular orientation in dimple and groove sites and explored the shell structure of these complexes.

1. Introduction

Adsorption of gases on carbonaceous materials could be exploited for safe and efficient storage of fuels on board of vehicles used for public and private transportation. Beside safety aspects, storage capacities in inexpensive low-weight containers are a main goal. The best candidates are natural gas (mainly CH_4) and hydrogen but one could also think of C_2H_4 or more complicated molecules.

Besides these technological aspects intriguing questions of basic physics arise in these systems. How does the corrugation of the fullerene surface influence storage capacities and the orientations of the molecules? Can we find particular, strongly bound commensurate phases, where each face of the fullerene is occupied by exactly one adsorbate molecule? What are the consequences of the different curvature of fullerenes and graphite or graphene? We addressed those issues in our recent joint experimental and theoretical works on $C_{60}(H_2)_n$ [1], $(C_{60})_m(CH_4)_n$ [2, 3], $(C_{60})_m(C_2H_4)_m$ [4], and $(C_{60})_m(CO_2)_n$ [5]. In the present contribution we show our latest simulation results of ethylene adsorption and compare them with adsorption of H_2 and CH_4.

2. Simulation methods and challenges

Ethylene is a planar molecule with a significant quadrupole moment. Contrary to He and CH_4, the interaction strength strongly depends on the relative orientation of two C_2H_4 molecules and ranges from 59.6 meV in T-shaped configuration to 2.4 meV for parallel planes [6]. Even if atomic charges are varied in the fitting of the parameter set this anisotropy complicates the search for analytical pair potentials. To better sample the whole potential energy surface we complemented an extensive set of CCSD(T)/AVTZ energies (12 different molecular configurations of Kalugina et al. [6]) with random configurations. Using this larger sample we were able to fit a force field that shows the correct trends concerning the relative orientation and that gives good agreement with the CCSD(T)/AVTZ dimer structure and binding energy. We also constructed a force field for C_{60}-C_2H_4 interactions based on DFT-D calculations (ωB97X-D/6-31g(d,p) [7-10]). For the C_{60}-C_{60} interaction we resorted to the Girifalco potential [11]. With these force fields we performed Molecular Dynamics (MD) simulations and optimizations using our own code. We also performed plane-wave DFT re-optimizations in vasp 5.2.
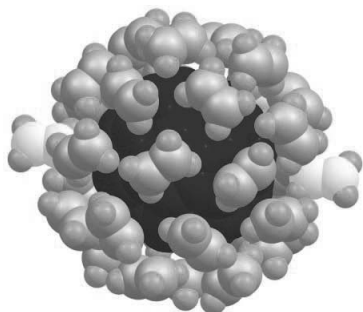
3. Simulation results

Figure 1: Two molecules (light grey) in $C_{60}(C_2H_4)_{32}$ stand up.

A single C_{60} fullerene with 32 adsorbed molecules is shown in Fig.1. There is not enough space for all 32 molecules to lie flat (C=C parallel to the C_{60}-faces) but the footprint of C_2H_4 can be lowered if its C=C axis is radially oriented; as a result two of them (light grey) stand up. Such an effect could not be observed for the relatively symmetric methane molecules. The molecular plane of all other 30 ethylene molecules is slightly tilted.

Ethylene on graphite and graphene offers a variety of different phases from solid-like to liquid-like low and high density phases [12-18]. The temperature (T) dependence of pairwise relative orientation and of molecular rotation was calculated by tracking three angles during heating of $C_{60}(C_2H_4)_{32}$ shown in Fig. 1. In general at T < 40-60 K, C_2H_4 is confined in its position and its mobility is gradually increased with T. The molecules start switching between a vertical and parallel C=C position at around 40-50 K. The tilt angle of the molecular plane allows flat orientation at T > 55 K. The relative orientation (angle γ) of neighboring C_2H_4
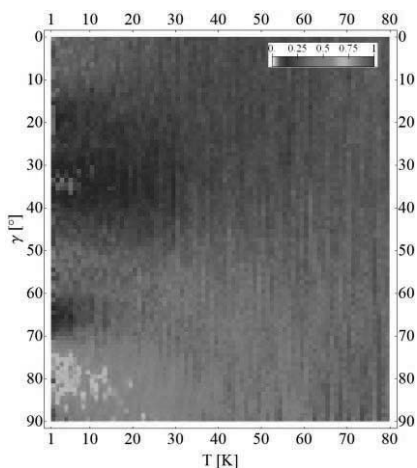
Figure 2: *Temperature dependence of the pairwise orientation of C₂H₄*

molecules is measured by a double projection on the fullerene faces and its T-dependence is shown in Fig. 2. 45 % of the molecules contribute to the peak at 80° at low T. A herring-bone pattern [17, 18] ($\gamma = 60°$ and $0°$) is not possible on C_{60}.

We also performed MD simulations of $(C_{60})_m(C_2H_4)_n$ clusters with m=1-5 and n up to 500. We could identify particulary stable structures that are responsible for anomalies in the ion yield (magic numbers) including dimple sites, groove sites and complete solvation shells. A comprehensive report of all simulated and measured results shall be found in [4].

Acknowledgement

References

[1] Kaiser A, Leidlmair C, Bartl P, Zöttl S, Denifl S, Mauracher A, et al. Adsorption of hydrogen on neutral and charged fullerene: Experiment and theory. J Chem Phys 2013;138(7):074311-13.

[2] Kaiser A, Zöttl S, Bartl P, Leidlmair C, Mauracher A, Probst M, et al. Methane Adsorption on Aggregates of Fullerenes: Site-Selective Storage Capacities and Adsorption Energies. ChemSusChem 2013;6(7):1235 – 44.

[3] Zöttl S, Kaiser A, Bartl P, Leidlmair C, Mauracher A, Probst M, et al. Methane Adsorption on Graphitic Nanostructures: Every Molecule Counts. J Phys Chem Lett 2012;3(18):2598-603.

[4] Zöttl S, Kaiser A, Daxner M, Goulart M, Mauracher A, Probst M, et al. Ordered Phases of Ethylene Adsorbed on Charged Fullerenes and their Aggregates. Carbon 2013;submitted.

[5] Mauracher A, Kaiser A, Probst M, Zöttl S, Daxner M, Postler J, et al. Decorating $(C_{60})_n{}^+$, n = 1–3, with CO_2 at low temperatures: Sterically enhanced physisorption. Int J Mass Spectrom;in print.

[6] Kalugina YN, Cherepanov VN, Buldakov MA, Zvereva-Loete N, Boudon V. Theoretical investigation of the ethylene dimer: Interaction energy and dipole moment. J Comput Chem 2012;33(3):319-30.

[7] Grimme S. Semiempirical GGA-type density functional constructed with a long-range dispersion correction. J Comp Chem 2006;27(15):1787-99.

[8] Chai J-D, Head-Gordon M. Long-range corrected hybrid density functionals with damped atom-atom dispersion corrections. Phys Chem Chem Phys 2008;10(44):6615-20.

[9] Ditchfield R, Hehre WJ, Pople JA. Self-Consistent Molecular-Orbital Methods. IX. An Extended Gaussian-Type Basis for Molecular-Orbital Studies of Organic Molecules. J Chem Phys 1971;54(2):724-8.

[10] Hehre WJ, Ditchfield R, Pople JA. Self-consistent molecular orbital methods. XII. Further extensions of Gaussian-type basis sets for use in molecular orbital studies of organic molecules. J Chem Phys 1972;56(5):2257-61.

[11] Girifalco LA, Lad RA. Energy of Cohesion, Compressibility, and the Potential Energy Functions of the Graphite System. J Chem Phys 1956;25(4):693-7.

[12] Grier BH, Passell L, Eckert J, Patterson H, Richter D, Rollefson RJ. Neutron-Scattering Study of Ethylene Motions on Graphite Surfaces. Phys Rev Lett 1984;53(8):814-7.

[13] Inaba A, Morrison JA. Ethylene on Graphite - Heats of Adsorption and Phase-Diagram. Phys Rev B 1986;34(5):3238-42.

[14] Klein ML, Morrison JA. Gas Surface-Potentials and the Interpretation of Experiments on the Ethylene Graphite System Using Molecular-Dynamics Calculations. Carbon 1987;25(1):23-30.

[15] Larese JZ, Passell L, Heidemann AD, Richter D, Wicksted JP. Melting in 2-Dimensions - the Ethylene-on-Graphite System. Phys Rev Lett 1988;61(4):432-5.

[16] Kim HK, Feng YP, Zhang QM, Chan MHW. Phase-Transitions of Ethylene on Graphite. Phys Rev B 1988;37(7):3511-23.

[17] Moller MA, Klein ML. The Low-Temperature Structure of Ethylene Monolayers Physisorbed on the Graphite Basal-Plane. Can J Chem 1988;66(4):774-8.

[18] Cheng A, Klein ML. Melting Transition of Ethylene on Graphite. Langmuir 1992;8(11):2798-803.

Pendular-state wavepacket dynamics and non-adiabatic effects of state-selected OCS molecules

Sebastian Trippel,[1] Terry Mullins,[1] Nele Müller,[1] Jens Kienitz,[1, 2] and Jochen Küpper,[1,2,3]

[1] Center for Free-Electron Laser Science, DESY, Notkestraße 85, 22607 Hamburg, Germany
[2] Department of Physics, University of Hamburg, Luruper Chaussee 149, 22761 Hamburg, Germany
[3] Center for Ultrafast Imaging, University of Hamburg, Luruper Chaussee 149, 22761 Hamburg, Germany

The behavior of molecules subject to strong laser fields has been a rapidly growing topic in molecular physics and chemistry during the last few years. In particular the investigation of alignment and orientation has attracted a huge amount of interest [1, 2] with possible applications ranging from molecular dynamics and stereochemistry [3], through quantum computation [4] and rotational coherence spectroscopy [5], to torsional control for potential future ultrafast molecular switches [6, 7]. Previous work focused, theoretically as well as experimentally, on the exploration of two limiting regimes, adiabatic and impulsive alignment. In the adiabatic case ($\tau_{Laser} > \tau_{rot}$), the interaction with the external electric field creates pendular states that correlate adiabatically with the field-free rotational eigenstates [8]. Therefore, a molecule is smoothly transferred from its initial field free rotational state to the corresponding directional hybridized state as the laser pulse is switched on. When the laser field fades away it returns to its initial state. The second limit employs laser pulses much shorter than the rotational period of the molecule ($\tau_{Laser} << \tau_{rot}$). In this case the molecule is left behind in a coherent superposition of rotational Eigen states created by the interaction with the short and strong laser-field [9]. The intermediate regime ($\tau_{Laser} \approx \tau_{rot}$) was only investigated theoretically so far. The temporal evolution of the degree of alignment during and after the laser pulse was discussed and modulations in the degree of alignment during the laser pulse and revival structure after the laser pulse were predicted [10, 11]. A comparison of the intermediate pulse-duration regime with both, adiabatic and impulsive, temporal limits was performed [12].

The availability of high intensity femtosecond laser systems and options to strongly stretch them make experimental studies in the intermediate regime now possible. The duration of the laser pulse can be adjusted between a few ten femtoseconds to a few

hundred picoseconds [14]. This tunablity provides a continuous control parameter for small molecules regarding the adiabaticity of the alignment process.

We performed a combined theoretical and experimental study in the intermediate pulse length regime on aligned carbonyl sulfide (OCS) in the absolute ground state. A wave packet of pendular states was created by the rising edge of a chirped picosecond laser pulse. The rise time was shorter than the rotational period of OCS (Trot ≈ 80 ps) and, therefore, the molecules could not follow the temporal profile adiabatically. The resulting wave packet dynamics of the pendular states is observed and characterized by the degree of alignment.

In addition we have studied the adiabaticity in mixed field orientation of OCS. We observe a strong non-adiabatic behaviour in the orientation for pulse lengths much larger than the rotational period of the molecule [15]. The non-adiabaticity manifests itself in a pronounced field free rotational revival structure. Our approach provides direct experimental insight into the induced wave packet dynamics.

References

[1] H. Stapelfeldt and T. Seideman, *Rev. Mod. Phys.* **75**, 543 (2003).

[2] L. Holmegaard, J. H. Nielsen, I. Nevo, H. Stapelfeldt, F. Filsinger, J. Küpper, and G. Meijer, *Phys. Rev. Lett.* **102**, 023001 (2009).

[3] J. Larsen, I. Wendt-Larsen, and H. Stapelfeldt, *Phys. Rev. Lett.* **83**, 1123 (1999).

[4] K. F. Lee, D. M. Villeneuve, P. B. Corkum, and E. A. Shapiro, *Phys. Rev. Lett.* **93**, 233601 (2004).

[5] A. Przystawik, *et al.*, *Phys. Rev. A* **85**, 052503 (2012).

[6] S. Ramakrishna and T. Seideman, *Phys. Rev. Lett.* **99**, 103001 (2007).

[7] C. B. Madsen *et al.*, *Phys. Rev. Lett*. **102**, 073007 (2009).

[8] B. Friedrich and D. Herschbach, *Phys. Rev. Lett.* **74**, 4623 (1995).

[9] T. Seideman, J. Chem. Phys. **103**, 7887 (1995).

[10] J. Ortigoso, M. Rodriguez, M. Gupta, and B. Friedrich, *J. Chem. Phys.* **110**, 3870 (1999).

[11] T. Seideman, Phys. Rev. Lett. 83, 4971 (1999).

[12] R. Torres, R. de Nalda, and J. P. Marangos, Phys. Rev. A 72, 023420 (2005).

[13] N. Owschimikow, B. Schmidt, and N. Schwentner, Phys. Rev. A 80, 053409 (2009).

[14] S. Trippel et al., Mol. Phys. 111, 1738 (2013).

[15] J. Nielsen *et al.*, *Phys. Rev. Lett.* **108**, 193001 (2012)

Mass spectrometric investigation of reaction intermediates

Anton Škríba and Jana Roithová

Department of Organic Chemistry, Faculty of Science, Charles University in Prague, Hlavova 2030/8, 12843 Prague 2
Corresponding author: jana.roithova@natur.cuni.cz

Introduction

One of the most studied reactions nowadays is the C-C_{Ar} bond formation. Reactions known as Stille, Suzuki-Miyaura, Sonogashira or Negishi coupling represent the most prominent examples. The drawback of these transformations is the need of functionalized starting materials like aryl halides, which can be expensive or difficult to access in the case of complicated molecules. With respect to the modern atom economical concept [1], where minimum steps to reactants are required and minimum side products should be formed, the chemists focused on the direct C-H activation catalyzed by transition metals [2].

Gas phase study

We have been investigating the mechanistic aspect of the reaction (Figure 1) between pyridine and terminal alkynes catalyzed by the ruthenium complex [CpRu(py)$_2$(PPh$_3$)]$^+$ [3]. Using mass spectrometry and collision induced dissociation experiments we were able to detect several intermediates proposed in the reaction cycle and test their reactivity. With IRMPD (infrared multiphoton dissociation spectroscopy) [4] we were able to characterize the key intermediates in the reaction cycle (Figure 2). Obtained results were combined with theoretical calculations.
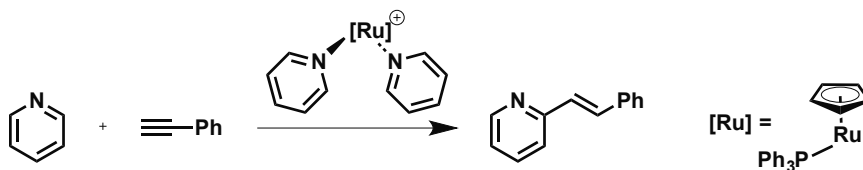

Figure 1: *Formation of styrylpyridine from pyridine and phenylacetylene catalyzed by ruthenium catalyst.*
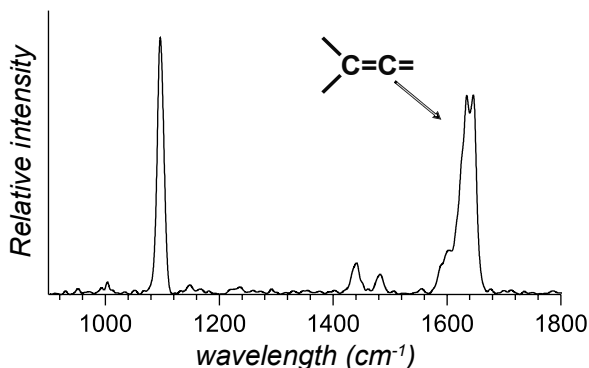
Figure 2: Experimental IRMPD spectrum (CLIO laser, Paris) showing vinylidene vibration of the possible reaction intermediate.

Acknowledgement

References
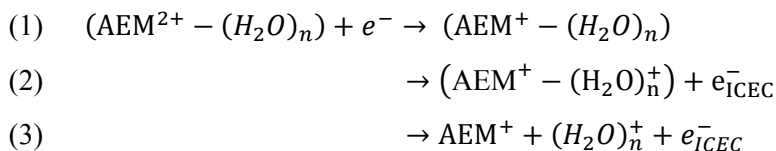
[1] B. Trost, *Science* **254**, 1471 (1991)
[2] V. Ritleng, C. Sirlin, M. Pfeffer. *Chem. Rev.* **102**, 1731 (2002)
[3] D. G. Johnson, J. M. Lynam, N. S. Mistry, J. M. Slattery, R. J. Thatcher, A. C. Whitwood, *J. Am. Chem. Soc.* **135**, 2222 (2013)
[4] J. Roithová, *Chem. Soc. Rev.* **41**, 547 (2012)

Intermolecular Coulombic electron capture driven electron emission of hydrated alkaliearth metal dications

Kevin Klawitter, Jusuf M. Khreis, Stephan Denifl
Institute for Ion Physics and Applied Physics,
University of Innsbruck, Technikerstr. 25/3, A-6020 Innsbruck

Based on the environment dependent autoionization mechanism called interatomic or intermolecular Coulombic decay (ICD), an environment dependent electron capture mechanism has been described in theory by Cederbaum and Gokhberg in 2009 [1], named interatomic or intermolecular electron capture (ICEC). In ICEC the system uses the excess energy after an electron capture to ionize neighbor atoms or molecules and subsequently emits a low energetic electron. This is a competitive process to the photorecombination where isolated atoms or molecules emit a photon that carries away the excess energy.

At the moment first investigations to approve the predicted ICEC experimentally for the proposed hydrated alkali earth metal (AEM) system [1] are carried out by us. In this system the ICEC mechanism for hydrated AEM dications is shown in equations below.

$$(1) \quad (AEM^{2+} - (H_2O)_n) + e^- \rightarrow (AEM^+ - (H_2O)_n)$$

$$(2) \quad \rightarrow \left(AEM^+ - (H_2O)_n^+\right) + e^-_{ICEC}$$

$$(3) \quad \rightarrow AEM^+ + (H_2O)_n^+ + e^-_{ICEC}$$

The AEM dication is surrounded by an arbitrary number of water molecules (left side of eq. 1). After catching the electron one positive charge of the AEM will be neutralized (right side of eq. 1) and the captured electron will go into the highest unoccupied orbital by releasing energy. This energy is utilized to ionize the neighboring water molecules (eq. 2), subsequently both cations undergo a coulomb explosion and a low energetic electron is emitted (eq. 3).

To carry out the ICEC investigations for the hydrated AEM's an electrospray ionization (ESI) ion source and an electron gun is connected to a mass spectrometer. Latter is an double focusing reverse Nier-Johnson type sector field mass spectrometer [2].

The hydrated AEM dications are produced by spraying a dissolved AEM-salt with the ESI source. The dications then are guided via an octupole ion guide to the

magnetic field sector of the mass spectrometer. There the AEM ions were mass selected dependent on the number of water molecules before they cross a low energetic electron beam to capture them. After that the kinetic energy release of the ionized water molecules is monitored by scanning the electric field of the electric sector. This technique of monitoring the kinetic energy release is called 'mass-analyzed ion kinetic energy scan (MIKES) [3].

Acknowledgement

References

[1] K. Gokhberg and L.S. Cederbaum. Environment assisted electron capture. Journal of Physics B: Atomic, Molecular and Optical Physics, 42 (23): 231001, 2009.

[2] John De Laeter and Mark D Kurz. Alfred Nier and the sector field mass spectrometer. Journal of Mass Spectrometry, 41 (7): 847-854, 2006.

[3] J Laskin and C Lifshitz. Kinetic energy release distributions in mass spectrometry. Journal of Mass Spectrometry, 36 (5): 459-478, 2001.

Ion-Surface Collisions of Low-Energy Ions Ar$^+$, N$_2^+$ and D$_2^+$ with Surfaces of Mixed Beryllium-Tungsten Thin Films

Martina Harnisch, Paul Scheier

Institute for Ion Physics and Applied Physics, University of Innsbruck

Zdenek Herman

J. Heyrovský Institute of Physical Chemistry, Academy of Sciences of the Czech Republic

Interactions of ionic projectiles (Ar$^+$, N$_2^+$, D$_2^+$) at incident energies from 20 eV up to 100 eV with surfaces of mixed beryllium-tungsten thin films of different composition were investigated at temperatures ranging from room temperature up to 450°C.

The aim of the measurements was to find differences between the different projectiles and a dependence of the Be$^+$ contribution to the spectra on the Be content in the surface sample. Besides various hydrocarbon contributions and sputtering of Be$^+$ from the surface, also reactions between the projectiles and the surface constituents could be observed in the interactions of D$_2^+$ with the surface samples.

1. Introduction

Research and development of feasible fusion devices in the connection with new sources of energy require fundamental information on plasma-wall interactions. Erosion and re-deposition of first-wall material in ITER (Be) can lead to the generation of mixed materials particularly Be-W mixed layers which have different properties than pure W compounds. This might reduce the performance of the PFCs. Hence the investigation of interactions of the involved plasma projectiles with these mixed material layers is required to provide important input data for modeling and computational science for the pioneering project ITER [1], [2].

Involved plasma projectiles are on the one hand the fusion fuels (deuterium and tritium), and on the other hand the gases planned to be used for cooling of the divertor region by impurity seeding (argon and nitrogen).

2. Experimental Setup

The experimental setup BESTOF in Innsbruck is described in large detail in previous publications [3]. It consists of two mass spectrometers arranged in tandem geometry (Fig. 1).
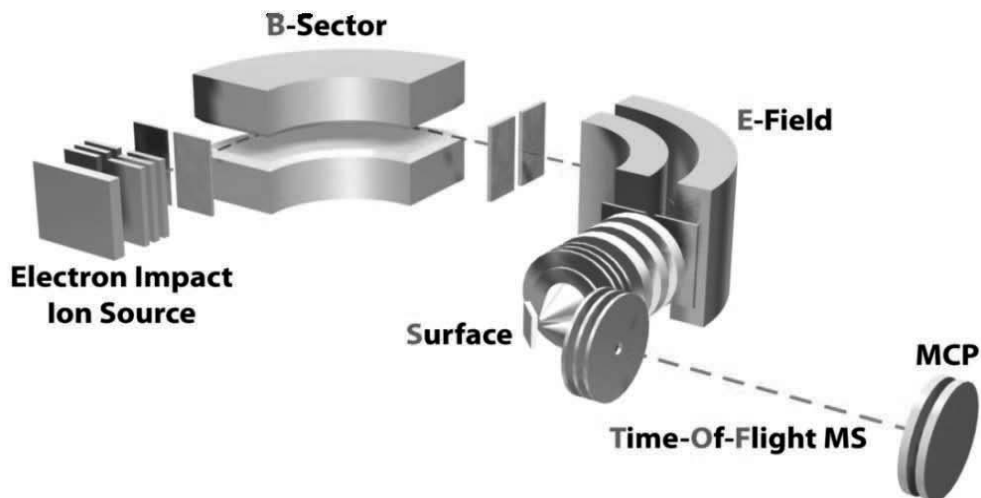
Figure 1: *Schematics of the tandem mass spectrometer BESTOF. A mass and energy selected ion beam interacts with a surface, the product ions are analyzed by a TOF mass spectrometer.*

Ions are produced in a Nier-type electron ionization source and extracted into the first mass analyzer, a reverse-geometry two-sector-field mass spectrometer. Subsequently, the beam of m/z-selected projectile ions is focused on a surface sample, which can be heated up to 600°C. There the projectile ions interact with the target surface at an incident angle of 45° and at well-defined incident energies ranging from a 20 eV up to 100 eV. Ions produced during this interaction are extracted into a linear time-of-flight mass analyzer and recorded with a multi-channel-plate detector.

3. Results and Discussion

Ion-surface interactions of Ar^+ with three BeW surfaces of different Be/W ratios have been investigated (BeWO(60:22:11), BeW(50:50), BeW(90:10)). The spectra show contributions of sputtered beryllium, hydrocarbons coming from cracked pump oil depositing on the surface, and – at higher temperatures – alkali contaminants. A connection between the amount of beryllium in the surface sample used and the ion yield of Be^+ in the spectra could not be seen (see figure 2).
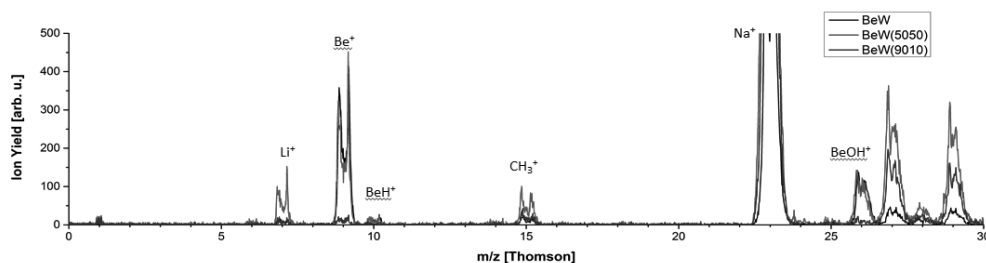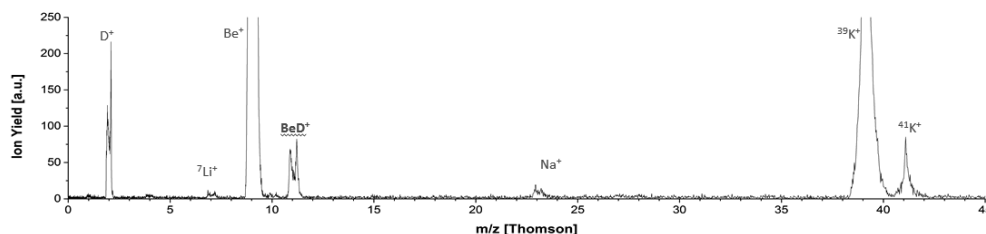
Figure 2: *Product ion spectrum of interactions of Ar$^+$ with different BeW mixed surface samples at a projectile incident energy of 70eV and a surface temperature of 300°C, showing Be$^+$ and Be products, remaining hydrocarbons and alkali contaminations.*

Interactions of D$_2^+$ with BeW(50:50) have been investigated at different surface temperatures ranging from room temperature to 450°C. While at room temperature reaction products of the interaction of D$_2^+$ with the surface hydrocarbons and very little beryllium can be seen in the spectra, at higher temperatures the hydrocarbon layer is efficiently removed and the Be$^+$ contribution increases remarkably. Beside the alkali contaminations also reactions of the projectile and the surface constituents to BeD$^+$ can be observed (see figure 3)

Figure 3: *Product ion spectrum of interactions of D$_2^+$ with a BeW(50:50) mixed surface sample at a projectile incident energy of 70eV and a surface temperature of 450°C, showing contributions of alkali contaminants, the dissociated projectile D$^+$, sputtered surface material Be$^+$ and the reaction product BeD$^+$.*

Acknowledgement

References

[1] EFDA work programme 2014 – Issue 3 – 15. October 2013

[2] A. Keim, M. Harnisch, P. Scheier, Z. Herman, *Int. J. of Mass Spectrom.*, Collisions of low-energy ions Ar^+ and N_2^+ with room temperature and heated surfaces of tungsten, beryllium and mixed beryllium-tungsten thin film, *in press*

[3] C. Mair, T. Fiegele, F. Biasioli, Z. Herman, T. D. Märk, *J. Chem. Phys.,* **111**, 2770 (1999)

# Revealing the Gas Phase Structure of Cationic Gold(I) Complexes by Ion Spectroscopy

Jiří Schulz and Jana Roithová

Department of Organic Chemistry, Faculty of Science, Charles University in Prague, Hlavova 2030/8, 128 43 Prague 2, Czech Republic

Introduction

The cationic gold(I) complexes are amongst the workhorses of the contemporary homogeneous catalysis[1]. This is due to their substantial Lewis acidity and thereof emerging ability to activate carbon-carbon multiple bonds towards an addition of various nucleophiles. The initial addition of a nucleophile often serves as an instigator for more complex reaction sequences affording typically carbocycles or heterocycles. The remarkably broad reaction scope may be achieved particularly in gold(I) catalysed oxidation reactions of alkynes[2,3]. The reactivity in this type of transformations have been rationalized by formation of highly reactive intermediates, *i.e.* gold(I) α-oxo carbenoids, that are strong electrophiles amenable to intra- as well as intermolecular trapping by reaction with available nucleophile [2,3]. Nevertheless, the involvement of gold(I) α-oxo carbenoids in the cascade reactions initiated by gold(I) catalysed oxidation reaction of alkynes have never been substantiated. Moreover, some of the recent studies aimed at the investigation of reaction mechanisms of such a type of transformations argue against the intermediacy of gold(I) α-oxo carbenoids while proposing alternative reaction schemes [4,5].

Knowing the above mentioned we decided to make use of techniques of tandem mass spectrometry as well as ion spectroscopy in study of the gas phase structure of cationic gold(I) complexes involved in gold(I) catalysed oxidation reactions of selected terminal as well as internal alkynes. The ions of interest have been generated by spraying from the solution of pyridine *N*-oxide, alkynes $R^1C\equiv CR^2$ (R^1/R^2 = Me/Me, Me/Ph, Ph/Ph, H/Ph) and cationic gold(I) complexes $[LAu]^+$ (Scheme 1). The species formed have been studied by energy resolved collision induced dissociation experiments together with infrared multiphoton dissociation spectroscopy [6,7]. The performed experiments conclusively showed that the putative gold(I) α-oxo carbenoids (**B**) undergo in the gas phase the Wolff rearrangement[8] yielding respective gold(I) ketene complexes (**C**), while the ions originally ascribed to initial alkyne–pyridine *N*-oxide adduct (**A**) may instead constitute an important resting state of gold(I) α-oxo carbenoids in the reaction mechanism.
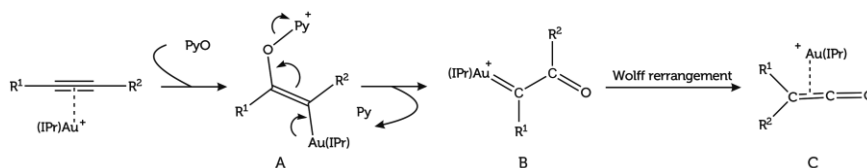
*Scheme 1: Generation of cationic gold(I) complexes **A–C**.*

Acknowledgement

References

[1] A. S. K. Hashmi, *Chem. Rev.* **107**, 3180–3211 (2007)

[2] J. Xiao, X. Li, *Angew. Chem., Int. Ed.* **50**, 7226–7236 (2011)

[3] M. C. Blanco, A. S. K. Hashmi, in: Modern Gold Catalysed Synthesis, A. S. K. Hashmi and F. D. Toste Eds, Wiley-VCH, Weinheim, Germany

[4] B. Lu, Y. Li, Y. Wang, D. H. Aue, Y. Luo, L. Zhang, *J. Am. Chem. Soc.* **135**, 8512–8524 (2013)

[5] G. Henrion, T. E. J. Chavas, X. Le Goff, F. Gagosz, *Angew. Chem., Int. Ed.* **125**, 6397–6402 (2013)

[6] L. Mac Aleese, A. Simon, T. B. McMahon, J. M. Ortega, D. Scuderi, J. Lemaire, P. Maitre, *Int. J. Mass. Spectrom.* **249**, 14–20 (2006).

[7] J. Roithová, *Chem. Soc. Rev.* **41**, 547–559 (2012).

[8] W. Kirmse, *Eur. J. Org. Chem.*, 2193–2256 (2005)

Electrical conductance of single molecules measured with conductive AFM

Benjamin Lachmann, Doreen Schütze

Institut für Physikalische Chemie, Christian-Albrechts-Universität zu Kiel,
Olshausenstraße 40, 24098 Kiel, Germany

Martin K. Beyer

Institut für Ionenphysik und Angewandte Physik,
Leopold-Franzens-Universität Innsbruck, Technikerstraße 25
6020 Innsbruck, Austria

Measurement of single molecule conductance is an essential step in the development of future electrical devices. Xu *et al.* demonstrated the reproducible measurement in break-junction experiments in organic solutions [1]. The molecular system of 1,8-Octanedithiol (ODT) in toluene showed an electrical contact between an Au-substrate and an Au-coated AFM-tip after repeatedly building and breaking the mechanical contact between those electrodes. The current as a function of Z-piezo driving distance showed plateaus with integer multiples of a fundamental current. However the uncertainty in the data analysis is a big problem in obtaining the objective values of interest.
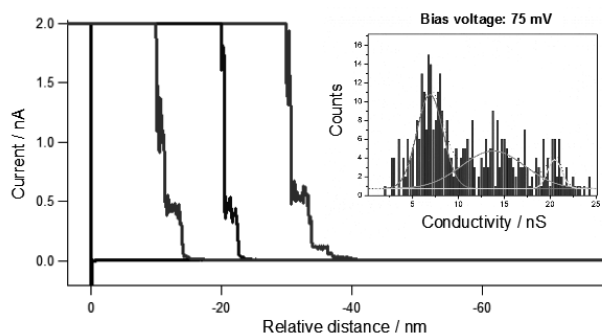
Figure 1: *(left) Example current/distance curves of break-junction experiments with 4,4'-Bipyridine at 75 mV; (upper right corner) statistical analysis via histogram#*

Here we present a general way of interpretation of one dimensional current and force curves with focus on monomolecular properties and molecular contact rupture

behavior using the example of 4,4-Bipyridine in toluene. While the results are in good agreement with literature [2], measurements at different bias voltages show the opportunity to simulate IV-curves of single or a couple of molecules connected in parallel, respectively. The advantages are given by the opportunities to directly investigate the ohmic behavior of quantum contacts under ambient conditions and dependency of the current flow on the applied force.

The conductance of aliphatic and aromatic molecules is studied as a first step towards mechanically switchable systems.

References

[1] B. Xu, X. Xiao, N. J. Tao, *J.Am.Chem.Soc.* **2003**, *125*, 16164-16165

[2] M. Frei, S. V. Aradhya, M. Koentopp, M. S. Hybertsen, L. Venkataraman, *Nano Lett,* **2011**, *11*, 1518-1523

Non-adiabatic dynamics of electronically excited rare-gas cluster cations

Martin Stachoň

IT4Innovations National Supercomputing Center & Department of Applied Mathematics, VSB – Technical University Ostrava, 17. listopadu 15/2172, Ostrava – Poruba, Czech Republic

Ivan Janeček

Institute of Geonics v.v.i., Academy of Sciences of the Czech Republic, Studentská 1768, Ostrava – Poruba, Czech Republic

René Kalus

IT4Innovations National Supercomputing Center & Department of Applied Mathematics, VSB – Technical University Ostrava, 17. listopadu 15/2172, Ostrava – Poruba, Czech Republic

1. Introduction

The rare-gas cluster cations are, from theoretical point of view, both objects highly appropriate for numerical modelings and simulations as well as objects of huge numerical demands, in particular if larger cluster sizes are involved. The former is due to the fact that highly accurate models for intracluster interactions based on the *diatomics-in-molecules* (DIM) [1] technology are available for singly ionized rare-gas clusters which are, on the other hand, still sufficiently fast to be involved in explicit dynamical calculations. The latter then relates to the fact that many electronic states are involved even if energy intervals of only a few eV are considered, which leads to the necessity of using true non-adiabatic dynamics simulation methods. For an Rg_N^+ cluster, the number of relevant (interacting) electronic states amounts to $3N$, i.e., many electronic states are to be taken into account even for moderate cluster sizes.

The rare-gas clusters were also studied to a large extent experimentally [2], mostly some twenty years ago. However, the experimental data, often obtained for cluster sizes of several tens of atoms, have still been waiting for a proper theoretical interpretation due to numerical demands of needed calculations. Only with the advent of powerful supercomputers of the tier-0 level (i.e., of petaflops peak performance) such calculations have become practicable. In the present contribution, results we obtained from numerical simulations on electronically excited rare-gas clusters of

sizes up to $N = 19$ will be presented. The data have been obtained thanks to the support from the PRACE research initiative [3] who granted us an allocation of 16 million core-hours on one of the European tier-0 supercomputers.

2. Methods

A mean-field semiclassical method has been used for dynamical calculations [4]. The electronic degrees of freedom have been treated via the non-stationary Schrödinger equation projected on a minimal valence-bond basis set (as proposed within the DIM method applied to rare gases [5]) and the nuclei have been approximated by classical particles moving in the mean field of quantum electrons. Both relativistic effects [6] as well as quantum decoherence processes [7] have been taken into account. Several simulation frameworks, as introduced in ref. [7] and implemented in our MULTIDYN code [8], have been used and the numerical data obtained for them compared to each other. Since the length of a direct dynamical simulation has been limited up to integration times of $t_{int} \approx 0.5 - 1.0$ ns due to computational demands while the life-time of metastable intermediate fragments were reported to span scales of several to several tens of microseconds in experiments [8], a multiscale model based on the chemical kinetics approach [9] has been used to extend the direct, nanosecond simulation data to longer times.

3. Results

Two families of non-adiabatic processes in the Rg_N^+ clusters have been studied: a) the photodissociation of the clusters in the VIS and UV region of the electromagnetic spectrum and b) the post-ionization fragmentation of their neutral precursors ionized by an impacting particle. Three rare-gases have been considered, argon as the rare gas having been probably most extensively studied in the past and as a species for which relativistic electronic effects are not much important, xenon as a representative of heavy elements with a lot of relativity coming into play in their electronic subsystems, and finally krypton as a mid-way element between relativistic xenon and "non-relativistic" argon. The main focus of the present contribution is on the internal conversion of the initial electronic excitation and on the production of long-lived, metastable intermediate fragments. As an illustration of the results obtained from simulations, the dependence of the average size of ionic fragments resulting from the photodissociation of argon cluster cations is plotted against the size of parent clusters in Fig. 1 and compared with available experiments.
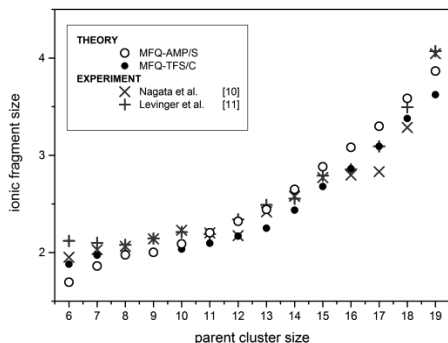
Figure 1: *Average size of ionic fragments emitted from Ar_N^+, N = 6 – 19, upon photoexcitation by a photon of E_{phot} = 2.35 eV.*

Acknowledgements

References

[1]   F. O. Ellison, J. Am. Chem. Soc. 85 (1963) 3540.
[2]   H. Haberland, Ed. *Clusters of Atoms and Molecules*, Springer, Berlin 1994.
[3]   http://www.prace-ri.eu
[4]   I. Janeček, D. Hrivňák, R. Kalus, and F. X. Gadéa, J. Chem. Phys. 125 (2006) 104315.
[5]   P. J. Kuntz and J. Valldorf, Z. Phys. D 8 (1988) 195.
[6]   M. Amarouche, G. Durand, and J. P. Malrieu, J. Chem. Phys. 88 (1988) 1010.
[7]   I. Janeček, S. Cintavá, D. Hrivňák, R. Kalus, M. Fárník, and F. X. Gadéa, J. Chem. Phys. 131 (2009) 114306.
[8]   http://moldyn.vsb.cz
[9]   I. Janeček, T. Janča, P. Naar, R. Kalus, M. Fárník, and F. X. Gadéa, J. Chem. Phys. 138 (2013) 044303.
[10] T. Nagata and T. Kondow, J. Chem. Phys. 98 (1993) 290.
[11] N. E. Levinger, D. Ray, M. L. Alexander, and W. C. Lineberger, J. Chem. Phys. 89 (1988) 5654.

Reactions of isotopically labeled vinyl acetate and acrylic acid with hydrated electrons in the gas phase

Amou Akhgarnusch, Sascha Frick, K. Philip Jäger, Robert F. Höckendorf, Patrick Liedtke, Bernd Hartke and Martin K. Beyer

Institut für Physikalische Chemie, Christian-Albrechts-Universität zu Kiel, Olshausenstraße 40, 24098 Kiel, Germany

FT-ICR Mass Spectrometry is a useful method to investigate the reactivity of gas-phase clusters, in particular transient species solvated in water clusters. The experiments are performed on a modified Bruker/Spectrospin CMS47X Fourier transform ion cyclotron resonance (FT-ICR) mass spectrometer [1,2]. Reactions of hydrated electrons $(H_2O)_n^-$ with acrylic acid, vinyl acetate and methyl acrylate have recently been studied without isotopic labeling [3]. For acrylic acid, oligomerization was observed, with acrylic acid radical anions serving as starters. The results with methyl acrylate suggest that the primary radical anion undergoes a radical addition followed by 5-exo-trig cyclization with a second reactant molecule. For vinyl acetate bond cleavage is observed, with a strong dependence on the size of the hydration shell [3]. However, due to mass overlap in the experiments with acrylic acid and vinyl acetate, important questions remained open. Isotopically labeled $CH_2CH^{13}COOH$ and $CH_3COO^{13}CH^{13}CH_2$ are used to resolve these issues. With labeled acrylic acid, a kinetic and nanocalorimetric analysis [2] becomes possible. The reaction rate for the formation of the acrylic acid oligomers was determined as well as the reaction enthalpy for the charge transfer process. The dissociation product of vinyl acetate after the charge transfer could be identified. The $^-O^{13}CH^{13}CH_2$ anion remains in the cluster, while the $CH_3CO^\bullet$ radical evaporates. Quantum chemical calculations employing global geometry optimization methods [4] support the experimental findings with vinyl acetate. The calculations also show the peculiar size dependence of the electron-induced C-O bond cleavage in vinyl acetate.

References

[1] C. Berg, T. Schindler, G. Niedner-Schatteburg, V. E. Bondybey, *J. Chem. Phys*. 1995, **102**, 4870-4884.

[2] Robert F. Höckendorf, O. Petru Balaj, Christian van der Linde, Martin K. Beyer, *Phys. Chem. Chem. Phys*. 2010, **12**, 3772–3779.

[3] K. Philip Jäger, Robert F. Höckendorf, Martin K. Beyer, *Int. J. Mass Spectrom*. 2012, **330/332**, 3772–3779.

[4] J. M. Dieterich, B. Hartke, Mol. Phys. 2010, **108**, 279. See also: http://www.ogolem.org.

IRMPD Spectroscopy in the Chemistry of Pyronin

Jiří Váňa, Jana Roithová

Faculty of Science, Department of Organic Chemistry, Charles University in Prague, Hlavova 2030/8, CZ-128 43 Prague 2, Czech Republic

Peter Šebej, Petr Klán

Department of Chemistry, Faculty of Science, Masaryk University, Kamenice 5/A8, 625 00, Brno, Czech Republic, and Research Centre for Toxic Compounds in the Environment, Faculty of Science, Masaryk University, Kamenice 126/3, 625 00 Brno, Czech Republic

The electrospray ionization and mass spectrometry in combination with Infrared Multiphoton Dissociation Spectroscopy (IRMPD) is very useful tool for study of reaction mechanisms. The ESI-MS enables isolation of transient reaction intermediates occurring in the reaction mixture in only negligible amounts. So obtained information is limited to molecular mass and fragmentation patterns of these ions. In order to further substantiate the identity of reactive intermediates, the mass-selected ions are further irradiated by Free Electron Laser (FEL) pulses and fragments abundance as a function of laser wavelength provides the so called action spectra. These are similar to the classical IR spectra and could be easily compared to the spectra predicted by theoretical calculations.

This approach for getting important information about reaction mechanisms was used in the study of photochemically induced C-C bond cleavage in pyronin analogues (Scheme 1).
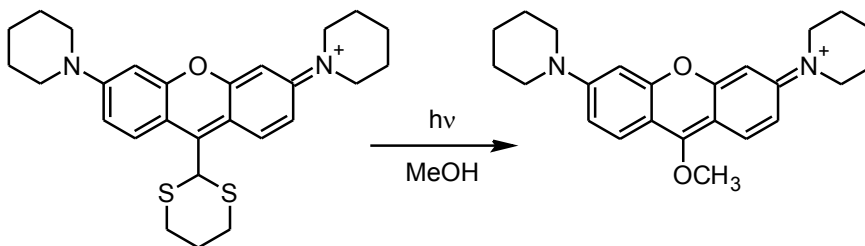
Scheme 1.

It was found that 1,3-dithian-2-yl derivatives of pyronin iminium salts upon irradiation in methanol undergo C-C bond cleavage to form its methoxy analogue. In this work we tried to examine this reaction using mass-spectrometry in combination with IRMPD and characterize possible reaction intermediates.

The ESI-MS spectrum of irradiated reaction mixture contains signals at m/z 497, 481, 465 (starting material), 439, 407 and 377 (product) that indicates complicated multistep reaction mechanism. More than one logical structure could be proposed for the individual detected ions thus their IRMPD spectra were recorded and analysed. Based on the obtained information, the reaction mechanism will be presented.
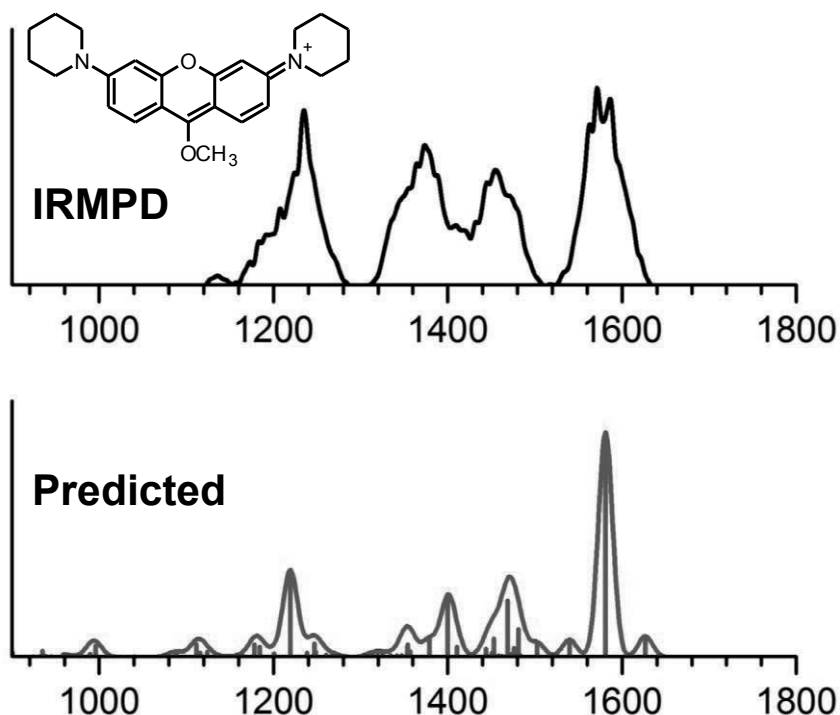
References

[1] J. Roithova, *Chem. Soc. Rev.*, 41, **2012**, 547-559.
[2] P. Stacko, P. Sebej, A. T. Veetil, P. Klan, *Org. Lett.*, 14, 18, **2012**, 4918-4921.

Inter-atomic Coulombic Decay (ICD) of Neon clusters upon electron ionization

Elias Jabbour Al Maalouf, Paul Scheier, Stephan Denifl

Institute for Ion and Applied Physics, University of Innsbruck, Technikerstrasse 25, A-6020-Innsbruck, Austria

In recent years the Interatomic Coulombic decay (ICD) has become known as an important decay process in weakly bound systems. Thereby electronic excess energy deposited by excitation or ionization by far ultraviolet photons or energetic particles like ions is transferred by exchange of a virtual photon to a neighboring particle that becomes ionized [1]. The results showed that ICD may be an abundant source for low energy electrons [2] which may further react in matter by electron capture or recombination. High-end experimental techniques using synchrotron ionization and reaction microscopes have been used to characterize ICD processes with weakly bound clusters. However, much less is known about ICD induced by electrons as impact species. This is a somewhat surprising situation, since electrons represent an abundant species as secondary particle formed in the interaction of ionizing radiation with matter [3]. It was also shown in many previous studies, that electron induced chemistry is very rich and find applications in many fields of physics and chemistry. For example, it was shown that low energy electrons can induce severe damage of DNA by the induction of single and double strand breaks, which may lead in accumulation to lethal harm of DNA in living cells [4]. Also in material sciences a high relevance of electron scattering processes is expected for processes on the nanometer scale [5]. The lack of ICD data for electron impact arose due to the experimental challenges in using electron beams as well from the physics of the electron impact process, where an *a priori* unknown amount of excess energy is deposited by the impacting electron. The deposited energy however may be substantial and may amount up to few tens of eV. This may lead to substantial fragmentation in clusters and also to Coulomb explosion following double ionization. Thus one main challenge in electron ionization experiments is to differentiate ICD processes from other fragmentation processes.

In the present study mass spectrometry is used to investigate the presence of ICD relaxation mechanism in neon clusters. This is done by measuring the kinetic energy of ions after electron impact with the clusters. The clusters are created via expansion of pressurized neon gas (2-10 bars), through a 10µm nozzle which is cooled down to temperatures around 40K by a cryostat, into vacuum. The mass spectrometer used is a

double focusing two sector-field mass spectrometer of reversed Nier–Johnson type geometry. Ions created in the source will be accelerated by 3 kV and subsequently the mass and the energy will be analyzed. Electron currents up to 1mA can be set and the mass range of the analyzer part is up to 5 000 Da with a mass resolution (m/Δm) of about 1 000. A pair of z-deflectors which allows the determination of the kinetic energies of the ions extracted out of the ion source. (The z-axis was chosen to observe the kinetic energies on, due to the fact that the double focusing does not affect the energy in the z-direction).

Acknowledgement

References

[1] U.Hergenhahn, J. Electron Spectrosc. Relat. Phenom **184** (2011) 78.
[2] H.K. Kim, J. Titze, M. Schöffler, F. Trinter, M. Waitz, J. Voigtsberger, H. Sann, M. Meckel, Ch. Stuck, U. Lenz, M. Odenweller, N. Neumann, S. Schössler, K. Ullmann-Pfleger, B. Ulrich, R.C. Fraga, N. Petridis, D. Metz, A. Jung, R. Grisenti, A. Czasch, O. Jagutzki, L. Schmid, T. Jahnke, H. Schmidt-Böcking, and R. Dörner, PNAS **108** (2011) 11821.
[3] S.M. Pimblott, J. A. Laverne. Radiation Physics and Chemistry **76** (2007) 1244.
[4] B. Boudaïffa, P. Cloutier, D. Hunting, M. A. Huels, L. Sanche. Science **287** (2000) 1658.
[5] C. R. Arumainayagam, H.-Lu Lee, R. B. Nelson, D. R. Haines, R. P. Gunawardane. Surface Science Reports **65** (2010) 1.

The catalytic effect of carbon surfaces on H_2 dissociation on Al_n clusters by DFT

Francesca Costanzo, Marc C. van Hemert, Geert-Jan Kroes
Gorlaeus Laboratories, Leiden Institute of Chemistry, Leiden University, P. O. Box 9502, 2300RA Leiden, The Netherlands

Recent experiments [1,2,3,4] show that carbon nanomaterials, such as carbonnanofibers, may be used to catalyse the dehydrogenation and rehydrogenation of hydrogen storage materials, such as the benchmark complex metal hydride $NaAlH_4$. However it is not clear how the carbon material can accomplish the dissociation (or recombination) of H_2. In this work we investigate the dissociation of H_2 on Al_n (n=2,4,6) clusters supported by coronene and graphene substrates using density functional theory (DFT), where coronene and graphene are taken as models for nanographitic surfaces. We account for van der Waals interactions by adapting the correlation part of the PBE exchange-correlation functional with the Grimme [5] and Langreth [6] corrections and we use NEB [7] to calculate the minimum energy reaction path for the dissociation of H_2. Analysis of the minimum barrier reaction paths and the associated dissociation barriers of H_2 on Al_n clusters interacting with the modeled carbon surfaces shows that the investigated carbon materials have a promoting effect on the dissociation of H_2 on the Al_n clusters, resulting in barrierless dissociation of H_2 on Al_4 (Fig.1) and Al_6 supported on coronene. The calculations on coronene suggest that the promoting effect comes from a stabilization of the singlet states of Al_4.
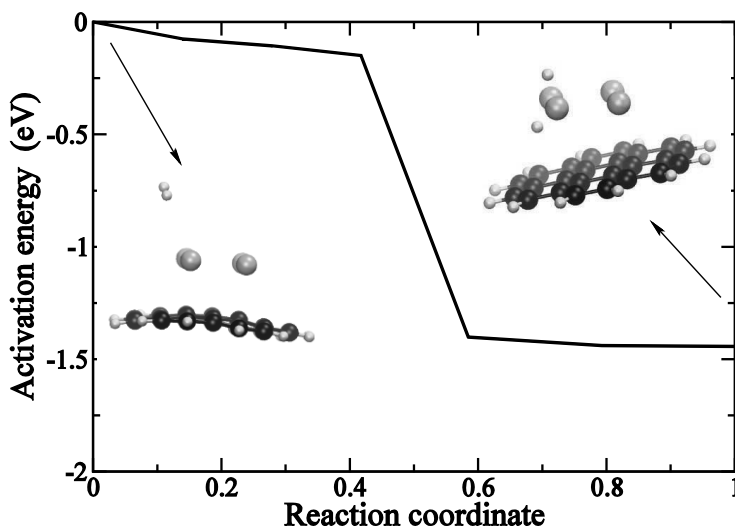
Figure 1: *(Color on line) Minimum energy dissociation pathway of H₂ molecule on Al₄ clusters atoms interacting with coronene (C). The initial and final states, correspond to the physisorbed and chemisorbed state of H₂ on Alₙ-C, respectively.*

References

[1] P. Adelhelm and P. E. de Jongh, J. Mater. Chem., 2011, 21, 2417–2427.

[2] C. P. Balde, B. P. C. Hereijgers, J. H. Bitter, and K. P. de Jong, Angew. Chem. Int. Ed., 2006, 45, 3501–3503.

[3] P. Adelhelm, K. P. de Jong, and P. E. de Jongh, Chem. Comm., 2009, 41, 6261–6263.

[4] J. Gao, P. Ngene, I. Lindemann, O. Gutfleisch, K. P. de Jong, and P. E. de Jongh, J. Mater. Chem., 2012, 22, 13209–13215.

[5] S. Grimme, *J. Comput. Chem.*, 2004, *25*, 1463–1473.

[6] M. Dion, H. Rydberg, E. Schröder, D.C. Langreth, and B.I. Lundqvist, *Phys. Rev. Lett.*, 2004, *92*, 246401.

[7] G. Henkelman and H. Jónsson, J. Chem. Phys., 2000, 113, 9978–9985.

Overtone spectroscopy of methanol: Supersonic-jet diode-laser spectra of OH-stretch overtone $2\nu_1$

Veronika Horká-Zelenková,Vít Svoboda, Ondřej Votava, and Petr Pracna
J. Heyrovský Institute of Physical Chemistry, Dolejškova 2155/3, 182 23 Prague 8, Czech Republic

1. Introduction

Molecular vibrational overtone absorption bands are found through the visible and near IR spectral range and coincide with the available solar radiation in lower atmosphere. Processes initiated via overtone excitation may contribute to atmospheric photochemistry when the UV-initialized processes are unavailable or inefficient. Molecules possessing functional groups with high vibrational frequencies (OH, NH and CH,...) are likely candidates for such processes, because only a few quanta of vibrational excitation are needed to reach chemically relevant levels of excitation.

CH_3OH is a good prototype molecule to study overtone pumping in polyatomic molecules. High resolution spectra provide information about energy flow within the molecule. Couplings between the OH chromophore and other internal modes cause quite complicated structure of overtone spectra and even for this simple molecule the ro-vibrational structure is not fully understood. The spectra in general show highly congested rotational structure at room temperature although methanol is relatively light molecule. Up till now only moderate resolution ($\Delta\nu \sim 0.1 \text{cm}^{-1}$) spectra in the $2\nu_1$ range have been measured at low temperature in supersonic jet by Rizzo and coworkers [1]. Consequently complete modeling of the band has not been possible so far.

In this contribution we report new experimental jet-cooled Doppler limited spectra of the first OH-stretch overtone, $2\nu_1$ in the spectral range of 7180-7220 cm^{-1}. The measurements were carried out by a cw-diode laser spectrometer in combination with slit jet supersonic expansion. In addition, the spectra were measured at two temperatures (30 and 70 K) in order to determine empirical lower state energies using the two temperature technique [2,3]. Such analysis will aid further assignments of rotational-vibrational lines of $2\nu_1$ overtone band.

2. Experimental set up

Measurements were carried out on apparatus that combines pulsed slit-jet supersonic nozzle with tunable diode laser direct-absorption spectrometer. Extended cavity diode laser in Littmann configuration utilized as a radiation source, is tunable in the range 7070-7300 cm^{-1}. The laser output power is 3 mW and the band width of the laser mode

is typically 1 MHz. Direct absorption signal is detected using custom designed dual-beam autoballanced photodetector. The spectra are frequency calibrated by Michelson wavemeter and temperature stabilized Fabry-Perot interferometer. The absolute frequency is determined using absorption line of jet cooled H_2O measured in the tuning range of the laser and is better than 3×10^{-4} cm^{-1}. The supersonic expansion was produced by a pulsed jet with slit nozzle (0.1×40 mm^2). Such configuration permits high sensitivity direct absorption measurements with sub-Doppler resolution. The temperature in supersonic jet expansion depends sensitively on the expansion conditions. Our jet system is capable to operate in a wide temperature range of 30-100K (for CH_3OH). For measurements at higher temperature we use a He/CH_3OH mixture and for the lower temperature we use a Ar/CH_3OH mixture.

3. Determination of empirical rotational quantum numbers

Integrated absorption line strength $S(T)$ at equilibrium temperature T is proportional to the lower state population given by Boltzmann distribution. The ratio of the intensities at two different temperatures T_1 and T_2 for a particular spectral line is given by relation:

$$R(T_1, T_2) \equiv \frac{S(T_1)}{S(T_2)} = \frac{Q(T_1)}{Q(T_2)} e^{\frac{E_{JK}^{''}}{k_B}\left(\frac{1}{T_1} - \frac{1}{T_2}\right)} \qquad Q(T) = \sum_i g_i e^{\frac{-E_{JK}^{''}}{k_B T}}$$

where $Q(T)$ is the partition function. The lower state rotational energy and consequently the lower state rotational quantum numbers can therefore be in principle determined from measured integrated intensity ratios. We have already applied such analysis to the rotational-vibrational spectra of NH_3 and CH_4 representing the symmetric and spherical top molecules, respectively [2,3].

4. Results and discussion

Methanol absorption spectra were recorded in the range of 7180-7220 cm^{-1}. To determine empirical quantum numbers, the ratios of the line intensities from 70K and 30K spectra were calculated. The dataset consists of 630 lines measured at 70K and 280 lines at 30K.
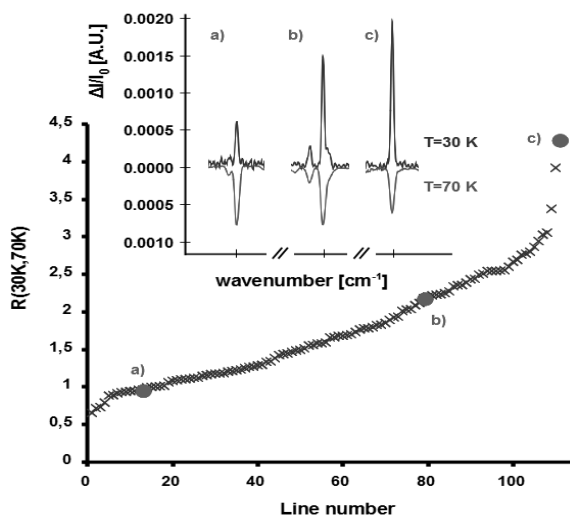
Figure 1: *Distribution of observed intensity ratios R(30K, 70K). Selected spectral lines are shown to highlight the differences in the relative intensities and their ratios are indicated by points in the plot.*

Temperature of the spectra was calculated from the Doppler broadening of the lines. The line strength was obtained as an integrated absorbance. For graphical representation of the data in figure 1 the intensity ratios of all transitions were ordered with increasing value R. The results do not show clear stepwise structure as in the case of methane [4] because rotational constants are quite small $B{\approx}C{=}0.79$ cm^{-1}, thus the differences in rotational energies are small ($\Delta E \ll k_B T$). Consequently, the two temperature analysis in this case can not provide precise values of rotational quantum numbers but still gives a range of possible E'' for given transition in the spectra. This information can be used to aid spectral assignments (rule-out improbable assignments).

At this point the Loomis-Wood technique has been applied (using the LWW program [4]) to identify P- and R-branch of $K{=}0{\leftarrow}0$ lines of the A sub-band, as indicated in figure 2. The assignments were confirmed by ground state combination differences. Band origin based on this preliminary assignment was determined as $\nu_0{=}7203.74$ cm^{-1}.
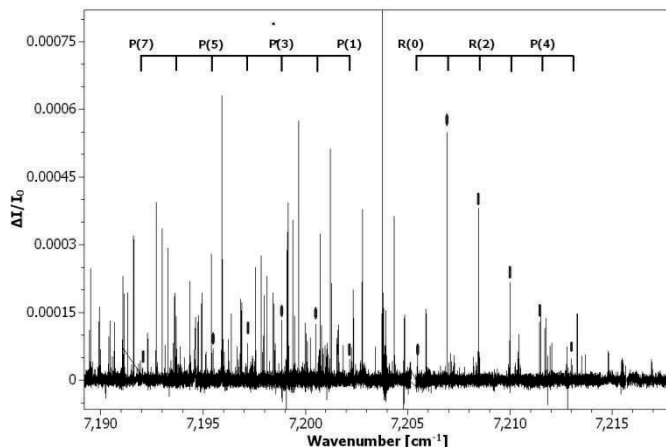
Figure 2: *CH₃OH spectrum of 2ν₁ band at 30K with   K= 0←0 assignments of A subband.*

Acknowledgement

References

[1] O. Rueda, V. Boyarkin, T.R. Rizzo, I. Mukhopadhyay, D. S. Perry, *J. Chem. Phys.* 2002, *116*, 91

[2] O. Votava, M. Mašát, P. Pracna, S. Kassi, A. Campargue, *Phys. Chem. Chem. Phys.* 2010, *12*, 3145.

[3] M. Mašát, P. Pracna, D. Mondelain, S. Kassi, A. Campargue, O. Votava, *J. Mol. Spectrosc.* 2013, *291*, 9.

[4] W.Lodyga, M. Kreglewski, P. Pracna, et al., *J. Mol. Spectrosc.* 200**7**, *243*, 182.

Formation of NCO⁻ by dissociative electron attachment to thymine in different environments

Michael Neustetter, Julia Aysina, Paul Scheier and Stephan Denifl
Institut für Ionenphysik und Angewandte Physik, Universität Innsbruck
Technikerstrasse 25, A-6020 Innsbruck, Austria

Whenever energetic radiation, such as X- or γ-rays as well as fast electrons or ions, interacts with living cells, a set of secondary species is created along the ionization track. In order to understand the on-going processes, investigations on the reactions of secondary particles with biomolecules is necessary. The most abundant ones are secondary electrons with low energies (< 20eV). These electrons can induce single- and double-strand breaks in plasmid DNA [1,2] by dissociative electron attachment (DEA). In the DEA process the initial capture of an electron leads to a temporary negative ion (TNI), which may then decompose by spontaneous ejection of the electron or by dissociation into neutral and anionic fragments. One approach is to study DEA to isolated (small) biomolecules in the gas phase. DEA to isolated systems is an excellent method to determine the fundamental properties of the electron attachment process like resonance energies, bond and site selectivity in dissociation, sequential dissociation pathways and so on [3]. Although studying molecular constituents of DNA is still different from what actually happens in the physiological environment, it can be seen as the first step towards the complex molecular systems that are able to explain and predict the real range of damage that ionising radiation sets upon biological environments.

Studies with isolated molecules are limited when conclusions should be drawn concerning the environmental influence. By the latter fragmentation processes may change considerably because excess energy deposited by the electron may be transferred in the energy dissipating environment. While studies of processes in the bulk are complex and difficult to interpret, experimental studies with clusters of biomolecules already allow a qualitative conclusion of processes occurring in complex cell environments.

One possibility to form such biomolecular clusters is given by supersonic expansions forming for example helium droplets [4] which can be doped by the substance of interest. Due to the evaporative cooling effect the temperature inside the helium cluster is kept at a temperature of about 0.37K. At this low temperature the thermal motions and vibrations of the particles are as low that the creation of biomolecular complexes is also possible.

We recently started investigations on the DEA decomposition of thymine leading to the NCO$^-$ anion. The latter anion is formed by a complex unimolecular decomposition process with multiple bond cleavages in the pyrimidine ring. In DEA to thymine, NCO$^-$ is the most abundant fragment anion at higher electron energies between 5 and 12 eV. In the present contribution a detailed insight into the decomposition dynamics of the thymine molecule leading to NCO$^-$ is given. Results for the isolated thymine [5] as well thymine in cluster matrices [6] are shown.

Acknowledgements

References

[1] B. Boudaïffa, P. Cloutier, D. Hunting, M. A. Huels, and L. Sanche, *Science* 287, 1658 (2000).

[2] F. Martin, P. D. Burrow, Z. Cai, P. Cloutier, D. Hunting, and Léon Sanche, *Phys Rev Lett*. 93, 068101 (2004).

[3] S. Ptasinska, S. Denifl, V. Grill, T. D. Märk, E. Illenberger, P. Scheier, *Phys Rev Lett*. 95, 093201-4 (2005).

[4] S. Denifl, F. Zappa, I. Mähr, J. Lecointre, M. Probst, T.D. Märk, P. Scheier, *Phys Rev Lett.* 97, 04320-1-4 (2006).

[5] F.F. da Silva, C. Matias, A. Diogo, et al., *J. Am. Soc. Mass Spectrom.*24, 1787-1797 (2013).

[6] S. Denifl, F. Zappa, A. Mauracher, F.F. da Silva, A. Bacher, O. Echt, T.D. Märk, D.K. Bohme, P. Scheier, *ChemPhysChem* 9, 1387-1389 (2008).

Inelastic Electron Interaction with Adenine & Hypoxanthine

Katrin Tanzer, Peter Plattner, Paul Scheier, Stephan Denifl
Institute for Ion Physics and Applied Physics, University of Innsbruck,
Technikerstrasse 25, A-6020 Innsbruck

M. Michele Dawley, Sylwia Ptasinska
Radiation Laboratory, University of Notre Dame,
Notre Dame, IN 46556

Electron attachment and electron ionization experiments were performed with the biologically relevant molecules, adenine and hypoxanthine. With a high resolution electron monochromator device, electron energy scans for positive and negative ion formation were recorded and compared. Results are in good agreement for DEA to both molecules, and several fragments show similar peak shapes and positions. The appearance energies of the fragment ions measured are very similar for both hypoxanthine and adenine.

1. Introduction

Adenine (Ade) is one of the most important organic molecules because of the role it plays in general life. It is an essential component of DNA (desoxyribonucleic acid), RNA (ribonucleic acid) and ATP (adenosine triphosphate). Adenine belongs to the purine group of molecules [1]. Hypoxanthine (Hyp) is a derivative in purine metabolism, and the oxidative deamination of adenine leads to the formation of hypoxanthine. Hypoxanthine possesses a structure similar to the nucleobase guanine, but lacks its exocyclic 2-amino group, and so it has a H-bonding pattern that is complementary to cytosine. Thus, hypoxanthine can pair with cytosine forming a Hyp·Cyt base pair during DNA replication which could have mutagenic effects [2]. Hypoxanthine is also found as a minor purine base in tRNA [3].
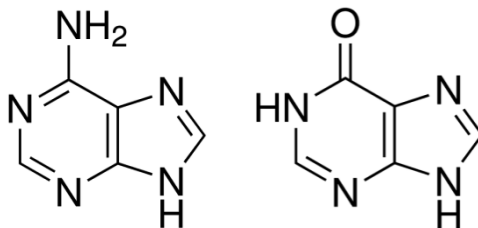
Figure 1: *Chemical structures of adenine (left) and hypoxanthine (right)*

Electron interactions with these biologically relevant molecules are important to study because of potential chemical transformations that can be induced by electrons. Low energy electrons are of particular interest because of the discovery that that the biological effects of high energy radiation are usually not produced by the impact of primary quanta but rather by the secondary species generated along the radiation track. Secondary electrons produced with energies below 20 eV are the most abundant of the secondary species and can induce single strand breaks and double strand breaks in DNA [4, 5].

2. Experimental Setup

All the present measurements were conducted with a high resolution hemispherical electron monochromator (HEM) instrument (Figure 1). The electron beam produced by the HEM had a typical energy resolution of 100 – 140 meV (full width at half maximum (FWHM)) and was crossed at right angles with a neutral biomolecular beam emitted from a capillary attached to a copper oven. The ions formed due to the interaction with electrons were extracted by a weak electric field towards the entrance of a quadrupole mass spectrometer (QMS) and were detected by a channeltron-type secondary electron multiplier.
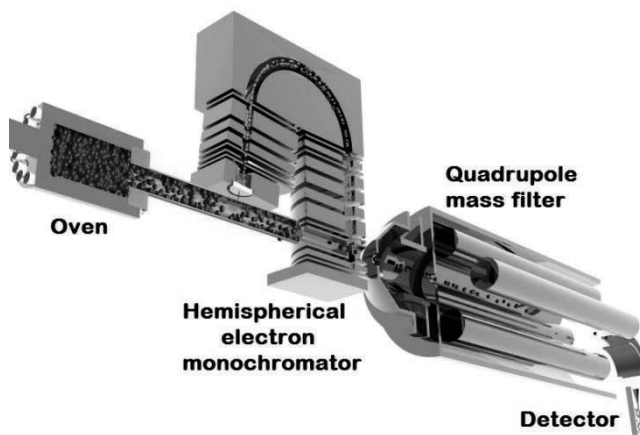
Figure 1: *Schematic of the high resolution experimental setup*

3. Results and Discussion

Several DEA studies to adenine have been published in previous years [6, 7, 8], and these results can be compared with hypoxanthine. Hypoxanthine was heated in a copper oven to approximately 490 K, and negative ion mass spectra at different

electron energies were obtained. Subsequently, ion efficiency curves were recorded as a function of electron energy. The mass spectra that were recorded at ~0-3 eV and 6 eV exhibit characteristic differences. While there is substantially less fragmentation occurring at energies close to 0 eV, the mass spectrum at 6 eV displays a rich fragmentation pattern, similar as previously found for adenine [8]. Also several of the most abundant fragment anions have corresponding masses found in the adenine spectrum. The ion efficiency curves for the principal fragment $[M-H]^-$ (135 Da for Hyp/134 Da for Ade) look similar. Both exhibit a sharp resonance at approximately 1.1 eV, although the scan for adenine displays features close to 0 eV and 2.2 eV that could not be resolved for hypoxanthine due to a slightly lower electron energy resolution. The fragments that show very similar resonances for both molecules include: $C_4H_3N_4^-$ (107 Da), $C_4H_2N_3^-$ (92 Da), $H_2C(CN)_2^-$ (66 Da) and $HC(CN)_2^-$ (65 Da) for hypoxanthine and adenine, respectively, $CH_2N_2^-$ (42 Da) and $CHN2^-$ (41Da) for hypoxanthine and adenine, respectively, and CN^- (26 Da). Additional fragments found for hypoxanthine are $C_5H_3N_3O^-$ (121 Da) and $C_3HN_3^-$ (79 Da).

In addition to DEA, we studied electron ionization of both adenine and hypoxanthine. While for Adenine no prior measurements exist to our best knowledge, threshold studies for hypoxanthine have been undertaken in the 1960s for the parent ion [9]. In the study presented here, we were able to determine the appearance energies (AE) of more than 10 fragments for both molecules. In contrast to previous threshold studies in which the threshold behavior of the ion yield was approximated by a linear fit without attention to the electron energy resolution, here we used a newly developed self-written evaluation program to determine the AE for each fragment that takes into account the resolution of the electron beam.

The results show very similar trends: while the AE of the parent ion is very low (~ 9.3 eV) for both molecules, fragment ions that can only be formed through one or more bond cleavages or ring cleavages tend to have higher appearance energies (14 – 17 eV). An example of this effect is the fragment ion with a mass of 53 Da ($C_2HN_2^+$). For this ion to form, it requires bond cleavage including double bonds. The $C_2HN_2^+$ appearance energy is the highest of all the fragments measured and lies above 18 eV for both adenine and hypoxanthine.

Acknowledgements

References

[1] S. Pilling et al., Rapid Commun. Mass Spectrom.; 21: 3646-3652 (2007)
[2] O. Brovaret et al., J Mol Model; 19; 4119-4137 (2013)
[3] O. Plekan et al., J. Phys. Chem.; 116; 5653-5664 (2012)
[4] B. Boudaiffa et al., Science; 287; 1658-1660 (2000)
[5] F. Martin et al., PRL; 94; 068101-1-4 (2004)
[6] S. Gohlke et al., Chem. Phys. Let.; 380; 595 (2003)
[7] H. Abdoul-Carime et al.; 35; 399 (2005)
[8] D. Huber et al.; J. Chem. Phys.; 125; 084304 (2006)
[9] C. Lifschitz et al.; Tetrahedron Letters; 46; 4583-4586 (1967)

Mass spectrometric studies of nucleobase/water clusters

Julia Aysina, Michael Neustetter, Paul Scheier, Stephan Denifl
Institute of Ion Physics and Applied Physics, University of Innsbruck, Innsbruck,
6020, Austria

In recent years there has been a significant interest in the understanding of damage processes of DNA, specially induced by low energy electrons. It has been suggested that ionizing radiation releases a large number of secondary electrons in cells with kinetic energies in the range of up to few of tens of eV [1, 2]. In this energy regime electron ionization and electron attachment processes may be responsible for chemical transformation of biological matter. The study by Sanche and co-workers [3, 4] demonstrated that these low energy electrons can induce single and double strand breaks in a film of plasmid DNA upon dissociative electron attachment (DEA). In DEA an electron attaches resonantly and the transient negative ion formed decays via dissociation of the molecule. This dissociation can be fast and often has only spontaneous electron emission as competitive channel. A large number of studies on electron ionization/electron attachment to various simple biomolecules (e.g. DNA bases, sugars, amino acids) in the gas phase have been carried out [5, 6]. Thereby, it turned out that biomolecule substantially decompose upon electron collisions. In addition, DEA is a very bond and site specific process, i.e. only certain bonds are cleaved in a molecule after electron attachment. For example, the dehydrogenated parent anion $(M-H)^-$ formed upon DEA to pyrimidine nucleobases is exclusively formed via H-loss from the nitrogen sites of the molecules [7].

However, for applications in radiotherapy it is highly important to understand how fragmentation process to biomolecules is modified by surrounding environment. It was shown lately that electron attachment to nucleobases embedded in helium droplets indicates significant changes in molecular fragmentation pattern upon solvation and thus the environment may cause strong modification of the DEA process [8, 9]. In this case extensive and slow fragmentation processes have been quenched effectively in the droplet, while direct dissociations via repulsive potential energy surface upon DEA cannot be avoided.

The studies with doped helium droplets represent a very first approach to investigate the effect of environment. Therefore, in the present study we use clusters of water (the main component of living cells) as a more realistic environment to study electron interaction with a biomolecule with respect to solvation effects. In order to understand the influence of a water matrix on electron ionization/DEA to a biomolecule we recently developed a new cluster source. Details on development,

implementation and first results of mass-spectrometric studies of pure water clusters and mixed nucleobase/water clusters will be presented.

Acknowledgement

References

[1] C von Sonntag 1987 The Chemical Basis for Radiation Biology
[2] A F Fuciarelli et al 1995 Radiation Damage in DNA: Structure/Function Relationships at Early Times
[3] B Boudaiffa et al 2000 Science 287 1658
[4] F Martin et al 2004 Phys. Rev. Lett. 93 068101
[5] I Bald et al 2008 Int. J. Mass. Spec. 277 4
[6] I Baccarelli et al 2011 Physics Reports - Review Section of Physics Letters 508 1.
[7] S Ptasinska et al 2005 Phys. Rev. Lett. 95 093201
[8] S Denifl et al 2006 Phys. Rev. Lett. 97 043201
[9] S Denifl et al 2008 ChemPhysChem. 9 1387

Two- and Three-Photon Double Ionization of Lithium

Michael Schuricke, Christian Dornes, and <u>Alexander Dorn</u>
Max-Planck-Institut für Kernphysik, Saupfercheckweg 1, 69117 Heidelberg,
Germany

Joachim Ullrich
Physikalisch-Technische Bundesanstalt, Bundesallee 100, 38116 Braunschweig,
Germany

Gregory Armstrong, James Colgan
Theoretical Division, Los Alamos National Laboratory, Los Alamos, NM 87545,
USA

Anatoli Kheifets
Research School of Physical Sciences and Engineering, Australian National
University, Canberra, Australia

The advent of free electron laser sources, as origin of intense and short VUV-laser pulses, paved the way to investigate new regimes in light-matter interaction. In these the most fundamental reactions are constituted by the interaction of few-photons with few-electrons, resulting in multiple ionization of the parent atom or molecule. In the VUV-regime, the electric field of the laser radiation, in contrast to multiple ionization in the infra-red, does neither shift the atomic states considerably nor influence the electrons motion in the continuum. This emphasizes the importance of electron correlations at all times of multiphoton ionization and challenges theory to accurately describe the observed dynamics. These simple reactions take place whenever intense VUV-radiation meets matter. Therefore, they are not only of supreme scientific interest but also of practical importance for FEL research in general. Pioneering differential experiments performed at FLASH on two-photon double ionization (TPDI) of the closed shell atoms helium and neon [1,2] combined with ab-initio theoretical approaches, could already identify the direct (non-sequential), sequential and virtual sequential removal of the electrons. The results presented here aim to explore the next step in complexity. How do two or three photons interact with two electrons in different shells? Thus, exploring the effect of correlations for significantly differing binding energies.

Therefore, a cold and dense lithium target, confined in magneto-optical trap (MOT), was set up at FLASH and combined with a many-particle momentum spectrometer (REMI) [4,5]. Consequently, recoil ion momentum distributions, giving insight into the electrons sum momentum and mutual emission angle, have been recorded.

Figure 1 illustrates the obtained results for photon energies of (a) 59 eV and (b) 50 eV, respectively. In the former case TPDI proceeds via an intermediate resonance and can also be discussed in terms of photon-double ionization of excited and aligned lithium. In contrast, at $E_\gamma = 50$ eV (Fig. 1(b)) DI can only take place by non-sequential absorption of at least two-photons.

The results of both measurements will be discussed and compared to two state-of-the-art calculations. These apply the convergent close coupling (CCC) [6] and time-dependent close coupling (TDCC) [7] approach and reach excellent agreement with the experimental data.

Figure 1. *Recoil ion momentum distributions of (a) TPDI at $E_\gamma = 59$ eV and (b) TPDI at $E_\gamma = 50$ eV . The data is integrated over the missing momentum component and ε marks the polarization direction.*
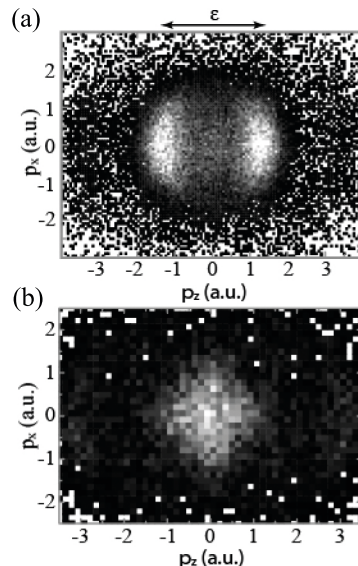
References

[1] M. Kurka *et al., New J. of Phys.* **12,** 073035 (2010)
[2] A. Rudenko *et al., Phys. Rev. Lett.* **101,** 073003 (2008)
[3] J. Feist *et al., Phys. Rev. A* **77,** 043420 *(2008)*
[4] M. Schuricke *et al., Phys. Rev. A 83* 023413 (2011)
[5] A. Kheifets *et al., Phys. Rev. A* **80** *063413 (2009)*
[6] G. Armstrong *et al.,* private comunication

Irregular cluster shapes in supersonic expansion of water vapor

J. Fedor, J. Kočišek

Department of Chemistry, University of Fribourg, Chemin du Musée 9, CH-1700 Fribourg

J. Lengyel, V. Poterya, A. Pysanenko, P. Slavíček, M. Fárník

J. Heyrovský Institute of Physical Chemistry ASCR, Dolejškova 3, CZ-18223 Prague, Czech Republic

Water clusters produced in supersonic expansions are widely used as a laboratory model system that mimics variety of environments. For example, water clusters can serve as a nanosolvation support to study system with biological relevance and probe the transition from behavior of isolated molecules to bulk solution. Another broad area of experiments with water clusters involves atmospherically relevant systems where the clusters represent aerosols or atmospheric ice nanoparticles. It has been shown recently [1] that the key steps in the atmospheric particle nucleation occur in a sub-2-nanometer size range and that the neutral formation pathways are prevalent. This size range corresponds to water clusters composed of several hundreds of water molecules.

The initial steps of nucleation - successive pickup of water molecules on the initial cluster - can be probed in laboratory by passing the neutral cluster beam through a pickup chamber filled with water vapor. Such experiments deliver pickup cross sections which, apart from providing understanding of the growth process, reflect also structural properties of the clusters themselves. The actual cross sections are evaluated from the velocity decrease of the neutral cluster beam.

In this Contribution we report evidence that the large water clusters (with the mean size $N \geq 300$) considerably differ from the spherical or close-to-spherical structures that correspond to the lowest potential energy structure and are often assumed to occur. This conclusion is based on the measured anomalously large cross sections of such clusters which are not consistent with their spherical shape. To verify the experimental method and support the conclusions, we have also performed the pickup experiments for argon ($Ar_N + Ar$). In this case the measured cross sections agree with the spherical model of argon clusters very well. The results are supported by molecular dynamics (MD) simulations which (i) confirm the validity of the analytical model for spherical clusters and (ii) confirm the increase of the pickup cross section with emergence of the irregular cluster shapes.
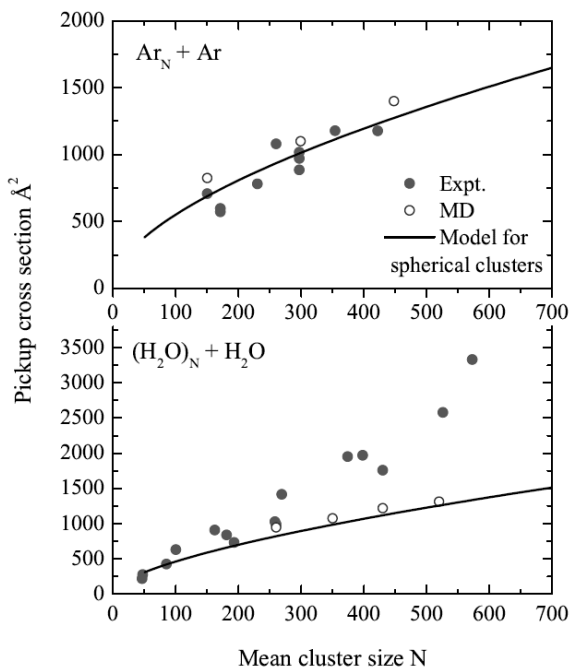
Figure 1. *Top panel: Cross section for pickup of Ar atom on Ar_N clusters. Bottom panel: Cross section for pickup of H_2O molecule on $(H_2O)_N$ clusters. In both cases N represents the mean cluster size in the beam. Red points: experimental data, blue points: molecular dynamics simulations, line: analytical model for spherical clusters.*

References

[1] M. Kulmala et al., *Science* **339**, 943 (2013)
[2] J. Fedor et al., *J. Chem. Phys.* **135**, 104305 (2011)
[3] J. Lengyel et al., *J. Chem. Phys.* **135**, 034304 (2012)

Ionic Detection of TNT-diesel mixture by electron ionization and electron attachment

Jusuf Khreis, Carolina Matias, Johannes Postler, Paul Scheier, Stephan Denifl
Institut für Ionenphysik und Angewandte Physik, Technikerstr. 25 / 3, A-6020 Innsbruck, Austria

Ralf Zimmermann
Helmholtz Zentrum München - German Research Center for Environmental Health (GmbH), P.O.Box 1129, D-85758 Neuherberg / Munich, Germany

The constant and actual need for detection of explosives and the development of techniques to distinguish them among several other similar yet unperilous substances has increased over the last years due to the high risk of terrorist attacks. One of the key issues is the fast capability to distinguish explosives amongst a background of other nitrogen-containing compounds. A large variety of mass spectrometric methods have been suggested for rapid explosive detection including laser photon ionization [1], ion mobility spectrometry [2], chemical ionization mass spectrometry [3], and negative ion mass spectrometry based on free electron capture [4]. The latter method may benefit from the remarkably high electron attachment cross sections of explosive compounds. In recent years a series of studies on dissociative electron attachment (DEA) to several isolated nitro compounds used as explosives have been undertaken [5-9]. These investigations have been performed in crossed electron-molecular beam experiments with high-energy resolution (~70 meV) or high sensitivity (utilizing ~10 µA of electron current). Thereby capture of an excess electron with virtually no kinetic energy leads to formation of a variety of DEA fragments reflecting therefore the explosive nature of the compounds, whereas in the latter the ultra-cold environment efficiently quenches all the gas-phase dissociation channels. DEA studies to explosives yielding NO_2^- formation, allowed to consider this fragment to serve as a fingerprint for the identification of the neutral compound.

These previous studies have been performed with isolated explosive molecules. However, in order to show the possible application even under more realistic conditions we recently performed studies, where the vapour of a diesel-explosive mixture was introduced into the ion source from an external gas inlet. Different concentrations of the explosive TNT in the diesel solvent were investigated and ion yields from the vapour were measured by electron ionization and electron attachment. The results indicated that for positive ion formation the mass spectra shows enormous complexity due to high efficiency of TNT and solvent ionization,

while for negative ions only anions from TNT can be detected in a considerable abundance. Implications for analytical chemistry will be discussed.

References

[1] C. Mullen, A. Irwin, B.V. Pond, D.L. Huestis, M.J. Coggiola, H. Oser, *Anal. Chem.* **78**, 3807-3814 (2006)

[2] L. Song, A.D. Wellman, H. Yao, J.E. Bartmess, *J. Am. Mass Spectrom.* **18**, 1789-1798 (2007)

[3] J. Kozole, J.R. Stairs, I. Cho, J.D. Harper, S.R. Lukow, R.T. Lareau, R. DeBono, F. Kuja, *Anal. Chem.* **83**, 8596-8603 (2011)

[4] J.A. Laramee, P. Mazurkiewicz, V. Berkout, M.L. Deinzer, *Mass Spect. Rev.* **15**, 15-42 (1996)

[5] P. Sulzer, F. Rondino, S. Ptasinska, E. Illenberger, T.D. Märk, P. Scheier, *Int. J. Mass Spectrom.* **272**, 149-153 (2008)

[6] P. Sulzer, A. Mauracher, F. Ferreira da Silva, S. Denifl, T.D. Märk, M. Probst, P. Limão-Vieira, P. Scheier, *J. Chem. Phys.* **131**, 144304 (2009)

[7] F. Ferreira da Silva, P. Sulzer, S. Denifl, T.D. Märk, P. Limão-Vieira, P. Scheier, *Int. J. Mass Spectrom.* **309**, 39-43 (2012)

[8] V. Vizcaino, S.E. Huber, P. Sulzer, M. Probst, S. Denifl, P. Scheier, *Eur. Phys. J. D* **66**, 27-31 (2012)

[9] J. Postler, M.M. Goulart, C. Matias, A. Mauracher, F. Ferreira da Silva, P. Scheier, P. Limao-Vieira, S. Denifl, *J. Am. Mass Spectrom.* **24/5**, pp. 744 – 752 (2013)

Two Photon IR-Laser Induced Population Transfer in NH_3 – First Steps to Measure Parity Violation in Chiral Molecules

Peter Dietiker, Eduard Milogyadov, Martin Quack, Andreas Schneider, Georg Seyfang

Physical Chemistry, ETH Zürich, Wolfgang Pauli Stasse 10, 8093 Zürich, Switzerland

1. Introduction

According to ordinary quantum chemistry including only the electromagnetic interaction the ground state energies of enantiomers of chiral molecules are exactly equal by symmetry. However, this symmetry is broken by the electroweak interaction and a slight energy difference $\Delta_{PV}E$ is introduced between the ground states of the two enantiomers resulting in a reaction enthalpy $\Delta_{PV}H_0^o$ for the stereomutation [1-7]

$$R = S, \qquad \Delta_{PV}H_0^o = N_A\Delta_{PV}E \qquad (1)$$

For the example for CHFClBr $\Delta_{PV}H_0^o \approx 10^{-11}$ Jmol^{-1} is predicted [4]. Although the theoretical calculation of the parity violating energy difference in molecules is now well established its experimental verification is still missing and is one of the great challenges in physics and chemistry [2-7]. The difference of the parity violating energy differences ($\Delta_{PV}E' - \Delta_{PV}E''$) between two rotational or rovibrational states can be obtained in an ultrahigh resolution microwave or infrared absorption measurement. Early attempts along this line have been made already after 1976 and are still pursued [8-12]. However, also an absolute value of the parity violating energy difference $\Delta_{PV}E$ itself can be obtained in an experiment proposed more than 25 years ago [1]. In this experiment a superposition state of the two enantiomers R and S with well defined parity is prepared in a two photon absorption/stimulated emission process. If the tunnelling splitting in the hypothetical symmetric potential is much smaller than the parity violating energy difference, the period of interconversion of the two parity states is then determined by the parity violating energy difference $\Delta_{PV}E$. This interconversion time can be measured by following the rotationally resolved line spectra of the parity isomers with time [1].

In preparation for the above-mentioned experiment we have chosen the achiral molecule NH_3 as a test molecule. The molecule has large rotational constants and only the lowest rotational levels (J = 0,1) are populated in a supersonic molecular beam. A two step population transfer process to a higher rotational level can be studied through the absorption of an IR-photon to reach an excited vibrational state

and the subsequent stimulated IR-emission down to a higher, initially unpopulated rotational level of the vibrational ground state. Also the UV-spectrum of NH_3 is well understood and molecules prepared in the higher rotational level can be probed efficiently by a 2+1 or 3+1 REMPI scheme through the electronically excited B-state (E'') or the C-state (A_1') [13,14].

2. Experimental Setup

From the calculated values for $\Delta_{PV}E$ a conversion time for the two parity states between 0.1 s and some seconds is expected. But with a sufficiently high sensitivity for the detection process an evolution time of 5 to 10 ms should be enough to determine $\Delta_{PV}E$ from the initial evolution of the population of the initially unpopulated parity state. During this evolution time the prepared molecules have to be shielded completely from any interaction with their surroundings. To minimize the disturbance by molecular collisions the experiments are performed in a skimmed supersonic expansion. Using Ar as a carrier gas the required evolution time corresponds to a flight path of 2 to 4 m between preparation and detection. The transferred population is probed with high sensitivity by a REMPI process in a time of flight mass spectrometer.

 Two continuous wave OPOs (Qioptiq) with idler powers of 0.6 to 1.2 W are used for the preparation step. Both OPOs are locked to a self-referenced frequency comb (Menlo Systems FC 1500-250) and a frequency stability of better than 5 kHz is obtained for the idler radiation for an integration time of 1ms. To avoid Rabi oscillations in the preparation step the molecules have been exposed to frequency chirped laser radiation [15]. The molecules in the supersonic expansion are exposed to chirped laser pulses if the laser radiation is focused by a f = 200 mm lens to a spot at 20-40 mm ahead (positive chirp) or behind (negative chirp) of the molecular beam. The UV-radiation for the multiphoton ionization in the detection step is delivered from a frequency doubled dye laser (Radiant Dyes, Narrow Scan D) pumped by the second harmonic of an Nd-YAG laser (Continuum 9010). A wavemeter (High Precision WS/6) is used for frequency calibration of the dye laser radiation. To avoid AC-Stark broadening of the REMPI signal the UV pulse energy had to be reduced to 1 mJ.

3. Results

The efficiency of the population transfer has been investigated in two steps. In a first step the one step population transfer from the $J_K = 0_0$-state to the $J_K=1_0$-state of the vibrationally excited ν_1-mode was investigated. Tuning the REMPI laser to the transition from the ($J_K=0_0$, a, v=0)-state of the electronic ground state to the ($J_K=2_0$,

$v_2=5$)-state of the electronically excited B-state a nearly complete depletion (95%) of the REMPI signal was obtained if the IR-laser (P = 0.5 W) is scanned across the IR-transition at 3355.00725 cm^{-1} (100'580'587 MHz). The population transfer to the v_1-fundamental is probed on the transition from the ($J_K = 1_0$, $v_1=1$, a) –state of the electronic ground state to the ($J_K = 1_0$, $v_2=2$)-state of the electronically excited C-state. A line width of 6 to 8 MHz is obtained for the efficiency of the population transfer where the width is dominated by lifetime and transit time broadening.

In the second step the finally required two photon population transfer was verified. As in the one step process the population was first transferred to the $J_K = 1_0$-state of the v_1-mode and afterwards down to the $J_K=2_0$-state of the vibrational ground state. To investigate the two photon population transfer to the final state the REMPI laser is set to the transition from the ($J_K=2_0$, a, v=0)-state of the electronic ground state to the ($J_K=3_1$, $v_2 = 5$)- state of the electronically excited B-state. The frequency dependence of the population transfer for the stimulated emission is shown in figure 1 with the pump laser for the first step locked to 3355.00725 cm^{-1}. The upper curve of figure 1 indicates the depopulation of the ($J_K=1_0$, $v_1=1$)-state by the probe laser scanned around $\tilde{v}_0$=3295.38782 cm^{-1} with P_{probe} = 0.65 W resulting in a transfer efficiency of 80% at the line centre. The lower curve shows the population transfer to the final $J_K=2_0$ state.

Figure 1
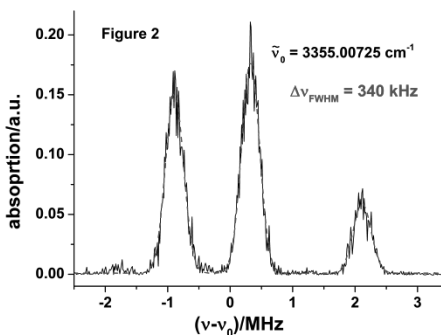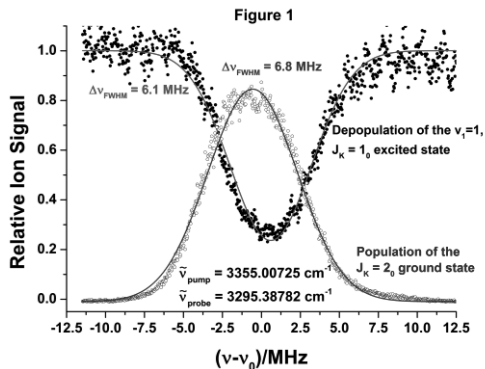
In a third experiment we have removed the chirp of the laser pulse. To avoid transit time and lifetime broadening we have increased the laser beam diameter from 0.8 mm to 3.1 mm and reduced the laser power to 25 mW. To minimize the residual Doppler broadening resulting from the divergence of the molecular beam the flight path between preparation and detection area was increased from 250 to 800 mm and a skimmer with a diameter of 0.9 mm was placed before the detection zone. With this altered setup a line width of 340 kHz was obtained which was small enough to resolve the hyperfine structure in the infrared transition resulting from nuclear spin of the ^{14}N. The measured spectrum for the ($J_K=0_0$, a, v=0) $\rightarrow$ ($J_K=1_0$, s, $v_1=1$) transition

is shown in figure 2. Using the published quadrupole coupling constant eQq(v=0,a) = -4.0898 MHz of the vibrational ground state [16] the quadrupole coupling constant for the (v_1=1,s)-state eQq(v_1=1,s) = -4.023(10) MHz is derived from the fit of the measured line positions.

Acknowledgment

References

[1]   M. Quack*, Chem. Phys. Lett*. **132**, 147 (1986)
[2]   A. Bakasov, T.-K. Ha, M. Quack, *J. Chem. Phys.* **109**, 7263 (1998)
[3]   R. Berger and M. Quack, *J.Chem. Phys*. **112**, 3148 (2000)
[4]   M. Quack and J. Stohner, *Phys. Rev. Lett.* **84**, 3807 (2000)
[5]   M. Quack and J. Stohner, *J.Chem. Phys*. **119**, 11228 (2003)
[6]   M. Quack, J. Stohner, M. Willeke, *Annu. Rev. Phys. Chem.* **59**, 741 (2008)
[7]   M. Quack, 'Fundamental Symmetries and Symmetry Violations from High-resolution Spectroscopy', in Handbook of High-resolution Spectroscopy, Vol.1, pages 659 – 722, M.Quack and F.Merkt (eds.), Wiley, Chichester 2011
[8]   O. N. Kompanets, A. R. Kukudzhanov, V. S. Letokhov, L. L. Gervits, *Opt. Commun.* **19**, 414 (1976).
[9]   E. Arimondo, P. Glorieux, and T. Oka, *Opt. Commun*. 23, 369 (1977).
[10] A. Bauder, A. Beil, D. Luckhaus, F. Müller, M. Quack, *J. Chem. Phys.* **106**, 7558 (1997).
[11] C. Daussy, T. Marrel, A. Amy-Klein, C. T. Nguyen, C. Bordé, and C. Chardonnet, *Phys. Rev. Lett.* **83**, 1554 (1999)
[12] S. K. Togunaga, C. Stoeffler, F. Auguste, A. Shelkovnikov, C. Daussy, A. Amy-Klein, C. Chardonnet, B. Daroqué, *Mol. Phys*. **111**, 2363 (2013)
[13] A. Douglas and J. M. Hollas, *Can. J. Phys*. **39**, 479 (1961)
[14] [14] J. M. Allen, M. N. R. Ashfold, R. J. Stickland, C. M. Western, *Mol. Phys*. **74**, 49 (1991)
[15] C. Liedenbaum, S. Stolte, J. Reuss, *Infrared Phys*. **29**, 397 (1989)
[16] G. Cazzoli, L. Dore, C. Puzzarini, *Astron. Astrophys.* **507**, 1707 (2009)

Low-energy electron attachment to dimethyl disulphide

Carolina Matias, Andreas Mauracher, Paul Scheier and Stephan Denifl
Institut für Ionenphysik und Angewandte Physik, Universität Innsbruck,
Technikerstr. 25 / 3, A-6020 Innsbruck, Austria

Paulo Limão-Vieira
Laboratório de Colisões Atómicas e Moleculares, CEFITEC, Faculdade de Ciências
e Tecnologia, Universidade Nova de Lisboa, 2829-516 Caparica, Portugal

Several studies involving the role of sulphur containing molecular species in the field of atmospheric chemistry have been reported (e.g. see [1–3]). Disulphide bond activation has also been identified as relevant within the context of biochemical processes closely related to the stabilizing role on the structure of several proteins [4]. Within the disulphide containing peptides, conformational structures vary according to the disulphide-reduced against disulphide-oxidized forms [5], which in turn mean different cellular functions [6, 7]. Reduction processes have been identified as crucial in biological systems meaning that any additional studies will allow fully understanding the underlying mechanisms of such processes. Here we are particularly interested on the role of low-energy electron interactions with bare dimethyl disulphide molecules ($C_2H_6S_2$).

Dissociative electron attachment (DEA) experiments to $C_2H_6S_2$, yielding three fragment anions have been performed by Modelli et al. [8]. Modelli and co-workers reported on the role of σ^* shape resonances involving S–C and S–S antibonding orbitals in low-energy electron transmission spectroscopy experiments [9].

In the present work gas phase electron attachment experiments have been performed with dimethyl disulphide by means of a crossed electron-molecular beam experiment. Anion efficiency curves for negatively charged fragments have been measured at low electron energies (0–15 eV) with a resolution of ~ 1 eV. Several new fragment anions have been detected for the first time in comparison to previous DEA studies to $C_2H_6S_2$. In total 19 anions ion yields have been measured including a long lived (metastable) non-dissociated parent anion which is formed at energies close to 0 eV. The by far dominant signal can be assigned to SCH_2^- formation whereas the parent anion has a comparably low intensity. Many of the dissociative electron attachment product anions observed at low-energy arise from surprisingly complex reactions associated with multiple bond cleavages and structural and electronic rearrangement. Results from thermochemical calculations will be presented in order to identify possible reaction pathways.

Acknowledgements

References

[1] V. Aquilanti, M. Ragni, A. C. P. Bitencourt, G. S. Maciel, and F. V. Prudente, J. Phys. Chem. A 113 (2009) 3804.

[2] P. Limão-Vieira, S. Eden, P. A. Kendall, N. J. Mason, S. V. Hoffmann, Chem. Phys. Lett. 366 (2002) 343.

[3] E. A. Drage, P. Cahillane, S. V. Hoffmann, N. J. Mason, P. Limão-Vieira, Chem. Phys. 331 (2007) 447.

[4] S. D. Dai, C. Schwendtmayer, P. Schurmann, S. Ramaswamy, H. Eklund, Science 287 (2000) 655.

[5] G. A. Rickard, J. Bergès, C. Houeè-Levin, and A. Rauk, J. Phys. Chem. B 112 (2008) 5774.

[6] H. Nakamura, K. Nakamura, J. Yodoi, Annu. Rev. Immunol. 15(1997) 351.

[7] A. Baker, C. M. Payne, M. M. Briehl, G. Powis, Cancer Res. 57 (1997) 5162.

[8] A. Modelli, D. Jones, G. Distefano and M. Tronc, Chem. Phys. Lett. 181 (1991) 361.

[9] C. Dezarnaud-Dandine, F. Bournel, M. Tronc, D. Jones and A Modelli, J. Phys. B: At. Mol. Opt. Phys. 31 (1998) L497.

Quantum interferometry with clusters in the time domain

Nadine Dörre, Philipp Haslinger, Philipp Geyer, Jonas Rodewald, Stefan
Nimmrichter and Markus Arndt
*University of Vienna, Faculty of Physics, Vienna Center for Quantum Science and
Technology, Boltzmanngasse 5, A-1090 Vienna, Austria*

The wave – particle duality of light and matter is one of the fundamental and most intriguing concepts in quantum physics. Over the last decades, research in matter wave interferometry has become a thriving field for studying fundamental phenomena and precision metrology [1]. Coherence experiments with large molecules and clusters [2] may allow for establishing new bounds on theoretical predictions that modify standard quantum mechanics [3] and are interesting for measuring molecular properties.

We present a time domain matter-wave interferometer (OTIMA) for nanoparticles which uses three pulsed optical gratings [4,5]. Standing light waves realized by the reflection of UV laser beams from a single mirror act as absorptive structures for neutral particles by single photon ionization in the antinodes. In contrast to material absorptive masks, such gratings allow to be operated in a pulsed mode, which makes the longitudinal motion of the particles negligible and thus brings gain in visibility and measurement precision.

We recorded first interference patterns with clusters of various organic molecules that also serve as a motivation to explore cluster properties with time domain metrology and absorption spectroscopy [6]. Our setup allows to extract information on photoionization properties of the interfering particles. Also photodissociation and fluorescence can be studied since emitted particles carry which-path-information and thus influence the visibility.

The experiment is universally applicable in the sense that it allows working with a large class of nanoparticles. It may act on atoms, molecules but also giant clusters as long as ionization is the principal response to photon absorption at the grating laser wavelength (λ=157 nm). Possible candidates therefore range from metal and semiconductor clusters to biomolecular complexes.

References

[1] Cronin, A. D., Schmiedmayer, J. & Pritchard, D. E. Optics and interferometry with atoms and molecules. *Rev. Mod. Phys.* **81**, 1051-1129 (2009).

[2] Hornberger, K., Gerlich, S., Haslinger, P., Nimmrichter, S. & Arndt, M. Colloquium: Quantum interference of clusters and molecules. *Reviews of Modern Physics* **84**, 157-173 (2012).

[3] Bassi, A. & Ghirardi, G. Dynamical Reduction Models. *Phys. Rep.* **379**, 257-426 (2003).

[4] Haslinger, P. *et al.* A universal matter-wave interferometer with optical ionization gratings in the time domain. *Nature Phys* **9**, 144-148 (2013).

[5] S. Nimmrichter, P. H., K. Hornberger, M. Arndt. Concept of an ionizing time-domain matter-wave interferometer. *New J. Phys.* **13**, 075002 (2011).

[6] Nimmrichter, S., Hornberger, K., Ulbricht, H. & Arndt, M. Absolute absorption spectroscopy based on molecule interferometry. *Phys. Rev. A* **78**, 063607 (2008).

Electron Attachment to Perfluorotetrahydrofuran

Jaroslav Kočišek, Radmila Janečková, Juraj Fedor
Department of Chemistry, University of Fribourg, Chemin du Musée 9, CH-1700, Fribourg, Switzerland

We present experimental absolute cross sections for negative ion formation after an electron attachment to $c\text{-}C_4F_8O$ in the 0 eV – 6 eV electron energy range. Electron attachment results into the formation of long‑living parent ion in the resonance ~ 0.9 eV as well as rich fragmentation into 12 anions which are formed in the three main resonances at, ~ 1.7 eV, at ~ 2.5 eV and at ~ 3.4 eV.

Introduction

One of the best electron scavengers ever synthesised is SF_6. It forms long living parent anion in an s-wave electron attachment process with huge cross section rising up to 10^{-16} m^2 in the near 0 eV region [1]. This behaviour is crucial for the application of SF_6 as the high voltage insulator.

The high stability of the molecule and high ionization threshold makes SF_6 ideal for practical applications. On the other hand it makes the molecule also extremely dangerous for the environment. The atmospheric residence time of more than 3000 years makes the molecule one of the most dangerous greenhouse gases. Together with high absorption cross section, it results into the value of global warming potential 23900 (GWP of CO_2 is 1). Therefore there is an intensive search for the SF_6 alternative.

One of the proposed compounds is the perfluorotetrahydrofuran studied in the present experiment. It has much lower GWP of 8700 [2], high stability as well as compatibility with other materials [3]. It was already tested in applications in Cherenkov detectors [4] and as a cleaning gas during the PECVD process [2]. However, a basic electron driven chemistry of the molecule is still not known. Such knowledge is crucial for the possible $c\text{-}C_4F_8O$ application as a dielectric gas as well as other electro technical and electro chemical applications. In present study, we perform precise measurements of absolute cross sections for the electron attachment to this molecule.

Experiment

The experiment was carried out by means of the total ion-collection apparatus described elsewhere [5]. The apparatus is a combination of the pulsed electron source which incorporates the trochoidal electron monochromator, the reaction cell and the

discrimination - free TOF spectrometer. Electrons were accelerated to the required energy in 0 eV-6 eV range. FWHM of the electron distribution function was kept under 0.3 eV during present experiments and electron currents in the continuous mode were ~ 10 nA. The electrons were introduced to the reaction cell filled with ~0.1 Pa of the studied gas. Negative ions formed during the 200 ns electron pulse were extracted with 200 ns delay to the 15 cm long TOF spectrometer with total accelerating voltage of 600 V. The ions were detected by the BURLE MCP – scintilator – photomultiplier detector with 3kV post acceleration voltage. The operating frequency of the experiment was 50 kHz. 3D electron energy – m/z – ion intensity spectra were recorded, which allow the extraction of mass spectra at specific electron energy as well as energy dependent ion yields for the particular fragments.

The experiments were performed in the mixtures of c-C_4F_8O with CO_2 and HCOOH calibration gases. The $HCOO^-$/HCOOH resonance at 1.4 eV which has the integrated cross section of 98.4 pm^2 [6] and O^-/CO_2 resonance at 4 eV which has the integrated cross section of 13.3 pm^2 [5] were used to calibrate the cross sections.

Results & Discussion

The electron attachment to c-C_4F_8O results into effective decomposition of the molecule as it is demonstrated on the negative ion mass spectra on the Fig. 1.
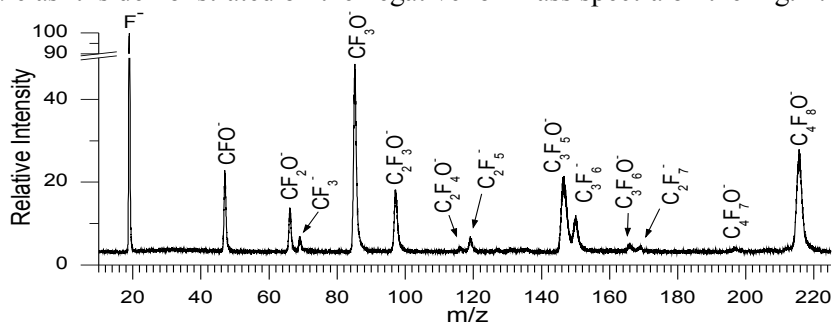
Figure 1: *Negative ion mass spectrum of the c-C_4F_8O molecule summed over 0 eV – 6 eV range.*

The parent anion is formed in resonance which peaks at ~ 0.9 eV with threshold ~ 0.3 eV. DFT calculation shows that the electron affinity of the c-C_4F_8O is ~ 0.5 eV. Therefore one can expect strong s-wave attachment similar to other halogenated compounds. However, in comparison to symmetric molecules like SF_6 or CCl_4 an additional electron in c-C_4F_8O results into significant change of the geometry (see Fig. 2). Such difference in the geometries together with high value of vertical

detachment energy (~1eV based on simple DFT estimate) is an indication of the possible barrier formation in between the anion and neutral states in contrast to barierless transition in the previously mentioned systems showing the near 0 eV resonance.
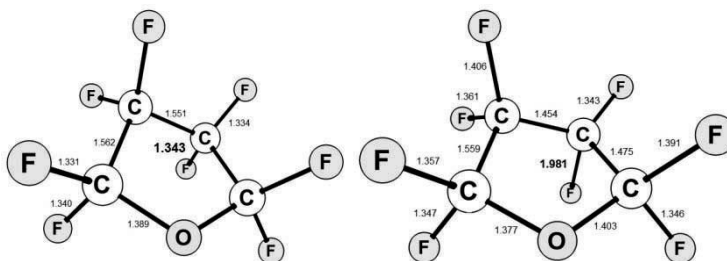
Figure 2: *C_4F_8O neutral structure (left) and anion structure (right) as a result of DFT B3LYP calculation in 6-311++G(2df) basis.*
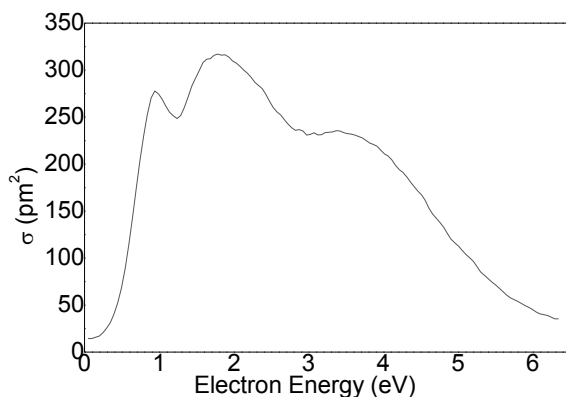
m/z	anion	Resonance +/-0.3eV
216	$C_4F_8O^-$	0.9 eV
97	$C_2F_3O^-$	1.64 eV 2.9 eV
85	CF_3O^-	2.3 eV 3.5 eV
47	CFO-	2.3 eV 3.4 eV
19	F-	2.4 eV 3.9 eV

Figure 3 *Total cross section for negative ion formation after electron attachement to C_4F_8O (left) and positions of the resonances for most intense ionic fragments (right).*

Parent ion is the only ion which shows the low energy resonance at ~ 0.9 eV. All the other ions are formed at higher energies. It is interesting that several ions, which require the cycle breaking during the formation are observed already at energies ~1.6 eV. In the case of the hydrogen analogue of c-C_4F_8O – tetrahydrofuran (c-C_4H_8O) such ions were observed exclusive in high energy resonances at ~ 7eV [7].

The high electron affinity of fluorine makes the molecular orbitals more delocalized and the ring structure less stable against dissociation. Also the absolute value of the total negative ion formation cross section in 1 eV - 5 eV region is order of magnitude higher then cross section of other fluorinated technical gasses like C_2F_6, C_3F_8, SF_6 or NF_3[8,9].

Conclusions

The perfluorotetrahydrofuran is an interesting alternative to other halogenated technical gasses. Even it does not posses the s-wave attachment as a prerequisite of high dielectric strength it has a large cross section for negative ion formation of hundreds of pm^2 up to several eVs. Except the technical applications it can be used like intense source of reactive ions in plasmas where e.g. the cross section for F-formation is nearly 40 times larger in comparison to the often used NF_3.

References

[1] Hotop H. et al.; Advances in atomic, molecular, and optical physics 49; 85-216, 2003
[2] Pruette, L. et al.; in Environmental Issues in the Electronics and Semiconductor Industries, L. Mendicino, L. Simpson editors; The Electrochemical Society, Inc.; Pennington 1999, p.20-29
[3] BTeV-RICH detector material compatibility test; available at http://www.phy.syr.edu/~nraja/btev/materialcompat/
[4] Artuso, M. et al.; Nucl. Instrum. Meth. A558; 2006, 373-387
[5] May, P. et al.; Physical Review A 80, , 2009, 012706
[6] Janečková, R. et al.; PRL 2013, accepted
[7] Sulzer, P. et al.; J. Chem. Phys. 125, 2006, 044304
[8] Nandi, D.; et al. Int. J. Mass Spec., 205(1-3) 2001, 111–117
[9] Christophoru L.G.; Olthoff J.K; J. Phys. Chem. Ref. Data 29, 2000, 267-330
    Christophoru L.G.; Olthoff J.K; J. Phys. Chem. Ref. Data 27 1998 998-911
    Christophoru L.G.; Olthoff J.K; J. Phys. Chem. Ref. Data 27 1998 1-29

Alignment of state-selected OCS: Rotational dynamics and the complete determination of the molecular eigenstate

Terry Mullins,[1] Sebastian Trippel,[1] Nele Müller,[1] Jens Kienitz,[1, 2] and <u>Jochen Küpper</u>[1,2,3]

[1] *Center for Free-Electron Laser Science, DESY, Notkestraße 85, 22607 Hamburg, Germany*
[2] *Department of Physics, University of Hamburg, Luruper Chaussee 149, 22761 Hamburg, Germany*
[3] *Center for Ultrafast Imaging, University of Hamburg, Luruper Chaussee 149, 22761 Hamburg, Germany*

State-selected and aligned molecular ensembles are excellent samples for studying ultrafast dynamics of physical and chemical processes in the molecular frame [1]. Using laser alignment the rotational dynamics of the target molecules are manipulated to ensure the molecular and laboratory frames coincide [2]. Cooling molecules in a supersonic expansion followed by passage through an electrostatic deflector produces ensembles amenable to strong alignment at kHz repetition rates [3].

Here, we present experiments to determine the exact rotational quantum state distribution of OCS molecules after passage through an electrostatic deflector, a critical parameter when good molecular alignment is desired. The spatial state distributions after the deflector are determined using a combination of rotational coherence spectroscopy [4] and the characteristic spatial probability density distributions resulting from angular momentum polarization of the sample in the deflector.

In addition, we present pump-probe experiments on the alignment dynamics of the state-selected molecular samples over the full range of laser interaction time-scales from adiabatic to impulsive. In the adiabatic case of long, 500-ps, laser pulses the dynamics are determined by the ground pendular eigenstates. In the impulsive case of short, 50-fs, pulses the dynamics are well described by field-free quantum rotation. Intermediate laser-pulse duration results in complex dynamics, both during the laser pulse as well as afterwards, with accumulated quantum phases strongly affecting the usual revival structures. The dynamics are theoretically understood and

explained in a full quantum-mechanical picture and are applicable to alignment of larger molecular systems as well as to surface-adsorbed molecular switches [5].

References:

[1] Holmegaard, PRL 2009; J. Hansen, et al., *Phys. Rev. Lett.* **106**, 073001 (2011)

[2] H. Stapelfeldt and T. Seideman, *Rev. Mod. Phys*. **75**, 543-557 (2003).

[3] S. Trippel et al., *Mol. Phys*. **111**, 1738 (2013).

[4] P. M. Felker, *J. Phys. Chem.*, **96**, 1844-1851 (1992).

[5] M. G. Reuter et al. *Phys. Rev. Lett*. **101**, 208303 (2008).

Highest resolution FTIR spectroscopy of indene (C₉H₈) with synchrotron radiation

S. Albert[a,b], Ph. Lerch[b], M. Quack[a] and A. Wokaun[c],

[a]Physical Chemistry, ETH Zürich, CH-8093 Zürich, Switzerland,

[b]Swiss Light Source, Paul-Scherrer-Institute, CH-5232 Villigen, Switzerland,

[c]Energy Research Department, Paul-Scherrer-Institute, CH-5232 Villigen,

Switzerland.

1. Introduction

One of the great challenges of astronomical infrared spectroscopy is the identification of the Unidentified Infrared Bands (UIBs) found in several interstellar objects. Polycyclic Aromatic Hydrocarbons (PAHs) and saturated polycyclic hydrocarbons have been proposed to be the carrier of the UIBs [1]. In this context we have started to extend our previous investigations of naphthalene [2], indole [2], azulene [3] and biphenyl [4] towards compounds consisting of an aromatic and a saturated carbon ring. Among them indene (C_9H_8) is one of the simplest bicyclic compounds. We have measured the IR spectrum of indene with our ETH prototype and ETH-SLS interferometers [2,5-7] using a resolution of 25 MHz and have obtained the first rotationally resolved infrared spectra of this compound. We discuss an analysis of the c-type bands of indene at 690.61 cm^{-1} and 766.08 cm^{-1}. In addition, we compare these bands with UIBs in the range 10 to 15 μm.

2. FTIR spectra of indene

The FTIR spectra of indene in the range 620 to 880 cm^{-1} as shown in Figure 1 have been measured with the FTIR setup at the SLS. The Synchrotron radiation extracted out of the storage ring is steered along three segments of 1:1 optics using Al coated mirrors kept under vacuum. From the third focal point, the beam is further steered through dedicated transfer optics to the FTIR spectrometer. Figure 1 shows three c-type bands of indene corresponding to the out-of-plane fundamentals ν_{39}, ν_{40} and ν_{41}. The Loomis Wood diagrams illustrate the c-type character of the indene bands.
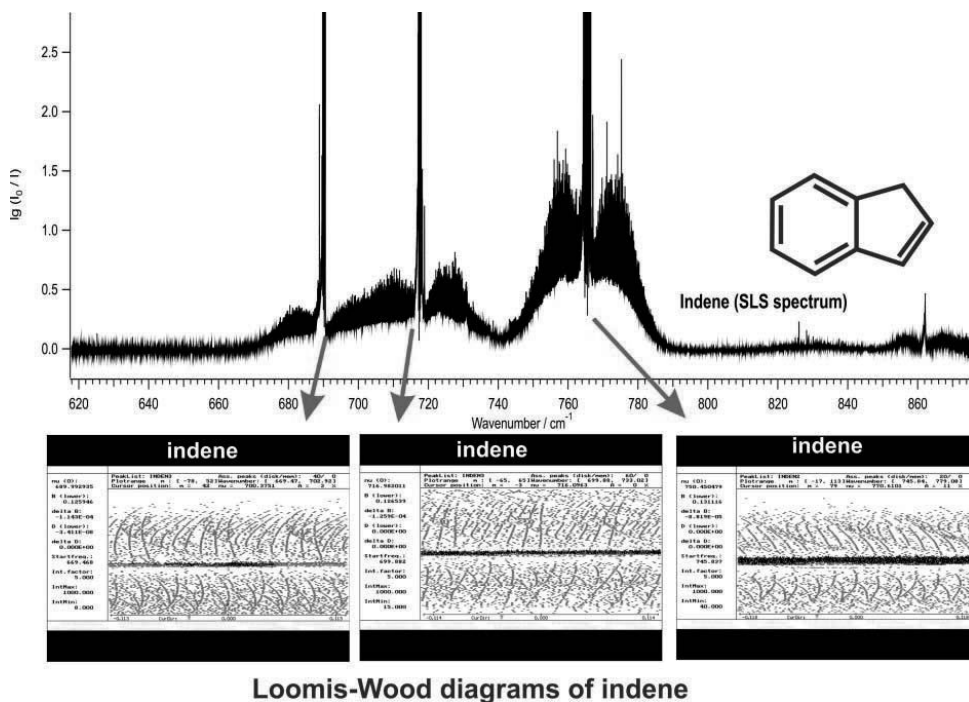
Loomis-Wood diagrams of indene

Figure 1: *FTIR-SLS spectrum of indene between 620 and 880 cm^{-1}. The lower part shows the Loomis Wood diagrams of three bands.*
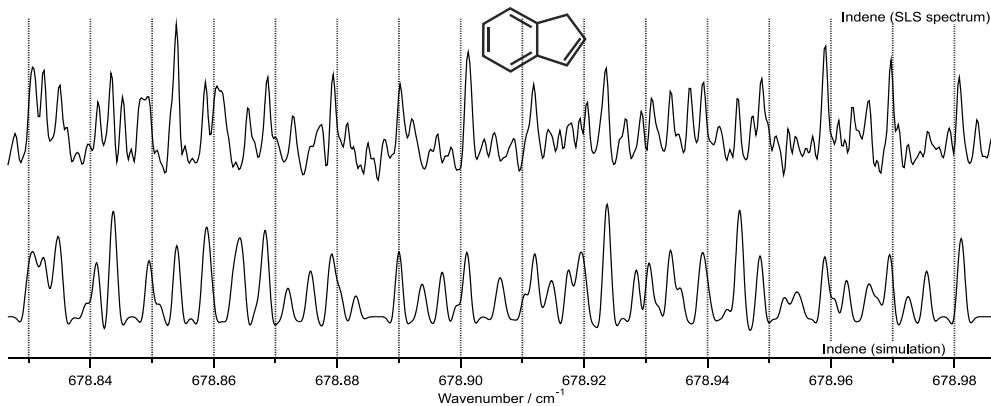
Figure 2: *Comparison of the measured (upper trace) and simulated (lower trace) spectrum of the c-type band of indene at 690.6074 cm^{-1}.*

3. Analysis of the indene fundamentals

The indene fundamentals at 690.6074 and 766.0764 cm^{-1} have been analysed using Watson´s Hamiltonian [7]. The ground state constants have been taken from Ref. [8]. The spectra have been simulated using the adjusted spectroscopic constants. A comparison of the measured fundamentals and their simulations is illustrated in Figures 2 and 3. As one can see there is a reasonably good agreement between the measured and simulated spectrum considering the omission of hot bands and the natural isotopomers in the simulation.
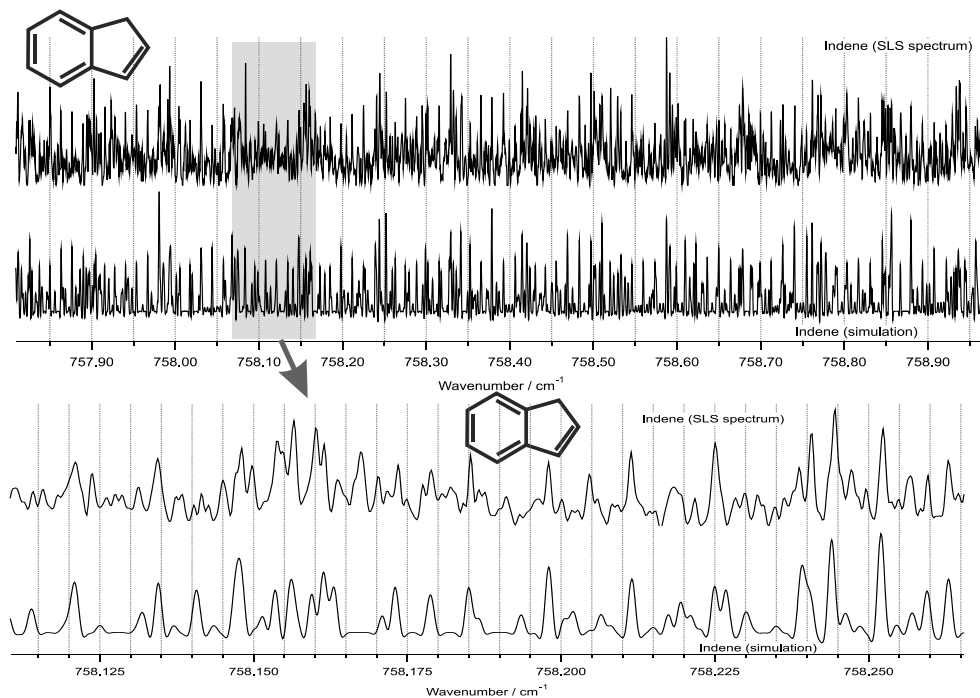
Figure 3: *Comparison of the measured (upper trace) and simulated (lower trace) spectrum of the c-type band of indene at 766.0764 cm^{-1}.*

4. Comparison of the fundamentals with UIBs

A comparison of the indane, indene, naphthalene, biphenyl and cyclohexane fundamentals displayed in Figure 4 shows the excellent coincidence between the UIBs at 13.55 and 14.3 µm with the biphenyl bands and at 12.78 µm with a naphthalene band. The coincidence with indane and indene bands is less pronounced.
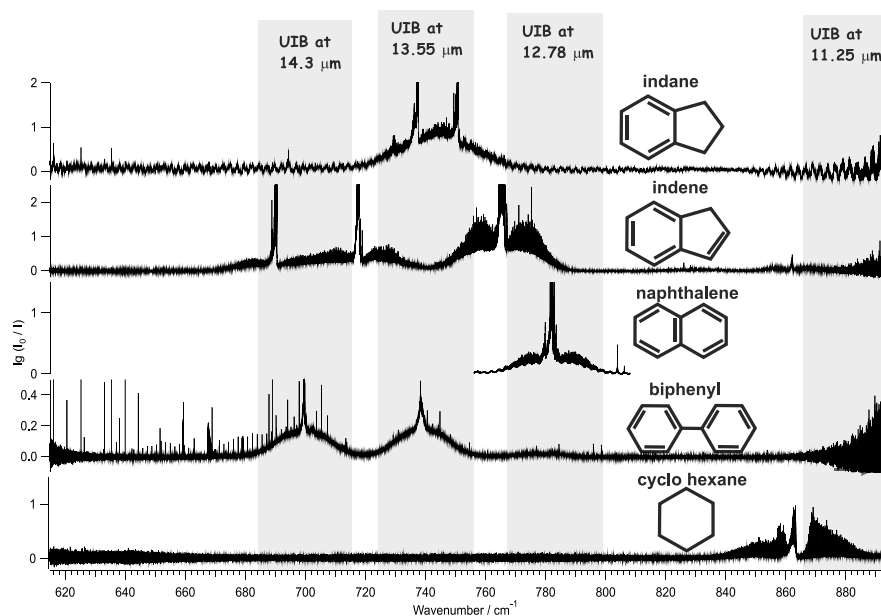
Figure 4: *Comparison of the indane, indene, naphthalene, biphenyl and cyclohexane bands in the 620 to 880 cm^{-1} range with the UIBs.*

References

[1] A.G.G.M. Tielens, Annu. Rev. Astron. Astrophys. 2008, 46, 289-337.

[2] S. Albert, K.K. Albert, Ph. Lerch, M. Quack, Faraday Discuss. 2011, 150, 71-99.

[3] S. Albert, Ph. Lerch, M. Quack, ChemPhysChem 2013, 14, 3204-3208

[4] S. Albert, K.K. Albert, Ph. Lerch, M. Quack, Faraday Discuss. 2011, 150, 146-151.

[5] S. Albert, K. K. Albert, and M. Quack, TOPS 2003, 84, 177.

[6] S. Albert and M. Quack. ChemPhysChem 2007, 8, 1271-1281.

[7] S. Albert, K. K. Albert and M. Quack, High Resolution Fourier Transform Infrared Spectroscopy, in Handbook of High-Resolution Spectroscopy, Vol. 2, (Eds. M. Quack and F. Merkt), Wiley, Chichester (2011), 965-1021.

[8] D. Luckhaus and M. Quack, *Mol. Phys.*, 68, 745 (1989).

[9] W. Caminati, *J. Chem. Soc. Faraday Trans.* **1993**, *89*, 4153-4155.

The infrared spectrum of methane up to 12000cm^{-1}

O. N. Ulenikov[a;b], E. S. Bekhtereva[a;b], S. Albert[a],

S. Bauerecker[a;c], H.-M. Niederer[a], and M. Quack[a]

[a]*Physical Chemistry, ETH Zurich, CH-8093 Zürich, Switzerland,*

[b]*Laboratory of Molecular Spectroscopy, Physics Department,*

Tomsk National Research University, Tomsk, 634050, Russia;

[c]*Technische Universitut Braunschweig, D - 38106, Braunschweig, Germany.*

1. Introduction

Methane is the prototypical hydrocarbon and of great importance for our understanding of chemical bonding and structure from the early days of chemistry [1]. Its current interest ranges from quantum dynamics and chemical reactions on potential hypersurfaces on the one hand [2–4] and atmospheric and astrophysical spectroscopy including its effects as a greenhouse gas on the other hand [5,6]. Methane combustion with a reaction enthalpy of $\Delta_R H^0 = -800$ kJ mol^{-1} is also among the largest chemical processes of mankind at a technical scale for energy production in the TJ range per year. On the other hand, the tiny energetic effects of parity violating potentials in the methane molecule in the range of fJ mol^{-1} have been discussed to be of interest for fundamental physics as well [7,8]. Although there has been substantial spectroscopic work on methane for more than a century, due to its obvious importance, the understanding of the high resolution infrared spectrum is incomplete to a surprising degree, particularly as far as the higher energy ranges of overtone absorption are concerned. Therefore we have started some time ago, a major experimental effort to measure the complete infrared spectrum of methane CH_4 and its stable isotopomers, and several aspects of our previous work on the spectra on various partially deuterated isotopomers have been reported in recent previous publications from this effort [9-12]. The analysis of the infrared spectrum of $^{12}CH_4$ and $^{13}CH_4$ is now fairly complete up to the energy range of the octad (i. e. below about 5000 cm^{-1}) [13, 14]. In the present work we aim at a partial analysis extending towards 12'000 cm^{-1}.

2. FTIR spectra

The Fourier transform infrared (FTIR) spectra of $^{12}CH_4$ and $^{13}CH_4$ have been recorded at 80 K in the wavenumber range from 1200 to 12500 cm^{-1} with the Zürich FTIR spectrometer Bruker IFS 125 prototype 2001 [15,16] using a resolution of

0.0027 to 0.01 cm^{-1} resulting in almost Doppler limited spectra. A multireflection collisional cooling cell based on White optics and embedded in a Dewar filled with liquid Nitrogen was used for recording the cold spectra [17].

3. Analysis

From the ground state only vibrational transitions to levels of F_2 symmetry species are strongly allowed in absorption. However, one expects numerous resonance interactions as found in the lower N-polyads. These can perturb the rotational structure of the allowed F_2 bands, but also contribute to appearance in the spectrum of bands of the A_1, A_2, E, or F_1 vibrational symmetry, by rovibrational interactions. Therefore, in general, an assignment of all lines is needed in a careful step-by-step rovibrational analysis in order to obtain the vibrational band centers and rovibrational parameters. However, in some spectral regions, where the spectrum is not excessively complex, even a simple approximate assignment provides the possibility to obtain beyond doubt the centers ($J = 0$ energy levels) of a set of the F_2−type vibrational bands. For that reason the P(1) line, corresponding to the $J = 0 \leftarrow J'' = 1$ transition of the band must be assigned. One obtains the upper level by adding the ground state energy 10.48164867 cm^{-1} (for the ^{12}CH$_4$ molecule) or 10.48213260 cm−1 (for ^{13}CH$_4$) to the P(1) line. This technique has been used successfully by us in the context of supersonic jet CRD laser spectroscopy of methane [18,19]. In the present work we use the method for the analysis of the cold FTIR spectra of CH$_4$. We were able to assign new lines for ^{12}CH$_4$ and also 9 new bands for ^{13}CH$_4$, those centers obtained from experimental transitions are presented in column 3 of Table 1. Column 5 and 6 of that table give the predicted values of the corresponding band center using a preliminary effective Hamiltonian analysis.

Table 1. Band Centers of the $^{13}CH_4$ Molecule (in cm^{-1})

Band	$(J' = 0 \leftarrow J'' = 1)$	Band	Ref.	Predict.-I	Predict.-II
1	2	3	4	5	6
$\nu_4(F_2)$	1292.2984	1302.7805	[tw]	1302.56	1302.57
$2\nu_4(F_2)$	2588.1590	2598.6411	[tw]	2597.91	2597.72
$\nu_2 + \nu_4(F_2)$	2811.9708	2822.4529	[tw]	2823.33	2823.35
$\nu_3(F_2)$	2999.0640	3009.5461	[tw]	3009.01	3008.96
$3\nu_4(1F_2)$	3837.9044	3848.3865	[tw]	3847.25	3848.74
$3\nu_4(2F_2)$	3897.0171	3907.4992	[tw]	3907.18	3906.46
$\nu_2 + 2\nu_4(F_2)$	4116.8741	4127.3563	[tw]	4127.47	4127.38
$\nu_1 + \nu_4(F_2)$	4203.3421	4213.8243	[tw]	4216.23	4216.12
$\nu_3 + \nu_4(F_2)$	4290.8153	4301.2974	[tw]	4301.43	4301.46
$\nu_2 + \nu_3(F_2)$	4523.5728	4534.0549	[tw]	4533.44	4533.44
$\nu_3 + 2\nu_4(1F_2)$	5552.9354	5563.4175	[tw]	5564.49	5565.36
$2\nu_3(F_2)$	5976.5657	5987.0478	[tw]	5986.22	5986.25
$\nu_2 + 2\nu_3(F_2)$	7482.676	7493.159	[tw]	7493.52	7493.59
$\nu_1 + \nu_3 + 2\nu_4(1F_2)$	8383.137	8393.620	[tw]	8394.37	8394.98
$2\nu_1 + \nu_3(F_2)$	8779.219	8789.700	[tw]	8792.75	8792.68
$3\nu_3(1F_2)$	8870.389	8880.871	[tw]	8880.92	8880.92
$3\nu_3(2F_2)$	9009.107	9019.589	[tw]	9016.17	9016.36
$\nu_1 + \nu_2 + 2\nu_3(F_2)$	10089.331	10099.813	[tw]	10098.11	10098.11
$2\nu_1 + \nu_2 + \nu_3(F_2)$	10273.830	10284.312	[tw]	10287.56	10287.60

References

[1]   L. Pauling, The Nature of the Chemical Bond, Oxford Uni., London, 1940.

[2]   S. Peyerimhoff, M.Lewerenz and M. Quack, Chem. Phys. Lett., 109, 563 (1984).

[3]   H. Hollenstein, R. Marquardt, M. Quack, and M. A. Suhm, J. Chem. Phys. 101, 3588 (1994).

[4]   R. Marquardt and M. Quack, J. Phys. Chem. A 108, 3166 (2004).

[5]　M. A.K. Khalil, Ann. Rev. of Energy and the Environment 24, 645 (1999).

[6]　P. G. J. Irwin, K. Sihra, N. Bowles, F. W. Taylor and S.B. Calcutt, Icarus 176, 255 (2005).

[7]　M.J.M. Pepper, I. Shavitt, P. v. Rague Schleyer, M. N. Glukhovtsev, R. Janoschek, and M. Quack, J. Comp. Chem. 16, 207 (1995).

[8]　A. Bakasov, T. K. Ha and M. Quack, J. Chem. Phys. 109, 7263 (1998).

[9]　O.N. Ulenikov, E.S. Bekhtereva, S.V. Grebneva, H. Hollenstein and M. Quack, Phys. Chem. Chem. Phys. 7, 1142 (2005).

[10] O.N. Ulenikov, E.S. Bekhtereva, S.V. Grebneva, H. Hollenstein and M. Quack, Mol. Phys. 104, 3371 (2006).

[11] O.N. Ulenikov, E.S. Bekhtereva, S. Albert, S. Bauerecker, H. Hollenstein and M. Quack, J. Phys. Chem. A 113, 2218 (2009).

[12] O.N. Ulenikov, E.S. Bekhtereva, S. Albert, S. Bauerecker, H. Hollenstein, and M. Quack, Mol. Phys. 108, 1209 (2010).

[13] S. Albert, S. Bauerecker, V. Boudon, L. Brown, J.-P. Champion, M. Loëte, A. Nikitin and M. Quack, Chem. Phys. 356, 131 (2009).

[14] H.M. Niederer, S. Albert, S. Bauerecker, V. Boudon, J.P. Champion and M. Quack, Chimia 62, 273 (2008).

[15] S. Albert, K. K. Albert and M. Quack, High Resolution Fourier Transform Infrared Spectroscopy, in Handbook of High-Resolution Spectroscopy, Vol. 2, (Eds. M. Quack and F. Merkt), Wiley, Chichester (2011), 965-1021.

[16] S. Albert and M. Quack. ChemPhysChem 2007, 8, 1271-1281.

[17] S. Albert, S. Bauerecker, M. Quack, and A. Steinlin, *Mol. Phys.*, 105, 541-558 (2007).

[18] M. Hippler and M. Quack, J. Chem. Phys. 116, 6045 (2002).

[19] C. Manca Tanner and M. Quack, Mol. Phys. **110**, 2111 (2012).

Quantum chemical approach to He^{*-} and He$_2$$^{*-}$ in helium nanodroplets

S. E. Huber and A. Mauracher

Institut für Ionenphysik und Angewandte Physik, Universität Innsbruck,
Technikerstraße 25/3, A-6020 Innsbruck, Austria

In gas phase the metastable excited species $He^{*-} \hat{=} He(1s2s2p\ {}^4P)$ and $He_2{}^{*-} \hat{=} He_2(1\sigma_g^2 1\sigma_u 2\sigma_g 1\pi_u\ {}^4\Pi_g)$ have received large attention over many decades both from experiment [1, 2] and theory [3].

In a recent study [4] we focused on said anions and their behaviour inside helium nanodroplets (HNDs). One aspect of this research was to test the capabilities of standard quantum chemical tools to describe these states and their interaction with ground state helium, $He \hat{=} He(1s^2\ {}^1S)$ (see figure 1). Our method was quantum mechanical calculations of the CCSD(T) type [5] and q-aug-cc-pVXZ, X = T, Q basis sets [4]. All calculations were corrected for basis set superposition errors (if applicable) [6].
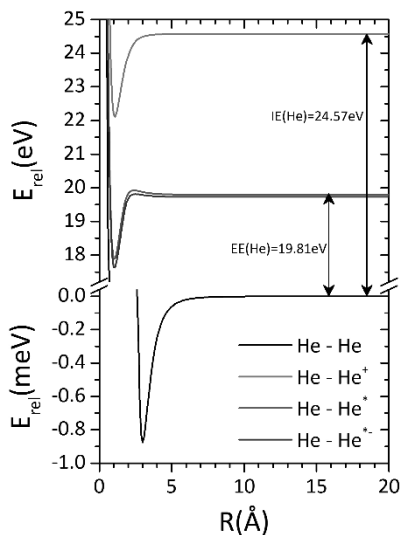
Figure 1 – *Interaction of ground state helium with various helium species. Results obtained at CCSD(T)/q-aug-cc-pVQZ.*

In this presentation we will give a validation that standard quantum chemical tools are capable of describing these states and interactions of interest and an interpretation of following aspects:

(a) The formation of He^{*-} and He_2^{*-}.

(b) The mobility of He^{*-} and He_2^{*-} within HNDs.

(c) The reactivity of He^{*-} with foreign molecules in HNDs.

(d) The suppressed reactivity of He_2^{*-} (which is in contrast to c.).

Acknowledgements

References

[1] P. Reinhed, A. Orbán, J. Werner, S. Rosén, R. D. Thomas, I. Kashperka, H. A. B. Johansson, D. Misra, L. Brännholm, M. Björkhage, H. Cederquist and H. T. Schmidt, Phys. Rev. Lett. **103**, 213002 (2009).

[2] T. Andersen, L. H. Andersen, N. Bjerre, P. Hvelplund and J. H. Posthumus, J. Phys. B At., Mol. Opt. Phys. **27**, 1135 (1994).

[3] L. Adamowicz and T. Pluta, Phys. Rev. A **44**, 2860 (1991).

[4] S. E. Huber and A. Mauracher, Mol. Phys., accepted.

[5] J. A. Pople, M. Head-Gordon and K. Raghavachari, J. Chem. Phys. **87**, 5968 (1987).

[6] S. F. Boys and F. Bernardi, Mol. Phys. **19**, 553 (1970).

Detection of Negative Charge Carriers in Superfluid Helium Droplets: The Metastable Anions He^{-*} and He_2^{-*}

Andreas Mauracher, Matthias Daxner, <u>Johannes Postler</u>, Stefan E. Huber, Stephan Denifl, Paul Scheier
Institut für Ionenphysik und Angewandte Physik, Universität Innsbruck, Technikerst. 25 / 3, A-6020 Innsbruck, Austria

J. Peter Toennies
Max Planck Institut für Dynamik und Selbstorganisation, Am Fassberg 17, D-37077 Göttingen, Germany

One of the fundamental questions in liquid helium research is the mechanism of charge transportation. While there are several negative charge carriers, one of them was identified before as an unusually fast moving one and therefore was named the "exotic fast negative carrier" (EFNC) [1]. There haven been extensive discussions which particle can be assigned to the EFNC in the past. Next to the two metastable excited species He^- and He_2^-, also electron bubbles containing either one or two electrons were under consideration [1-3]. We now have directly observed He^- as well as He_2^- in mass spectra of helium nano droplets (HND) of different sizes. The experiments, together with quantum chemical calculations at CCSD(T)/q-aug-cc-pVTZ level of theory, indicate that the EFNC can be attributed to helium anions.

We observed the creation of helium anions upon electron impact on HNDs in three distinct resonances in the energy range of about 22 eV to 25 eV. These energies coincide very well with the resonances reported by Henne and Toennies [4] for the formation of negatively charged HND. The observed resonances were explained by elastic scattering of an electron with a Helium atom, exciting the latter into its metastable 2^3S state and leaving behind an electron bubble. However, it now seems more reasonable to explain this behaviour via formation of He^-, which is heliophilic and therefore readily stays inside the droplet.

Moreover, most parent anion formation processes of molecules embedded in HNDs show a "repetition" of low energy resonances around 22 eV which were attributed to ionization by aforementioned electron bubbles until now [5]. However, the new experimental data suggests that this phenomenon can be explained via the formation of He^- and subsequent ionization due to charge transfer.

We can prove the higher mobility of He^- compared to He_2^- by doping the HND with SF_6. While the He_2^- signal is only slightly affected, the He^- yield drops significantly. This can be explained by the ability of He^- to reach the SF_6 molecule, which resides

in the center of the droplet, whereas He_2^- is not mobile enough and moreover will stay at the surface of the HND.

The formation process of He^-, its properties and the consequences on the interpretation of previous studies will be presented in this contribution.
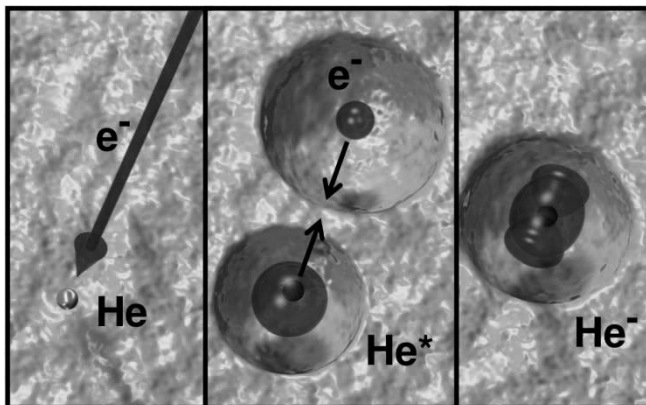
References

[1] G. G. Ihas and T. M. Sanders, Phys. Rev. Lett. 27, 383 (1971).
[2] T. M. Sanders and G. G. Ihas, Phys. Rev. Lett. 59, 1722 (1987).
[3] A. G. Khrapak and W. F. Schmidt, Low Temp. Phys. 37, 387 (2011).
[4] U. Henne and J. P. Toennies, J. Chem. Phys. 108, 9327 (1998).
[5] S. Denifl et al., Phys. Rev. Lett. 97, 043201 (2006).

Ejection of Low-Mass Ions from Large Helium Nanodroplets

Michael Renzler, David Stock, Paul Scheier
Institute for Ion Physics and Applied Physics
University of Innsbruck

1. Introduction

The size distribution of the cluster ions formed via ionization of (pure) helium nanodroplets (HND) obtained by mass spectrometry generally reach to a maximum cluster size of about 1000 helium atoms [1]. This value is surprisingly insensitive of the average size of the neutral precursor droplets. In contrast, simple deflection of the ionized cluster beam with a pair of plates or retarding field analysis of the ionized droplets indicate that charged species with a mass of up to several million He atoms are formed too [2-3]. The latter two methods rely on the fact that the velocity of all masses in a neutral cluster beam is exactly the same and depends on the temperature of the gas before the expansion (in the present case between 7.5 and 9K). The kinetic energy of a large HND ($>10^6$ atoms) is in the keV range and thus such massive ions are hardly affected by typical potentials applied to electrostatic lenses in mass spectrometers. Utilizing a combination of the deflector plate and retarding field method we analyzed the size distribution of charged HND as a function of the expansion conditions and ionization parameters (i.e., electron energy and electron current). These results are compared with mass spectra measured under identical conditions where low-mass ions up to a few 100 He atoms are formed in the interaction region of the neutral HND and electron beam. Thereby we obtain new insight on the processes that lead to formation and ejection of low-mass ions from large HND.

2. Experimental Setup

In a new instrument we implemented both, a pair of electrostatic deflector plates and a set of grids for a retarding field analysis and measured the cluster size distribution of massive charged HND. Helium with a purity >99.9999% is cooled at a pressure of 20 bar with a closed cycle cryo-cooler to temperatures between 7.5K and 9K and expanded through a 5μ diameter pinhole nozzle. The resulting beam of HND passes a 0.4mm diameter skimmer and is ionized in a differentially pumped region (pressure $<10^{-5}$ Pa) by a crossed beam ionizer (Nier-type ion source, with a magnetically collimated electron beam). The ions pass a pair of deflector plates where the charged HND are separated according to their kinetic energy which is proportional to their

mass (all neutral HND have the same velocity). Further down-stream a set of highly transparent grids can be operated as a retarding field analyzer which enables high electrostatic field strengths due to a minimum distance between the grids of about 1.5mm. Ions that pass this region are then detected by a channel electron multiplier operated in a single ion counting mode.

3. Results

Figure 1 shows a typical size distribution obtained for ionized HND formed upon electron ionization at electron energies of 40eV (black), 60eV (red) and 100eV (blue). The neutral HND were produced at a temperature of 8K and a pressure of 20bar.
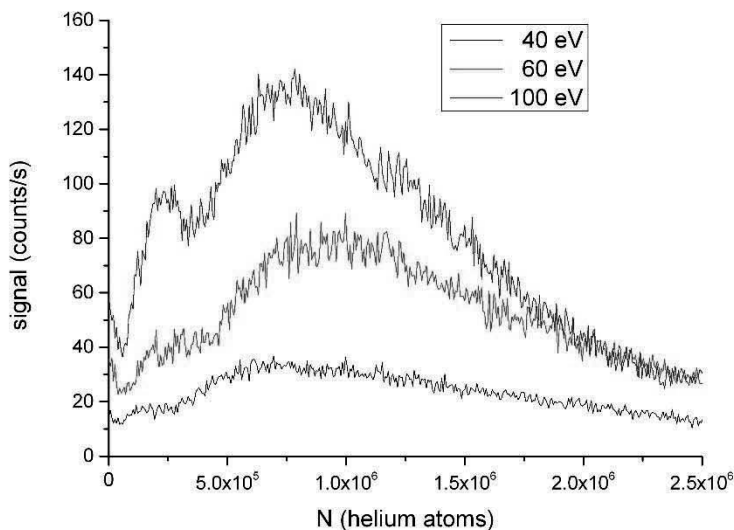
Figure 1: size distributions of HND

At electron energies above the threshold for double ionization (49.2 eV = 2×24.6eV), a second maximum at a cluster size of about N=300 000 appears. We contribute this low-mass peak to the fragmentation of large multiply charged HND that break-up symmetrically. The appearance of this maximum is also dependent on the electron current, since higher currents can lead to multiple ionization processes via sequential electron hits, even at electron energies below the above mentioned threshold.

Figure 2 shows the ion yield for charged clusters of size N=225 000 (red) and N= 580 000 (black) as a function of the voltage applied to the retarding field analyzer.

The dashed green lines represent the total kinetic energy of the mass selected cluster ions. In both cases most of the helium droplets are lost at counter voltages that create a potential barrier which matches the kinetic energy of the clusters. For all cluster sizes we observe a pronounced rise in the ion yield at a counter voltage that is slightly lower than the kinetic energy of the mass selected charged droplet. We attribute this to lensing effects, since this hump always appears, regardless of ionization energy or electron current.
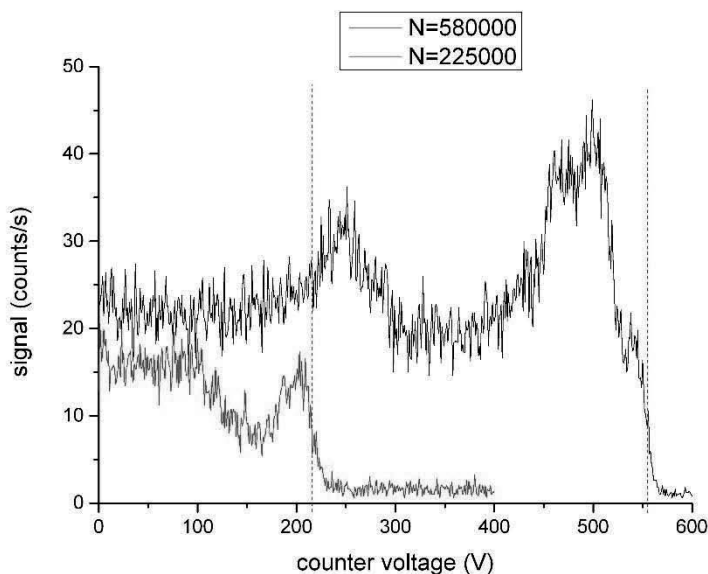
Figure 2: *Ion signal vs. counter voltage*

4. Discussion

The present results demonstrate that ionic cores are tightly bound to large HND and cannot be extracted by electric fields having strengths of several kV/cm which are typical values in mass spectrometry. However, results obtained from a mass spectrometer system indicate that low-mass ions are ejected from large HND immediately after the ionization event. The dependence of the ion yield of these low-mass ions on the electron energy and electron current suggest that Coulomb repulsion between the ionic cores of multiply charged HND is essential to eject most of these ionic cores as low-mass ions from large HND. In contrast the residual HND, most likely single charged, cannot be detected in all mass spectrometer instruments due to the high kinetic energy of the neutral HND which is strongly mass dependent.

Additional measurements are planned for negatively charged HND and to probe the heavy, charged droplets formed upon electron collisions with doped HND.

Acknowledgement

References

[1] H. Schöbel, et al., The European Physical Journal D **63**, 209 (2011)
[2] E. L. Knuth and U. Henne, J. Chem. Phys. **110**, 2664 (1999)
[3] T. Jiang and J. A. Northby, Physical Review Letters **68,** 2620 (1992)

Energetic properties of pentaerythritol

S. Ralser, M. Daxner, B. Puschnigg, M. Renzler, N. Weinberger, P. Scheier
University of Innsbruck, Institute for Ion Physics and Applied Physics

Pentaerythritol (PETP, Figure 1), when deposited on a cold, clean copper surface, and measured with a scanning tunnelling microscope, shows two different morphologies of mono-molecular films. The first one, the so called rectangular phase, can be seen after deposition of the molecule and is stable below 230K. The second one, the striped phase appears at higher temperatures or when a voltage ramp is applied to the rectangular phase with the help of a STM – Tip [1].

Figure 7: *Chemical structure of PETP*

Electron driven reactions such as dissociative electron attachment are possible mechanisms for such a phase transition. Thus in the present study we investigate electron driven reactions of isolated PETP molecules and clusters of PETP molecules embedded in superfluid He nanodroplets.
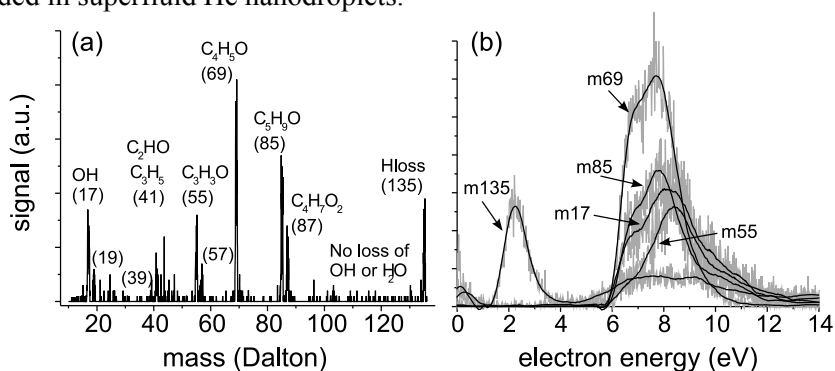
Figure 8: *(a) Mass spectrum of negative ions formed upon dissociative electron attachment to PETP in gas phase at 8eV electron energy. (b) Anion efficiency curves of the most abundant product anions.*

Figure 2(a) shows a mass spectrum of negative ions formed upon dissociative electron attachment of 8eV electrons with gas phase PETP. At this electron energy the majority of product ions are formed via two overlapping core excited resonances (see Figure 2(b)). The dehydrogenated closed-shell anion [PETP-H]$^-$ at a mass of 135 Dalton is an exception as this anion is preferentially formed via a resonance at an electron energy of 2eV.

If PETP is embedded into a helium droplet, several reaction channels are quenched via rapid energy transfer to the surrounding helium matrix and evaporative cooling of helium atoms. Furthermore, this environment enables the possibility of PETP-cluster formation inside the droplet and subsequent ion-molecule reactions between neighbouring molecules and initially formed ions are possible.

Figure 3(a) shows a section of a mass spectrum of anions formed upon around 22eV electron collisions with PETP doped helium nanodroplets. In contrast to the gas phase measurement, this experiment shows, next to the loss of hydrogen, the formation of a fragment anion that has lost 33 Dalton which we assign as the deprotonated PETP which lost an addition methanol molecule. A second weaker series of anions with the mass of the stoichiometric cluster minus 51 Dalton is likely the result of a sequential methanol and water loss from the corresponding dehydrogenated parent anions. As the loss of 51 Dalton is only observed once even for large clusters we conclude that polymerization of PETP clusters is not happening inside the He droplets. Furthermore, the attachment of methanol to the closed shell anions [(PETP)$_n$-H]$^-$ is observed for all cluster sizes.
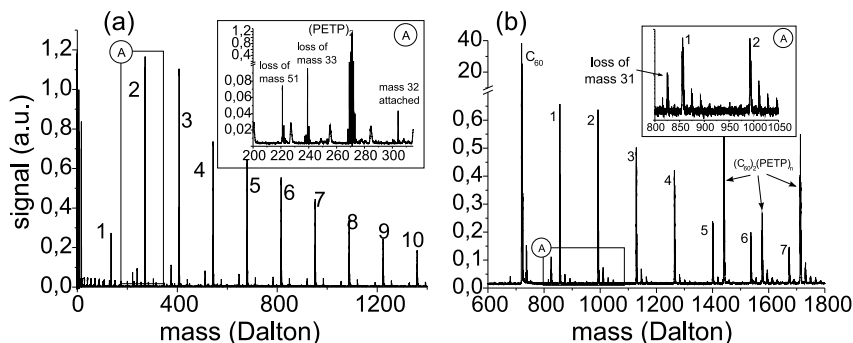
Figure 9: *Mass spectra of negative ions formed upon electron bombardment of PETP doped helium nanodroplets (helium temperature=9.66K, helium pressure=24bar, electron energy=22eV). (a) pristine PETP clusters and (b) PETP-decorated C$_{60}$ clusters.*

The fragmentation pattern deduced from the negative ion mass spectrum of He nanodroplets doped with PETP and C_{60} (Figure 3(b)) differs substantially from the mass spectrum obtained without the C_{60}. Only the monomer of PETP complexed with a C_{60} exhibits bond cleavage of the PETP unit. Larger numbers of PETP show exclusively parent molecules and additional pickup of residual gas water which strongly binds via hydrogen bridges to the PETP units. Similar to fullerenes decorated with other hydrogen containing molecules [2-4] we interpret the relatively strong signal for $[PETP-H]C_{60}^-$ and $[PETP-CH_2OH]C_{60}^-$ as covalently bound complexes where the PETP radical opens an aromatic bond of the fullerene.

These measurements clearly show that most of the fragmentation reactions of PETP are quenched by the superfluid He matrix and even more by the additional presence of fullerenes.

Possible implications of the dissociative electron attachment processes investigated for isolated PETP molecules and clusters of PETP in doped He nanodroplets for the phase transitions of monomolecular films observed via Scanning tunnelling microscopy will be discussed on the poster.

Acknowledgement

References

[1] Hager M. et al., *Spatiotemporal evolution of reaction fronts trigger by tunneling electrons*, XXVII INTERNATIONAL CONFERENCE ON PHOTONIC, ELECTRONIC AND ATOMIC COLLISIONS (ICPEAC 2011)
[2] Denifl S. et al., Angew. Chem. Int. Ed. 48 (2009) 8940-8943
[3] Leidlmair C. et al., Astrophys. J. 738 (2011) L4
[4] Zött. S. et al., J. Phys. Chem. Lett. 3 (2012) 2598–2603

State-resolved sticking probabilities of methane studied with double resonance excitation

P.M. Hundt, M.E. van Reijzen, H. Ueta, and R.D. Beck
Surface Dynamics Group, ISIC – LCPM - EPFL,
1015 Lausanne, Switzerland

State resolved measurements of the sticking probability for dissociative chemisorption of CH_4 on several transition metal surfaces have shown that vibrational exciation of the incident molecule can strongly enhance its reactivity and provided evidence for mode-specificity in methane chemisorption.

To probe the role of vibrational symmetry on reactivity of vibrationally excited methane, we prepared CH_4 in the different symmetry components of the first overtone ($2v_3$) of the antisymmetric C-H stretch normal mode. While direct overtone excitation from the vibrational ground state (v=0) used in our previous experiments provides access only to the $2v_3$-F_2 vibration, we can prepare any of the three symmetry components (A_1, E, and F_2) of the $2v_3$ overtone vibration of CH_4 by step-wise double resonance excitation via the v_3-F_2 state in a molecular beam.

Combining IR-IR double resonance excitation of the CH_4 reactant in a molecular beam by two independently tunable IR optical parametric oscillators, with product detection by reflection absorption infrared spectroscopy (RAIRS), we compared the state resolved CH_4 reactivity for the different $2v_3$ vibrational symmetry components to obtain evidence for the effect of vibrational symmetry on the CH_4 reactivity on Pt(111).

Electronically adiabatic and non-adiabatic collisions of OH(A$^2\Sigma^+$) + Kr, Xe

Mark Brouard*, Garreth McCrudden and Tom Perkins
Department of Chemistry, University of Oxford, Physical & Theoretical Chemistry Laboratory, South Parks Road, Oxford, UK

F. Javier Aoiz and Diego Herráez-Aguilar
Departamento de Química Física, Facultad de Química, Universidad Complutense, 28040 Madrid, Spain

Millard H. Alexander[#] and Jacek Kłos
Department of Chemistry and Biochemistry and [#]Institute of Physical Science and Technology, University of Maryland, College Park, MD 20742, USA

Paul J. Dagdigian
Department of Chemistry, The Johns Hopkins University, Baltimore, Maryland 21218-2685, United States

1. Introduction

The OH(A$^2\Sigma^+$) + Rg systems, where Rg = Kr or Xe, are characterised by very strong attractive interactions (up to the order of a chemical bond) in linear geometries, and repulsion in side-on configurations [1]. Several energy transfer pathways are available in a collision:

a) rotationally elastic   OH(A, N) + Rg $\rightarrow$ OH(A, $N' = N$) + Rg
b) rotationally inelastic   OH(A, N) + Rg $\rightarrow$ OH(A, $N' \neq N$) + Rg
c) electronically inelastic   OH(A, N) + Rg $\rightarrow$ OH(X$^2\Pi$, N') + Rg

In the electronically adiabatic pathways (a and b), the ***j–j'*** correlation is also of great interest. The collisional depolarisation of ***j*** quantifies the 'tilt angle' between the initial and final planes of rotation, and is a very sensitive probe of the intermolecular potential.

In contrast to other lighter Rg atom collisions, in the case of Kr and Xe, electronic quenching plays an essential role in the overall dynamics. The potential is strongly attractive for linear HO—Rg configuration [2], due to a conical intersection between

the 1A' and 2A' PESs and it is precisely at these configurations where electronic quenching takes place.

Quenching thus competes directly with rotational energy transfer (RET) and collisional depolarisation in these collisions, and the presence of electronic quenching suppresses the RET and depolarisation cross-sections from the predicted adiabatic value. Similar effects are observed in the OH(A, $v=1$) + Kr system, which displays more quenching than in $v = 0$. It is thought that the region of greatest coupling becomes more accessible as the OH bond is allowed to stretch.

In this work, cross-sections have been measured for electronic quenching, rotational energy transfer and collisional depolarisation in both rotationally elastic and inelastic collisions.
These cross-sections have been compared to quasi-classical trajectory calculations as described below.

2. A three-state trajectory surface-hopping QCT model, including roto-electronic couplings

Due to the significant degree of non-adiabaticity in the OH(A) + Kr, Xe systems, single-surface (adiabatic) quasi-classical trajectory (QCT) and quantum mechanical (QM) calculations have thus far failed to accurately model the collision dynamics for the range of rotational states where quenching is significant. This stands in contrast to our previous studies of OH(A) with lighter rare gases [3], and NO(A), where adiabatic QCT and QM calculations were in excellent agreement with each other and with the experimental results.

In non-linear configurations, the symmetry of the OHRg system is reduced from $C_{\infty v}$ to C_s, and the doubly degenerate $X^2\Pi$ ground state is split into states of A' and A'' symmetry with respect to reflection in the scattering plane. For symmetry reasons, electrostatic coupling can only link the excited, $2A'$ surface with the $1A'$ surface.

Coupling between the electronic $1A''$ and $2A'$ states is possible via a rotation of A'' symmetry – so-called *Coriolis* coupling. In a similar way, rotation of the triatomic complex also mediates the Renner-Teller coupling between the $1A'$ and $1A''$ states [4]. Therefore the $1A''$ state can also be included in quenching, as seen experimentally where the product OH(X) lambda-doublet ratio is approximately equal [2].

Trajectory surface-hopping QCT has been used to reproduce the experimental quenching, RET and collisional depolarisation cross-sections. When considering a two-state model (1A' and 2A') featuring electrostatic coupling only, electronic quenching is underestimated for both Kr and Xe colliders, but the calculated cross-sections have the correct trend.

A theory has been developed to include all electronic and roto-electronic couplings in a full three-state trajectory surface-hopping calculation. For OH(A) + Kr, experimental and theoretical cross-sections are brought into excellent agreement, and the theory also succeeds in reproducing the quenched OH(X) rotational state distributions and lambda-doublet ratios measured by Lester *et al* [2]. For OH(A) + Xe, agreement is also much improved compared to the two-state model, though further work is still needed.
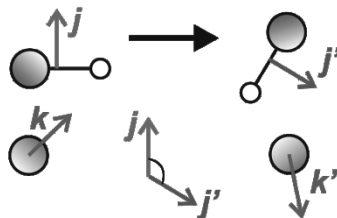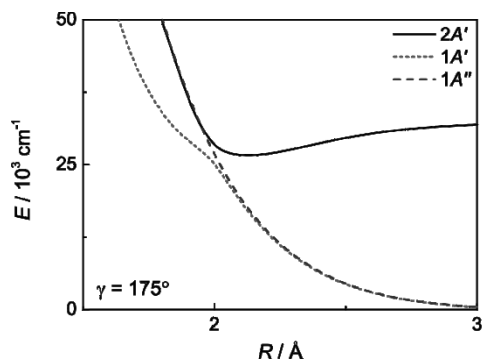
References

[1] A new potential energy surface for OH(A$^2\Sigma^+$)-Kr: The van der Waals complex and inelastic scattering. H. Chadwick *et al., J. Chem. Phys.* **137**, 154305 (2012)

[2] Electronic Quenching of OH A $^2\Sigma^+$ Induced by Collision with Kr Atoms. J. H. Lehman *et al., J. Phys. Chem. A,* dx.doi.org/10.1021/jp407035p (2013)

[3] See for example: *J. Chem. Phys.* **130**, 044305 (2009), *J. Chem. Phys.* **130**, 044306 (2009), *J. Chem. Phys.* **131**, 104307 (2009), *J. Phys. Chem. A* **113**, 15156 (2009)

[4] Trajectory-Surface-Hopping Study of the Renner-Teller Effect in the N(^{2}D) + H$_2$ Reaction. F. Santoro *et al.*, *J. Phys. Chem. A,* **106**, 8276 (2002)

Rotational dependence of the competition between H$^+$ (D$^+$) - transfer and charge transfer reaction: HCl$^+$ (DCl$^+$) + HCl

Till Uhlemann, Jens Wallauer and Karl-Michael Weitzel
Philipps-Universität Marburg, Fachbereich Chemie, 35032 Marburg, Germany
email: Weitzel@chemie.uni-marburg.de

In order to understand and eventually control ion-molecule reactions, it is necessary to complement conventional thermal studies by the investigation of the influence of translational and internal energy of the reacting agents in a state-selective experiment. We have recently described an approach for measuring cross sections for ion molecule reactions over a wide range of the collision energy and internal quantum state of the ion [1,2].

In this contribution we extend our previous work to situations where two reactions may compete. To this end we have measured the cross sections for reactions (1) to (3) as a function of collision energy and rotational quantum state in the ion. State-selected HCl$^+$-ions with rotational quantum numbers controllable from 0 up to 6 were prepared by resonance enhanced multiphoton ionization (REMPI) [3]. A guided ion beam apparatus was used to measure cross section σ.

$$
\begin{array}{llll}
\text{HCl}^+ + \text{HCl} & \rightarrow & \text{Cl} + \text{H}_2\text{Cl}^+ & (1) \\
\text{DCl}^+ + \text{HCl} & \rightarrow & \text{HDCl}^+ \ + \ \text{Cl} & (2) \\
& & \text{DCl} \quad + \quad \text{HCl}^+ & (3)
\end{array}
$$

The cross section $\sigma(E_{c.m.}, N^+)$ for reactions (2) and (3) are shown in Fig. 1. Details will be discussed in this presentation.
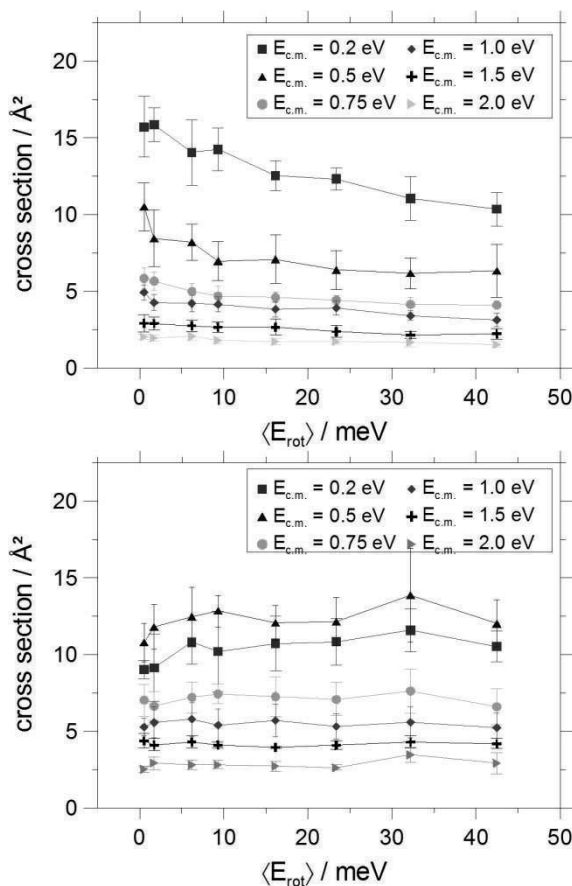
Figure 1: *Absolute cross section for the deuteron transfer (left) and the charge transfer (right) in the reaction DCl$^+$ + HCl as a function of (state-selected) rotational energies at different center of mass collision energies (E$_{c.m.}$) as indicated.*

References

[1] Paetow, L.; Unger, F.; Beichel, W.; Frenking, G.; Weitzel, K.-M. J. Chem. Phys. 132, 174305 (2010)

[2] Paetow, L.; Unger, F.; Beutel, B.; Weitzel, K.-M. *J. Chem. Phys.*, 133, 234301 (2010)

[3] Michel, M.; Korolkov, M.V.; Weitzel, K.-M. *J. Phys. Chem. A*, 108, 9924-9930 (2004)

[4] Uhlemann, T.; Wallauer, J.; Weitzel, K.-M., in preparation

Analysing Destruction Channels of interstellar Hydrocarbon Anions with a 22pol Ion-Trap

Eric Endres, Olga Lakhmanskaya, Thorsten Best, Daniel Hauser, Sunil Kumar, and Roland Wester

Universität Innsbruck, Institut für Ionen und Angewandte Physik, Technikerstr. 25/3
6020 Innsbruck , Austria

The space in between the stars of the galaxies is called the interstellar Medium (ISM). Here, one can find accumulations of atoms, molecules and ions, the so called molecular clouds. The molecular clouds are important as birthplaces for new stars and likely new solar systems. These clouds exist in a vast range of temperatures and densities. Such circumstances give rise to a large number of surprisingly complex molecules. The reactions forming many of these molecules are yet to be elucidated. In particular, ion-molecule reactions are believed to play a key role. The detection of the first interstellar anions [1]-[4] has raised new interest in the quantitative composition of the ISM and the underlying reaction network. To date, six anions have been detected, three of which are unsaturated hydrocarbon chains, namely C_4H^-, C_6H^- and C_8H^-.

Characteristics of these carbon chain anions have been investigated previously via photodetachment measurements [2] and via reactions with atomic partners H, N and O at room temperature [3]. Reactions with molecular hydrogen are assumed to take place slowly [3]. However, because of the abundance of H_2 in the ISM, a precise knowledge of the reaction rates are still important.

A cryogenic 22-pol radio frequency ion trap is the ideal tool to observe rare reactions. With the qualities of an ion trap it is possible to be sensitive to reaction rates lower than 10^{-16} cm^3s^{-1}. Furthermore trapped ions can be cooled down to less then 10K [5] which allows us to analyse temperature effects on reactions. An additional feature is the optical access to the trap. This provides the possibility to make precise photodetachment measurement and spectroscopy. The properties of the 22-pol ion trap allows us to simulate the conditions of the ISM and analyse possible destruction channels for hydrocarbon anions of interstellar interest. Temperature dependent measurements of the reaction rates for the reaction between hydrocarbon

chain anions and H_2 will be presented. Moreover, results of the absolute photodetachment cross-section measurements will be shown.

References

[1] M. C. McCarthy, C. A. Gottlieb, H. Gupta, and P. Thaddeus. Laboratory and astronomical identification of the negative molecular ion C_6H^-. *The Astrophysical Journal Letters*, 652(2):L141, 2006.

[2] T. Best, R. Otto, S. Trippel, P. Hlavenka, A. von Zastrow, S. Eisenbach, S. Jzouin, R. Wester, E. Vigren, M. Hamberg, and W. D. Geppert. Absolute photodetachment cross-section measurements for hydrocarbon chain anions. *The Astrophysical Journal*, 742(2):63, 20

[3] Brian Eichelberger, Theodore P. Snow, Cynthia Barckholtz, and Veronica M. Bierbaum. Reactions of H, N, and O atoms with carbon chain anions of interstellar interest: An experimental study. *The Astrophysical Journal*, 667(2):1283, 2007.

[4] J. Cernicharo, M. Gulin, M. Agndez, K. Kawaguchi, M. McCarthy, and P. Thaddeus. Astronomical detection of $C4H^-$, the second interstellar anion. *A&A*, 467(2):L37–L40, 2007.

[5] Oskar Asvany and Stephan Schlemmer. Numerical simulations of kinetic ion temperature in a cryogenic linear multipole trap. *International Journal of Mass Spectrometry*, 279(2–3):147 – 155, 2009

Collision induced dissociation of aliphatic aminoacids

P Limão-Vieira, F Ferreira da Silva, G Meneses, D Almeida
Laboratório de Colisões Atómicas e Moleculares, CEFITEC, Departamento de Física, Faculdade de Ciências e Tecnologia, Universidade Nova de Lisboa, 2829-516 Caparica, Portugal

G García
Instituto de Física Fundamental, Consejo Superior de Investigaciones Científicas, Serrano 113-bis, 28006 Madrid, Spain

Negative ion formation in electron transfer experiments by potassium collisions with alanine ($C_3H_7NO_2$) and valine ($C_5H_{11}NO_2$) is investigated in the energy range from 15 to 100 eV. The time-of-flight (TOF) fragmentation patterns obtained in the unimolecular decomposition are compared for both amino acids as function of the collision energy. In the case of alanine, the most prominent feature in the collision regime is the relative decrease of the dehydrogenated parent anion signal with respect to the hydrogen anion as the collision energy increases. In the low collision energy regime this can be rationalized in terms of autodetachment inhibition, whereas at higher energies the negative molecular ion can be formed with an excess of internal energy which might even result in fragmentation. Regarding valine, such behaviour was not observed which has been interpreted as a result of side chain effect contributing to an increase of the internal degrees of freedom in comparison to alanine [1].

References

[1] F Ferreira da Silva, J Rafael, T Cunha, D Almeida and P Limão-Vieira, Int. J. Mass Spectrom., (2014) submitted.

State-resolved studies of chemisorptions reactions of water and methane on single crystal surfaces

P. Morten Hundt, Maarten van Reijzen, Helen Chadwick and Rainer D. Beck

Laboratoire de Chimie Physique Moléculaire
Ecole Polytechnique Fédérale de Lausanne, Switzerland.

This contribution will review recent results from our laboratory on quantum state resolved reactivity measurements for the dissociative chemisorption of methane and water (and its deuterated isotopologues) on Ni and Pt surfaces. Using state-selective reactant preparation by infrared pumping in a molecular beam, we prepare the incident reactant molecules in a specific ro-vibrational quantum state and measure the state-resolved reactivity on a single crystal surface using surface analytical techniques such Auger electron spectroscopy, King & Wells beam reflectivity, and reflection absorption infrared spectroscopy of the surface bound reaction products. The results of our measurements provide evidence for mode- and bond-specificity as well as steric effects, which show that chemisorption reactions cannot be described by statistical rate theory but require a dynamical model including all internal degrees of freedom of the dissociating molecule. Comparison of our experimental data with the results   ted.
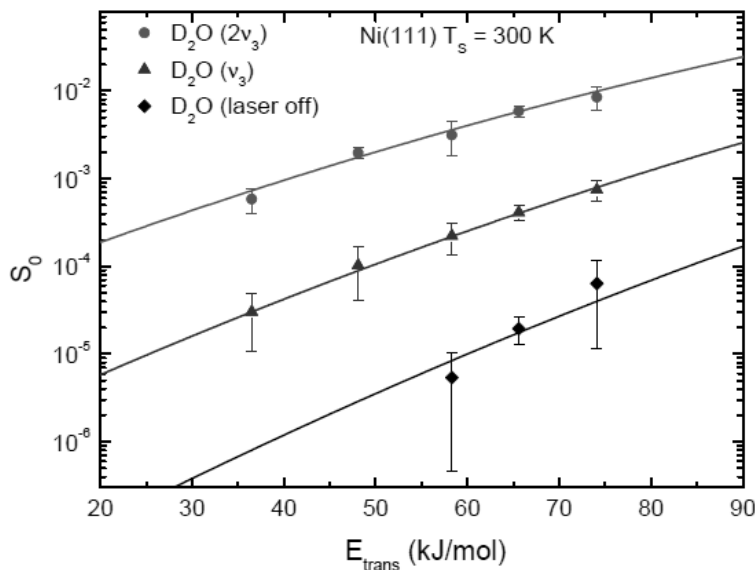
Figure 1: *Quantum state resolved dissociation probability of D₂O on Ni 111).*

Stereodynamic effects in collisions of NO(X) + Ar

M. Brouard[1]*, H. Chadwick[1], C. J. Eyles[1], S. D. S. Gordon[1], B. Hornung[1], B. Nichols[1], F. J. Aoiz[2], S. Stolte[3]

[1]*Department of Chemistry, University of Oxford, United Kingdom*
[2]*Departmento de Química Física, Universidad Complutense, Spain*
[3]*Atomic and Molecular Physics Institute, Jilin University, China*

* Email: mark.brouard@chem.ox.ac.uk

Inelastic scattering measurements have been made for collisions of oriented NO(X) with Ar using a crossed molecular beam apparatus coupled with velocity mapped ion imaging, for a selection of spin-orbit conserving and spin-orbit changing transitions. The initial state of the NO(X) was selected using a hexapole field and the final state by (1+1') REMPI, allowing full Λ-doublet resolution of both the initial and final quantum state. The bond axis of the NO molecule was oriented prior to the collision using a static electric field generated by a four rod setup. Fast switching between the orientation field and velocity mapping conditions is needed to be able to image the scattered NO after the collision[1].

The state to state oriented differential cross-sections for scattering of NO with Ar have been measured, building on previous work on the steric asymmetry[2-3]. Complementary quantum mechanical calculations have also been performed and the agreement between the experimental and theoretical differential cross-sections is reasonable. The normalised difference between the two oriented DCSs varies with scattering angle, and can be qualitatively reproduced by model calculations that consider the interferences between four limiting scattering paths[4].

Preliminary measurements of the product rotational angular momentum alignment following collisions of NO(X) with argon have also been performed experimentally. The differences between the two orientations are not as pronounced as for the oriented differential cross sections. The results obtained can be explained classically by considering a simple kinematic apse[5] model, in which the projection of *j* onto the apse is conserved throughout the collision. Again, the polarisation parameters obtained from the experimental data are in good agreement with those obtained theoretically.

References

[1] L. M. Lipciuc, A. J. van den Brom, L. Dinu, M. H. M. Janssen, *Rev. Sci. Inst.,* **76**, 123103 (2005)

[2] J. J. Van Leuken, J. Bulthuis, S. Stolte and J. G. Snijders, *Chem. Phys. Lett.,* **260**, 595 (1996)

[3] M. J. L. de Lange and M. M. J. E. Drabbels and P. T. Griffiths and J. Bulthuis and S. Stolte and J. G. Snijders, *Chem. Phys. Lett.*, **313**, 491 (1999)

[4] C. J. Eyles, M. Brouard, C.-H. Yang, J. Kłos, F. J. Aoiz, A. Gijsbertsen, A. E. Wiskerke and S. Stolte, *Nature Chemistry*, **3**, 597 (2011)

[5] A. J. McCaffery, M. J. Proctor and B. J. Whitaker, *Annu. Rev. Phys. Chem.*, **37**, 223 (1986)

Temperature diagnostics of anions in 22 pole trap

<u>O. Y. Lakhmanskaya</u>, T. Best , S. Kumar, E. Endres, D. Hauser, R. Wester
Institut für Ionenphysik und Angewandte Physik, Leopold-Franzens-Universität Insbruck, Technikerstraße 25, 6020, Innsbruck, Austria

R. Otto
Department of Chemistry and Biochemistry, University of California San Diego, 9500 Gilman Drive, La Jolla, CA 92093, USA

S. Eisenbach
Physikalisches Institut, Albert-Ludwigs-Universitat Freiburg, Hermann-Herder-Str. 3, 79104 Freiburg, Germany

A. von Zastrow
Institute for Molecules and Materials, Radboud University Nijmegen, Heijendaalseweg 135, 6525 AJ Nijmegen, The Netherlands

Investigation of ion-molecule reactions and spectroscopy measurements require internally and translationally thermalised molecular ions with a well defined temperature. The widely used technique for this is a buffer gas cooling. Collisions with neutral buffer gas molecules (or atoms) cool both internal and external degrees of freedom (for example [2, 3]). High order multipole traps are very suitable for such ion preparation ([1, 4]). They have a large field free region and as a result reduced rf heating and long lifetimes of ions.

There are a number of precise temperature measurements of molecular ions in a 22 pole trap. Most of them are based on spectroscopic studies of ions [3, 5 – 9]. These measurements indicate the existence of a discrepancy between ion temperature and buffer gas temperature and significant deviation of ion rotational temperature from the trap temperature in the range of 10-23 K [2].
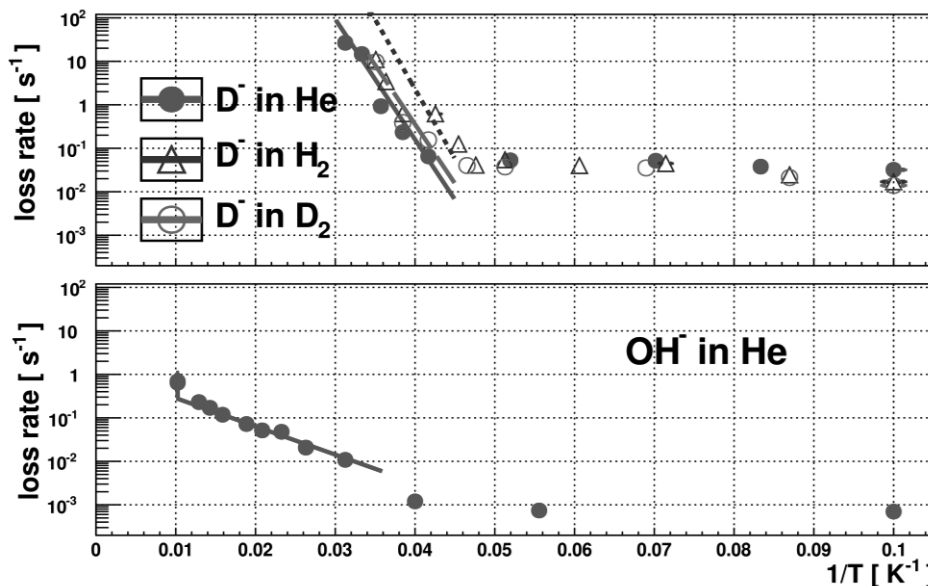
Figure 1: *Translational temperature diagnostics via evaporation for OH⁻ and D⁻ anions in a 22 pole trap. The lines are the exponential fits of experimental data.*

We present a scheme for translational temperature diagnostics of ions and present data for OH⁻ and D⁻ anions in a 22 pole rf trap. We observed a breakdown of thermalisation at 20-25K (fig. 1) and investigate this feature in more detail. The experimental studies show an independence of this feature from both the buffer gas to ion mass ratio and the trapping parameters. We also investigate the distortions of the trap potential caused by the end cap electrodes and discuss an applicability of a new translational thermometry scheme based on loss rate measurements.

References

[1] R. Wester, Radiofrequency multipole traps: tools for spectroscopy and dynamics of cold molecular ions, J. Phys. B: 42 (2009) 154001.

[2] R. Otto, A. von Zastrow, T. Best, R. Wester, Internal state thermometry of coolled trapped molecular anions, Phys. Chem. Chem. Phys. 15 (2013) 612.

[3] O. Asvany, O. Ricken, H. S. P.Müller, M. C. Wiedner, T. F. Giesen, S. Schlemmer, High-resolution rotational spectroscopy in a cold ion trap: H_2D^+ and D_2H^+, Phys. Rev. lett. 100 (2008) 233004.

[4] D. Gerlich, Inhomogeneous rf fields: A versatile tool for the study of processes with slow ions, Adv. Chem. Phys. 82 (1992) 1.

[5] J. Mikosch, H. Kreckel, R. Wester, R. Plasil, J. Glosik, D. Gerlich, D. Schwalm, A. Wolf, Action spectroscopy and temperature diagnostics of H^+ by chemical probing, J. Chem. Phys 121 (2004) 11030.

[6] H. Kreckel, D. Bing, S. Reinhardt, A. Petrignani, M. Berg, A. Wolf, Chemical probing spectroscopy of H_3^+ above the barrier to linearity, J. Chem. Phys. 129 (2008) 164312.

[7] S. Schlemmer, T. Kuhn, E. Lescop, D. Gerlich, Laser excited N^+ in a 22-pole ion trap: Experimental studies of rotational relaxation processes, Int. J. Mass Spectrom. 185-187 (1999) 589.

[8] S. Schlemmer, E. Lescop, J. von Richthofen, D. Gerlich, M. A. Smith, Laser induced reactions in a 22-pole ion trap: $C_2H^+ + h\nu^- \rightarrow C_2H^+ + H$, J. Chem. Phys 117 (2002) 2068.

[9] J. Glosik, P. Hlavenka, R. Plasil, F. Windisch, D. Gerlich, A. Wolf, H. Kreckel, Action spectroscopy of H_3^+ and D_2 using overtone excitation, Phil. Trans. R. Soc. London, Ser. A 364 (2006) 2931.

Towards THz spectroscopy of OD⁻ by threshold photodetachment measurements

S. Lee, D. Hauser, K. Geistlinger, E. Endres, O. Y. Lakhmanskaya, S. Kumar, T. Best, R. Wester

Institut für Ionenphysik und Angewandte Physik, Leopold-Franzens-Universität Insbruck, Technikerstraße 25, 6020, Innsbruck, Austria

Buffer gas cooling of trapped molecular ions in a radiofrequency trap cools molecular ions both in external and internal degrees of freedom. This allows one to prepare molecular ensembles in only few rotational states [1]. Photodetachment spectroscopy of anions has been demonstrated as a suitable technique to investigate rotational levels in the ground vibrational state under high resolution [2]. The photodetachment cross section also provides an understanding of the destruction of anions in various plasma environments or in the interstellar medium.

For molecules such as OH⁻ and OD⁻ , the lowest rotational transitions from $J=0$ to 1 of OH⁻ and OD⁻ are 1.12 and 0.6 THz respectively. These frequencies were difficult to access due to a lack of THz radiation sources [3-5]. Recent developments have made it possible to access in these freqency ranges with cw THz radiation sources, based on frequency difference mixing of two diode lasers [6]. This may give a control over the population distribution in the low rotational states.

In the present work, we combine a cryogenic 22 pole ion trap with a cw THz radiation source to investigate a rotationally resolved THz-spectroscopy and rovibronic inelastic collisions of cold trapped OD⁻ anions. Using a narrow band (< 2MHz) cw THz radiation source tunable upto 1.8 THz, a THz photon drives the rotational transition from $J=0$ to 1 and the electron is detached by a second photon. We will present progress towards THz spectroscopy of trapped ions.

References

[1] R. Wester, Radiofrequency multipole traps: tools for spectroscopy and dynamics of cold molecular ions, *J. Phys. B : At., Mol. Opt. Phys.*, **42**, 154001 (2009)

[2] R. Otto, A. von Zastrow, T. Best, R. Wester, Internal state thermometry of cooled trapped molecular anions, Phys. Chem. Chem. Phys. 15 612 (2013)

[3] G. Cazzoli, C. Puzzarini, Observation of OD⁻ by microwave spectroscopy, *J. Chem. Phys.* **123**, 041101 (2005)

[4] F. Matsushima, T. Yonezu, T. Okabe, K. Tomaru, Y. Moriwaki, Frequency measurement of pure rotational transitions of OH⁻, *J. Mol. Spectrosc.* **235**, 261 (2006)

[5] T. Yonezu, F. Matsushima, K. Takahashi, J. Onmaya, Y. Moriwaki, Frequency measurement of pure rotational transitions of OD⁻, *J. Mol. Spectrosc.* **253**, 16 (2009)

[6] A. J. Deninger, T. Göbel, D. Schönherr, T. Kinder, A. Roggenbuck, M. Köberle, F. Lison, T. Müller-Wirts, P. Meissner , Precisely tunable continuous-wave terahertz source with interferometric frequency control , Rev. Sci. Instrum. **79**, 044702 (2008)

Author index